

*De-novo-* Light Harvesting Complexes as  
Model System to study Chromophor-protein  
Interactions in the Native Membrane

vorgelegt von  
Adela García-Martín  
Dissertation zur Erlangung des Doktorgrades der Fakultät für  
Biologie  
der  
Ludwig-Maximilians-Universität München  
München 2007

1. Berichterstatter: PD Dr P. Braun  
2. Berichterstatter: Prof. Dr. H. Scheer  
Tag der mündlichen Prüfung: 30.03.2007

## DANKSAGUNG

Erst mal will ich mich bei Paula bedanken, da sie im Labor "meine Mutter" und vor allem meine Freundin gewesen ist. Sie hat mir mit allem geholfen.

Ich wollte auch Prof. Scheer fuer seine Zeit, seine Humanitaet und aussergewoehnliche Persoendlichkeit danken. Ich werde immer sein Werk bewundern.

Ich wollte meine Dankbarkeit Dr Robert Gif-sur-Yvette, France, fuer die Raman messungen

Am meine Bublein, fuer die Zeiten in kaltem November Deutschlands, fuer unsere "Essen" und viel mehr..

Ines, fuer ihre Reden ueber Liebe, Leben und am meisten ueber uns selber.

"Birgitte", mit dir war es immer lustig und ernst auf ein mal. Ich erinnere mich immer noch an unsere Obst und Verbenkonjunktionen ...

Allen meinen Kollegen im Labor dafuer, dass alle an mich etwas gemacht haben und ich habe mit allen so zu sagen gewachsen...

Allen meinen "Alten Kollegen" dafuer, dass ich von euch viel gelernt habe und viel Spass gehabt habe.

Patricia, fuer unsere gute und schlechte Momente auf spanisch... Monika fuer ihre Freundschaft und Gewissen..

Ich bedanke mich besonders bei Claudia.. ohne dich haette ich nie damit angefangen. Du hast mich immer gehort und mir geholfen, vielen dank!!

MEINEN ELTERN dafuer, dass sie an mir immer geglaubt haben und mich immer unterstuetzt haben. Ohne euch haette ich Nichts in meinem Leben gesachfft..Vielen dank!!!!Meinem Bruder, fuer seine Unterstuetzung in jeder Hinsicht, fuer seine Tippen

Ich bedanke mich auch bei allen meinen Freundinnen in Spanien, fuer eure mails, Anrufen und Gemuet. Ich danke euch alle, die mich in messenger ausgehalten habt (Ana, Susana, Natalia, Pepa Popa, ...)

Und am Ende, aber nicht zuletzt, ich danke dir Joerg, fuer deine Hilfe und Liebe....

An ALLEN..... Vielen dank, von meinem Herz....

## AGRADECIMIENTOS

En primer lugar a mi “mami” en el laboratorio, Paula, por haber sido y ser un apoyo y una amiga....gracias de corazón

Al Prof. Hugo Scheer, por su humanidad y personalidad...! Además de haberme hecho un hueco en su laboratorio!

A mi pequeña Bubi, por esos momentos en el frío y oscuro noviembre y durante todo el año, siempre estabas ahí. Por nuestra “comida” y mucho más....

A Ines, por nuestras conversaciones sobre el amor, sobre la vida y sobre nosotras, porque sobretodo hemos hablado de nosotras.... que es lo que importa ¿no?.

A mi “Birguite”, contigo siempre fue todo muy divertido a la vez que serio, hablando de “frutas y declinaciones verbales”, que interesante...

A todos mis colegas del laboratorio, porque todos a “vuestra manera”, me habéis ayudado a conocerme un poquito más.

A todos los antiguos colegas, porque con vosotros he aprendido mucho y lo mejor... ¡me he divertido!

A Patricia, por nuestros buenos y malos momentos en español y porque siempre estuvo ahí, a Mónica por su amistad y conocimientos.

Uno muy especial va para Claudia, sin ti nunca hubiera empezado esta aventura, porque siempre me escuchaste y ayudaste, ¡gracias!!!

A mis padres, porque sin ellos nunca hubiera alcanzado nada en mi vida, y esto es una de las cosas más importantes, porque siempre habéis creído en mí, y lo seguís haciendo...

A mi hermano, por su apoyo en todos los sentidos, por sus consejos y regañinas, y sus visitas...

A todas mis amigas de España, por sus mails, llamadas y ánimo, por nuestras bodas “gitanas” y Navidades inolvidables. A todas las que me habéis aguantado en el ¡bendito Messenger! (Ana, Susana, Natalia, Beatriz, Pepa, Popa...)

Y por último pero no menos importante, a Joerg, por su amor y ayuda incondicional...

¡A todos GRACIAS de verdad...de corazón!!!!!!!!!!!!!!!!!!!!

# Contents

<b>Abbreviations</b> .....	<b>v</b>
<b>1. Chapter 1. Introduction</b> .....	<b>1</b>
<b>1.1 Photosynthesis in purple non-sulfur bacteria</b> .....	<b>1</b>
<b>1.2 The peripheral antenna complex, LH2, from purple non-sulfur bacteria</b> .....	<b>4</b>
<b>1.3 The light harvesting active cofactors in the LH2 antenna</b> .....	<b>5</b>
<b>1.4. Spectroscopic properties of the LH2 antenna</b> .....	<b>8</b>
<b>2. Chapter 2. Materials and methods</b> .....	<b>11</b>
<b>.2.1 Materials</b> .....	<b>11</b>
2.1.1 Chemicals.....	11
2.1.2 Enzymes.....	11
2.1.3 Kits.....	12
2.1.4 DNA length and protein molecular weight standards.....	12
2.1.5 Bacterial strains and plasmids.....	12
2.1.6 Plasmids and vectors.....	13
2.1.7 Oligonucleotides.....	13
2.1.8 Antibiotic stock solutions.....	15
2.1.9 Computational work.....	15
<b>.2.2 Methods</b> .....	<b>16</b>
2.2.1 Molecular biology and protein biochemical work.....	16
2.2.1.1 Growth conditions of <i>E. coli</i> DH5 $\alpha$ cells for plasmid preparation.....	16
2.2.1.2 Small-scale plasmid isolation from <i>E. coli</i> (miniprep).....	16
2.2.1.3 Large-scale plasmid isolation from <i>E. coli</i> by CsCl density centrifugation.....	17
2.2.1.4 Restriction analysis of plasmid DNA.....	18
2.2.1.5 Preparation and analysis of DNA by agarose gel electrophoresis.....	18
2.2.1.6 Isolation of DNA fragments from agarose gels.....	18
2.2.1.7 Preparation of vector DNA for ligation.....	18

2.2.1.8 Ligation of DNA fragments.....	19
2.2.1.9 Polymerase chain reaction for cloning.....	19
2.2.1.10 Site directed mutagenesis.....	20
2.2.1.11 Treatments of PCR derived DNA.....	21
2.2.1.12 Determination of content of DNA.....	21
2.2.1.13 Transformation of <i>E.coli</i> .....	21
2.2.1.14 Plasmid transfer by conjugation of <i>Rhodobacter sphaeroides</i> .....	21
2.2.1.15 Cultivation of <i>Rhodobacter sphaeroides</i> .....	22
2.2.1.16 Preparation of intracytoplasmatic membranes.....	23
2.2.1.17 Isolation of the LH2 complex.....	24
2.2.1.18 Protein analysis by gel electrophoresis.....	25
2.2.1.19 Pigment quantification by HPLC.....	26
2.2.1.20 Protein determination.....	26
2.2.2 Statistical analyses in PS I and PS II.....	26
2.2.3 Biophysical analyses.....	27
2.2.3.1 “ <i>In situ</i> ” absorbance spectroscopy.....	27
2.2.3.2 Absorbance spectroscopy.....	27
2.2.3.3 Fluorescence spectroscopy.....	28
2.2.3.4 Circular dichroism spectroscopy.....	28
2.2.3.5 Resonance Raman spectroscopy.....	28
<b>3. Chapter 3: Identification of critical assembly factors at the Bacteriochlorophyll-protein interface in LH2.....</b>	<b>30</b>
<b>3.1 Introduction.....</b>	<b>30</b>
<b>3.2 Results and discussion.....</b>	<b>33</b>
3.2.1 Model high resolution structure from <i>Rhodobacter sphaeroides</i> .....	33
3.2.2 Model LH2 protein.....	34
3.2.3 Permutation of the LH2 $\alpha$ -residue at position -4 at the Bacteriochlorophyll-protein interface in model LH2 complex.....	39
3.2.4 Structural stability of LH2 complexes.....	44

3.2.5 Hydrogen bonding interactions at the Bacteriochlorophyll-protein interface.....	46
3.2.6 Permutation of the LH2 $\alpha$ -residue at position -4 at the bacteriochlorophyll-protein interface in LH2 WT complex.....	50
<b>3.3 Conclusions.....</b>	<b>62</b>
<b>4. Chapter 4: Role of the stereochemical ligation of Bacteriochlorophyll.....</b>	<b>63</b>
<b>4.1 Introduction.....</b>	<b>63</b>
<b>4.2 Results and discussions.....</b>	<b>66</b>
4.2.1 Disruption of the hydrogen bond in LH2 $\alpha$ WT <sub>S-4/G</sub> .....	66
4.2.2 Thermal stability of the LH2 $\alpha$ WT <sub>S-4/G</sub> complex.....	73
4.2.3 Statistical analysis of (Bacterio)chlorophyll-protein interactions depending on the chlorophyll ligation state.....	75
<b>4.3 Conclusions.....</b>	<b>78</b>
<b>5. Chapter 5: Identification of critical (protein) factors for binding and functional modulation of carotenoids.....</b>	<b>80</b>
<b>5.1 Introduction.....</b>	<b>80</b>
<b>5.2 Results and discussion.....</b>	<b>84</b>
5.2.1 Modelling the carotenoid-protein interface in LH2 from <i>Rhodobacter sphaeroides</i> .....	84
5.2.2 Study of carotenoid binding in model LH2 $\alpha$ AL <sub>20/S-4</sub> .....	87
5.2.3 Carotenoid content in model LH2 $\alpha$ AL <sub>20/S-4</sub> .....	95
5.2.4 Study of critical protein-carotenoid interactions in LH2 from <i>Rhodobacter sphaeroides</i> .....	99
5.2.5 Study of the role of phenylalanine in carotenoid binding in LH2 from <i>Rhodobacter sphaeroides</i> .....	102
5.2.6 Statistical analysis of carotenoid-protein interactions in photosystems I and II.....	109
5.2.7 Thermal stability of LH2 depending on the carotenoid contents.....	114
<b>5.3 Conclusion.....</b>	<b>118</b>
<b>6. Summary.....</b>	<b>119</b>

<b>7. References.....</b>	<b>121</b>
<b>EhrenwörtlicheVersicherung.....</b>	<b>133</b>
<b>Publications.....</b>	<b>134</b>
<b><i>Curriculum vitae</i>.....</b>	<b>135</b>

## Abbreviations

aa	amino acid
ADP	adenosine diphosphate
ATP	adenosine triphosphate
APS	ammonium peroxodisulfate
BChl	bacteriochlorophyll
bp	base pairs
BSA	bovine serum albumin
Car	carotenoid
CD	circular dichroism
Chl	chlorophyll
Cyt	cytochrome
DEAE	diethylaminoethyl
DNA	deoxyribonucleic acid
DNase	deoxyribonuclease
dNTP	deoxyribonucleoside triphosphate
DTT	dithiothreitol
EDTA	ethylene diamine tetra acetic acid
H	hydrogen
HEPES	N-2-hydroxyethylpiperazin-N'-2-ethansulfonic acid
HPLC	high performance liquid chromatography
<i>i.e.</i>	<i>id et</i>
IPTG	isopropyl $\beta$ -D-thiogalactopyranoside
LB	<i>Luria bertani broth</i>
LDAO	N,N-dimethyldodecylamin-N-oxid
LH	light harvesting
MOPS	3-(N-morpholino)propanesulfonic acid

---

NE	neurosporene
NIR	near infrared
OD	optical density
PCR	polymerase chain reaction
PS	photosystem
O $\beta$ G	octyl- $\beta$ -glucoside
RC	reaction center
RNA	ribonucleic acid
RR	resonance Raman
RT	room temperature
SE	spheroidene
SDS	sodium dodecyl sulphate
SO	spheroidenone
T <sub>m</sub>	midpoint temperature
T <sub>m</sub>	midpoint of denaturation
TEMED	tetra-methyl-ethylendiamin
TM	transmembrane
Tris	2-amino-2(hydroxymethyl)-1,3-propandiol
UV	ultra violet
WT	wild type

## CHAPTER 1

### General Introduction

Photosynthesis is probably the most important biochemical process on earth. In this process solar energy is converted into chemical energy, which is used to produce organic matter, the indispensable nutritional resource for heterotrophic organisms. As a by-product of photosynthesis  $O_2$  is produced, as results of which there is the oxygenic atmosphere on earth. The photosynthetic machinery generally consists of functionally distinct pigment-protein complexes, the light harvesting (LH) and reaction center (RC) complexes. Chlorophyll (Chl) and carotenoid (Car) molecules of the LH systems absorb light and transfer electronic excitation energy to special Chl molecules in the RC (primary donor). The role of the primary donor is to initiate the directional transfer of electrons across a biological membrane. This charge separation, which takes place in RC, is ultimately used to generate energy-rich metabolites, such as ATP, used by subsequent  $CO_2$  fixation reactions. Both the elementary energy transfer (ET) and primary electron transfer reactions are ultra fast, occurring between  $10^{-13}$  and  $10^{-11}$  seconds, whereas the  $CO_2$  fixation proceeds at a much slower rate.

## 1.1 Photosynthesis in bacteria

Photosynthetic bacteria do not have chloroplasts (or any other organelles); instead, photosynthesis takes place directly within the cytoplasmic membrane. Chloroplasts found in eukaryotes likely evolved from an endosymbiotic relation with cyanobacteria. Cyanobacteria often contain thylakoid membranes to which phycobilisomes are attached. The phycobilisomes act as light harvesting complexes for the photosystems, where oxygen is produced in photosystem II. All other photosynthetic bacteria, however, do not produce oxygen during photosynthesis. Purple bacteria which belong to the diverse group of proteobacteria, are both capable of producing energy through photosynthesis, or heterotrophically by oxidation of organic compounds depending on the environmental conditions. In photosynthetic purple sulfur bacteria, the electron donor is either sulfide or elemental sulfur. The purple non-sulfur bacteria typically use hydrogen or organic compounds. The purple bacterium, *Rhodobacter (Rb.) sphaeroides*, which is used as model organism in this work, belongs to the genus *Rhodobacter*, within the family *Rhodobacteraceae*.

The photosystems (PS) of purple non-sulfur bacteria are embedded in the so called intracytoplasmatic membranes (ICM), which are invaginations of the cytoplasmatic membranes with -depending on the bacterial species- morphologies ranging from sacs to tubes, or sheets. By the invaginations the available surface area is increased to house the PS complexes. In all purple photosynthetic bacteria, the RC is surrounded by a “core” antenna complex termed LH1. In most of them, an additional LH system exists, the peripheral antenna, called LH2, which transfers excitation energy to the RC *via* the core antenna. Some produce an additional peripheral complex, LH3 (McLuskey et al 2001) or LH4 (de Ruijter et al 2004) which are present under particular growth conditions. Excitation energy is transferred, by mechanisms still only partly understood, from the peripheral via the core antenna to the RC (Robert et al 2003) (figure 1.1). The level of LH2 complexes relative to the RC is not fixed but adjusted to efficiently absorb light under varying light intensities.

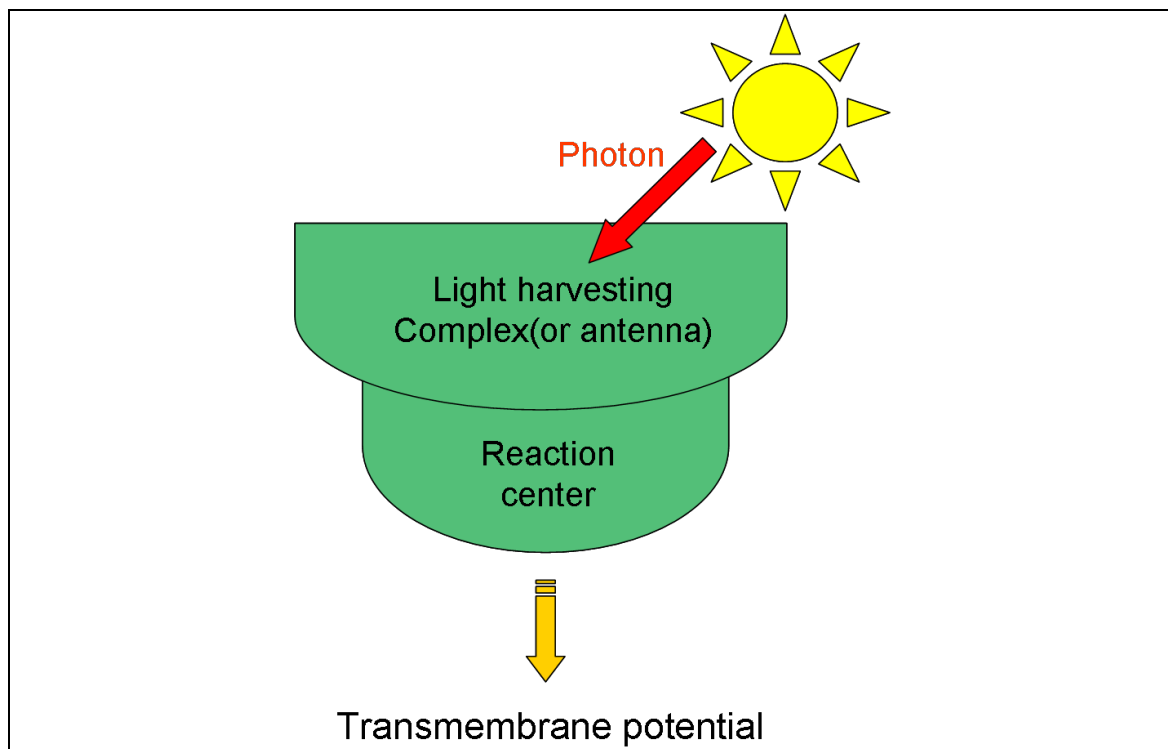


**Figure 1.1: Way of the photons in the photosynthesis.**

In purple bacteria LH complexes are oligomers formed from elementary subunits, usually two transmembrane (TM) polypeptides,  $\alpha$  and  $\beta$ -subunits, which bind the LH active pigments, BChl and Car. In LH complexes Cars are primarily used for light absorption and energy transfer (ET), although they do also function in photoprotection (chapter 5). The protein matrix not only binds these pigments but also arranges them to efficiently perform their different functions.

Each pigment has characteristic absorption spectra: BChl *a* is a cyclic tetrapyrrole carrying a characteristic isocyclic five-membered ring, which is biosynthetically derived from C-13 propionic acid side-chain of the common heme and Chl precursor protoporphyrin IX (Moss 1988). The absorption spectra of the BChl *a* show the electronic transitions along the x axis of the BChl running through the two nitrogen (N) atoms of rings B and D and the y axis along A and C and the two nitrogen (Scheer 2006) (figure 1.2). BChl has two pairs of absorption bands in the blue (B or Soret band) and in the red and NIR (Q bands) spectral regions. One band of each pair is polarized along the x-axis ( $B_x$ ,  $Q_x$ ), the other along the y-axis ( $B_y$ ,  $Q_y$ ). The polarisations of the transitions along the axes are called x and y (Scheer 2006). BChl *a* is not symmetrical along both axes, in solution the  $Q_y$  band is located near 780 nm and the  $B_y$  ~360 nm and the  $Q_x$  ~580 nm and  $B_x$  ~390 nm (not shown). The Cars generally tetraterpenes that contain a chain of conjugated

double bonds, they are found in almost any organisms, also in purple bacteria. In fact, purple bacteria are purple due to the absorption of their Cars rather than BChl *a*.

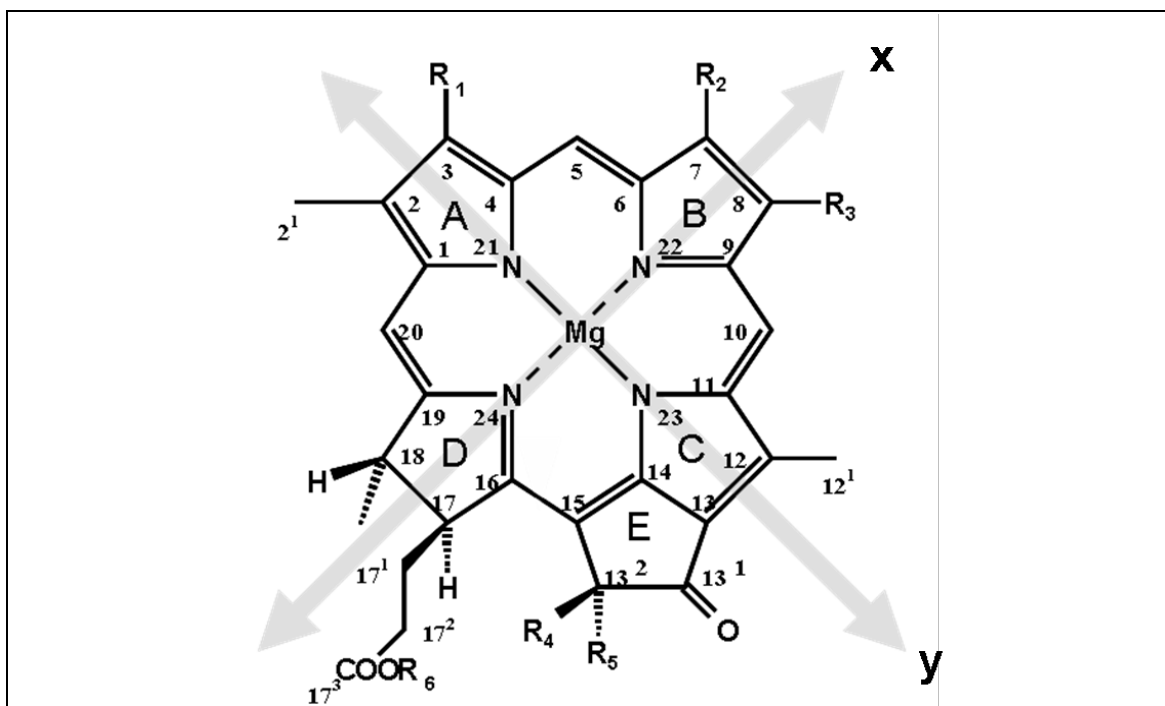


**Figure 1.2: Structure of (B)Chl:** The arrows indicate the y and x transition. R1 is either acetyl (BChl) or vinyl (Chl). Note, that R3, (ethyl), R5, (carbomethoxy) and R4, (hydrogen) are identical in BChl and Chl.

The  $\alpha$  and  $\beta$  polypeptides of the LH2 complexes are small (4-7 kDa), consisting of 40 to 70 amino acid residues and are very hydrophobic. They have been sequenced in a large number of species (for example Brunisholz & Zuber 1992, Robert et al 2003). Both polypeptides have a tripartite structure consisting of polar N- and C-terminal domains and a central, single TM  $\alpha$ -helical domain. The N-terminus is located on the cytoplasmic side of the membrane and the C-terminus on the periplasmic side (Zuber 1986). Native antenna complexes are ring-like oligomers of this minimal subunits composed of the  $\alpha\beta$ -polypeptides and non-covalently bound BChl *a* and Car pigment molecules.

Structural biology and, in particular, protein crystallography has been extremely successful in revealing the structures of photosynthetic proteins from purple bacteria. The RC from *Rhodospseudomonas (Rps.) viridis* was the first integral membrane protein to be solved to high resolution by X-ray crystallography (Deisenhofer et al. 1984). There are also structures of the RC (Allen et al 1987) and LH1-RC "core" (Law et al 1998) complex from *Rb. sphaeroides* and the LH2 from *Rhodospirillum, (Rsp.) molischianum* (Koepeke et al 1996) and from *Rps. acidophila* (McDermott et al 1995, Cogdell et al 2003, Papiz et al 2003). Electron microscopy studies have resulted in a low resolution projection of the LH1

complex from *Rps. rubrum* (Karrasch et al 1995), two dimensional crystal structures from LH1-RC core complexes from *Rb. sphaeroides* (Walz et al 1998), and the LH2 complexes from *Rhodovulum (Rv.) sulfidophilum* (Montoya et al 1995) and from *Rb. sphaeroides* (Walz et al 1998, Scheuring et al 2003). There are also atomic force microscopy studies of LH2 crystal from *Rb. sphaeroides* (Frese et al 2004).

## 1.2 Peripheral antenna LH2

The high resolution structure of LH2 from *Rps. acidophila* (McDermott et al 1995, Cogdell et al 2003, Papiz et al 2003) shows that this complex is a nonamer of elementary subunits. The TM helices of 9  $\alpha\beta$ -hetero dimers form two concentric rings with radii of 18 Å and 34 Å, with most of the BChl sandwiched in between (Prince et al 2003) (figure 1.3). The helices of the  $\alpha$ -subunits lie perpendicular to the plane of the membrane whereas those of the  $\beta$ -apoproteins are tilted by about 15° with respect to it. No helix-helix interactions occur within the TM domains of the complex (Freer et al 1996), but extensive pigment-pigment interactions dominate the TM structure (Law et al 2004). The N- and C-termini of both apoproteins fold over and interact with one another to enclose the cytoplasmic and periplasmic surfaces of the ring. The whole structure is interlocked by hydrogen bonds formed between aromatic residues located at the C-termini of both apoproteins and the BChl a molecules which form an excitonically coupled ring at the C-terminal ends of the helices (McDermott et al 1995, Freer et al 1996). It is important to emphasize that the ring of LH2 does not form without the cofactors BChl and Car.

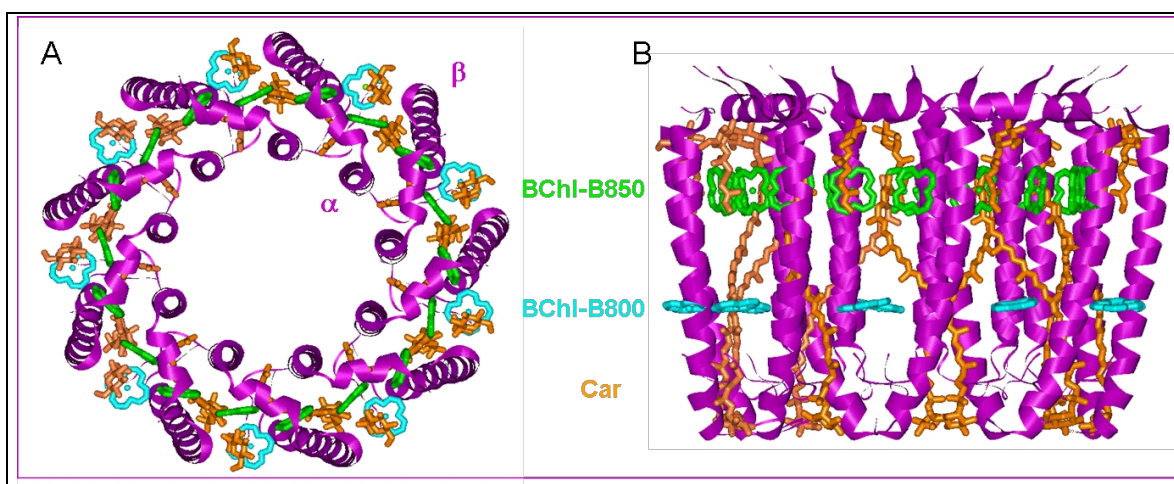


**Figure 1.3: The structure of the LH2 complex from *Rps. acidophila* at a resolution of 2.0 Å:** (Cogdell et al 2003). **(A):** Viewed parallel to the plane of the membrane with the periplasmic side on the top. **(B):** Looking down from the periplasmic side of the membrane. The  $\alpha$ - and  $\beta$ -subunit, are

shown in purple, the BChl-B50 (see below) are shown in green, the BChl-B800 (see below) are shown in turquoise, and the Car are shown in orange.

### 1.3 The light harvesting active cofactors in the LH2 antenna complex

Each minimal  $\alpha\beta$ -subunit of the complex binds a total of three BChl *a* and one Car (Gall et al 2006, Cherezoy et al 2006) giving a total of 27 BChl and 9 Car molecules in the holocomplex. In each dimer unit, two of the three BChl molecules are arranged near the periplasmic surface of the complex as a closely coupled dimer, with the plane of their bacteriochlorin rings approximately perpendicular to the plane of the membrane. These BChl-dimers form a ring of 18 overlapping pigments that are sandwiched between the  $\alpha$ - and  $\beta$ -apoproteins of the fully assembled LH2 complex. These BChls are termed BChl-B850 having the maximum absorption of the red-most transition at 850 nm. The distance between the BChl-B850 molecules within a dimer is  $\sim 9.5$  Å and between two dimers is  $\sim 8.9$  Å.

Each BChl-B850 molecule is coordinated *via* the central Mg to highly conserved histidine residues located in the hydrophobic stretch of each  $\alpha$ - and  $\beta$ -polypeptide. Histidine are most frequently found to coordinate the central Mg atom of BChl or Chl molecules in nearly all bacterial and plant LH complexes (Brunisholz & Zuber 1992, Jordan et al 2001). Next to the Mg coordination, multiple interactions exist between the protein subunits and the (B)Chl molecules, in particular, the peripheral substituents.

The other type of BChl molecules in LH2, BChl-B800 (due to the maximal of absorption at 800 nm), are monomeric, and are located at the N-terminal side of the LH2 complex. Their bacteriochlorin rings lie in a plane parallel to the plane of the membrane. Each BChl-B800 is separated from the neighbour by a distance of  $\sim 21$  Å. In *Rps. acidophila*, the BChl-B800 molecules are ligated to a carboxylate moiety of the N-terminal  $\alpha$ -methionine (Papiz et al 2003).

There is a single Car molecule per  $\alpha\beta$ -subunit (Gall et al 2006, Cherezoy et al 2006). This Car has a typical *all-trans* conformation and spans the whole depth of the complex. In the LH2 from *Rps. acidophila* the Car is rhodopin glucoside and in the LH2 from *Rb. sphaeroides* it is spheroidene (SE) and spheroidenone (SO) in varying ratios depending on the growth conditions (Yelissev et al 1996, Yelissev et al 1997). There are a number of

mutant strains of *Rb. sphaeroides* which have as major Car neurosporene (NE), the biosynthetic precursor of spheroidene (chapter 5, figure 5.3).

Some of the underlying principles as the binding and spectral adaptation of (B)Chl by polypeptide have been clarified by classical mutagenesis in native complexes. This includes ligation of the BChls' central Mg ion by nucleophilic amino acid residues and H-bonding between aromatic residues and the C3-acetyl group, but many of the determinants responsible for recognition of (B)Chl, stable binding and spatial arrangement by the protein scaffold remain unravelled. Even less is known concerning the Car binding and recognition by the polypeptides.

Purple bacteria, in particular, *Rb. sphaeroides* have been extensively used as model organism for photosynthesis. The spectroscopic properties of these bacterial systems are relatively straightforward as they possess only one major chlorin type pigment and the resonant absorption bands arising from this chromophore are generally well resolved. This makes this bacterial system ideal as a model for studying photosynthesis in general.

Based on these studies the spectral bands in the LH2 spectrum are clearly assigned to specific molecules in the LH2 molecule. An absorption band occurring at 800 nm is due to a monomeric BChl *a* pigment oriented perpendicular to the membrane normal (figure 1.5). An absorption band occurring at ~ 850 nm has been assigned to the extensively coupled BChl *a* pigments with dipoles oriented parallel to the membrane normal. It is a combination of excitonic and protein-pigment interactions that cause the absorption maximum of these BChls to red-shift dramatically, from about 770 nm for monomeric BChl *a* in organic solvents to about 850 nm in LH2 (figure 1.5).

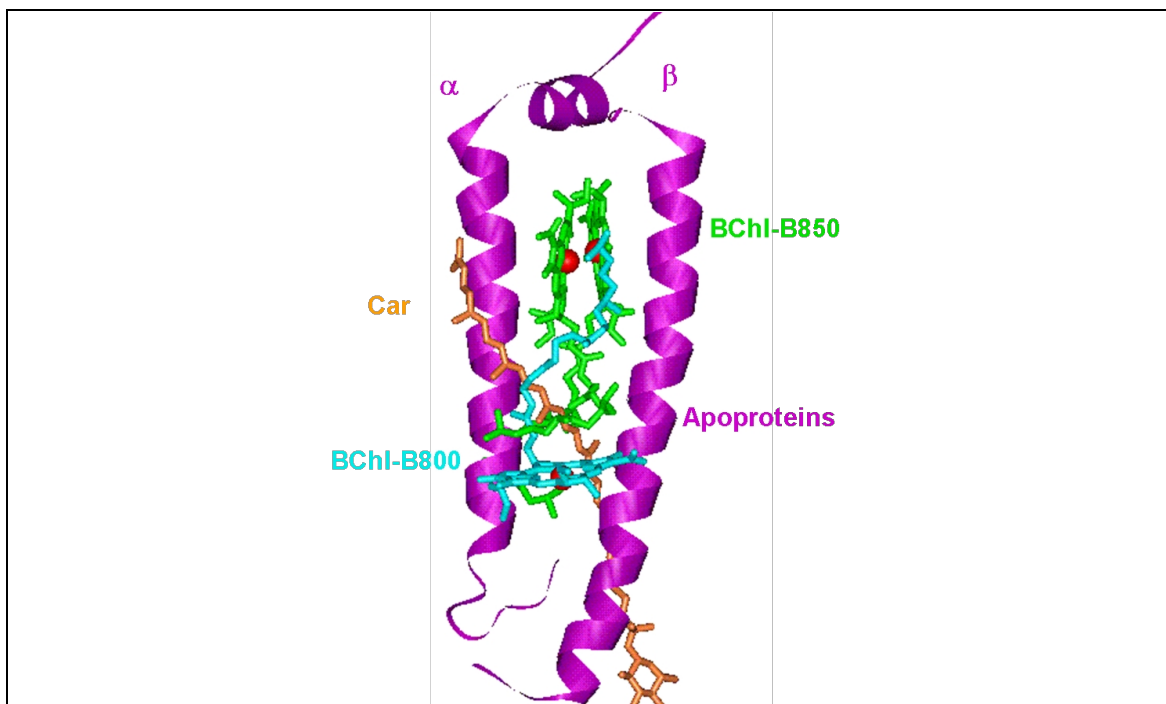


**Figure 1.4: Schematic view of the LH2 elementary subunit from *Rps. acidophila*** (McDermott et al 1995) The  $\alpha$  and  $\beta$ -subunits (purple), 2 BChl-B850 (green), one BChl-B800 (turquoise), and one Car (orange).

## 1.4 Spectroscopic properties of LH2

The structure of LH2 reveals an organization that is beautifully adapted to optimize the orientation of the BChl molecules for a rapid and efficient ET. The ET occurs from Car to BChl-B800 and to BChl-B850 (Robert et al 2003). The spectral properties of individual pigments within LH2 are strongly dependent on the interactions with their immediate environment. These interactions are responsible both for the transition frequencies of the pigments and for the static disorder which leads to a BChl-B850 with largely homogeneously broadened absorption transitions. The close proximity the BChl-B850 molecules provokes that they interact strongly with each other and therefore they act almost like a super molecule, and only so one can understand the spectroscopic properties. The BChl-B850 band is the sum of the electronic transition of all pigment (Robert et al 2003). The CD signal also reflects this character. The LH2 exhibit a conservative CD signal in the BChl-B850 region (Cogdell & Scheer 1985).

Within the LH2 complex a number of factors are discussed to contribute to the tuning of the spectra. Most importantly and apparent from the three-dimensional structure are: (i) interactions between neighboring pigments within the cyclic structure and (ii) hydrogen bonding interactions between the BChls'  $C_3$  acetyl groups and aromatic residues of the protein. Coupling between pigments has long been presumed (van Grondelle 1985,

Cogdell & Scheer 1985, Braun et al 1990, Braun & Scherz 1991, Koolhaas et al 1998) and confirmed by observation of van der Waals contacts between the pigment molecules in the high resolution structures. This has been shown to be the main factor in determining the spectral properties by a number of calculations (for example Scherz et al 1996, Sauer et al 1996a). It has been demonstrated that a certain proportion of the red shift observed in the BChl  $a$   $Q_y$  transition is due to hydrogen bonding of the C3 acetyl group to aromatic residues (Fowler et al 1994, Sturgis et al 1995a, Sturgis et al 1995b, Sauer et al 1996b, Sturgis et al 1997).

The absorption spectrum of LH2 from *Rb. sphaeroides* is depicted in figure 1.5. In contrast to the situation observed in the NIR region of the spectrum, the positions of the  $Q_x$  transition and Soret absorption bands of all three BChl populations are less affected by the chemical environment of their binding sites. They all have their Soret absorbance located at  $\sim 380$  nm and that of their  $Q_x$  transition located at  $\sim 590$  nm. The absorption between 450 nm and 550 nm arises from the Car.

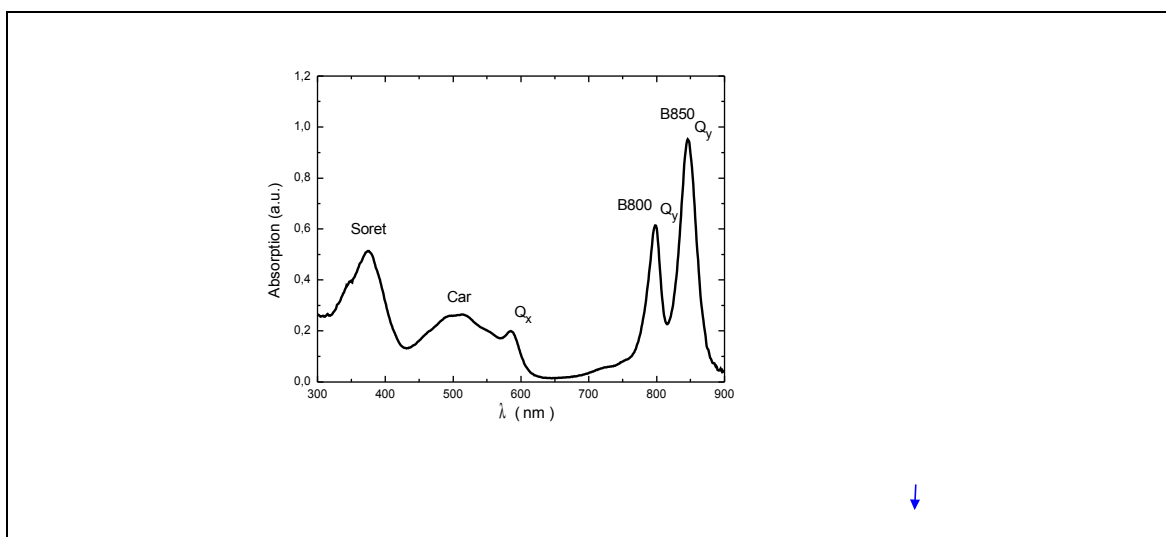


**Figure 1.5: Typical absorption spectrum of LH2 complexes from *Rb. sphaeroides*.** The absorption bands of the BChl molecules are: at  $\sim 800$  and  $\sim 850$  nm ( $Q_y$  transition), at  $\sim 580$  nm ( $Q_x$ ) and at  $\sim 380$  nm (Soret band). The region of the Car molecules is shown at 450-550 nm. Spectra are taken of LH2 complex in detergent O $\beta$ G (material and methods).

ET among the pigments of LH2 has been examined, for example, by fluorescence excitation spectroscopy. The excitation spectra of LH2 complexes principally show similar features as the absorption spectra when detecting at 850 nm. The broad excitation band at 450-550 nm originates from Car and the 800 nm excitation band from BChl-B800. Both, the absorption and fluorescence excitation spectra may change in response to alterations

in the binding to the TM proteins or between the pigments. Thus, these spectra, in particular of the BChl-B850, may be used as sensitive endogenous probes for the proper assembly of the LH2 complex.

In this thesis, it is tried to define which factors hold together and assemble the structure LH2 complex, to that end a combination of biochemical, bioinformatics and spectroscopic methods are used. More precisely, it is aimed at shedding further light on the critical interactions between the light harvesting cofactors and their binding proteins in the complex LH2 of *Rb. sphaeroides*, which has as ligands the pigments BChl and Car.

The presented work is divided into two major parts. In the first part, the critical interactions at the BChl/protein interface are examined and in the second part, Car/protein binding and functional assembly are explored. For the exploration of the critical *in vivo* interactions between the chromophores and proteins, an experimental model system had first to be established, which assembles in the native membrane. This is first greatly simplified in the region of the chromophore binding sites, which by insertion of particular residues in turn enables the systematic study of the determinative BChl-protein and Car-protein interaction motifs in the model sequence context.

The main goals of this work have been to further the understanding of (i) the role of intramembrane H-bonding at the BChl/protein interface, (ii) the role of the diastereotopic ligation of (B)Chl, and (iii) the role of the aromatic residues in binding and functional modulation of Car in TM proteins by the combination of spectroscopic and biochemical analyses. Complementary to the experimental approach, the identified Car and BChl-binding motifs should be further substantiated by a bioinformatical approach. The results are accordingly discussed in three chapters, which each have an individual introduction specific for the theme.



## CHAPTER 2

# Materials and methods

## 2.1 Materials

### 2.1.1 Chemicals

All chemicals used in this work had a suitable degree of purity and were provided by Merck (Darmstadt, Germany), Pharmacia (Uppsala, Sweden), Roth (Karlsruhe, Germany), Serva (Heidelberg, Germany), and Sigma-Aldrich Chemie GmbH (Taufkirchen, Germany). Other chemicals, buffers, and additional materials are described in the corresponding methods.

### 2.1.2 Enzymes

Enzymes were obtained from the following companies, if not indicated otherwise: Invitrogen (Karlsruhe, Germany), MBI Fermentas (St. Leon-Rot, Germany), New England Biolabs (Frankfurt/Main, Germany), Promega (Mannheim, Germany), Qiagen (Hilden; Germany), Roche Diagnostics (Mannheim, Germany), and Stratagene (Heidelberg, Germany).

T4-DNA Ligase	Invitrogen, Germany
DNase I, Rnase-free	Roche Diagnostics GmbH, Penzberg, Germany
DNA polymerase	TaKaRa Ex Taq™, Takara Bio INC., Shiga, Japan
RNase Inhibitor	Roche, Mannheim, Germany
Proteinase K	Invitrogen, Karlsruhe, Germany
Dpn I	Invitrogen, Karlsruhe, Germany
Kpn I	Invitrogen, Karlsruhe, Germany
Nde I	Invitrogen, Karlsruhe, Germany
Pfu DNA	Promega, Mannheim, Germany
Hind III	Promega, Mannheim, Germany

BamH I	Promega, Mannheim, Germany
ExoSap -IT PCR	USB (Amersham Pharmacia Biotech)
Lysozyme	Serva, Heidelberg, Germany

### 2.1.3 Kits

QIAprep Spin Miniprep Kit	Quiagen, Hilden, Germany
Plasmid Midi Kit	Quiagen, Hilden, Germany
QIAquick PCR Purification Kit	Quiagen, Hilden, Germany
QIAquick Gel Extraction Kit	Quiagen, Hilden, Germany
RNeasy MiniElute Cleanup Kit	Quiagen, Hilden, Germany
Mini Quick Spin DNA Columns	Roche, Mannheim, Germany
QuickChange	Stratagene, La Jolla CA, USA
QuickChange XL site-directed mutagenesis	Stratagene, La Jolla, CA, USA

### 2.1.4 DNA length and protein molecular weight standards

GeneRuler™ 1Kb DNA ladder (MBI Fermentas, St. Leon-Rot, Germany), yielding fragments between 250 to 1000 bp, and  $\lambda$  DNA, restricted with *EcoRI* and *HindIII*, yielding fragments between 564 to 21226 bp, were used as DNA length standard. GeneRuler™ 100bp DNA ladder was used for small fragments.

As a standard for the determination of the molecular weight of proteins, SDS-PAGE molecular weight standards from Biorad (26625, 16950, 14437, 6512, 3496, 1423 kDa and Kaleidoscope standards (38600, 25000, 16300, 7800, 3400 kDa) were used.

### 2.1.5 Bacterial strains and plasmids

Strain/Plasmid	Relevant characteristics	Source/Reference
<b>Strain</b>		
<i>E. coli</i>		
DH5 $\alpha$	<i>supE44, <math>\Delta</math> lac</i> U169 ( $\phi$ 80Z $\Delta$ M15) <i>hsd R17</i> , (Sambrook et al 1989) <i>rec A1, end A1, gyr A96, thi-1, rel A1</i>	
S17-1	<i>thi, pro, hsdR-, hsdM, recA</i> , RP4-2 (Tc::Mu Km::Tn7)	
<i>Rb. sphaeroides</i>		
NCIB 8253	Wild type	(Nidemann RA 1974)
DPF2	Genomic deletion of <i>puf BALMX</i> ; insertion of Km <sup>R</sup> gene	
DG2	Major Car NE	
DD13	Major Car SO, SE. Strain DPF2 with genomic deletion of <i>pucBA</i> ; insertion of Sm <sup>R</sup> gene	
<b>Plasmid</b>		
pRK415	Tc <sup>R</sup> derivate of RK2; mobilizate	
pRKCBC1	Tc <sup>R</sup> ; 3.8 kb <i>BscI</i> fragment encompassing <i>pucBA</i> with engineered KpnI site and unique BamHI site (in pRK415)	

### 2.1.6 Vectors

Name	Application	Resistance	Company

pGEM-T Easy Vector	For cloning products	of PCR	Ampicillin	Promega (Mannheim, Germany)
TA-TOPO	For cloning products	of PCR	Kanamycin Ampicillin	Invitrogen (Karlsruhe, Germany)

## 2.1.7 Oligonucleotides

All oligonucleotides used for PCR reactions, cloning or sequencing have been synthesized by Thermo Electron (Ulm, Germany).

Use	Primer designation	Sequence (5'→3')
Sequencing	LH2 $\alpha$ -BamHf	ACCATGACCAACGGCAAATC
	LH2 $\alpha$ -BamHr	AACCCAAGGATCCCGGCC
Sequencing	LH2-Kpn1-f	GAAACCGACCGTCGGGGTACCGCTGTTCTCAGCG
	LH2-Kpn1-r	CGCTGAGGAACAGCGGTACCCCGACGGTCCGTTTC
Mutagenesis	LH2 $\alpha$ AL <sub>16S-4/T</sub> -f	GCTGCCCTGCTCGCCWCTCTCCTGATACACG
	LH2 $\alpha$ AL <sub>16-4S/T</sub> -r	CGTGTATCAGGACGCWGGCGAGCAGGGCAGC
Mutagenesis	LH2 $\alpha$ AL <sub>16S-4/N-H</sub> -f	GCTGCCCTGCTCGCCMCTCTCCTGATACACG
	LH2 $\alpha$ AL <sub>16-4S/N-H</sub> -r	CGTGTATCAGGACGCTGGCGAGCAGGGCAGC
Mutagenesis	LH2 $\alpha$ AL <sub>16S-4/Q-K</sub> -f	GCTGCCCTGCTCGCCMCTCTCCTGATACACG
	LH2 $\alpha$ AL <sub>16-4S/Q-K</sub> -r	CGTGTATCAGGACGCKGGCGAGCAGGGCAGC
Mutagenesis	LH2 $\alpha$ AL <sub>16S-4/E-D</sub> -f	GCTGCCCTGCTCGCCSCTCTCCTGATACACG
	LH2 $\alpha$ AL <sub>16-4S/E-D</sub> -r	CGTGTATCAGGACGCSGGCGAGCAGGGCAGC
Mutagenesis	LH2 $\alpha$ AL <sub>16S-4/C-F-Y</sub> -f	GCTGCCCTGCTCGCCDCTCTCCTGATACACG
	LH2 $\alpha$ AL <sub>16-4S/C-F-Y</sub> -r	CGTGTATCAGGACGCHGGCGAGCAGGGCAGC
Mutagenesis	LH2 $\alpha$ AL <sub>16/S-4L-12/S-10</sub> -f	GGCGATGACGGCAGCGGGCAGCAACAGCGGAACGCCGAC
	LH2 $\alpha$ AL <sub>16/S-4/L-12/S-10</sub> -f	GTCGGCGTTCCGCTGTTGCTCGCCGCTGCCGTATCGCC
Mutagenesis	LH2 $\alpha$ AL <sub>16/S-4/L-12</sub> -f	GTCGGGGTACCGCTGTTACTGTCCGCTGCCCTGCTCGCCTCTC
	LH2 $\alpha$ AL <sub>16/S-4/L-12</sub> -r	GAGAGGCGAGCAGGGCAGCGGACAGTAACAGCGGTACCCCGAC
Mutagenesis	LH2 $\alpha$ AL <sub>16/S-4/A-10</sub> -f	GACCGTCGGGGTACCGCTGTTCTGGCCGCTGCCCTGCTCGCC
	LH2 $\alpha$ AL <sub>16/S-4/A-10</sub> -r	GGCGAGCAGGGCAGCGGCCAGGAACAGCGGTACCCCGACGGTC
Mutagenesis	LH2 $\alpha$ WT <sub>F-12/L</sub> -f	GAAACCGACCGGCGTTCCGCTGTTGCTCAGCGCTGCCGTCATCGC CTCC
	LH2 $\alpha$ WT <sub>F-12/L</sub> -r	GGAGGCGATGACGGCAGCGCTGAGCAACAGCGGAACGCCGGTCCG GTTTC

Mutagenesis	LH2 $\alpha$ WT <sub>S-10/A</sub> -f	GACCGGCGTTCCGCTGTTCTCGCCGCTGCCGTCATCGCCTCCGT C
	LH2 $\alpha$ WT <sub>S-10/A</sub> -r	GACGGAGGCGATGACGGCAGCGGCGAGGAACAGCGGAACGCCG GTC
Mutagenesis	LH2 $\beta$ WT <sub>A/G-8</sub> -f	CATCCTCGGCACCCGCGTCGSCGGTGGCATGGCGCTCATC
	LH2 $\beta$ WT <sub>A/G-8</sub> -r	GTAGGAGCCCGTGGGCGCAGCSGCCACCGTACCGCGAGTCG
Mutagenesis	LH2 $\alpha$ WT <sub>A-4</sub> -f	GCTGCCGTCATCGCCGCCGTCGTTATCCACG
	LH2 $\alpha$ WT <sub>A-4</sub> -r	CGTGGATAACGACGGCGGCGATGACGGCAGC
Mutagenesis	LH2 $\alpha$ WT <sub>L/V-4</sub> -f	GCTGCCGTCATCGCCSTGGTCGTTATCCACGCTG
	LH2 $\alpha$ WT <sub>L/V-4</sub> -r	CAGCGTGGATAACGACCASGGCGATGACGGCAGC
Mutagenesis	LH2 $\alpha$ WT <sub>H/N-4</sub> -f	GCTGCCGTCATCGCCMATGTCGTTATCCACGCTG
	LH2 $\alpha$ WT <sub>H/N-4</sub> -r	CAGCGTGGATAACGACATKGGCGATGACGGCAGC
Mutagenesis	LH2 $\alpha$ WT <sub>Q/K-4</sub> -f	GCTGCCGTCATCGCCMAGGTCGTTATCCACGCTG
	LH2 $\alpha$ WT <sub>Q/K-4</sub> -r	CAGCGTGGATAACGACCTKGGCGATGACGGCAGC
Mutagenesis	LH2 $\alpha$ WT <sub>E/D-4</sub> -f	GCTGCCGTCATCGCCGASGTCGTTATCCACGCTG
	LH2 $\alpha$ WT <sub>E/D-4</sub> -r	CAGCGTGGATAACGACSTCGGCGATGACGGCAGC
Mutagenesis	LH2 $\alpha$ WT <sub>G-4</sub> -f	GCTGCCGTCATCGCCGGCGTCGTTATCCACGCTG
	LH2 $\alpha$ WT <sub>G-4</sub> -r	CAGCGTGGATAACGACGCCGGCGATGACGGCAGC
Mutagenesis	LH2 $\alpha$ WT <sub>C/F/Y-4</sub> -f	GCTGCCGTCATCGCCTDTGTCGTTATCCACGCTG
	LH2 $\alpha$ WT <sub>C/F/Y-4</sub> -r	CAGCGTGGATAACGACAHAGGCGATGACGGCAGC
Mutagenesis	LH2 $\alpha$ WT <sub>M/L-4</sub> -f	GCTGCCGTCATCGCCATSGTCGTTATCCACGCTG
	LH2 $\alpha$ WT <sub>M/L-4</sub> -r	CAGCGTGGATAACGACSATGGCGATGACGGCAGC
Mutagenesis	LH2 $\alpha$ WT <sub>G+4</sub> -f	CGTCGTTATCCACGCTGCTGTGGGACGACCACCACCTGGCTGCC C
	LH2 $\alpha$ WT <sub>G+4</sub> -r	GGGACCCAGGTGGTGGTCGTCCCCACAGCAGCGTGGATAACGA CG
Mutagenesis	LH2 $\alpha$ WT <sub>G+3</sub> -f	CGTTATCCACGCTGCTGGGCTGACGACCACCACC
	LH2 $\alpha$ WT <sub>G+3</sub> -r	GGTGGTGGTCGTGTCAGCCAGCAGCGTGGATAACG
Mutagenesis	LH2 $\alpha$ WT <sub>G-1</sub> -f	GTCATCGCCTCCGTCGTTGGCCACGCTGCTGTGCTGACG
	LH2 $\alpha$ WT <sub>G-1</sub> -r	CGTCAGCACAGCAGCGTGGCCAACGACGGAGGCGATGAC
Mutagenesis	LH2 $\alpha$ WT <sub>G-4</sub> f	GTCTTCGGTGGCATGGGGCTCATCGCGCACTCC
	LH2 $\alpha$ WT <sub>G-4</sub> r	GGAAGTGC CGATGAGCCCCATGCCACCGAAGAC

## 2.1.8 Antibiotic stock solutions

Ampicillin	10 mg/ml dissolved in water
Kanamycin	10 mg/ml dissolved in water

Streptomycin	20 mg/ml dissolved in water
Neomycin	10-20 mg/ml dissolved in water

### 2.1.9 Computational work

Origin 7.0	Northampton, USA
Spectacle 1.8 (Lab Control)	Moenchengladbach, Germany
Microsoft Word 2003	Germany
Microsoft Excel 2003	Germany
Adobe Photoshop	Schaumburg, USA
Accelrys Gene 2.0	Cambridge, UK
WebLab Viewer Pro 3.7	Geneva, Swiss
Deep View /PDB View (version v 3.7)	Geneva, Switzerland
Swiss- Pdb Viewer 3.7	Geneva, Switzerland
WHAT IF 6.0	Heidelberg, Germany
	Nijmegen, Netherlands

## 2.2 Methods

### 2.2.1 Molecular biology and protein biochemical work

#### 2.2.1.1 Growth conditions of *E. coli* DH5 $\alpha$ cells for plasmid growth

LB-medium: 10 g/l bacterial peptone, 5 g/l yeast extract, 10 g/l NaCl, pH 7.2

LB-agar: 15 g/l agar for solid medium

Ampicillin 10 mg/ml dissolved in water

In a falcon tube, 10 ml of LB medium with ampicillin, are inoculated with a single colony of *E. coli* DH5 $\alpha$  harbouring the plasmid of interest. The culture was incubated overnight on a platform shaker at 37°C and 210 rpm. From this culture, the cells were harvested by centrifugation (18000 x *g*, 5 min) and the plasmid DNA was purified as described below. That was made for all the plasmids except for pRKCBC (see section 2.2.1.3).

### 2.2.1.2 Small-scale plasmid isolation from *E. coli* (miniprep)

Plasmids (in Topo), were isolated from the correspondent bacterial cells using QIAprep Spin Miniprep Kit (Qiagen, Hilden, Germany) according to the manufacturer's protocol. DNA was eluted from the columns by addition of 50 µl elution buffer, with subsequent centrifugation (14000 x *g*, 2 min, RT).

### 2.2.1.3 Large-scale plasmid isolation from *E.coli* by CsCl density centrifugation

LB-medium: 10 g/l bacterial peptone, 5 g/l yeast extract, 10 g/l NaCl, pH 7.2

LB-agar: 15 g/l agar for solid medium

Tetracycline 10 mg/ml dissolved in water or ethanol

TE buffer: 10 mM Tris-HCl, pH 8.0, 1 mM EDTA

Solution I: 10 g/l glucose, 3 g/l TRIS, 4 g/l EDTA

Solution II: 0.2 M NaOH, 1% SDS

Solution III: 0.4 M NaOH 2% SDS

The plasmid pRKCB was prepared from 400 ml cultures of transformed *E.coli* DH5α in LB medium essentially as described by (Sambrook et al 1989) and was separated from RNA and genomic DNA by centrifugation through a CsCl gradient in a Beckman 70.1 Ti rotor at 360000 x *g* for 24 h at 18°C. Intact plasmid DNA was removed from the centrifuge tubes using wide gauge needles and the ethidium bromide extracted with caesium chloride-saturated isopropanol. Each sample was then dialysed against TE buffer for 24 h with a minimum of four changes of buffer to remove the CsCl. One colony was inoculated into 10 ml LB, tetracycline incubated at 37°C with shaking 180 rpm for 8 h.

The 400 ml LB was pre-warmed in a 2 l flask at 37°C for ~30 min, the tetracycline is added and the medium was inoculated with the 10 ml starting culture. The cultures were incubated overnight at 37° with continuing shaking (180 rpm).

The cells were centrifuged at 4500 x *g* for 10 min at 4°C in a Beckman JA10/JLA 10.500 or equivalent. The pellet was suspended in 10 ml of Solution I and chilled on ice for 5 min. Solution II was added and mixed by gentle swirling for 1-2 min. Then, 15 ml of the Solution III was added and mixed by gentle swirling and incubation on ice for 15 min. The samples were centrifuged at 7200 x *g* for 35 min at 4°C in a Beckman JA14.

The supernatant was transferred to a fresh JA14 bottle, and the 6-fold volume of isopropanol was added. The mixture was stored at RT for 15 min and centrifuged for 45 min at  $7200 \times g$  at  $18^{\circ}\text{C}$  with slow deceleration. The supernatant was decanted carefully and the pellet was washed with  $\sim 50$  ml of 70% ethanol. Subsequently, the ethanol was removed and the pellet was dried by vacuum.

The pellet was resuspended in 8 ml of TE buffer and 8 g CsCl. When it had fully dissolved, 400  $\mu\text{l}$  of 10 mg/ml ethidium bromide solution were added, and the mixture was loaded in Beckman QuickSeal tubes for the TY 65/Ti 70.1. The tubes were filled completely with 1 g/ml CsCl in TE solution, balanced, and sealed. Afterwards, the tubes were centrifuged at  $200000 \times g$  for  $\sim 16$  h at  $18^{\circ}\text{C}$ ; the lower band was collected with a syringe. The DNA was washed and dialysed for 24-48 h.

#### **2.2.1.4 Restriction analysis of plasmid DNA**

Plasmid DNA was digested with restriction endonuclease(s) by mixing 1-10 ng template preparation, 10 units of each restriction endonuclease in a total volume of 10  $\mu\text{l}$  of 10x ideal buffer. After incubation at  $37^{\circ}\text{C}$  for 2 h the DNA has been analyzed on agarose gel as described below. If the conditions for two enzymes are incompatible with each other, the DNA was digested successively with the respective enzymes.

#### **2.2.1.5 Preparation and analysis of DNA by agarose gel electrophoresis**

TAE Buffer: 4.84 g/l Tris base, 1.142 ml/l Glacial acetic acid, 2 ml/l 0.5 M EDTA.

Agarose gel electrophoresis of DNA was performed in submarine gel tanks of appropriate size. All agarose gels used throughout this work were run in 1x TAE buffer and were prepared by dissolving from 1 to 2 % agarose and ethidium bromide in a concentration of 0.5  $\mu\text{g}/1\text{ml}$  in 1x TAE buffer. Samples containing an appropriate amount of DNA were mixed with 10x loading buffer prior to sample application. The gels were run at 60-70 V until optimal separation is achieved. The DNA was visualized via fluorescence excitation by illumination with UV light (302 nm). The marker GeneRuler™ 100 bp DNA ladder was used in 2% agarose and DNA/EcoRI+HindIII marker was used in 1% agarose.

#### **2.2.1.6 Isolation of DNA fragments from agarose gels**

After separation by agarose gel electrophoresis, DNA fragments used for cloning were cut from the gel and extracted by using the QIAquick® Gel Extraction Kit™ (Qiagen, Germany) according to the supplier's protocol.

### 2.2.1.7 Preparation of vector DNA for ligation

After the restriction described in section 2.1.4, the 5'-phosphate group was removed from the linearized DNA molecule by alkaline phosphatase treatment as follows: 5 units shrimp alkaline phosphatase were added for each  $\mu\text{g}$  of vector DNA solution. Incubation was for 30 min at 37°C followed by purification of the vector DNA from the reaction mixture as described (2.2.1.6) and stored at -20°C until further use.

### 2.2.1.8 Ligation of DNA fragments

The ratio between linearised vector and insert DNA in a reaction was ideally 3:1, roughly estimated by agarose gel electrophoresis. For standard, 50 ng of the vector DNA and 20ng of the insert DNA and were incubated with 1  $\mu\text{l}$  of T4 DNA ligase and of 5x ligation buffer and the reaction mix was brought to a final volume of 20  $\mu\text{l}$  and incubated 2 to 4 h in a water bath at 16°C or overnight at 4°C. The assay was used directly for transformation of *E. coli* cells without any further purification.

### 2.2.1.9 Polymerase chain reaction for cloning

Amplification of DNA fragments was performed in a 25  $\mu\text{l}$  reaction mixture with thin walled PCR tubes by ready-to-go PCR Beads from Amersham Pharmacia Biotech. The PCR Bead contains the dNTP mixture, PCR puffer and the *Taq* polymerase. The following reaction mixture is used:

template: 2-10 ng

primer 1 (15 pM): 1.5  $\mu\text{l}$  (final concentration 0.2 – 1 pM)

primer 2 (15 pM): 1.5  $\mu\text{l}$  (final concentration 0.2 – 1 pM)

H<sub>2</sub>O add to 25  $\mu\text{l}$ .

The PCR was performed with the following steps, if not otherwise stated:

- 1) initial denaturation at 94°C for 3 min,
- 2) denaturing at 94°C for 30 sec,
- 3) annealing usually at 50-65°C for 30 sec,
- 4) elongation at 72°C for approx. 1 min/1kb DNA,
- 5) termination at 72°C for 10 min,
- 6) cooling to 4°C.

The amplification procedure (steps 2-4) was repeated 30 times. The melting temperature of the primers depends on their GC content and was calculated by the following formula.

$$T_m = 81.5 + 0.41(\% \text{ GC}) - 675/N \text{ (N=number of bp)}$$

### 2.2.1.10 Site directed mutagenesis

Mutagenesis of DNA was performed in a 50  $\mu\text{l}$  reaction mixture with thin walled PCR tubes containing dNTP mixture, PCR buffer, and the *Pfu* turbo DNA polymerase from QuickChange XL site-directed mutagenesis kit (Stratagene, La Jolla, CA, USA). The following mixture was used:

template: 2 - 10 ng

5 $\mu\text{l}$  Promega buffer

primer 1 (1.5 pM): 1.25  $\mu\text{l}$  (final concentration 0.02–0.1 pM)

primer 2 (1.5 pM): 1.25  $\mu\text{l}$  (final concentration 0.02–0.1 pM)

1 $\mu\text{l}$  dNTP mix

3  $\mu\text{l}$  Quicksolution

H<sub>2</sub>O add to 50  $\mu\text{l}$ , then

1 $\mu\text{l}$  Pfu turbo polymerase was added.

The PCR was performed as follows, if not otherwise stated:

- 1) initial denaturation at 95 °C for 1 min,
- 2) denaturing at 95 °C for 50 sec,
- 3) annealing usually at 60 °C for 50 sec,
- 4) elongation at 68 °C for approx 1-2 min/1kb DNA,
- 5) termination at 68 °C for 7 min,
- 6) cooling to 4°C.

The amplification procedure (steps 2 to 4) was repeated 17 times. The melting temperature of the primers depends on their GC content and was calculated by the following formula.

$$T_m = 81.5 + 0.41(\% \text{ GC}) - 675/N - \% \text{ mismatch.}$$

### 2.2.1.11 Treatments of PCR-derived DNA

- DNA fragments for ligation

DNA amplified by PCR (see section 2.2.1.9) was purified with the QIAquick® PCR purification Kit (Qiagen, Hilden).

- DNA fragments for sequencing

The DNA after PCR is treated with ExoSap at 37°C for 15 min and 80°C for 15 min according to the provided protocol.

### 2.2.1.12 Determination of content of DNA

DNA concentrations were determined spectroscopically using an Amersham-Pharmacia (Ultraspec 3000) spectrometer. The absolute volume necessary for measurement was 100 µl. Concentrations were determined by measuring the absorbance at 260 and 280 nm. For pure double stranded DNA the absorption ratio A<sub>260</sub>/A<sub>280</sub> is approx. 2. Concentrations were calculated as follows.

Double stranded DNA [ $\mu\text{g ml}^{-1}$ ] = 50 x A<sub>260</sub> x dilution factor

### 2.2.1.13 Transformation of *E. coli*

LB-medium: 10 g/l bacterial peptone, 5 g/l yeast extract, 10 g/l NaCl, pH 7.2

LB-agar: 15 g/l agar for solid medium

SOC medium: 20 g/l Trypton, 5 g/l Yeast, 2 ml/l 5M NaCl

Tetracycline 10 mg/ml dissolved in water or ethanol

To 100 µl of competent *E. coli* DH5α cells, 2-3 µl of ligation mixture were added and incubated for 30 min on ice. After a heat shock (45 s, 42°C) and successive incubation on ice (3 min), 900 µl SOC-medium were added and the bacteria incubated at 37°C for 1 h on a rotary shaker. The cells were then centrifuged (10000 x g, 1 min, and 4 °C) and the supernatant removed. Cells were resuspended in 200 µl of LB medium and plated onto LB plates containing the appropriate antibiotics. Plates are incubated overnight at 37°C.

Transformation of DH5α chemically competent *E. coli* was done according to the manufacturer's protocol (Invitrogen).

### 2.2.1.14 Plasmid transfer by conjugation of *Rb. sphaeroides*

M22 Medium 2.6 g/l  $\text{KH}_2\text{PO}_4$ , 2.3 g/l  $\text{K}_2\text{HPO}_4 \cdot 3\text{H}_2\text{O}$ , 2.5 g/l Sodium Lactate, 0.5 g/l  $(\text{NH}_2)\text{SO}_4$ , 20 ml Solution C, 4.343 g/l Na Succinate, 0.27 g/l Na Glutamate, 0.04 g/l Aspartic Acid, pH adjusted to 7.6

Solution C (trace element): 10 g/l Nitriloacetic acid, 24 g/l  $\text{MgCl}_2$ , 3.35 g/l  $\text{CaCl}_2$ , 125 mg/l EDTA, 250 mg/l  $\text{ZnCl}_2$ , 250 mg/l  $\text{FeCl}_2$ , 90 mg/l  $\text{MnCl}_2$ , 9.25 mg/l  $(\text{NH}_4)_6\text{MoO}_7\text{O}_{24} \cdot 4\text{H}_2\text{O}$ , 7.75 mg/l  $\text{CuCl}_2$ , 12.5 mg/l  $\text{Co}(\text{NO}_3)_2$ , 5.75 mg/l Boric Acid

Vitamins 1 mg/l Nicotin acid, 0.5 mg/l Thiamine, 1 mg/l para-pAminobenzoic acid, 0.01 mg/ Biotin.

Neomycin 10-20  $\mu\text{g}/\text{ml}$  dissolved in water

Tetracycline 10  $\mu\text{g}/\text{ml}$  dissolved in water

The strains DD13 or DG2 were grown overnight, with 180 rpm shaking and at 34°C in 10 ml M22 medium in 100 ml flask with trace element, 0.1% casamino acid, 10  $\mu\text{l}/\text{ml}$  vitamin neomycin.

The mutant-plasmid was transformed in S17 *E. coli* on tetracycline agar plate overnight at 37°C.

The 10 ml starter cultures DD13 or DG2 were inoculated in 100 ml M22 medium in a 500 ml flask and were grown for 1 or 2 days. A single colony from S17 *E. coli* was transferred to a new plate.

The strains DD13 or DG2 culture was centrifuged at 6000 x *g* at 4°C for 5 min. The supernatant was discarded carefully. The pellet was resuspended in 10 ml of M22 medium. The *E. coli* from the agar plates were resuspended in 100  $\mu\text{l}$  of LB medium. The two cultures were mixed at ratio of 1:10 S17:DD13, plated on LB plates and kept in the dark at 34°C overnight.

Screening for expression of the mutant genes was conducted directly on the colonies using a Guided Wave reflexion probe, model SD2000 spectrophotometer equipped with a reflexion probe (Avantes, Ostfildern, Germany).

### 2.2.1.15 Cultivation of *Rb. sphaeroides*

LB Medium: 10 g/l bacterial peptone, 5 g/l yeast extract, 10 g/l NaCl, pH 7.2

M22 Medium see app 1.2.1.15

Vitamins	1 mg/l Nicotin acid, 0.5 mg/l Thiamine, 1 mg/l para-pAminobenzol acid, 0.01 mg/ Biotin
Neomycin	10-20 $\mu$ g/ml dissolved in water
Streptomycin	5 $\mu$ g/ml dissolved in water
Tetracycline	10 $\mu$ g/ml dissolved in water
TE buffer	10 mM Tris-HCl, pH 8.0, 1 mM EDTA.

*E. coli* strains were grown in LB with tetracycline used at a concentration of 10  $\mu$ g/ml.

A colony (figure 2.1A) was grown up in 10 ml of M22 medium containing 0.1% casamino acid, 10 $\mu$ l/ml vitamins, tetracycline, neomycin, and streptomycin at 28 to 34°C in the dark at 180 rpm in a shaker incubator. Cultives were grown in successively larger volumes, first 80 ml and then 1.5 l maintaining the growth conditions already outlined (figure 2.1B).

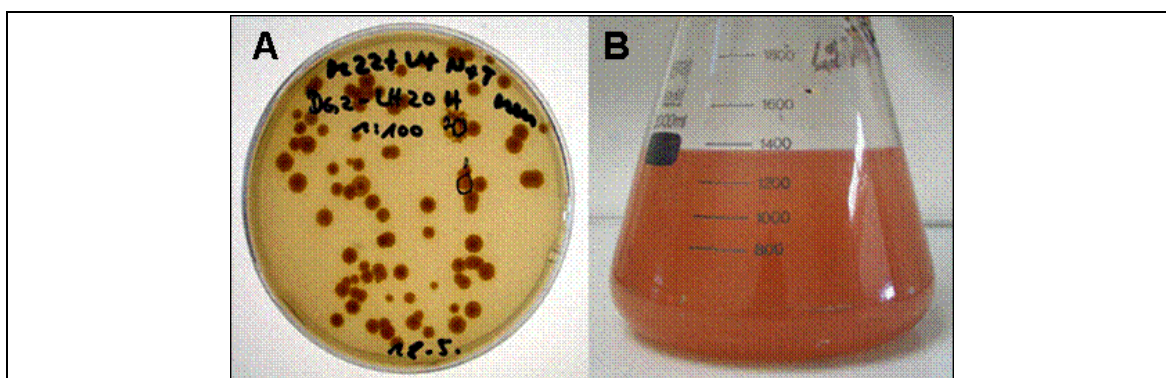


**Figure 2.1: Growth of *Rb. sphaeroides* DD13. (A): on growth plates and (B) in liquid cultures.**

The 1.5 l culture was harvested by centrifugation (20 min at 4500 x *g* in a Beckman JA-10 rotor at 4°C), and the cell pellet was resuspended in 20 ml of TE buffer. The concentrated cell suspension was frozen at -80°C.

### 2.2.1.16 Preparation of intracytoplasmatic membranes

- Membranes of LH2 from *Rb. sphaeroides* strain DD13 or DG2

TE buffer 10 mM Tris-HCl, pH 8.0, 1 mM EDTA.

Membranes were prepared from cells grown semi aerobically in the dark and these cell were broken by French press at 15000 psi for 3x. Previously, the cells were prepared with 1ml of lysozyme (10 mg/ml) and incubated in the dark for 30 min on ices. The cells were broken with a homogeniser after the addition of DNase I. The membranes were

purified by applying the solution on a sucrose step gradient (15%/40%, w/w) (figure 2.2) and centrifuged for 16 h at 175000 x *g*.



**Figure 2.2: Purification of *Rb. sphaeroides* membranes by sucrose gradient centrifugation**

The membranes were harvested from the interface and centrifuged (3 h at 280000 x *g*) to obtain a pellet. This pellet was solubilized with TE buffer.

- Membranes of LH2 from *Rb. sphaeroides* R26.1

Tris buffer: 20 mM Tris-HCl, pH 8.0.

The harvested cells of R26.1 were washed several times with 100 mM Tris-HCl (pH 8.0) and stored in a deep freezer as pellet. The chromatophores were obtained using a French Press at 15000 psi of the cells which were suspended in the above Tris buffer to which DNase had been added. The suspension was centrifuged twice at 25000 x *g* to remove debris. Then, the supernatant was centrifuged at 225000 x *g* for 90 min to pellet the chromatophores. They were washed several times and resuspended in Tris buffer, and stored at 4 °C.

### 2.2.1.17 Isolation of the LH2 complex

- Complex of LH2 from *Rb. sphaeroides* strain DD13 or DG2

Buffer I      10mM Hepes, 50mM NaCl, 1.5% Octyl  $\beta$ -D-glucopyranoside (O $\beta$ G)

Buffer II     10mM Hepes, 50mM NaCl, 0.65% O $\beta$ G

Buffer III    10 mM Hepes, 300 mM NaCl, 0.65% O $\beta$ G

Buffer IV     10mM Hepes, 0.65% O $\beta$ G

pH 7.5.

The LH2 complex was isolated from the membranes. To that end the purified membranes were incubated at an  $OD_{850} \sim 20$  in buffer I with 1.5% O $\beta$ G in the dark on ice for 20 min and subsequently centrifuged for 25 min at 2500000 x *g*. The supernatant was loaded on a DEAE-Sepharose ion exchange column which was activated with Buffer III and equilibrated with Buffer IV.

Column eluates were analysed for LH2 spectroscopically, pooled, and loaded on a gel filtration column, Superdex 200, equilibrated and eluted with Buffer IV.

○ Complex of LH2 from *Rb. sphaeroides* R26.1

The preparation of LH1 and LH2 complexes was based on a two-step solubilisation procedure using (1) lithium dodecyl sulfate (LDS) and (2) O $\beta$ G; each solubilisation was followed by fractionation by stepwise sucrose gradient centrifugation.

(i) The R26.1 chromatophores ( $OD_{860} \sim 25$ ) were solubilised with 1% LDS at RT for 1 min. (ii) The suspension was immediately diluted with 1 volumes of Tris buffer, and centrifuged at 45000 x *g* for 10 min. (iii) The supernatant was applied onto a stepwise sucrose gradient (0.75, 1.0, 1.5, and 2.0 M sucrose in Tris buffer containing 0.8% O $\beta$ G); and centrifuged at 225000 x *g* for 14 h. (iv) The LH2 was collected, dialyzed against Tris buffer with 0.8% O $\beta$ G.

### 2.2.1.18 Protein analysis by gel electrophoresis

Stacking gel:	5% acrylamide Solution, 1,5 M Tris-HCl, pH 6.8, 10% SDS (Sodium Dodecyl Sulfate) solution, 10% APS, TEMED, Deionized Water.
Separating gel	19% acrylamide Solution, 1 M Tris-HCl, pH 6.8, 10% SDS solution, 0.1% APS, TEMED, Deionized Water.
Tris/Tricine/SDS:	1.210 g/l Tris Base, 17.90 g/l Tricine, 10 ml/l 10% SDS solution
Tris/Glycine/SDS:	3.0 g/l Tris Base, 14.4 g/l Tricine, 10 ml/l 10% SDS solution
SDS gel-loading:	50 mM Tris-HCl (pH 6.8), 2% SDS, 0.1% Bromophenol blue, 10% glycerol, 100 mM dithiothreitol.

Complex protein mixtures or protein preparations were separated and analyzed by standard SDS-PAGE (Laemmli 1970). All minigels (Biorad) contained 19% acrylamide solution (ProSieve-50 Solution) in the separating gel and 5% in the stacking gel. Protein samples to be analyzed were denatured by adding 2x SDS sample buffer and incubated at 80°C for 5 min.

The gels were run by minigel electrophoresis (Biorad) at 130 to 180 V until the tracking dye reached the bottom of the gel. The molecular weight markers used was a Kaleidoscope Prestained Standards, low (4, 8.3, 16.5, 28.1, 36.7 kDa Biorad). Proteins were visualized by staining with Coomassie brilliant blue solution (0.025% Brilliant Blue R250 (Sigma), 25% ethanol, 8% acetic acid) and subsequent destaining (30% methanol, 10% acetic acid).

### 2.2.1.19 Pigment quantification by HPLC

The pigments of LH2, Car and BChl were extracted with a mixture of acetone/methanol 7:2 (v/v) and the extracts were evaporated to dryness under argon in the dark. For analyses, dried extract were resuspended in 20  $\mu$ l acetone and were applied to a 600E multisolvent/delivery system from Waters (Milford, USA) in a column Grom-Sil 120 ODS 5ST 5 mm, length 250 mm and ID 4 mm, Grom, Rottenburg-Hailfinger (Germany). The pigments were eluted with an acetone/water (95:5) solution at a flow rate of 1 ml/min. The spectra were analysed with spectacle program (Version 1.55) from LabControl. To maintain O<sub>2</sub> free conditions, the solvents were washed with helium during HPLC runs. The measurements were made at room temperature.

The extinction coefficients at 456 nm were taken to be  $E_{1\text{cm}}^{1\%} = 2,700$  for SE and  $E_{1\text{cm}}^{1\%} = 2,120$  for SO (Shneour 1962), both in acetone-methanol, 7:2 and for NE  $E_{1\text{cm}}^{1\%} = 2,918$  in hexane (416, 440, 470 nm) (Britton & Young 1993).

### 2.2.1.20 Protein determination

Total protein content in membranes was determined by using the BCATm kit (Pierce, Rockford, USA). Sample concentration ranges, used for protein determination were chosen such that the contribution at 562 was negligible (sample absorption  $OD_{562} < 0.01$ ).

For the estimation of LH2 protein content, the extinction coefficient of B850 BChl was taken as 120 [ $\text{mM}^{-1}\text{cm}^{-1}$ ] (Clayton & Clayton 1981b).

## 2.2.2 Statistical analyses in PS I and PS II

Car-peptide or BChl-peptide contacts at a radius  $\leq 5$  Å in PS I and PS II were determined by use of the program WebLab viewer 3.7. For each Car atom, the number of contacts to

polypeptide has been determined at radius  $\leq 5 \text{ \AA}$  in the structure of PS I and PS II both from *Synechococcus elongatus* and *Thermosynechococcus elongatus* respectively.

In addition, the determination of Car-protein or BChl-protein contacts was performed by a home-made Visual Basic® extension program for Microsoft®-Office Excel 2003, (Alexander Pazur), consisting of several functional modules. The PDB formatted files of PS I and PS II high resolution structures were used as sources for molecular data on atomic level, which were copied into an internal, multi-dimensional numerical array. This allowed a fast, random access to any atomic position without the slower process of addressing single cells on the spreadsheet. A user interface generated on an excel sheet enabled among others to enter the name of the residue, the acronyms of the first and last element of the searched molecule section, as well the interesting range of contact distances, here adjusted to  $d_{(\min, \max)} = 0.5\text{-}4 \text{ nm}$ . The calculation was performed by three obligate steps: The PDB data file was opened, analysed for compatibility and written into the array. Then distance  $r(n,m)$  from atom  $m$  of the search frame with the spatial coordinate  $p_{xyz}(m)$  to atom  $n$  of the array with the coordinate  $p_{xyz}(n)$  was calculated by

$$r(n,m) = \sqrt{(p_x(n) - p_x(m))^2 + (p_y(n) - p_y(m))^2 + (p_z(n) - p_z(m))^2} \quad (1)$$

And subsequently the contact criterion tested by

$$\langle d_{\min} \leq r(n,m) \leq d_{\max} \rangle c(m,a) \oplus 1 \quad (\text{With } a \in \mathbf{A}). \quad (2)$$

For a true condition the counter  $c(m, a)$  for the consecutively numbered functional atom specification  $a$  out the atom set  $\mathbf{A}$  was incremented by one.

## 2.2.3 Biophysical analyses

### 2.2.3.1 “In situ” absorbance spectroscopy

The investigation of whole cells in bacterial colonies (figure 2.1A) and polyacrylamide-embedded LH2 samples was performed on with Dual Fibre model SD2000 spectrophotometer equipped with a reflexion probe (Avantes, Ostfildern, Germany).

### 2.2.3.2 Absorbance spectroscopy

Absorption spectra are recorded on a Lambda 25 spectrophotometer (PerkinElmer Life Sciences) or Shimadzu UV-2401PC, in 1cm or 1mm quartz cuvettes. The spectra were taken in a range of 300-900 nm.

### 2.2.3.3 Fluorescence spectroscopy

Fluorescence is measured by FluoroMax spectrofluorometer (SPEX, NJ, USA). The excitation spectra were recorded in a range of 350-810 nm. For fluorescence excitation spectra, two filters, 370 and 420 nm, are used. The fluorescence emission is detected at 850 nm.

### 2.2.3.4 Circular dichroism spectroscopy

Circular dichroism spectra are recorded by a Dichrograph CD6 (Jobin Yvon, Paris, France) in a 1 cm cylindrical cuvette or by a Jasco J-810 spectripolarimeter. Purified membranes were adjusted to an  $A_{850} = 3 \text{ cm}^{-1}$  in TE buffer and the isolated complex were adjusted to an  $A_{850} = 1-3 \text{ cm}^{-1}$  in Hepes buffer with O $\beta$ G. In order to not denature the sample during the measurement the scans were obtained at 4°C and three of them were averaged.

Thermal denaturation of purified membranes and isolated complex were carried out in a 1 mm cylindrical quartz cuvette. The samples were heated from 4 or 15 to 95 °C at a constant rate of 1 °C min<sup>-1</sup>, and the CD signal at 845 nm was recorded every 0.05 °C (integration time, 0.2 s). Variations in sample turbidity were corrected by used of milk solution as standard but did not significantly affect the NIR-CD spectrum.

### 2.2.3.5 Resonance Raman (RR) spectroscopy

The Raman spectra were recorded in the laboratory of Bruno Robert, Gif-sur-Yvette, France.

FT resonance Raman spectra were recorded using a Bruker IFS 66 interferometer coupled to a Bruker FRA 106 Raman module equipped with a continuous coherent Argon laser (Innova 100). Excitation at 1064 nm was provided by a continuous Nd: Yag laser. The set-up, laser powers and sample behaviour are extensively described previously (Mattioli et al 1993).

The typical resolution of FT resonance Raman spectra was 4 cm<sup>-1</sup>. All spectra were recorded at room temperature with 180° backscattering geometry from pellets or concentrated solutions held in standard aluminium cups. Depending on the sample, spectra are the result of 5000-20000 co-added interferograms.

To calculate the ratio of BChl to Car is used FT Raman spectroscopy is used employing the 1064 nm fundamental from a Nd-YAG laser and the scattered light, is analysed using

an interferometer which, in part, compensates for the low Raman scattering efficiency at wavelengths in the NIR. By exciting at 1064 nm, in many cases one may circumvent the problem of spurious fluorescence because this excitation is usually at energies lower than the radiative states of most molecules (Mattioli et al. 1993).

## CHAPTER 3

# Identification of critical assembly factors at the Bacteriochlorophyll-protein interface in LH2

### 3.1 Introduction

The folding of helical TM proteins has been proposed to occur in two energetically distinct stages. In first stage the helices are formed and inserted into the membrane and, in the second stage, these preformed helices interact with each other and assemble to the final 3D structure .

TM helices are generally characterised by long stretches of hydrophobic residues flanked in many cases by aromatic and proline residues (von Heijne 1994). The driving force for membrane insertion derives primarily from the transfer of hydrophobic side chains from water to the apolar region of the lipid bilayer. Few polar residues and rarely charged residues are present in the TM helices (Landolt-Marticorena et al. 1993, Sipos & von Heijne 1993, von Heijne 1994). As a result of the tendency for the buried residues to be more polar than the lipid-exposed ones, many TM helices are slightly amphiphilic.

The packing of the helices with each other are often the basis for the stable assembly of membrane proteins (von Heijne 1994, Popot & Engelman 2000, Engelman et al. 2003). The  $\alpha$ -helix associations within the membrane are generally governed by electrostatic and van der Waals interactions. The packing of the helices in the membrane is apparently tighter than in soluble proteins . A critical factor for the packing of the helices is the packing value of individual amino acids residues. Serine and threonine, for example, have generally high packing values (it should be kept in mind that the packing values are not calculated separately for interfacial and noninterfacial residues and may differ significantly from case to case) supporting their close association with surrounding polypeptide residues. These residues have also another important role in the helix association. Small residues, in particular, the polar serine and threonine, stabilize the formation of helical oligomers by H-bonding interactions . Therefore serine and threonine are the most frequently occurring polar residues in the TM helices (Senes et al. 2000, Adamian & Liang 2002, Dawson et al. 2002). The highest packing values have the small residues (glycine and alanine), which also have an important role in helix-helix association (Russ &

Engelman 2000, Kleiger et al. 2002, Shlyk-Kerner et al. 2006),. The large and positively charged residues, lysine and arginine, however, have the lowest packing values, whereas the negatively charged residues, aspartate and glutamate, and the polar residues, asparagine and glutamine, have relatively high packing values . The aromatic amino acids have generally low packing values, while, histidine residues, have a high level of packing in comparison to other charged residues which is readily explained by their frequent role in cofactor ligation (normally, the amino acids which are ligated with a cofactor have a high level of packing, but that is not a general rule) . Other factors, such as ligand binding and folding of extramembranous loops , also contribute to the packing of TM helices .

In the case of the LH proteins, the interaction between the helices is of minor importance for their assembly. The TM helices make only limited contact with each other due to the abundance of the low-molecular weight cofactors, BChl and Car; which are attached non-covalently to the helices . In such cases interaction among the TM helices is largely replaced by pigment-protein and pigment-pigment interactions and the pigment is often the critical factor for the proper folding and assembly .

Multiple types of interactions exist between the (B)Chl and the surrounding polypeptide(s). The best understood interaction between the polypeptides and (B)Chl is the ligation of the central magnesium ion by a suitable amino acid residue, frequently a histidine . The multiple possibilities for these interactions between the (B)Chl and the surrounding polypeptide(s) are obvious from the complex structures of the (B)Chl with up to four peripheral carbonyl groups, several asymmetric centers, and long chain esterifying alcohol. The involvement of the carbonyl groups in intermolecular hydrogen bonds has been explored in detail for the acetyl and keto groups of BChl in photosynthetic complexes from purple photosynthetic bacteria. In the case of the C3 acetyl group, hydrogen bonding to neighbouring residues modulates the functional properties, specifically the excitation energies of the BChl *a* in LH complexes .

Hydrogen bonding to the C13<sup>1</sup> keto carbonyl, at the isocyclic ring which is common to all chlorophylls, seems to be widespread , but appears to have less or no effect on the electronic properties of (B)Chl . It has also been suggested that hydrogen bonding to the C13 keto group contributes to the tuning of the redox energies of P870 in bacterial RCs .

In the crystal structure of PS I , which comprises more than 10 TM helices and contains nearly 100 Chl-binding pockets, the majority of the polar groups of Chls, in particular the C13<sup>1</sup> keto group, are likely to be H-bonded by the polypeptide residues in close vicinity . It is not exactly understood, however, whether these H-bonds essentially contribute to the structural stability of the membrane-embedded (B)Chl proteins.

Four principal experimental approaches have hitherto been used to investigate the interplay between the proteins and the pigments in Chl and BChl-proteins. These are: firstly, exchange of the pigment with chemically modified pigment in natural pigment-protein complexes *in vitro* (Scheer & Hartwich 1995, Lapouge et al. 2000); secondly, chemical synthesis of the *novo* proteins or of truncated versions of natural proteins followed by reconstitution of the complex *in vitro* ; thirdly, mutagenesis and overexpression of the gene, followed by reconstitution of the pigments *in vitro* ; and fourthly, site directed or combinatorial mutagenesis combined with assembly of the complex *in vivo* .

Here, artificial, model TMHs are used to explore BChl-binding and assembly of LH systems in their native membrane environment . The model TMHs that consist of alternating alanine-leucine sequences and comprise the chromophore-binding site in the TM region have been fused at their N and C-terminal ends with native extrinsic sequences of the  $\alpha$ -subunit of LH2.

The focus of this work has been to identify and investigate the interactions at the pigment-protein interface which are essential for the functional and structural assembly of (B)Chl-protein complexes. To that end:

- a model LH protein is used in which the native contacts at the BChl-protein interface have been reduced and largely eliminated. In the model BChl-binding site the contribution of distinct amino acids to the functional assembly of the BChl-proteins can be readily assessed;
- the thus identified critical interactions are further examined by site-directed mutagenesis in WT sequence context;
- the experimentally identified interactions are modelled in model structures based on the existing high resolution structure of LH2 from *Rps. acidophila*.

## 3.2 Results and discussions

### 3.2.1 Model high resolution structure of *Rb. sphaeroides*

Hitherto, there are two structures of LH2, one from *Rps. acidophila* and one from *Rps. molischanum* , which have been solved at high resolution. Amino acids sequence identity between the LH subunits of *Rb. sphaeroides* and *Rps. acidophila* is 45,3% and between *Rb. sphaeroides* and *Rps. molischanum* is 37,7%. Therefore *Rps. acidophilla* was chosen for the modelling of the LH2  $\alpha$ -subunit from *Rb. sphaeroides*. In addition, recent studies in

which the projection map has been obtained of the tubular LH2 crystal from *Rb. sphaeroides* clearly show the nonameric organization of the ring as has been suggested by atomic force microscopy at 10 Å resolution. The LH2 in *Rps. acidophila* is also a nonamer and different from the octameric ring formed by LH2 from *Rps. molischianum*.

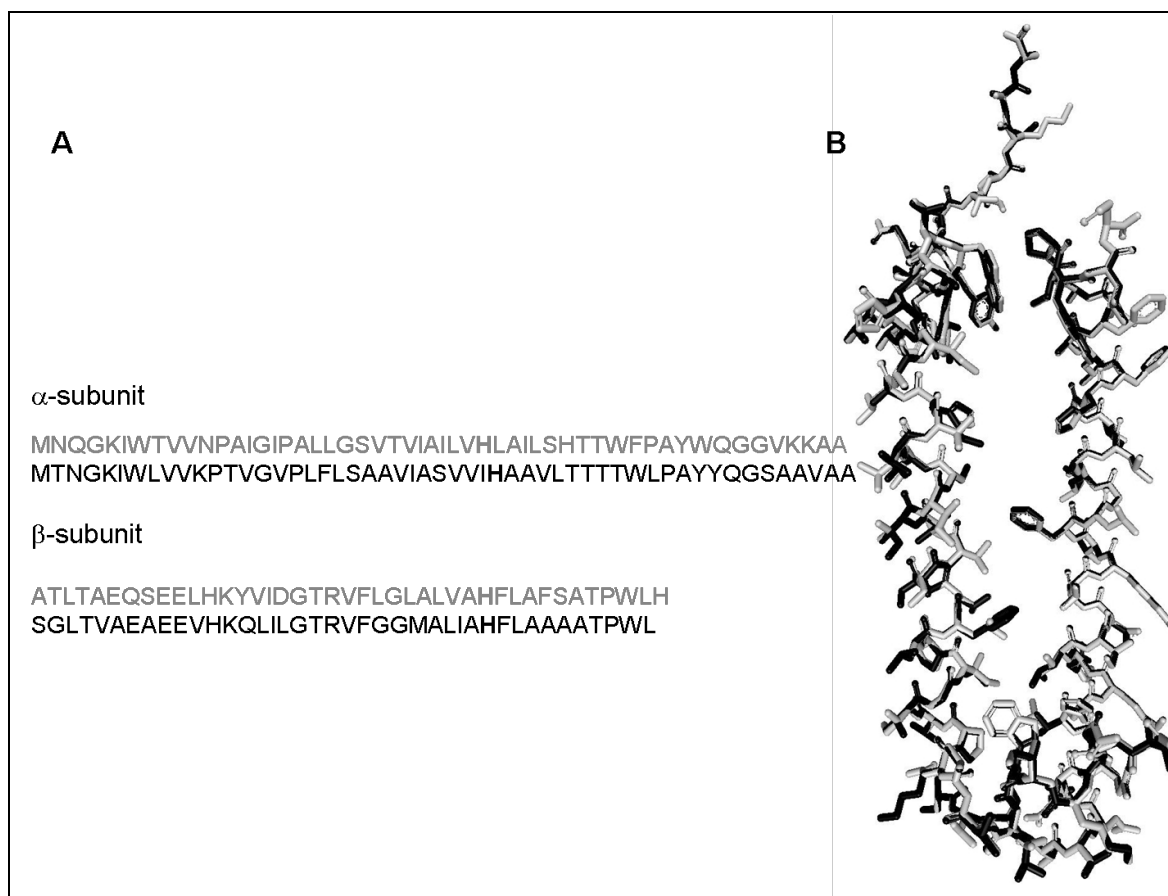


**Figure 3.1: Modelled LH2 protein structure.** Amino acid sequences of *Rps. acidophila* (grey) and *Rb. sphaeroides* (black) (A) and comparison of the  $\alpha\beta$  subunit structure of *Rps. acidophila* (light grey) and modelled structure of *Rb. sphaeroides* (black) (B).

In the model structure, every residue in the subunits of *Rps. acidophila* has been replaced by the residues of the subunits of *Rb. sphaeroides*. The backbone of the resulting model structure did not alter as compared to *Rps. acidophila*, while the side chain conformations obviously were modified in place where “mutations” took place (figure 3.1). Due to the lack sufficiently developed force field calculations for the (B)Chl (Linnanto et al. 2004, Palencar 2005), modelling of BChl is not easily available and the conformation and relative locations of the pigments are not changed during modelling. In the model structure the position of the mutant residues can be calculated and their contacts can be assessed. In general, the amino acids which are situated close to the pigments are not dramatically changed.

### 3.2.2 Model LH2 protein

To investigate BChl/protein interaction motifs a model BChl-protein has been designed which has a BChl binding site with an artificial “model” sequence. In this model protein, LH2  $\alpha$ AL<sub>16</sub>, a contiguous stretch of 14 residues from valine in position -7 to threonine in position +6 of the  $\alpha$ -subunit of LH2 have been replaced with a simplified alanine-leucine repeat sequence (figure 3.2). These residues include all the residues which interact with the BChl-B850 at a distance of  $\leq 3.5$  Å in the TM region. Neither the histidine in position 0 (the numbering specifies the amino acid position relative to the histidine, designated His 0, which binds the central magnesium of BChl-B850) nor the adjacent isoleucine in position -1 were replaced. The residues at positions -5, +1 and +2 happened to be alanine already, and the residue at position +4 is a leucine (figure 3.2) resulting in a total of 8 ‘new’ residues in LH2  $\alpha$ AL<sub>16</sub>. This mosaic  $\alpha$ -subunit was expressed together with the complement LH2 WT  $\beta$ -subunit in *Rb. sphaeroides* deletion strain DD13, which is devoid of endogenous BChl binding proteins (LH1<sup>-</sup>, LH2<sup>-</sup>, and RC<sup>-</sup>) but capable of BChl synthesis (figure 3.2). It should be noted here that a second set of LH2 genes have been recently identified in the genome of *Rb. sphaeroides* (Zeng et al 2003). Although these genes are expressed, these  $\alpha$ - and  $\beta$ -subunits cannot assemble into LH2 complex in the absence of the other set of LH2 subunits. It is clear that the  $\alpha$ -subunit of these second *puc* genes does not assemble with the *puc BA* to LH2. It is not known yet whether the  $\beta$ -subunits of the second gene participate in LH2 formation. In this chapter of my thesis, the  $\beta$ -subunits have not been altered (figure 3.2).

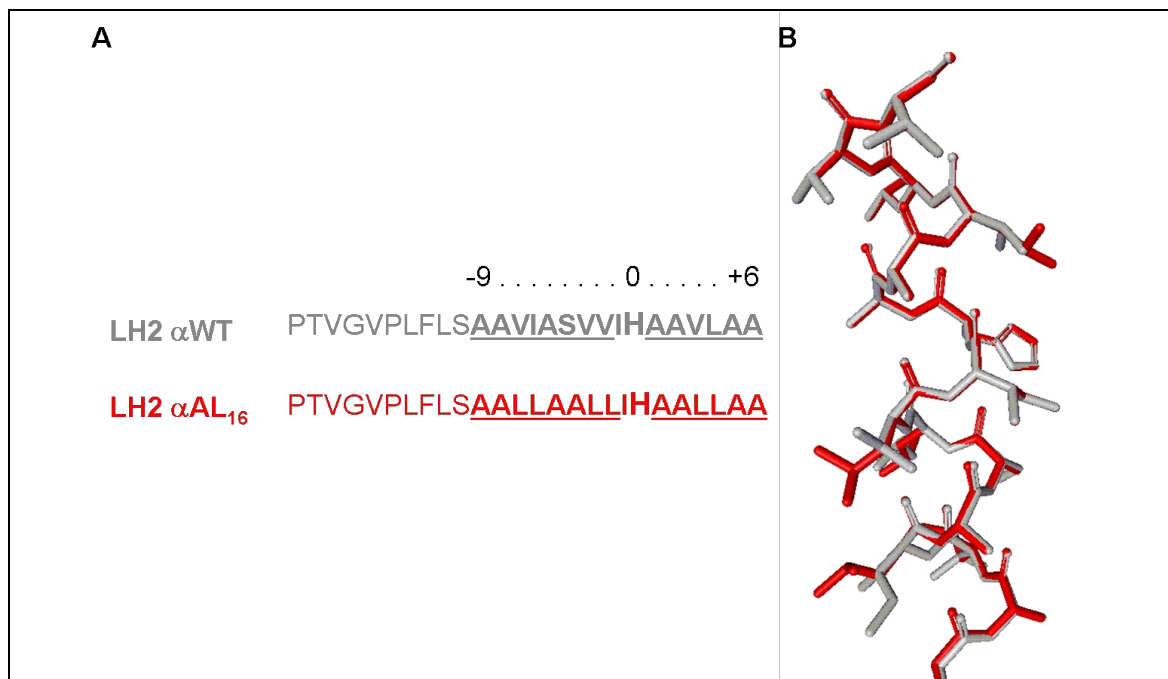


**Figure 3.2: Model LH protein: AA sequences of the LH2  $\alpha$ -TM helix from *Rb. sphaeroides* (grey) and model  $\alpha$ -TM helix LH2  $\alpha$ AL<sub>16</sub> (A).** The amino acid stretches, which are replaced by alanine-leucine are shown in bold and underlined. The His which ligates the central Mg is shown enlarged and defines the position 0. (B) Comparison of the modelled structures of *Rb. sphaeroides* LH2  $\alpha$ WT -subunit (black) (figure 3.1) and model subunit LH2  $\alpha$ AL<sub>16</sub> (red).

LH2 complexes have “typical” spectral properties due to the specific interactions of the BChl in this complex. Thus BChl can be used as endogenous probe for the folding and proper assembly of LH2 (see introduction). In figure 3.3A inset, the *in situ* absorption spectrum of LH2  $\alpha$ AL<sub>16</sub> is shown. The NIR absorption bands of BChl-B850 and BChl-B800 are closely similar to the bands of LH2 WT. The absorption band of BChl-B850 is slightly red shifted from  $\sim 848$  nm in LH2 WT to  $\sim 851$  nm in LH2  $\alpha$ AL<sub>16</sub>, which may point to certain, minor alterations in the BChl-B850 geometry. In addition, there is a shoulder at  $\sim 760$  nm in LH2  $\alpha$ AL<sub>16</sub> indicating elevated levels of free BChl (*i.e* BChl that is not (tightly) bound polypeptides and not assembled into pigment-protein complexes) mixed with metabolic precursors and/or degradation products of BChl. There are, however, no significant changes in the absorption spectrum of LH2  $\alpha$ AL<sub>16</sub> in comparison to LH2 WT. It should be emphasized that the absorption spectra maybe altered by mutation in the BChl-B850 binding sites .

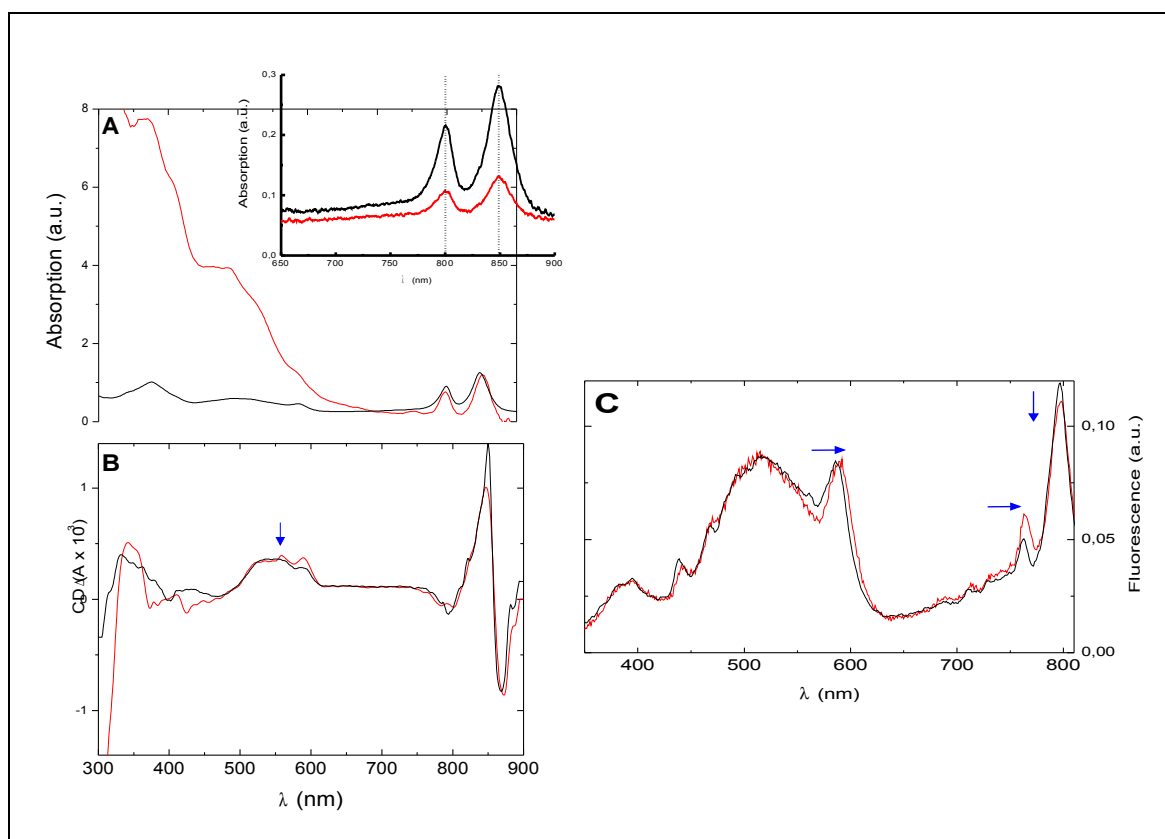


**Figure 3.3: Absorption (A), CD (B) and fluorescence (C) spectra of the model protein LH2  $\alpha$  AL<sub>16</sub>.** Shown are the spectra of LH2 WT (black) and LH2  $\alpha$ AL<sub>16</sub> (red). The *in situ* optical spectra (inset) are taken of *Rb sphaeroides* DD13 colonies. The absorption and CD spectra are normalised at the Q<sub>y</sub> BChl-B850 absorption maximum and CD extremum. The fluorescence spectra are normalised at the Q<sub>x</sub> band at ~ 590 nm. Spectra are taken from purified membranes. The arrows indicate spectral derivations from LH2 WT in LH2  $\alpha$ AL<sub>16</sub>.

The structural stability and assembly of LH2  $\alpha$ AL<sub>16</sub>, however, is clearly affected. Significantly less complex is stably assembled in the membrane in comparison to LH2 WT as obvious from the high level of scattering in the Soret region of the spectrum. That is also demonstrated by the quantification of total protein content *versus* LH2 content (as judged by the BChl-B850 absorption) in the membrane. The ratio of total protein/LH2 protein is estimated to be around 10:1 (w:w) for LH2 WT and 10:02 for LH2  $\alpha$ AL<sub>16</sub>, thus assembled LH2  $\alpha$ AL<sub>16</sub> is approximately five times less abundant in the membrane than LH2 WT.

In order to further examine the structural organisation of the pigments in the model LH2  $\alpha$  AL<sub>16</sub> in comparison to LH2 WT, the CD spectra are taken. As BChl-BChl couplings contribute mainly to the typical CD signal (Cogdell & Scheer 1985, van Grondelle 1985, Braun et al. 1990, Braun & Scherz 1991, Koolhaas et al. 1998) it is agreed that its exact shape serves as fingerprint for the BChl arrangement in the complex. No significant

alterations are observed in the CD spectrum of LH2  $\alpha$ AL<sub>16</sub> (figure 3.3B). The CD spectrum of LH2  $\alpha$ AL<sub>16</sub> shows a conservative, S-shaped CD signal in the NIR with peaks at 848 nm (+) and 872 nm (-), similar to LH2 WT. Moreover, in LH2  $\alpha$ AL<sub>16</sub> the optical activity of the BChl-B800 shows a negative trough near 800 nm. Apparently, the model LH2  $\alpha$ AL<sub>16</sub> support not only binding of BChl but also association into structures with a geometry like that of the BChl-B850 and BChl-B800 in LH2 WT.

The functional fitness of LH2  $\alpha$ AL<sub>16</sub> is examined by fluorescence excitation spectroscopy (figure 3.3C). As evident from the excitation bands, ET occurs from the Cars to BChl-B850 and from the BChl-B800 to BChl-850. There are some minor changes in the excitation spectra; the ET from the BChl-B800 to BChl-B500 is slightly reduced (by ~8 %) in comparison to LH2 WT. ET from Car to BChl has only been observed in pigment-protein complexes and never in BChl-Car mixtures.

It is remarkable that the major simplification of the BChl-B850 site has not produced significantly altered spectral properties (figure 3.3). This may indicate that residues in the immediate vicinity of BChl-B850 particularly in the TM binding site do not critically contribute to their geometrical arrangement and spectroscopic properties. It appears that few residues, in particular, the histidine which ligates the central Mg and the aromatic residues outside of the TM regions which contribute to H-bonding to the C3 acetyl group are sufficient to allow for the assembly of the complex. As reported by the group around Niederman, the combinatorial mutation of 3, 4, 5 and 6 residues in the  $\beta$ -subunit, however, caused spectral shifts of the BChl-B850 absorption. In the light of these findings it is remarkable that the simplified alanine-leucine sequence in the vicinity of BChl-B850 did not produce significantly altered spectral properties (figure 3.3).

In summary, the model BChl-B850 site apparently supports the assembly of the functional LH unit. Nevertheless, the distinct reduction in expression level and thermal stability (see below) suggest that interactions at the BChl-protein interface which are critical for the structural stability and thus stable assembly are absent. In the following, the model protein is used to identify such interactions and determine their contribution to the structural stability of this complex.

Sequence alignment studies of the TM region of the LH2 subunits show that there are only few amino acids that are highly conserved among different purple bacteria species. In figure 3.4 the individual alignment positions are coloured to reflect the evolutionary conservation of the residues at this position in  $\alpha$ -subunit. The residue positions with a high level of conservation are coloured blue and residue position with a low level of conservation are coloured red, increasing from yellow via green to blue. The red coloured

residues are considered to have undergone a high level of mutation. Such residue positions in the polypeptides are termed mutation hot spots. The multiple alignment of the LH2  $\alpha$ -subunit from ten different families of proteobacteria shows that the overall level of conservation of residues in the TM of  $\alpha$ -subunit is low. Only H(0) and P(-14) are very highly conserved and I(-1) and A(-4) are highly conserved (figure 3.4) . At position -4, there seems to be only alanine and serine residues (in *Rb. sphaeroides* and *Rb. sulphilus*) in the  $\alpha$ -subunit and exclusively alanine in the  $\beta$ -subunit of natural LH2 and mutant proteins . In addition, statistical analysis of the (B)Chl-binding pockets in plant photosystem have shown that the residues at positions -4, -1 and +4 have the highest contact frequencies with Chl molecules . Taken together, these observations point towards an important role of these residues in binding and assembly of (B)Chl-binding pockets. In my thesis, the impact of the residue at position -4 on the assembly of LH2 has been explored by permutating this residue in both LH2 WT and LH2  $\alpha$ AL<sub>16</sub>.

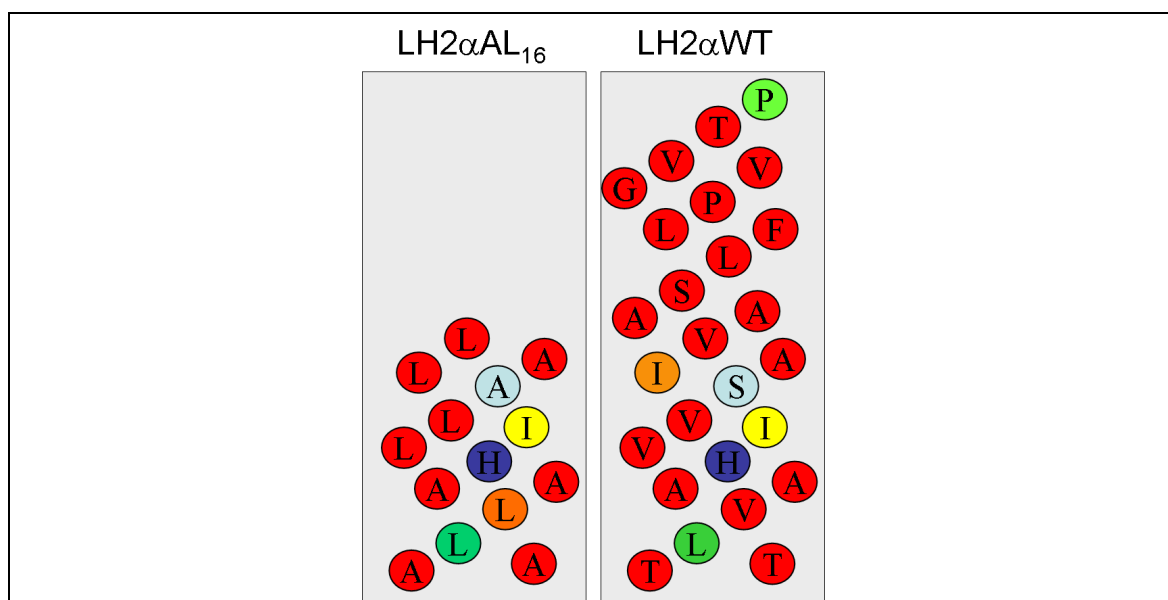


**Figure 3.4: Novel helix–BChl-B850 interface in the model TM helix.** Individual alignment positions are coloured to reflect the evolutionary conservation of residues at this position. Note, that only S(-4) from the highly conserved residues has been mutated.

### 3.2.3 Permutation of the LH2- $\alpha$ residue at position -4 at the BChl/protein interface in model LH2 complex

The LH2  $\alpha$ AL<sub>16/X-4</sub>, in which X is an amino acid, are identical to LH2  $\alpha$ AL<sub>16</sub>, except for the residue at position -4, which is alanine in LH2  $\alpha$ AL<sub>16</sub>. The *in situ* absorption spectra of LH2  $\alpha$ AL<sub>16</sub> and LH2  $\alpha$ AL<sub>16</sub> with 12 different amino acids at position -4 are shown in figure 3.5. Assembly of the model LH2  $\alpha$ AL<sub>16</sub> (as assessed by the “typical” absorption bands B800

and B850) is observed in detectable amounts only with serine, alanine, and threonine at position -4, whereas the others residues (cysteine, aspartate, glutamate, phenylalanine, glycine, histidine, lysine, asparagine, glutamine, and tyrosine) result in the loss of model LH2  $\alpha\text{AL}_{16}$  complex (figure 3.5). The assembly of the model LH2 is thus highly susceptible to the nature of the side chain at position -4, indicating that the residues at this position play a major structural role for the assembly of LH2. In turn, this demonstrates that critical interactions are readily identified in the model sequences due to the amplification of effects in the model sequence context and inherently instable system.

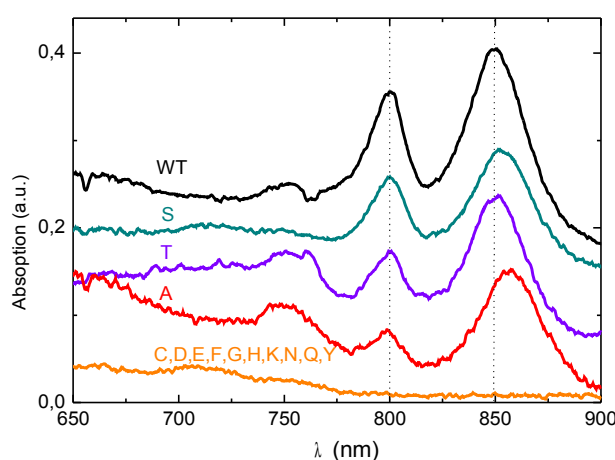


**Figure 3.5: *In situ* absorption spectra of model LH2  $\alpha\text{AL}_{16/X-4}$ .** “*In situ*” spectra are taken of *Rb. sphaeroides* colonies expressing LH2  $\alpha\text{AL}_{16/X-4}$ : LH2 WT (black), LH2  $\alpha\text{AL}_{16}$  (red), LH2  $\alpha\text{AL}_{16/S-4}$  (dark cyan), LH2  $\alpha\text{AL}_{16/T-4}$  (violet), LH2  $\alpha\text{AL}_{16/C-4}$ , LH2  $\alpha\text{AL}_{16/D-4}$ , LH2  $\alpha\text{AL}_{16/E-4}$ , LH2  $\alpha\text{AL}_{16/F-4}$ , LH2  $\alpha\text{AL}_{16/G-4}$ , LH2  $\alpha\text{AL}_{16/H-4}$ , LH2  $\alpha\text{AL}_{16/N-4}$ , LH2  $\alpha\text{AL}_{16/Q-4}$ , and LH2  $\alpha\text{AL}_{16/Y-4}$  (orange).

As obvious from figure 3.5 only three residues, alanine, threonine and serine, support the assembly of antenna complex, they are discussed in detail below.

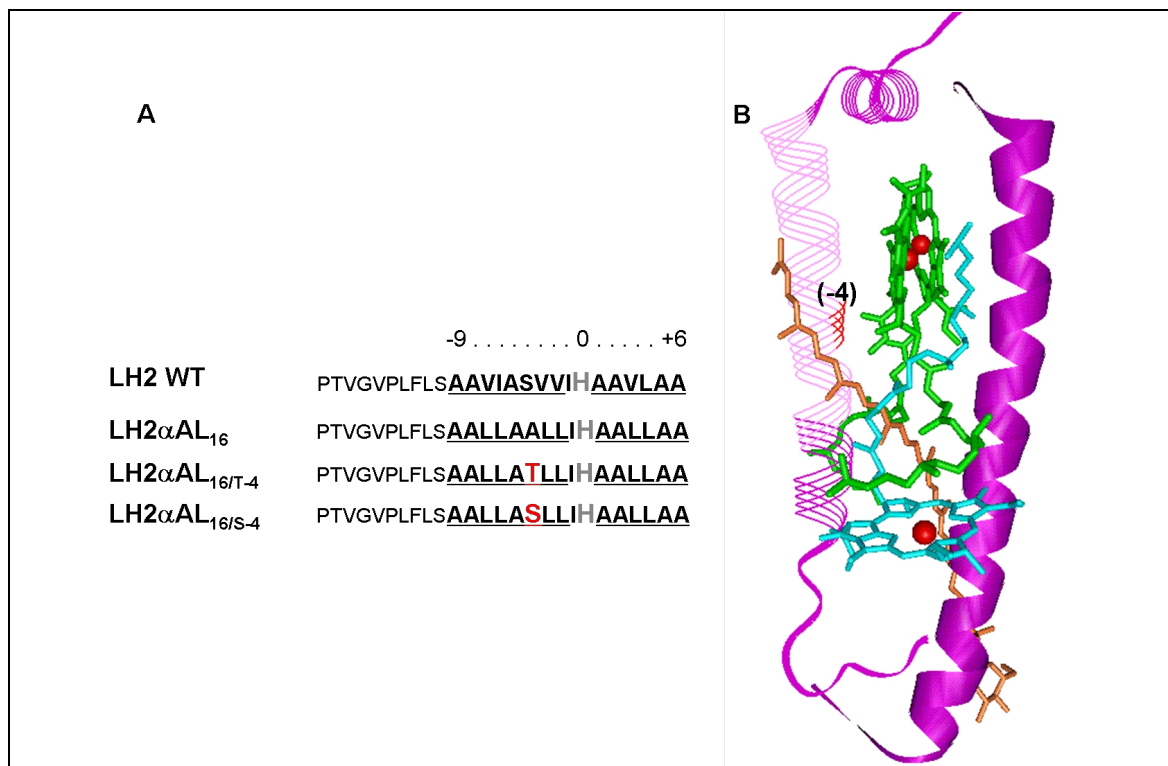


**Figure 3.6: Model LH2  $\alpha$ AL<sub>16/S-4</sub> and LH2  $\alpha$ AL<sub>16/T-4</sub>.** (A) AA sequence of model LH2  $\alpha$ AL<sub>16/S-4</sub> and LH2  $\alpha$ AL<sub>16/T-4</sub>. The residues which are replaced in the TM are underlined. The threonine and serine at position -4 are shown in red and underlined, and histidine (0) is shown in grey. (B) Schematic view of the model LH2  $\alpha$ AL<sub>16</sub> binding site, BChl-B850 (green), BChl-B800 (cyan) and Car (orange). The  $\alpha\beta$ -subunits are purple, the region of  $\alpha$ -TM protein, which is replaced by the alanine-leucine sequence is light purple and the position -4 is red.

Figure 3.7A exhibits the absorption spectra of LH2  $\alpha$ AL<sub>16/T-4</sub> and LH2 WT. The spectra are largely similar. There is a minor change in the red most absorption band which is shifted by  $\sim 1$  nm (from 848 nm to 849 nm). Moreover, the absorption ratio B800/B850 is reduced either indicative of a partial loss of BChl-B800 and/or structural reorganization of this site. The BChl-B800 absorption band is broadened to the blue side, and there is a shoulder at  $\sim 760$  nm indicative that there is “free” BChl due to either defects in the assembly and/or stability of LH2  $\alpha$ AL<sub>16/T-4</sub> as observed for LH2  $\alpha$ AL<sub>16</sub>.

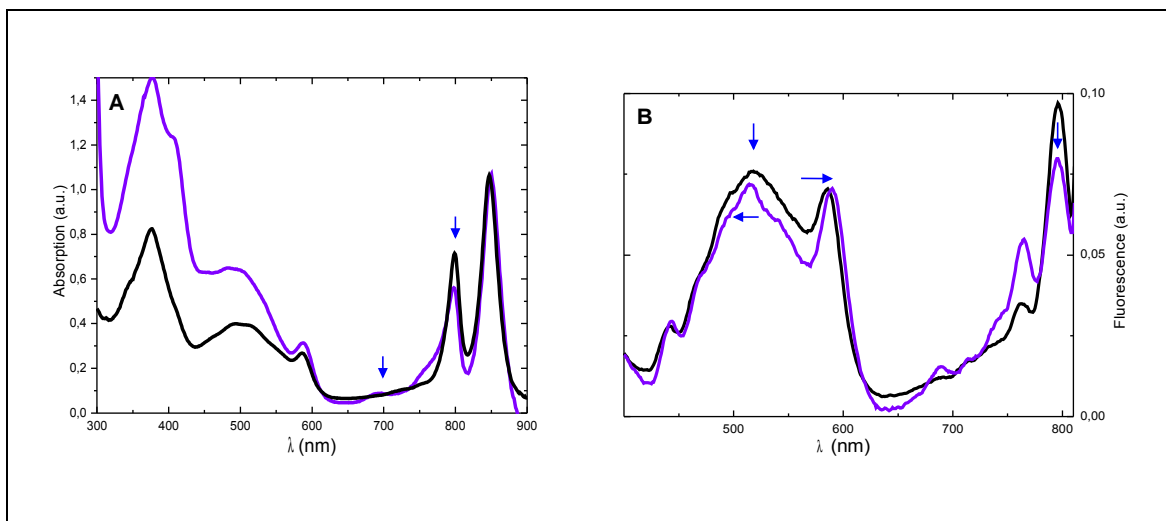


**Figure 3.7: Absorption spectra (A) and fluorescence excitation spectra (B) of LH2 WT (black) and LH2  $\alpha\text{AL}_{16/T-4}$  (violet).** The absorption spectra are normalised to the BChl-B850 peak at ~850 nm. The excitation spectra are normalised to the BChl  $Q_x$  transition at 598 nm. The fluorescence emission is detected at 850 nm. The arrows indicate the changes in LH2  $\alpha\text{AL}_{16/T-4}$ . Spectra are taken from purified membranes.

The fluorescence excitation spectrum of the mutant LH2  $\alpha\text{AL}_{16/T-4}$  is largely similar to the spectrum of LH2 WT, which indicates that ET from Car to BChl-B800 and BChl-B850 and from BChl-B800 to BChl-B850 takes place. Some minor changes are noticeable in LH2  $\alpha\text{AL}_{16/T-4}$ : (i) the ET of LH2  $\alpha\text{AL}_{16/T-4}$  in the Car region is slightly reduced (by 7%) and slightly blue-shifted (from ~517 nm in LH2 WT to ~514 nm in LH2  $\alpha\text{AL}_{16/T-4}$ ) and (ii) ET from BChl-B800 to BChl-B850 is reduced by ~ 12% (figure 1.7B).

The absorption spectrum of LH2  $\alpha\text{AL}_{16/S-4}$  is also similar to the one of LH2 WT (figure 3.8A), only a number of minor changes are observed: the red-most absorption band is slightly red-shifted from ~ 849 to ~ 853 nm in comparison to LH2 WT, indicative of minor structural rearrangements of the BChl-B850 dimer and the absorption ratio B800/B850 is reduced (figure 3.8A) either indicative of a partial loss of BChl-B800 and/or of structural reorganisation of this site .

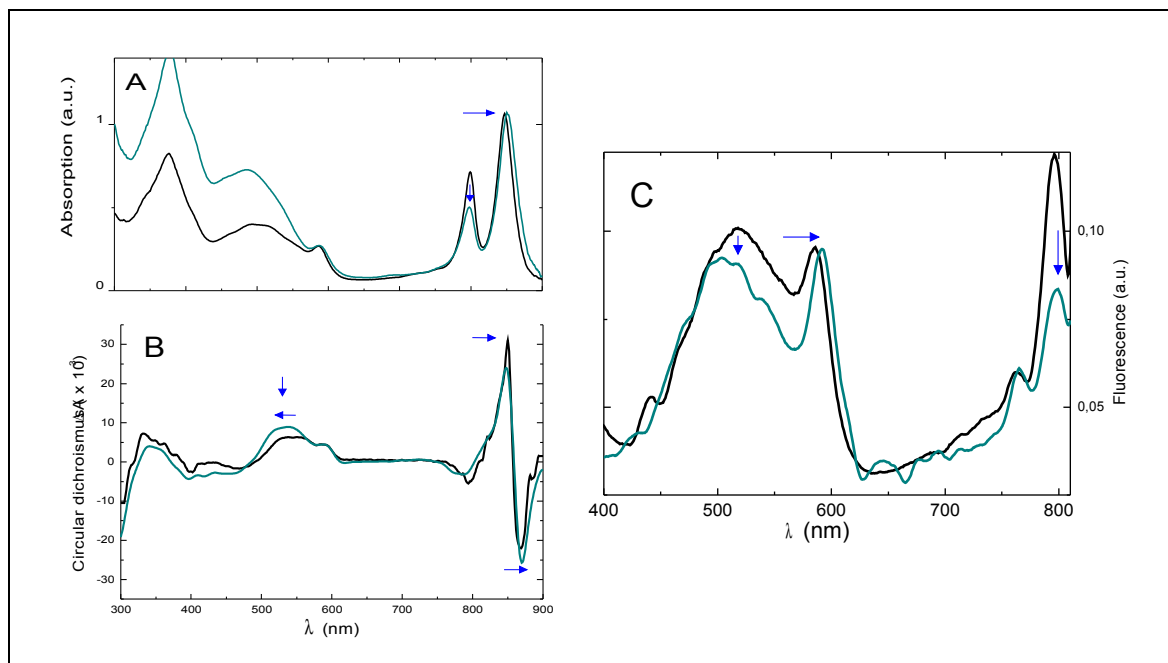


**Figure 3.8: Absorption (A), CD (B) and fluorescence (C) spectra of the model protein LH2  $\alpha$  AL<sub>16/S-4</sub>:** Spectra are taken from purified membranes of LH2 WT (black) and LH2  $\alpha$ AL<sub>16/S-4</sub> (dark cyan). The absorption spectra are normalised at the Q<sub>y</sub> BChl-B850. The fluorescence spectra are normalised at the Q<sub>x</sub> band at  $\sim$  590 nm.

The conservative, S-shaped CD signal in the near infrared with extrema at  $\sim$  848 nm (+) and  $\sim$  870 nm (-) and zero crossing at  $\sim$  857 nm, is similar for LH2 WT ( $\sim$  850 nm (+),  $\sim$  867 nm (-) and zero crossing  $\sim$  857 nm). Additionally, the optical activity of BChl-B800, seen as a negative through near 800 nm is somewhat reduced in comparison to LH2 WT. The signal of the Car (450-550 nm) is slightly blue-shifted, indicating a change in the Car binding site (see also chapter 5).

The ET from the Cars to BChl-B850 in LH2  $\alpha$ AL<sub>16/S-4</sub> is somewhat altered as compared with LH2 WT. The fluorescence excitation bands of Car are slightly blue shifted and decreased (approximately 10%) relative to the Q<sub>x</sub> transition of the BChl molecules at  $\sim$  600 nm. Moreover, the 800 nm excitation band is reduced in LH2  $\alpha$ AL<sub>16/S-4</sub> in comparison to LH2 WT (reduced in  $\sim$  50%).

The absorption spectrum from purified membranes of LH2  $\alpha$ AL<sub>16/S-4</sub> in *Rb. sphaeroides* DG2, in which, the major Car is NE (see materials and methods) is shown in figure 3.9A. This Car has well resolved vibrational absorption bands in the visible range, contrary to SO. Thus alterations in the Car region are better to note in the presence of NE due to the three characteristic absorption peaks. However, owing to the scattering effects in the blue range of the spectrum of LH2  $\alpha$ AL<sub>16/S-4</sub>, the changes in the Car region are not that clearly discernable. There is, however, a noticeable blue shift of two peaks of the NE in

comparison to LH2 WT, from  $\sim 491$  and  $\sim 457$  nm to  $\sim 481$  and  $\sim 450$  nm respectively (figure 3.9A).

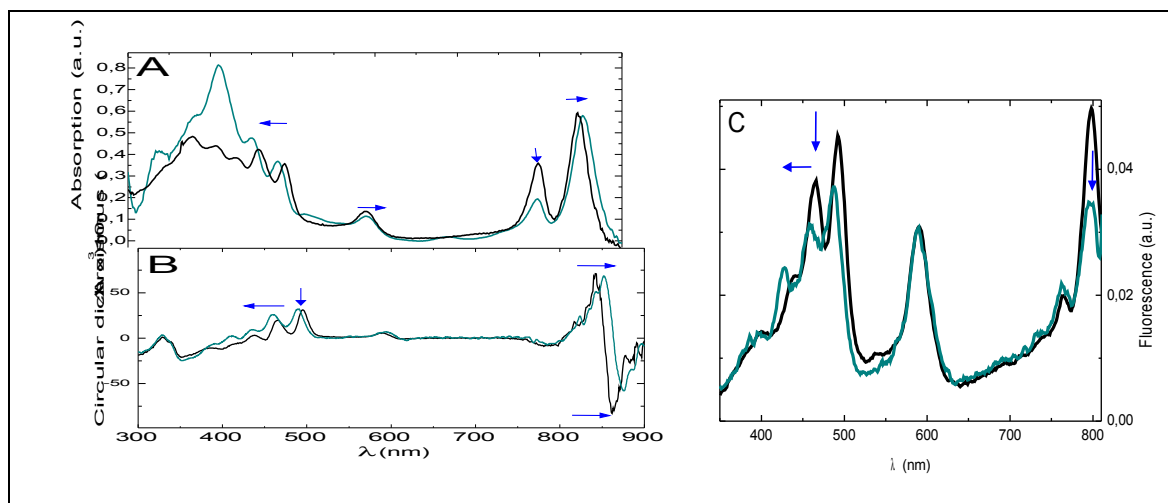


**Figure 3.9: Absorption (A), CD (B) and fluorescence excitation (C) spectra of LH2 WT (black) and LH2  $\alpha$ AL<sub>16/S-4</sub> (orange) expressed in DG2.** Spectra are taken of purified membranes from *Rb. sphaeroides* DG2. The spectra are normalised to the absorption and CD signal of BChl-B850. Fluorescence excitation spectrum, emission is detected at 850 nm. The arrows indicate the changes between the spectra.

The CD signal of the model LH2 in DG2 is similar to the signal of these complexes in strain DD13. In the Car region the maximal peaks are blue-shifted in comparison to LH2 WT, from  $\sim 495$ ,  $466$  and  $463$  nm to  $\sim 489$ ,  $458$ ,  $434$  nm, respectively (figure 3.9B).

The excitation spectrum (figure 3.9C) from isolated membranes of LH2  $\alpha$ AL<sub>16/S-4</sub> expressed in DG2 shows also changes in the Car region, closely similar to the changes of LH2  $\alpha$ AL<sub>16/S-4</sub> expressed in DD13 (figure 3.8C). The major intensity peaks of the Car are blue shifted in comparison to LH2 WT, from  $\sim 491$  nm to  $\sim 487$  nm,  $\sim 465$  nm to  $\sim 457$  nm and  $\sim 440$  nm to  $\sim 427$  nm. Furthermore in LH2  $\alpha$ AL<sub>16/S-4</sub>, the ET from Car to BChl-B850 is reduced by approximately 12% as compared with LH2 WT, and ET from BChl-B800 to BChl-B850 is reduced by approximately 65%. The spectra analysis of the mutant LH2  $\alpha$ AL<sub>16/S-4</sub> shows that there are additional alterations in the spectra as compared to LH2  $\alpha$ AL<sub>16</sub> and LH2 WT, the absorption ratio B800/B850 is reduced and the BChl-B850 is slightly red shifted. However, the assembly of LH2 is principally supported.

In summary, in LH2  $\alpha$ AL<sub>16/S-4</sub> and LH2  $\alpha$ AL<sub>16/T-4</sub>, there is a reduction in the intensity absorption band of BChl-B800 in comparison to LH2 WT or LH2  $\alpha$ AL<sub>16</sub>. Interestingly, in LH2  $\alpha$ AL<sub>16/S-4</sub> the reduction in ET from BChl-B800 to BChl-B850 as well as Car to BChl-B850 is more pronounced, as compared to LH2  $\alpha$ AL<sub>16/T-4</sub>. The absorption maxima of the Car are blue shifted in both LH2  $\alpha$ AL<sub>16/S-4</sub> and in LH2  $\alpha$ AL<sub>16/T-4</sub>. Curiously, LH2  $\alpha$ AL<sub>16/T-4</sub> has

spectroscopic characteristics similar to both LH2  $\alpha\text{AL}_{16}$  and LH2  $\alpha\text{AL}_{16/\text{S-4}}$ . Although, alanine and serine are more similar in size than threonine and alanine (alanine and serine have an identical surface ( $115 \text{ \AA}^2$ ) and almost the same volume ( $88.6 \text{ \AA}^3$  and  $89 \text{ \AA}^3$  respectively)). Apparently, the effect of the residues -4 at the BChl/protein interface depends on shape as well as other properties (see below). In any case, the critical importance of the residue at position -4 is demonstrated by the finding that out of the 12 residues tested in the model sequence context, only alanine, threonine, and serine support assembly the antenna complex.

To specifically explore the effects of the residues' physical and chemical properties at the BChl-protein interface, the residue at -4 is permuted in WT sequence context and explored in the LH2 modelled structure (see below).

### 3.2.4 Structural stability of model LH2 complexes

The LH2 complexes exhibit irreversible, cooperative thermal unfolding transitions and can be described as an irreversible two-state process. In the case of the irreversible two-state process, the denaturation is kinetically controlled and thus, depends on the heating rate. Upon heating, the dissociation/unfolding of the complex leads to disruption of the BChl-BChl coupling and consequently to the loss of the CD signal at  $\sim 845$  and  $\sim 862$  nm. The thermal stability of the LH2 model protein complexes has been determined by following the CD signal during heat denaturation in the native lipid environment. Figure 3.10 depicts the thermal denaturation curve of LH2 WT, LH2  $\alpha\text{AL}_{16}$ , LH2  $\alpha\text{AL}_{16/\text{S-4}}$ , and LH2  $\alpha\text{AL}_{16/\text{T-4}}$ . LH2  $\alpha\text{AL}_{16}$  is clearly the least stable complex with a midpoint of denaturation ( $T_m$ ) of  $\sim 30^\circ\text{C}$  (figure 3.10). Considering that the optimal growth temperature is  $\sim 34^\circ\text{C}$  for *Rb. sphaeroides*, it is not surprising that LH2  $\alpha\text{AL}_{16}$  is found in the membrane at considerable lower levels than LH2 WT (see below).

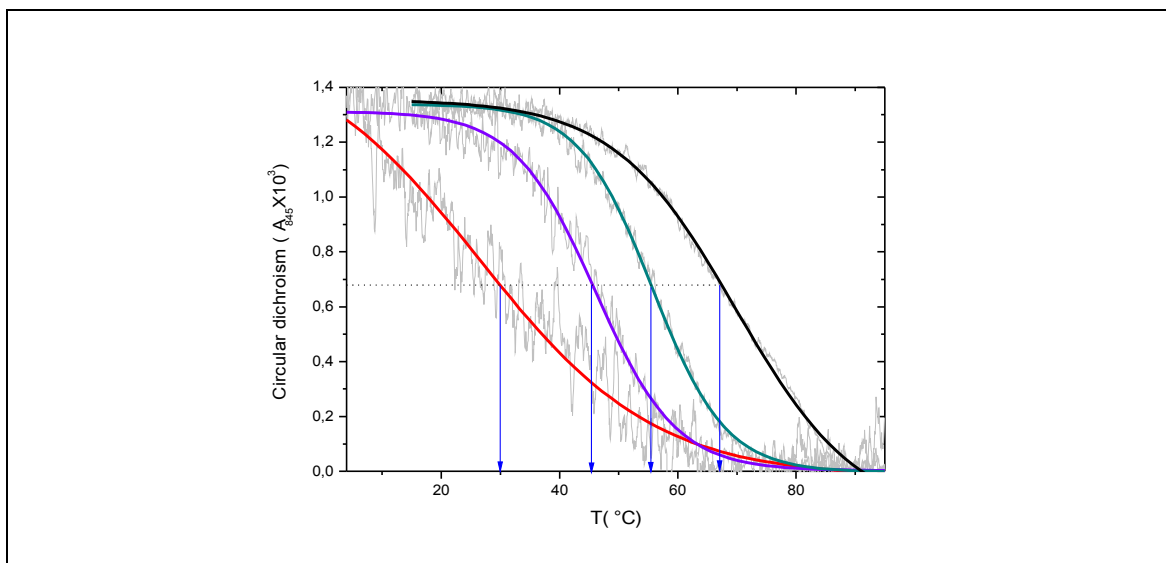


**Figure 3.10: Thermal denaturation of LH2 WT (black), LH2  $\alpha$ AL<sub>16</sub> (red), LH2  $\alpha$ AL<sub>16/S-4</sub> (dark cyan), and LH2  $\alpha$ AL<sub>16/T-4</sub> (violet).** Changes of the CD signal at 845 nm during heating of suspended membranes. The  $T_m$  values are indicated by the arrows. The denaturation curves (grey) have been fitted with by use of Origin curve fit program. Fitted curves are shown in color black, red, dark cyan and violet.

In LH2  $\alpha$ AL<sub>16/S-4</sub> which is identical to LH2  $\alpha$ AL<sub>16</sub>, except for the serine instead of alanine at position -4, the  $T_m$  is shifted to  $\sim 56^\circ\text{C}$ , thus approaching the  $T_m$  of LH2 WT ( $\sim 67^\circ\text{C}$ ). In LH2  $\alpha$ AL<sub>16/T-4</sub>, the  $T_m$  is  $\sim 46^\circ\text{C}$  and its stability is between LH2  $\alpha$ AL<sub>16/S-4</sub> and LH2  $\alpha$ AL<sub>16</sub>. The shape of the denaturation curve of LH2  $\alpha$ AL<sub>16/T-4</sub> is also closely similar to the curve LH2  $\alpha$ AL<sub>16/S-4</sub>. In addition the  $T_m$  of LH2  $\alpha$ AL<sub>16/S-4</sub> differs by in less than  $10^\circ\text{C}$ , from the  $T_m$  of LH2 WT, whereas, the  $T_m$  of LH2  $\alpha$ AL<sub>16</sub> is reduced by more than  $15^\circ\text{C}$  in comparison to LH2  $\alpha$ AL<sub>16/T-4</sub>. Remarkably, the substitution of alanine at position -4 by threonine or serine, especially, serine, results in a complex which is clearly more stable than LH2  $\alpha$ AL<sub>16</sub>, even though, only a single replacement, and, in addition, a fairly conservative (residues that are highly similar in their properties) has been made.

In the modelled structure (figure 3.11) there are different possible rotamers for serine -4 in LH2  $\alpha$ AL<sub>16/S-4</sub>. For each one, serine as well as threonine, exhibits a possible hydrogen bond (see below) to the BChl-B850. Both residues donate an hydrogen of the hydroxyl group to the C13<sup>1</sup> keto carbonyl atom of the BChl-B850. Thus, the relative stabilisation observed in LH2  $\alpha$ AL<sub>16/T-4</sub> as compared to LH2  $\alpha$ AL<sub>16</sub> may be related to H-bonding between the OH group of these residues at -4 and the C13 keto of one of the BChl-B850 molecules.

### 3.2.5 Hydrogen bonding interactions at the BChl-protein interface

As is obvious from the high resolution structure of *Rps. acidophila*, position -4 is in close vicinity of ring E and its substituents. The stabilizing effect of serine *versus* alanine in model LH2  $\alpha$ AL<sub>16</sub> may be related to the presence of the OH group which can participate in H-bonding to the C13 oxo groups. The hydrogen bond may be also present in the LH2  $\alpha$ AL<sub>16/T-4</sub>, since threonine has the OH group (see below, figure 3.13). There are works, which demonstrated that the threonine donates a putative hydrogen bond to (B)Chl and specifically the keto group C13<sup>1</sup> in PS I.

It is known that the keto carbonyl C13<sup>1</sup> of (B)Chl frequently participates in hydrogen bonding (Sturgis et al. 1995b, Witt et al. 2002, Kwa et al 2004a). This has been reported for the antenna-RC complex of PS I and in bacterial RCs, , . Additionally, the statistical analysis of the nearly 100 Chl binding sites in PS I confirm that the C13<sup>1</sup> keto carbonyl groups are repeatedly involved in H-bond interactions .

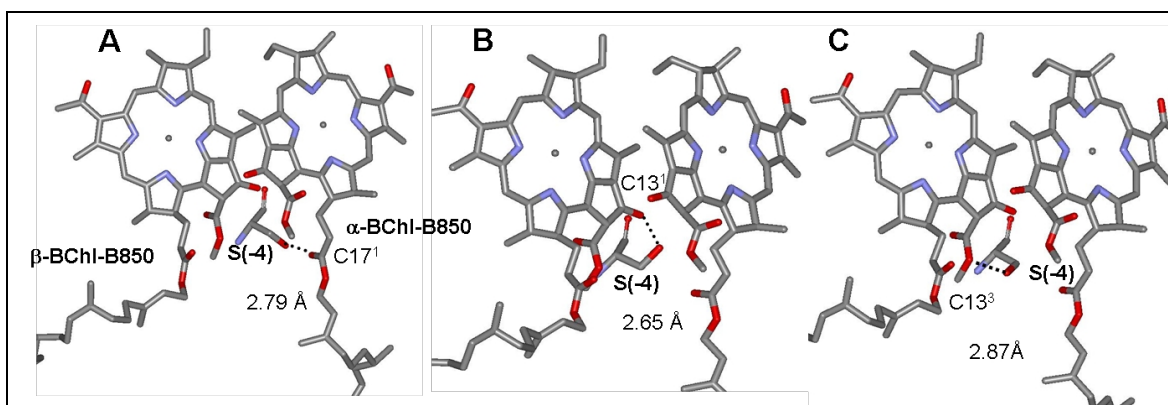


**Figure 3.11: Possible H-bonding of serine in position -4 and BChl-B850 in model from *Rb. sphaeroides*.** (A) Hydrogen bond between the hydroxyl of S(-4) and the C17<sup>1</sup> of  $\alpha$ -BChl-B850, (B) the C13<sup>1</sup> from  $\beta$ -BChl-B850 and (C) the C13<sup>3</sup> of the  $\beta$ -BChl-B850.

To further explore whether the significant rise in stability in LH2  $\alpha$ AL<sub>16/S-4</sub> (and partly LH2  $\alpha$ AL<sub>16/T-4</sub>) is related to H-bonding at BChl-protein interface, RR spectroscopy has been employed. RR spectroscopy is a method which is very useful in dissecting the physicochemical mechanisms underlying the interactions among (B)Chl and the surrounding polypeptide. In particular, the Raman bands are very sensitive to intermolecular interactions between the C13<sup>1</sup> keto and C3 acetyl groups, which are conjugated to the (B)Chl macrocycles'  $\pi$ -system, and their immediate polypeptide environments (Robert 1996), , .

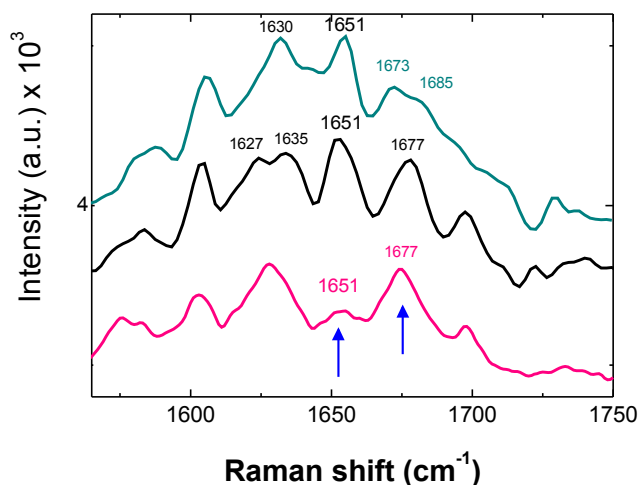


**Figure 3.12:** RR spectra of LH2 WT (black), LH2  $\alpha\text{AL}_{16/\text{S-4}}$  (cyan), and LH2  $\alpha\text{WT}_{\text{S-4/A}}$  (pink). The shift of the  $1651\text{ cm}^{-1}$  band to  $1677\text{ cm}^{-1}$  is indicated by the arrow.

The typical RR spectrum of LH2 WT has five bands in the carbonyl stretching modes region ( $1620\text{--}1710\text{ cm}^{-1}$ ), , , . Specifically, the bands at  $1627$  and  $1635\text{ cm}^{-1}$  have been attributed to the C3 acetyl groups of the BChl-B850 . The stretching mode of the acetyl carbonyl of the BChl-B800 also contributed in this frequency range, but is very weak in FT Raman spectra . The remaining bands have been attributed to the C13<sup>1</sup> keto carbonyl of the BChl-B850 ( $1651$  and  $1677\text{ cm}^{-1}$ ) and of the BChl-B800 ( $1701\text{ cm}^{-1}$ ), , , (Robert & Lutz 1985). The considerable downshift of one of the BChl-B850 C13<sup>1</sup> keto bands to  $1651\text{ cm}^{-1}$  has been proposed to reflect strong hydrogen bonding , , . The residue which participates in this bond has not yet been identified.

The Raman spectrum of LH2  $\alpha\text{AL}_{16/\text{S-4}}$  resembles the spectrum of the LH2 WT in the carbonyl region; in particular, the band at  $1651\text{ cm}^{-1}$  is clearly discernable (figure 3.12). There are some alterations; the two low frequency bands at  $1627$  and  $1635\text{ cm}^{-1}$  have been replaced by an intense band at  $1630\text{ cm}^{-1}$ . The merging of the  $1627\text{--}1635\text{ cm}^{-1}$  bands have been also observed in the spectra of LH2  $\alpha\text{WT}_{\text{S-4/A}}$  (figure 3.12) and from *Rb. sphaeroides* G1C, which produces as the major Car NE . In *Rb. sphaeroides* G1C, it has been attributed to a minor reorganization of the C-terminal end of the  $\alpha$  polypeptide, because of the change in chemical structure of the Car terminal groups. The band at  $1677\text{ cm}^{-1}$  is broadened and probably split into two bands with frequencies at  $\sim 1673$  and  $1685\text{ cm}^{-1}$ , whereas the intensity of the band at  $1701\text{ cm}^{-1}$  is strongly reduced. One possible explanation for these alterations may be that the BChl-B800 assumes an altered conformation in the model BChl-binding site (chapter 5), which leads to an increase in polarity around the keto group (which is located in the membrane interface close to the

cytoplasmatic lumen) and thereby shifts its Raman frequency by  $15\text{ cm}^{-1}$  to lower wave numbers. In accordance, the reduced ratio of the B800/B850 absorption bands (figure 3.8A and 3.9A) and the reduced B800 fluorescence excitation band (figure 3.8C and 3.9C) point to either a partial loss of the BChl- B800 or to a reduced extinction coefficient because of the alteration in this site . In any case, the modifications in the Raman spectra indicate that some rearrangement may occur upon the replacement of the BChl-B850 TM-binding domain in LH2  $\alpha\text{AL}_{16/\text{S}-4}$ .

The remaining spectrum of LH2  $\alpha\text{AL}_{16/\text{S}-4}$  is very similar to the spectrum of the LH2 WT. In particular, the band at  $1651\text{ cm}^{-1}$  which has been assigned to the hydrogen-bonded C13<sup>1</sup> of  $\beta$ -BChl-B850 is clearly present. In contrast, in the FT Raman spectrum of LH2  $\alpha\text{WT}_{\text{S}-4/\text{A}}$ , the band at  $1651\text{ cm}^{-1}$  is nearly absent, whereas the band at  $1677\text{ cm}^{-1}$  has gained intensity and is shifted to slightly lower energies (figure 3.12). The loss of the  $1651\text{ cm}^{-1}$  band indicates that in the mutant LH2  $\alpha\text{WT}_{\text{S}-4/\text{A}}$  the hydrogen bond to the C13<sup>1</sup> keto carbonyl group of  $\beta$ -BChl-B850 has been disrupted or weakened . This is further supported by similar alterations in the Raman spectra of the mutant LH2  $\alpha\text{WT}_{\text{S}-4/\text{G}}$ . In LH2  $\alpha\text{WT}_{\text{S}-4/\text{G}}$ , serine at position -4 is replaced by glycine, which does not have any side chain (see chapter 4) (Garcia-Martin 2006a). Conceivably, in LH2  $\alpha\text{AL}_{16}$ , with alanine, which does not have the hydroxyl group of the  $\alpha\text{S}(-4)$ , the keto carbonyl groups of  $\beta$ -BChl-B850 are free of strong polar intermolecular interactions. Equally, in LH2  $\alpha\text{WT}_{\text{S}-4/\text{G}}$  which lacks any side chain. The frequency of the Raman band at  $1677\text{ cm}^{-1}$  ('free' keto groups have bands around  $1700\text{ cm}^{-1}$ ) indicates, however, that there still are some polar interactions either with polar residues or a polar environment (figure 4.9, chapter 4).

Taken together, the FT Raman results strongly suggest that there is an hydrogen bond between S(-4) and the BChl-B850 in the model BChl-binding site of the LH2  $\alpha\text{AL}_{16/\text{S}-4}$  similar to the bond in LH2 WT . In the absence of either serine or threonine, and consequently the hydroxyl group parting in hydrogen bonding; the stable assembly of the model LH2 is significantly diminished. The critical input of this H-bond is further demonstrated by use of a model protein in which the entire BChl-B850 site is modified. In the model LH2 complex with entirely simplified binding sites on both the  $\alpha$ - and  $\beta$ -subunits, LH2  $\alpha\text{AL}_{16} + \beta\text{AL}_{12}$ , LH2-like complex is not even assembled to detectable amounts in the membrane . The assembly of LH2  $\alpha\text{AL}_{16} + \beta\text{AL}_{12}$  maybe "rescued" by the introduction of serine at position -4 . Apparently in this case, whether assembly takes place or not depends on the establishment of the H-bond at the BChl-B850/protein interface. Previously, the importance of intramembrane hydrogen bonding for the folding and assembly of the membrane proteins has been demonstrated . Here is shown that the

assembly of BChl proteins depends on intramembrane hydrogen bonding between the BChl and its binding polypeptide.

Surprisingly, in WT sequence context the H-bond between the serine hydroxyl and C13<sup>1</sup> of BChl-B850 seems not to be a major factor for the stability of LH2 (not shown). Recently, it has been suggested that certain CH groups, such as methyl hydrogens, could also acts as H-bonds donors (Ho & Curmi 2002, Desiraju 2002). It therefore may be possible that alanine at -4 is also involved in, albeit weaker, H-bond interactions with the C13<sup>1</sup> keto carbonyl and partly compensates for the disruption of the strong bond to serine. Alternatively, nearby  $\alpha$ -histidine at position 0 could closely interact with the C13<sup>1</sup> keto carbonyl group. Formation of hydrogen bond between these residues and BChl may partly compensate for the loss of the H-bond to the OH of the S(-4) and at the same time may be accountable for the relatively low stretching frequency of the keto group even in absence of serine. However, in LH2  $\alpha$ WT<sub>S-4/A</sub>, if such a bond is formed, it should be weaker than the H-bond with the hydroxyl group in LH2  $\alpha$ AL<sub>16/S-4</sub> as obvious from the Raman data and LH2 stability.

The RR of LH2  $\alpha$ AL<sub>16/T-4</sub> could not be measured due to the low expression level of this mutant which makes it impossible to obtain a reliable Raman spectrum. In the figure 3.13 the modelled structure of LH2  $\alpha$ AL<sub>16/T-4</sub>, however, is depicted. As shown  $\alpha$ -T(-4) has 3 possible rotamers which would allow for H-bonding with the BChl-B850.

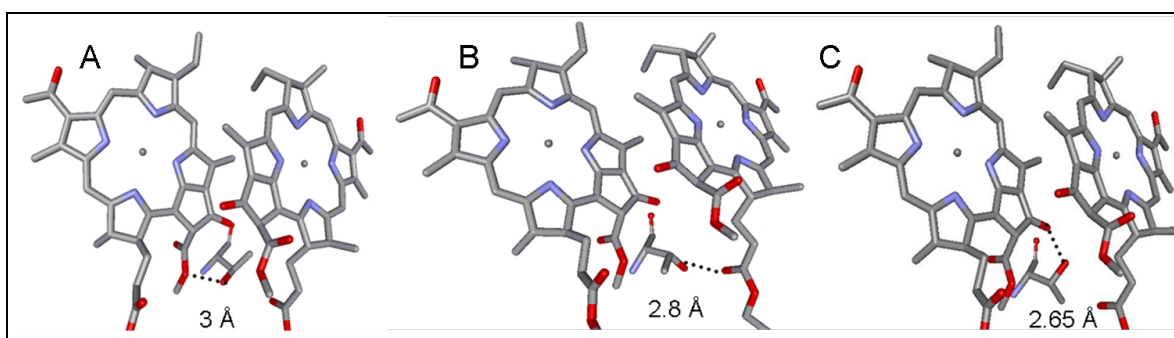


**Figure 3.13: Possible rotamers from the modelled structure of LH2  $\alpha$ WT<sub>S-4/T</sub>.** (A) Hydrogen bond between the hydroxyl of T(-4) and C13<sup>4</sup> of the  $\beta$ -BChl-B850, and (B) the C17<sup>1</sup> of  $\alpha$ -BChl-B850 and the (C) C13<sup>1</sup> of  $\beta$ -BChl-B850.

### 3.2.6 Permutation of the LH2- $\alpha$ residue at position -4 at the BChl/protein interface in LH2 WT complex

Assembly of a model-LH2 complex (see below) LH2  $\alpha$ AL<sub>16</sub> +  $\beta$ AL<sub>12</sub> has been shown to depend on a single serine residue at the BChl helix interface, which makes a H-bond between the hydroxyl of serine -4 and the C13<sup>1</sup> of the  $\beta$ -BChl-B850 . Exchange experiments using modified (B)Chl molecules showed that the substituents at ring E are critical structural factors for proper binding and assembly of BChl . Apparently, the interaction of these substituents is a critical factor in the recognition/binding of the BChl molecule by the polypeptide. In the statistical analysis of (B)Chl bindings pockets it has been observed that contacts to the residue at the position - 4 relative to the histidine ligand occur most frequently.

In this section, the effects of the amino acid side chain properties on LH2 assembly of the residue at position -4 of the  $\alpha$ -subunit which is in the close vicinity of the C13 substituents, have been systematically tested in WT sequence context. To that end serine at position -4, is replaced by 15 others amino acids and the assembly of the antenna complex is monitored by *in situ* optical absorption spectra (figure 3.14). The structures of the mutants are modelled by the program Deep View/Swiss- PDB View (version v 3.7) and WHAT IF to visualize its conformation and position relative to the BChl-B850. All the structures shown in this section of the chapter are based on the modelled structure of *Rb. sphaeroides*.

Each amino acid has several possible conformational positions in the structure; these positions are called rotamers. A rotamer is a set of allowed rotation angles of side-chain bonds, and restriction of rotamers is a major energy factor in protein folding, mainly for entropic reasons. Here, the rotamer of the mutants with the lower score are selected. The residue at position -4 in close vicinity of the BChl ring E is critical for LH2 assembly as demonstrated by use of the model LH2 (see below). To further understand of the role of this residue, it is systematically mutated in the model structure. Preliminary characterisation of these mutants is presented here, but thorough experimental analysis is still wanting but beyond the scope of this work.

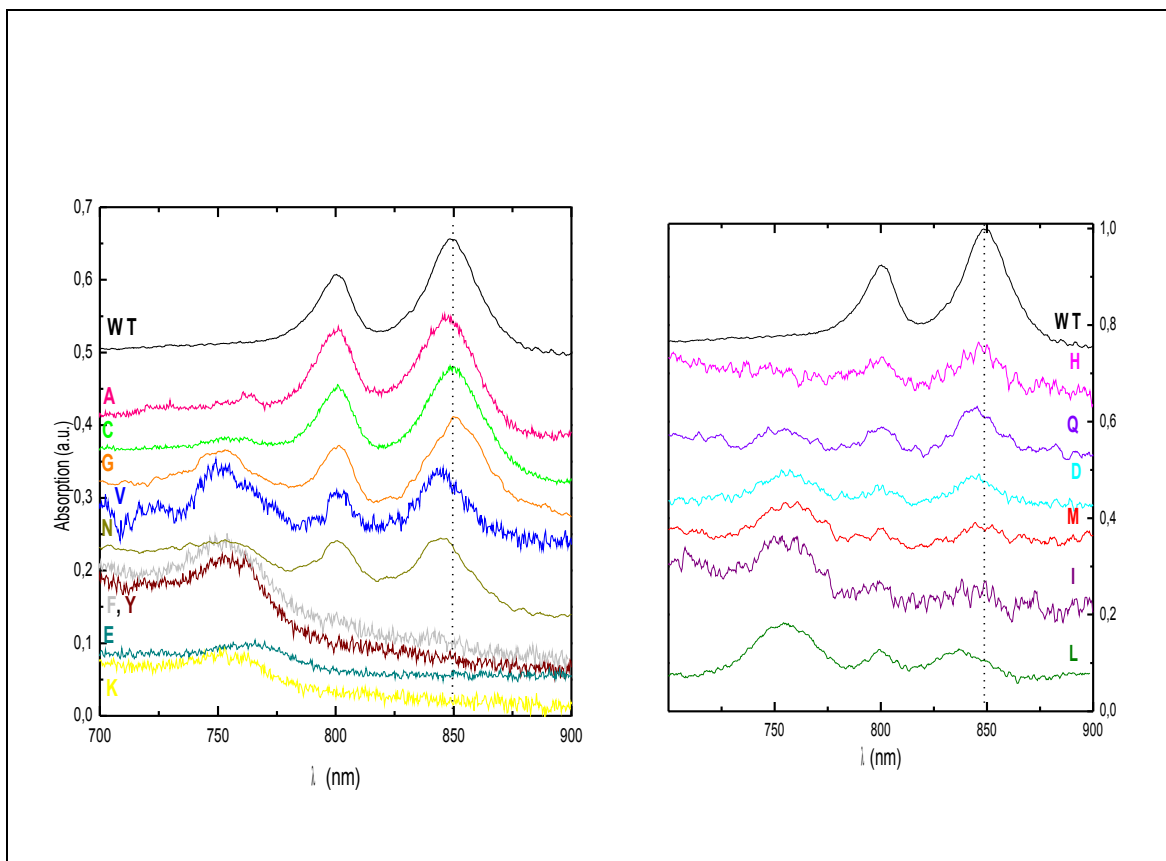


**Figure 3.14: Assembly of LH2 WT in dependence of the residues at position -4.** “*In situ*” spectra are taken of *Rb. sphaeroides* colonies expressing LH2 WT and LH2  $\alpha$ WT<sub>S-4/X</sub> with 15 different residues at position -4. Colour coding is indicated in graphs.

Glycine is the smallest amino acid (surface  $75 \text{ \AA}^2$  and volume  $60.1 \text{ \AA}^3$ ) with its side chain being a single hydrogen atom. Despite its small size glycine is an important amino acid for the folding and stability both in soluble and TM protein. It is very abundant in membrane helices (Popot & Engelman 2000). In TM helices, glycine does not have helix destabilising properties in contrast to its effects in soluble proteins (Popot & Engelman 2000). Since it has no large side chain to conflict with other structures it has much more flexibility of rotation than its larger “colleagues”.

With the replacement of the serine at position -4 with glycine in the mutant LH2  $\alpha$ WT<sub>S-4/G</sub>, the hydrogen bond between this amino acid and BChl-B850 is disrupted. This disruption is apparent from the Raman spectrum of this mutant (figure 4.9, chapter 4). LH2  $\alpha$ WT<sub>S-4/G</sub>, assembles to LH2-like complex, however, it shows a band at  $\sim 760 \text{ nm}$  (free BChl), and the intensity of the bands at BChl-B850 and BChl-B800 are reduced relative to BChl-B760 in comparison to LH2 WT (figure 3.14). Besides, this mutant shows a slight red shift of the absorption maximum of the BChl-B850 (from  $\sim 849$  to  $\sim 851 \text{ nm}$ ) (table 3.1) in comparison to the maximum of LH2 WT. In addition, the structural stability of this mutant is

significantly reduced possibly due to either the effective disruption of the H-bond and/or the emergence of a cavity in the protein interior at the BChl-protein interface (for further discussion of this mutant WT  $\alpha$ LH2<sub>S-4/G</sub> see in chapter 4).

	LH2 assembly	$\lambda_{\max}$ (nm) <sup>(a)</sup>	850/760 <sup>(b)</sup>	$\Delta$ OD (cm <sup>-1</sup> ) <sup>(c)</sup>	Surface of residue at -4 (Å <sup>2</sup> ) <sup>(d)</sup>	Volume of residue at -4 (Å <sup>3</sup> ) <sup>(e)</sup>
LH2 $\alpha$ WT	+	849		0x10 <sup>6</sup>	115	89
LH2 $\alpha$ WT <sub>S-4/G</sub>	+	851	2.4	2x10 <sup>6</sup>	75	60.1
LH2 $\alpha$ WT <sub>S-4/A</sub>	+	848	17	1x10 <sup>6</sup>	115	88.6
LH2 $\alpha$ WT <sub>S-4/V</sub>	+	844	0.7	6x10 <sup>6</sup>	155	140
LH2 $\alpha$ WT <sub>S-4/I</sub>	+	842	0.375	7x10 <sup>6</sup>	175	166.7
LH2 $\alpha$ WT <sub>S-4/L</sub>	+	837	0.6	12x10 <sup>6</sup>	170	166.7
LH2 $\alpha$ WT <sub>S-4/D</sub>	+	844	1	5x10 <sup>6</sup>	150	111.1
LH2 $\alpha$ WT <sub>S-4/N</sub>	+	845	2.25	4x10 <sup>6</sup>	160	114.1
LH2 $\alpha$ WT <sub>S-4/Q</sub>	+	843	1.6	6x10 <sup>6</sup>	180	143.8
LH2 $\alpha$ WT <sub>S-4/M</sub>	+	846	0.5	3x10 <sup>6</sup>	185	162.9
LH2 $\alpha$ WT <sub>S-4/C</sub>	+	850	16	1x10 <sup>6</sup>	135	108.5
LH2 $\alpha$ WT <sub>S-4/H</sub>	+	847	2.8	2x10 <sup>6</sup>	195	153.2
LH2 $\alpha$ WT <sub>S-4/E</sub>	—				190	138.4
LH2 $\alpha$ WT <sub>S-4/Y</sub>	—				230	193.6
LH2 $\alpha$ WT <sub>S-4/K</sub>					200	168.6
LH2 $\alpha$ WT <sub>S-4/F</sub>					210	189.9

**Table 3.1:** LH2 properties in dependence of the residue at position -4. (a) Maximal absorption of BChl-B850 Q<sub>y</sub> transition, (b) ratio between BChl-B800 and -B850, (c) blue shift of the maximal absorption of the Q<sub>y</sub> transition of BChl-B850, (d) the values are according to (Chothia 1976) (e) the values are according to (Zamyatin AA 1972 ).

In LH2  $\alpha$ WT<sub>S-4/A</sub> the serine at position -4 is replaced by alanine. Alanine has an identical surface (115 Å<sup>2</sup>) and similar volume (88.6 Å<sup>3</sup>) as serine. The *in situ* absorption spectrum of LH2  $\alpha$ WT<sub>S-4/A</sub> (figure 3.14) is closely similar (blue shift of ~1 nm) to the spectra of LH2 WT (table 3.1). Thus, the exchange of the serine by alanine apparently neither results in significant alterations of the BChl excitation energies nor in the pigment arrangement. In the modelled structure of *Rb. sphaeroides* from LH2  $\alpha$ WT<sub>S-4/A</sub> no hydrogen bond is indicated, because the methyl hydrogen atoms of C<sub>B</sub> of alanine are not considered to participate in H-bonding. However, it could be possible that this residue is involved, albeit weak, H-bond interactions with the C13<sup>1</sup> keto carbonyl and partly compensates for the disruption of the strong bond to serine -4. In any case, the Raman spectrum indicates that the hydrogen bond has been disrupted or significantly weakened (figure 3.12). However, the carbonyl resonance frequency is not as for free carbonyls groups, indicating either a polar environment or weak H-bonding. Stability is almost unchanged for the LH2  $\alpha$ WT<sub>S-4/A</sub>, whereas much reduced for LH2  $\alpha$ WT<sub>S-4/G</sub>, (figure 4. 10, chapter 4).

Summing up, the small residues, G and A, did not significantly affect the spectral properties of LH2. In both mutants there is a very minor shift in the absorption of BChl-B850 in comparison to WT. G and A residues, together with S and T, have the highest packing values in integral membrane proteins.

However, the planarity of the BChl-B850 macrocycle may not permit the simultaneous close packing of the very short glycine residue at position -4 and “longer” residues at other positions along the BChl-protein interface (see chapter 4).

The aliphatic residue, valine has a larger surface (155 Å<sup>2</sup>) and volume (140 Å<sup>3</sup>) as compared to serine and apparently has no capacity to form hydrogen bonds. In the modelled structure of LH2  $\alpha$ WT<sub>S-4/V</sub> (not shown) every rotamer has a good score and there are no bumps between the valine and the BChls. The *in situ* absorption spectrum of LH2  $\alpha$ WT<sub>S-4/V</sub> exhibit some changes in comparison to the spectrum of LH2 WT: (i) a red shift of the maximal band of BChl-B850, from ~ 849 to ~ 844 nm and (ii) a shoulder at ~ 760 nm (table 3.1), indicative of alterations in BChl-B850 geometry and some disturbance in stable assembly (figure 3.14). Thus, although valine is often favoured in the TM region due to its hydrophobicity, its side chain maybe unfavourable large, resulting in the above changes.

Leucine and isoleucine are both “long” aliphatic amino acid without the capacity to form H-bond. They have identical volumes (167.7 Å<sup>3</sup>); however, isoleucine (175 Å<sup>2</sup>) has slightly larger surface than leucine (by 5Å<sup>2</sup>). Curiously, the substitution of serine for leucine or isoleucine at position -4 permits the assembly of the antenna complex (figure 3.14). A

number of changes are recorded in the spectra of LH2  $\alpha$ WT<sub>S-4/L</sub> and LH2  $\alpha$ WT<sub>S-4/I</sub> as compared to LH2 WT (figure 3.14): (i) the mutants exhibit a strong absorption at  $\sim 760$  nm typical of free BChl, (ii) the BChl Q<sub>y</sub> absorption maximum is blue shifted by  $\sim 12$  nm (from  $\sim 849$  to  $\sim 837$  nm) in the case of LH2  $\alpha$ WT<sub>S-4/L</sub> and  $\sim 7$  nm (from  $\sim 849$  to  $\sim 842$  nm) in the case of LH2  $\alpha$ WT<sub>S-4/I</sub> (table 3.1) and (iii) the intensity of the band of BChl-B800 is higher than of the BChl-B850, probably due to broadening of the band of BChl-B850. It should be noted that the spectrum of LH2  $\alpha$ WT<sub>S-4/I</sub> is barely discernable and due to the low signal to noise ratio, the spectral properties maybe somewhat distorted.

In the modelled structure of LH2  $\alpha$ WT<sub>S-4/L</sub> there are 22 possible rotamers; two of them have a very good score (-3), but the majority have scores above 0 up to +11, indicative of the presence of single, double, triple, and quadruple bumps. The bumps occur with BChl-B850, particularly, with the atoms C13<sup>1</sup>, C13<sup>1</sup> oxo, C13<sup>3</sup>, C13<sup>3</sup> oxo, C13<sup>4</sup> and C13<sup>4</sup> oxo of the  $\beta$ -BChl-B850 as well as with C17<sup>1</sup> and C17<sup>3</sup> oxo of the phytol rest of  $\alpha$ -BChl-B850 (figure 3.15A).

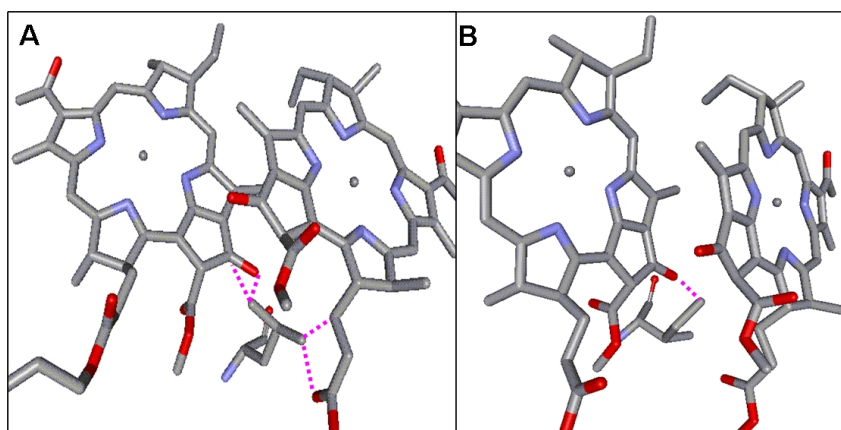


**Figure 3.15: Modelled structure of LH2  $\alpha$ WT<sub>S-4/L</sub> (A) and LH2  $\alpha$ WT<sub>S-4/I</sub> (B).** The purple lines indicate the bumps between the residues and the BChl. Note, that this rotamer of leucine has 4 bumps with BChl-B850.

On the contrary, the rotamers of the mutant LH2  $\alpha$ WT<sub>S-4/I</sub> only have simple or double bumps with the BChl-B850 (figure 3.15B). This indicates that isoleucine and leucine have, in spite of their general similarity, distinctly different conformations and thus contacts with their immediate environment, in particular, with substituents of the BChl-B850 at C13.

In summary, the aliphatic residues valine, leucine, and isoleucine support LH2 assembly. Interestingly, the replacement of serine by these residue results in blue shifting of the maximal absorption of the Q<sub>y</sub> transition of BChl-B850. In LH2  $\alpha$ WT<sub>S-4/L</sub> the shift is maximal

by  $\sim 12$  nm. These shifts are likely induced by changes in the geometry of the  $\beta$ -BChl-B850 in its binding pocket relative to the  $\alpha$ -BChl-B850 (see below) due to the presence of the long side chains.

Replacement of serine -4 with the non polar residue methionine (surface  $185 \text{ \AA}^2$  and volume  $162.9 \text{ \AA}^3$ ) permits complex assembly (figure 3.14). As judged from the ratio of the 760/850 bands, the expression level of assembled antenna complex is low. Surprisingly, the red most absorption band of BChl-B850 is only shifted by  $\sim 3$  nm to the blue (table 3.1), indicative of only minor disturbance in the BChl-B850 geometry. In the model structure the best rotamer has a score -1, but even in this conformation, clashes occur between the atom  $C_E$  of methionine and the  $C17^1$  of  $\alpha$ -BChl-B850. In other rotamers there are bumps between the  $S_D$  and/or  $C_E$  of the methionine -4 and the BChl-B850 molecules.

The *in situ* spectrum (figure 3.14) (table 3.1) of LH2  $\alpha$ WT<sub>S-4/F</sub>, shows that the replacement of serine by phenylalanine, (surface  $210 \text{ \AA}^2$  and volume  $189.9 \text{ \AA}^3$ ) results in the loss of the LH2 complex from the membrane. In the model structure, the best three rotamers have a score of 3, in which, there are bumps between F(-4) and the  $C13^1$  keto carbonyl of  $\beta$ -BChl-B850. This mutation does not permit assembly of a stable antenna complex, likely due to the bulky side chain which clashes with the BChl-B850, in particular, the oxo  $C13^1$  oxo of the  $\beta$ -BChl-B850. As obvious from the absence of the typical LH2 in the absorption spectrum (figure 3.14), the replacement of serine by tyrosine also results in abolishment of antenna from the membrane (see also table 3.1). Tyrosine has been shown to participate in hydrogen bonding with the C3 acetyl of the BChl-B850 in LH2 at the position -4, however, the tyrosine's size appears to be incompatible with either the folding and/or the stable assembly of LH2.

Similar to phenylalanine, the side chain of tyrosine has a considerable larger surface ( $230 \text{ \AA}^2$ ) and volume ( $193.6 \text{ \AA}^3$ ) than serine. In the model structure Y(-4) there are clashes with both BChl-B850 molecules, specially, the carbon atoms of the tyrosyl bumps ring bumps with the  $C13^1$  of  $\beta$ -BChl-B850 and with the C16, N16, and C19 of the  $\alpha$ -BChl-B850 macrocycle.

Threonine is often found in the TM region of proteins in spite its polar side chain largely due to its participation in hydrogen bonding between TM helices. In addition, threonine has a high packing value; supporting the close association with surrounding polypeptide residues. According to the modelling, threonine at position -4 makes hydrogen bonds to the BChl-B850. The figure 3.13 displays some of the threonine rotamers. In the model, the hydroxyl group of the threonine makes a hydrogen bond with either the keto carbonyl group  $C13^1$  (score -4) or  $C13^4$  (score -5) of the  $\beta$ -BChl-B850 or the  $C17^1$  (score -5) of the  $\alpha$ -

BChl-B850. Being quite similar to serine both are polar, and have relatively similar surfaces and volumes (serine:  $115 \text{ \AA}^2$ ,  $89 \text{ \AA}^3$ , threonine:  $40 \text{ \AA}^2$ ,  $116 \text{ \AA}^3$ ), and has the capacity to donate a hydrogen for H-bond interactions. Evidently, if the serine at position -4 is replaced for threonine in LH2  $\alpha\text{AL}_{16/\text{T}-4}$ , the assembly of the model complex is supported (see below).

Replacement of serine for aspartate permits assembly of LH2 complex as obvious from the *in situ* optical spectrum of LH2  $\alpha\text{WT}_{\text{S-4/D}}$  (figure 3.14). The red most absorption band of BChl-B850 is slightly blue shifted in comparison with LH2 WT (from  $\sim 849 \text{ nm}$  to  $\sim 844 \text{ nm}$ ). The band at  $\sim 760 \text{ nm}$  typical of free BChl (table 3.1), indicates some disturbance in complex assembly. In the model structure of this mutant (figure 3.16A) an hydrogen bond between aspartate and the oxo C13<sup>1</sup> of the  $\beta$ -BChl-B850 is indicated (score -3). The potential H-bond and the fairly small size of this residue appear to allow for the assembly of the LH2 complex, in spite of its potentially charged carboxyl side chain.

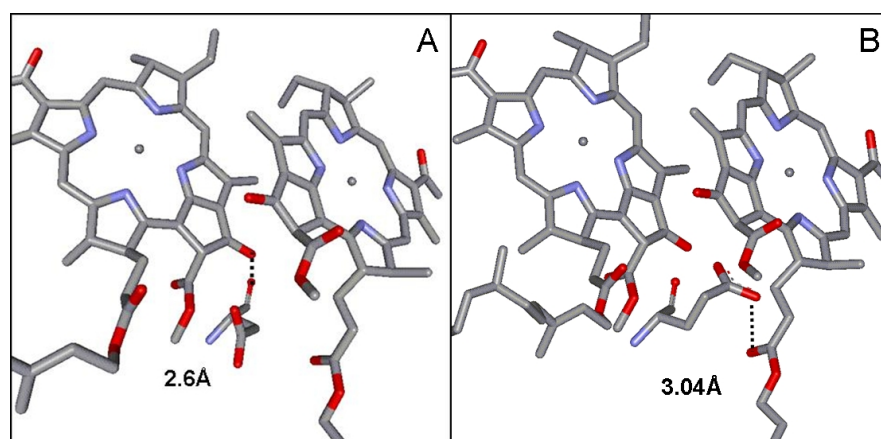


**Figure 3.16: Model structures of LH2  $\alpha\text{WT}_{\text{S-4/D}}$  (A) and LH2  $\alpha\text{WT}_{\text{S-4/E}}$  (B).** Note, the hydrogen bond between BChl-B850 and aspartate involve is the keto carbonyl C13<sup>1</sup> of  $\beta$ -BChl-B850 and the OH of the carboxyl side chain of Asp (-4) and the hydrogen bond between BChl-B850 and glutamate at position -4 involves the C17<sup>3</sup> oxo of  $\alpha$ -BChl-B850. The H-bonds are represented by dotted lines.

In contrast, the replacement of serine by glutamate in LH2  $\alpha\text{WT}_{\text{S-4/E}}$ , leads to loss of the LH2 complex from the membrane (figure 3.14), (table 3.1). Glutamate is very similar to aspartate, as both are negatively charged amino acids with a terminal carboxyl group which have only slightly different pKs (glutamate with 4.3 is higher than that aspartate 3,9). Glutamate, however, is the larger residue (glutamate:  $190 \text{ \AA}^2$ ,  $138.4 \text{ \AA}^3$ , aspartate:  $150 \text{ \AA}^2$ ,  $111 \text{ \AA}^3$ ).

The modelled structure of the mutant LH2  $\alpha\text{WT}_{\text{S-4/E}}$  shows that hydrogen bonding between the OH group of the glutamate carboxyl group and the oxo C17<sup>3</sup> (figure 3.16B) from the  $\alpha$ -

BChl-B850 could take place. There is, however, also multiple bumping due to the relatively large size of glutamate compared to serine and aspartate.

Usually, Glu and Asp are rarely found in TM helices except for the peripheral ends of the TM helices where the negative charged side chain favours interactions with the lipid head groups or charged groups from other amino acids. It has been shown that Glu and Asp may be placed in model poly Leu TM helices without inhibiting helix insertion nor inducing the break of the helix .

In accordance, replacement of serine -4 with aspartate which has a size (surface  $150 \text{ \AA}^2$  and volume  $111.1 \text{ \AA}^3$ ) fairly close to serine permits complex assembly. Curiously, replacement by glutamate (which has one carbon more in its side chain) results in the loss of LH2 from the membrane. The polar and charged groups of the carboxyl group are strongly unfavourable in the interior of the membrane and thus needs to be saturated by other polar and charged groups in close vicinity. The carboxyl of Glu may participate in H-bond to the C17<sup>3</sup> keto carbonyl of  $\alpha$ -BChl-B850, but at the same time bumping with the neighbouring amino acid residues is high. Thus, it appears that, in the case of glutamate, the combination of charge and steric hindrance results in the loss of LH2 from the membrane.

Replacement of the serine -4 by the positively charged residue lysine, results in the loss of LH2 complex (figure 3.14). This is easily rationalised because introduction of the positive charge of the imino group into the membrane is thermodynamically unfavourable, and additionally, the surface ( $225 \text{ \AA}^2$ ) and volume ( $173.4 \text{ \AA}^3$ ) of this residue results in multiples bumps with BChls-B850 and hence steric hindrance is likely to be significant.

In summary, it appears that out of the three charged residues tested only Asp at position -4 supports assembly of LH2. Substitutions of the Ser by Lys or Glu at position -4 results in the disruption of complex assembly. This suggests that principally potentially charged residues are tolerable at the BChl protein interface. From the modelling it is apparent that Asp may participate in H-bonding with the keto carbonyl group C13<sup>1</sup> of  $\beta$ -BChl-B850. Protonation of the carboxyl groups is likely to occur in the membrane interior . It has been shown by sequences analysis of PS I that aspartate is present at significantly higher frequency as expected from random at position -4 in Chl binding pockets . This further supports the fitness of aspartate at position -4 in the close vicinity of BChl and its potential stabilising role at the BChl-protein interface.

The side chain thiol group of the cysteine, although a soft H-bond donor (Popot & Engelman 2000), could participate in H-bonding to BChl-B850. Although less frequent, it is favoured in a low dielectric environment (Popot & Engelman 2000). However statistical

analysis (Adamian & Liang 2001) indicates that the disulfide bonds are not frequently found in membrane proteins and do not play important roles in maintaining the stability of the TM helix. Cysteine has a small surface ( $135 \text{ \AA}^2$ ) and volume ( $108.5 \text{ \AA}^3$ ), quite similar to serine, and also has capacity to form H-bond. As shown in the modelled structure of LH2  $\alpha\text{WT}_{\text{S-4/C}}$  one of the rotamers makes an H-bond with the C13<sup>1</sup> of  $\beta$ -BChl-B850 (figure 3.17). In accordance, the *in situ* absorption spectrum of LH2  $\alpha\text{WT}_{\text{S-4/C}}$  (figure 3.14) is very similar to the spectrum of WT (table 3.1).

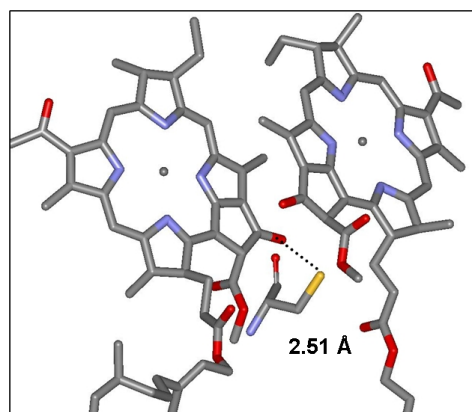


**Figure 3.17: Modelled structure of LH2  $\alpha\text{WT}_{\text{S-4/C}}$ .** Cysteine may participate in hydrogen bonding with the keto carbonyl C13<sup>1</sup> (score -4) of  $\beta$ -BChl-B850.

Histidine is not often found in TM helices; however, it is very important as ligand of prosthetic groups such as Chl and heme molecules. Histidine replaced the serine at position -4 in the mutant LH2  $\alpha\text{WT}_{\text{S-4/H}}$ . There is a possible hydrogen bond between the histidine and the C17<sup>3</sup> keto carbonyl or with the oxo C13<sup>1</sup> from the  $\alpha$ -BChl-B850. In LH2  $\alpha\text{WT}_{\text{S-4/H}}$ , there is only a minor blue shift in the red most absorption band (table 3.1). The level of assembled LH2  $\alpha\text{WT}_{\text{S-4/H}}$  is lower than that of LH2 WT, indicative of some disturbance in LH2 structural stability and/or in assembly (figure 3.14).

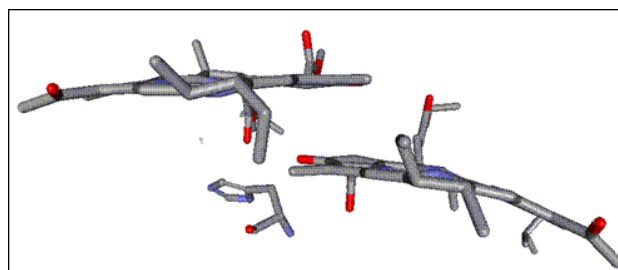


**Figure 3.18: A view of the structure from LH2  $\alpha\text{WT}_{\text{S-4/H}}$ .** Note that histidine and BChl-B850 are in parallel plane.

Curiously, although histidine has quite a large volume and surface (similar to Ile and Leu, see below), the spectral properties of the mutant LH2  $\alpha\text{WT}_{\text{S-4/H}}$  are not altered significantly

in comparison to LH2 WT. There are three rotamers of the His at position -4 in which the imidazole lies parallel to one ring of the macrocycle from BChl-B850 (figure 3.18). Possibly, the imidazole ring of histidine interacts favourably with the tetrapyrrol of the BChl-B850. Statistical analyses of plant photosystems have shown that histidine residues are frequently present in Chl-binding pockets, particularly often in the close vicinity of ring A of the macrocycle .

Asparagine is similar to aspartate, but has larger surface ( $160 \text{ \AA}^2$ ) and volume ( $114 \text{ \AA}^3$ ), and its side chain groups are not ionisable. The red most absorption band of LH2  $\alpha\text{WT}_{\text{S-4/N}}$  is blue shifted from  $\sim 849 \text{ nm}$  to  $\sim 845 \text{ nm}$ , and the band at  $\sim 760 \text{ nm}$  is clearly discernable indicating some disturbances in the complex assembly in the membrane (figure 3.14, table 3.1). According to the model structure, asparagine at position -4 could participate in H-bonding with C13<sup>1</sup> of the  $\beta$ -BChl-B850 (figure 3.19).

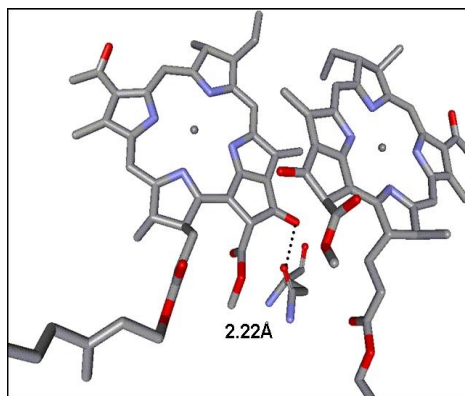


**Figure 3.19: Modelled structure of LH2  $\alpha\text{WT}_{\text{S-4/N}}$ .** Asparagine may participate in hydrogen bonding with the keto carbonyl C13<sup>1</sup> (score -5) of  $\beta$ -BChl-B850.

As obvious from the *in situ* absorption spectrum (figure 3.14), replacement of serine -4 by glutamine supports the assembly of complex. In contrast, glutamate, which is closely similar in structure and volume, inhibits assembly of the complex. However, glutamine is a residue with smaller surface ( $180 \text{ \AA}^2$ ) than glutamate ( $190 \text{ \AA}^2$ ), and its side chain is not ionisable. The model structure shows that the amino side chain group of Gln may participate in H-bonding to BChl-B850 (not shown).

In summary, from a total of 16 amino acid tested at position -4 of the  $\alpha$ -subunit (proline, arginine, tryptophan and threonine have not been tested), there are four residues which when substituting for serine inhibit the assembly of LH2 complex (figure 3.14). These are the either charged and relative large residues (lysine and glutamate) or very bulky aromatic residues (tyrosine and phenylalanine). Remarkably, most of the residues replacing serine at position -4, produced LH2 complex with some impediment in functional and structural properties. The critical importance of the residues at this position is thus

demonstrated by its influence on the absorption properties hence, the functional modulation of the light harvesting active BChl-B850. Apparently, there is a correlation between the volume of the residues at position -4 and the position of the maximal absorption of BChl-B850 (figure 3.20). In essence, the spectral shifting of BChl-B850 absorption band is linearly proportional to the residues volume (exceptions are the residues histidine and methionine which do not induce spectral changes). Lys, Tyr and Phe are the residues with the largest volume and surface tested, and in addition Lys possesses a charged side chain as well as Glu. These findings indicate that the volume is the critical parameter for complex assembly, but also charge is definitely destabilising. However, if the residues contribute to the stability favourably, like H-bonding and/or a suitable packing volume, a charged side chain is compatible even in the interior of the lipid bilayer at the BChl/protein interface.

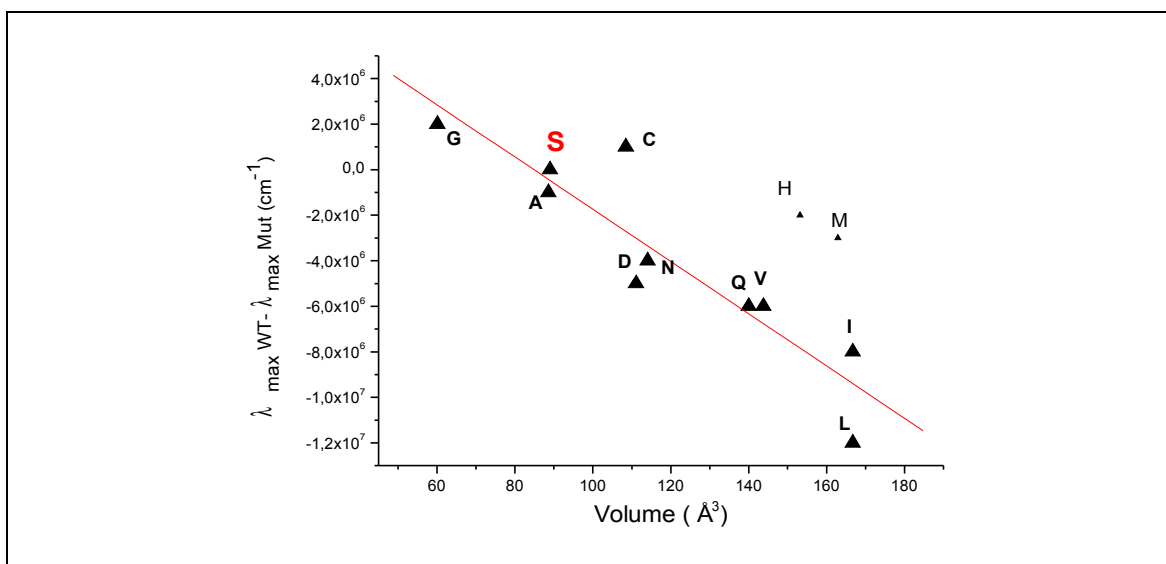


**Figure 3.20: Shift in the BChl-B850 absorption maximum as a function of residue (-4) volumes.** Note that the blue shifting is linearly increasing with the volume of the residue at position -4.  $\lambda_{\max}$  indicates the maximum of the BChl-B850 red most transition. Blue shifts are represented by negative and red shift by positive numbers.

Curiously, the correlation does not hold well for Leu and Ile, which have identical volumes but in LH2  $\alpha$ WT<sub>S-4/L</sub> the blue shift is larger than that in LH2  $\alpha$ WT<sub>S-4/I</sub>. The relationship between the shifting of the Q<sub>y</sub> absorption maximum of BChl-B850 and the surface of  $\beta$ -BChl-B850 that is covered by each amino acid is shown in figure 3.21.

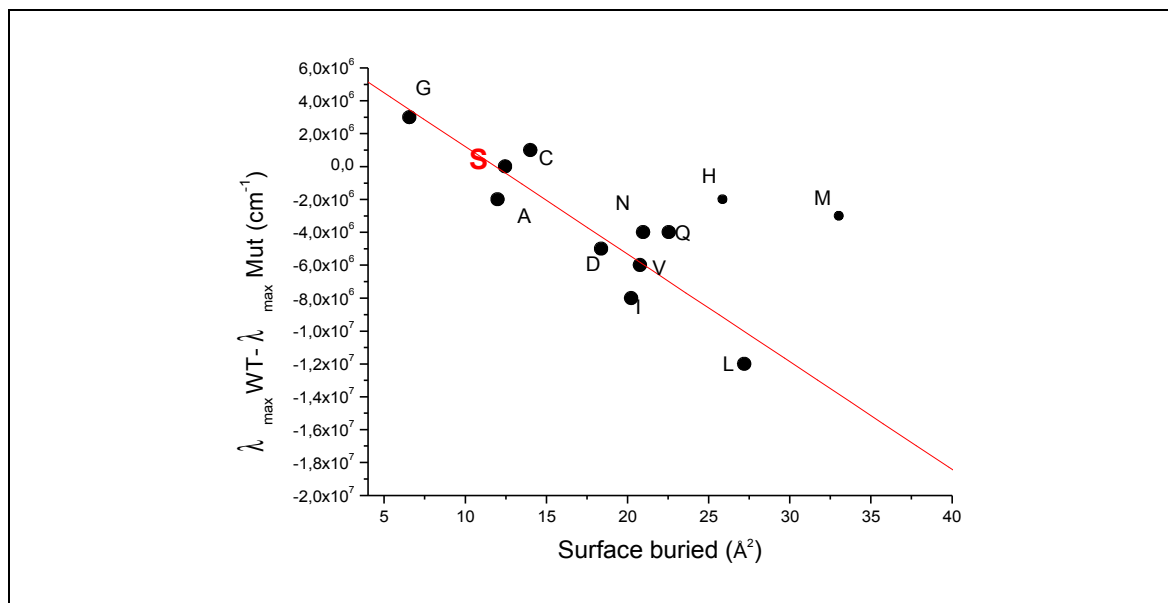


**Figure 3.21: Correlation between the shift in the BChl-B850 absorption maximum and the  $\beta$ -BChl-B850 surface buried by the residue at position -4.**

The linear correlation between the  $\beta$ -BChl-B850 and the blue shifting of the absorption maximum of BChl-B850 (figure 3.21) indicates that packing between residue -4 and the BChl critically influences the BChl geometry. It appears that in the case of the residues Ile and Leu, leucine has a larger contact surface with  $\beta$ -BChl-B850 than isoleucine. This may lead to a more pronounced displacement of the pigments from their original position and relative to each other, resulting in more pronounced shifts of the red most transition of BChl-B850.

In conclusion: the volume of the residue at position -4 is critical for the proper assembly of BChl-B850 possibly by modulating the exact BChl geometry/configuration in its pockets.

### 3.3 Conclusions

In the model protein LH2  $\alpha$ AL<sub>16</sub>, the absorption and CD spectra are nearly identical with those of the native LH2 complex, suggesting that the BChl-B850 geometry and overall complex assembly is retained. The fluorescence excitation spectrum of the mutant LH2  $\alpha$ AL<sub>16</sub> shows that the efficient energy transfer occurs from the Car and BChl-B800 to BChl-B850, and hence that the novel complexes function as LH units. However, structural stability is significantly reduced.

A hydrogen bond between the hydroxyl group of  $\alpha$ S(-4) and the C13<sup>1</sup> keto carbonyl group of the BChl-B850 is identified by Raman spectroscopy (figure 3.12) in the model LH2 and in WT LH2. The stability of the model LH2  $\alpha$ AL<sub>16/S-4</sub> is critically dependent on this H-bond.

On the contrary, the stability of the WT LH2 is little affected by the presence or absence of the hydroxyl group as demonstrated by the replacement of serine with alanine in LH2  $\alpha$  WT<sub>S-4/A</sub>. These findings indicate that the combination of H-bonding and residue packing at -4 determines its input to structure stability of BChl/protein assembly.

In essence, the residue at position -4 has a key function in the assembly of LH2 like BChl-proteins. Effects disruptive to the assembly may be amplified in the model sequence context devoid of native contacts, but could be compensated in the WT sequence by the cooperative contributions of the multiple native contacts at the BChl/protein interface.

The permutation of amino acids with different side chains showed that residues with large volume and charge are unfavourable at position -4 relative to the histidine ligand (glutamate, lysine, tyrosine, and phenylalanine) for the assembly antenna complex.

The volume of the residues appears to be the critical factor, clearly more important than charge, which is demonstrated, for example, by the fact that glutamate (pK 4,3) replacing serine at position -4, disrupts the assembly of the complex, while aspartate (pK 3,9), with very similar charge but smaller volume supports assembly. In addition, amino acids with large volume exhibit stronger changes in the maximal absorption band of the BChl-B850. The amino acids which have a larger interface with the  $\beta$ -BChl-B850 have also stronger blue shifts of the maximum absorption of BChl-B850. Even single replacements with aa abort the assembly of LH2 thus demonstrating the critical input of the residue at position -4. This indicates that the residue at position -4 critically contributes to the proper arrangement of BChl-B850 and the assembly of the LH2 antenna complex.

## CHAPTER 4

# Role of the stereochemical ligation of (bacterio)chlorophyll

### 4.1 Introduction

The folding and assembly of membrane proteins has been extensively studied during the last years. A detailed introduction on membrane protein folding has already been made in chapter 3, here the main points are briefly summarised again. The assembly of membrane proteins had been proposed to occur in two stages; in the first stage, the TM helices are inserted into a membrane. The driving force for insertion derives primarily from the transfer of hydrophobic side chains from water to the apolar region of the bilayer. In the second stage, the protein is then able to fold via the coalescence of the helices to form the native tertiary structure (Engelman & Steitz 1981, Popot & Engelman 1990, White & Wimley 1999).

The hydrophobic interactions play a role in the stabilizing the individual helices, the hydrophobic side chains make contact with the hydrophobic region the lipids, thus stabilizing a transbilayer location and, the hydrogens bonds that form in this process are strong in a low dielectric environment. Van der Waals packing forces play an important role in the folding of the membrane proteins, acting between helices, helices and lipids and between lipids. There are, also, interhelical H-bonds, which are particularly important for the stabilization of helix-helix interactions (Choma et al. 2000, Adamian & Liang 2002, DeGrado et al. 2003).

In cofactors binding proteins, the interactions between the cofactors and TM helices contribute significantly to the folding of the TM protein in the membrane. In photosynthetic proteins, the photoactive cofactors, Car and, particularly (B)Chl are very abundant and often contribute essentially to the assembly of the pigment protein complex. .

The (B)Chl belong to the cyclic tetrapyrroles, their central metals differentiate the major classes: iron in the hemes, and magnesium (and rarely zinc) in Chl and BChl. The presence of different peripheral substituents in the tetrapyrrole skeleton, as well as its hydrogenation state, further distinguishes these two groups of molecules. The structures of Chl and BChl are very similar (figure 4.1). The macrocycles of Chl *a* and BChl *a* differ

only at ring A and B BChl has one additional bond in ring B, and the substituent at ring A is an acetyl carbonyl group in BChl and a vinyl group in Chl.

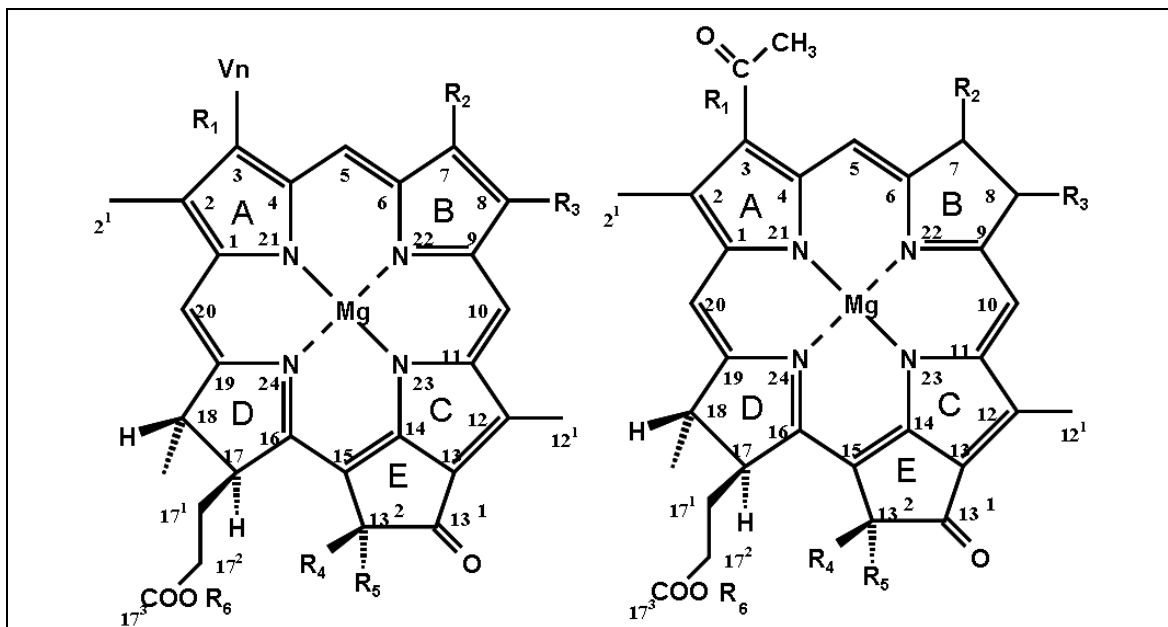


**Figure 4.1: Chlorin structures:** Left Chl a and right BChl a. Note that two structures differs only (i) in ring A in R1, vinyl for Chl and acetyl for BChl; (ii) Ring B in Chl a has a double bond. The numbering system is according to IUPAC rules. R1 is either acetyl (BChl) or vinyl (Chl). Note, that R3 (ethyl), R5 (carbomethoxy) and R4 (hydrogen) are identical in BChl and Chl.

The carbonyl groups frequently interact with the surrounding polypeptide and/or neighbouring pigment. H-bonding to the acetyl carbonyl of BChls has been recognized to modulate the spectral and, although still disputed, redox properties of these molecules. The H-bonding to the C13<sup>1</sup> keto carbonyl at the isocyclic ring, which is common to all Chls and BChls, seems to be widespread but appears to have less or no effects on their electronic properties. The PS I, whose structure has been solved at 2.5 Å comprises more than 10 TM subunits and contains nearly 100 Chl-pockets and thus constitutes a considerable data base for (B)Chl bindings studies. The majority of the polar groups of Chl, in particular the C13<sup>1</sup> keto carbonyl group, are likely to be H-bonded to polypeptide residues in close vicinity (see also in Chapter 3).

The ligation to the central magnesium has long been recognized to be critical for the binding of BChl and thus the assembly of BChl protein. However, only recently, the stereochemical aspect of (B)Chl ligation has been recognised in (B)Chl protein assemblies (Balaban 2003, Balaban 2005, Oba & Tamiaki 2002).

Usually, (B)Chl has 5 stereocenters, the two faces of (B)Chl are diastereotopicity distinct (figure 4.2). The sixth of the chiral centers is the Mg, which has, if attached to protein, as

fifth ligand an amino acid side chain. Another one is the 17-propionyl side chain connecting the phytol moiety to the macrocycle. Therefore, (B)Chl has an up and down face and depending on the positioning of the liganding residue relative to the (B)Chl face, the ligation is called  $\alpha$ - or  $\beta$ -ligation. If the amino acid ligand and the 17-propionic acid phytol ester are positioned on the same side of the (B)Chl macrocycle, the ligation is of the  $\beta$ -type and if they are on opposite sides, the ligation is of the  $\alpha$ -type (figure 4.2).

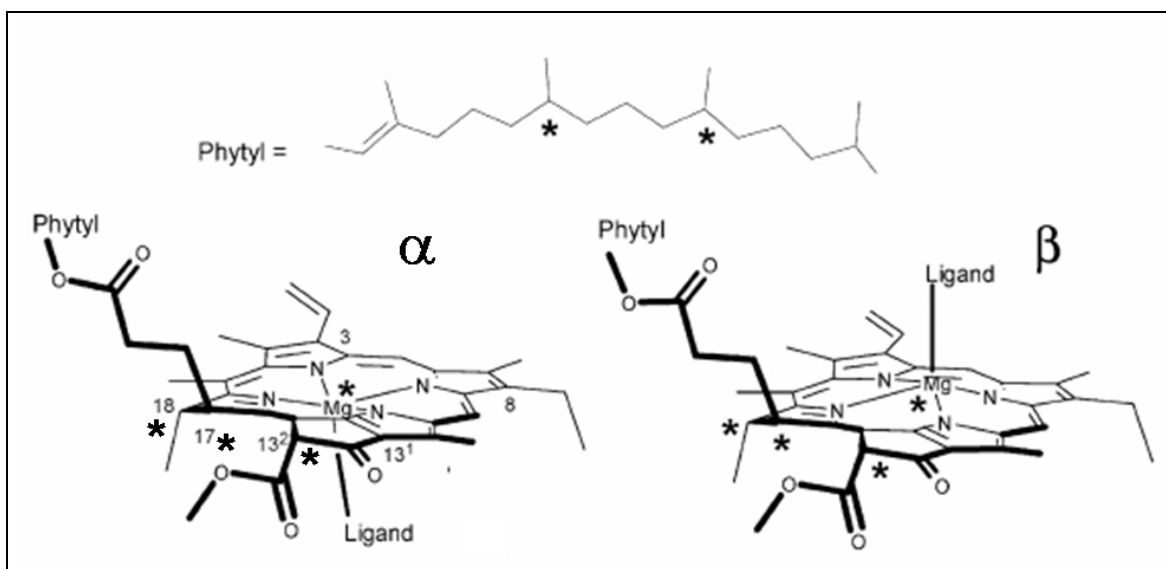


**Figure 4.2:** The diastereotopic  $\alpha$ - and  $\beta$ -ligation of tetrapyrroles. Asterisks denote chiral centers (Balaban 2005).

The two possible geometries lead to diastereomers which should have different chemical and physical properties. The  $\beta$ -ligation is energetic unfavourable in comparison to  $\alpha$ -ligation (Balaban 2003). The  $\alpha$ -ligation was estimated to be 4.3 kJ/mol more stable than the  $\beta$ -ligation (Oba & Tamiaki 2002). Additionally, in the absence of any ligand or oligomerization, a water molecule remains tightly bound to BChl. This H<sub>2</sub>O molecule has been encountered in the  $\alpha$ -orientation only (Balaban 2005). The  $\alpha$ -ligated (B)Chl are generally much more abundant in photosynthetic complexes compared to  $\beta$ -ligated (B)Chl (Balaban 2003, Balaban 2005). In PS I, for example, there are 96 Chls, and only 14 of them are ligated in  $\beta$ -position. In PS I, all the Chl ligands have been strictly conserved during evolution within different species, and the incorporation of the Chl in the protein matrix is a highly conserved process which does not occur randomly (Balaban 2003). In LHCII of green plants, there are 8 Chls *a* and 6 Chls *b*, and only 2 and 1 are in  $\beta$ -coordination, respectively. It has been noted that the  $\beta$ -coordination occupies key positions for the excitation energy transfer and also could quench their triplet states efficiently (Oba & Tamiaki 2002, Balaban 2005). It has been speculated that the  $\beta$ -ligation is correlated with strong excitonic interactions leading to the most red shifted pigments

and thus favouring the ET to either neighbouring complexes or directly to the special pair of (B)Chls within RC (Balaban 2003, Balaban 2005). This however has not been verified by experimental studies. The role of the diastereotopic distinct ligation of (B)Chls thus remains to be substantiated.

In LH2 there two BChl-B850 are ligated in  $\beta$ -position, and the BChl-B800 is ligated in  $\alpha$ -position. Thus, the LH2 from *Rb. sphaeroides* may serve as a model system for the elucidation of the role of stereochemical ligation of (B)Chl. The aim of the work described in this chapter has been to further explore this role by

- site-directed mutagenesis of the residues interacting with the  $\beta$ -ligated BChl-B850 in the TM proteins of LH2 from *Rb. sphaeroides*, and subsequent spectroscopic and structural characterization of these mutants;
- substantiating the mutagenetic work by statistical analysis of BChl-protein interactions, in particular, of  $\alpha$ - and  $\beta$ -ligated Chl, in PS I and PS II.

## 4.2 Results and discussion

### 4.2.1 Disruption of the H-bond in LH2 $\alpha$ WT<sub>S-4/G</sub>

In the peripheral antenna of *Rb. sphaeroides*, there are three BChl, two of them are ligated in  $\beta$ -ligation, and these are the BChl-B850, whereas the BChl-B800 is ligated in the  $\alpha$ -position (figure 4.3).

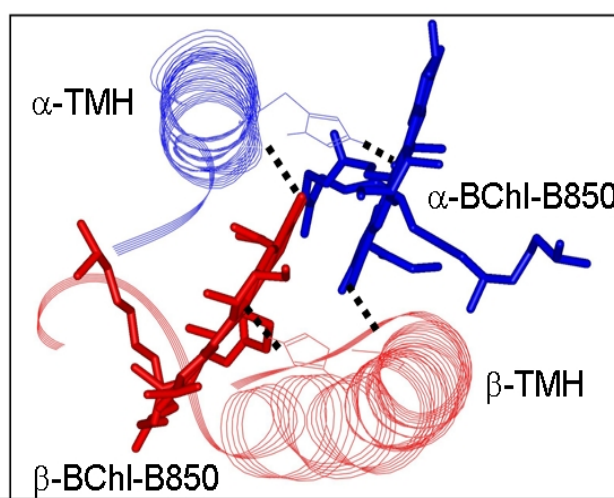


**Figure 4.3: The  $\beta$ -ligated BChl-B850 and the TM helices.** View of the  $\beta$ -ligated BChl-B850 and their binding helices in the LH2 high resolution structure of *Rps. acidophila*. The ligation to the central magnesium and putative H-bonds are indicated by lines.

It has previously been shown that the C13<sup>1</sup> keto carbonyl group of  $\beta$ -BChl-B850 is H-bonded to the hydroxyl group of the serine -4 of the  $\alpha$ -subunit (figures 3.11, 3.12, chapter 3). To study the impact of this H-bond on the assembly of LH2, the serine at position -4 has been replaced by glycine. Glycine is the smallest amino acid and its side chain is a single hydrogen atom. This mutation removes the side chain in the close vicinity of the C13<sup>1</sup> oxo of the  $\beta$ -BChl-B850 and should thus effectively disrupt the H-bond to the serine -4.

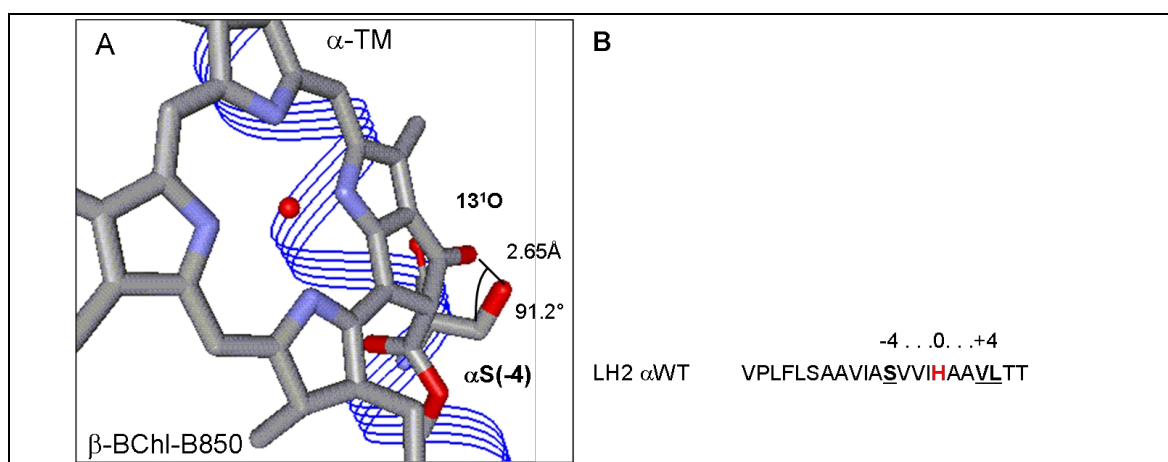


**Figure 4.4: H-bonding in peripheral antenna LH2.** **A.** Detail of the H-bond between the C13<sup>1</sup> oxo of the  $\beta$ -ligated BChl-B850 and the OH group of serine -4 in the modelled structure of *Rb. sphaeroides* (chapter 3). The distance between serine and C13<sup>1</sup> is 2.65 Å and the angle is 91.2°. **B.** Amino acid sequences of  $\alpha$ -TMH. The histidine is red and the residues mutated in this work are underlined.

The assembly of the LH2 complex may be monitored directly by absorption spectroscopy, because significant spectral alterations accompany the BChl-BChl and BChl-polypeptide association in this complex (figure 4.5). Most prominent of the typical LH2 absorption spectrum are the red-shifted NIR absorption bands at ~ 850 and 800 nm of the BChl-B850 and BChl-B800. In organic solvent BChl, when free of interactions with other pigments and/or protein, absorbs at ~ 770 nm. The *in situ* spectra of LH2  $\alpha$ WT<sub>S-4/G</sub> as compared to LH2 WT are shown in figure 4.5. The substitution of  $\alpha$ -serine at position -4 with glycine results in significant reduction of the absorption bands at ~850 and ~800 nm relative to the absorption band at ~760 nm. This indicates that the free BChl accumulates in cells expressing LH2  $\alpha$ WT<sub>S-4/G</sub> due to either significant disturbance in the association of LH2 or the enhanced disintegration of already assembled LH2 complexes.

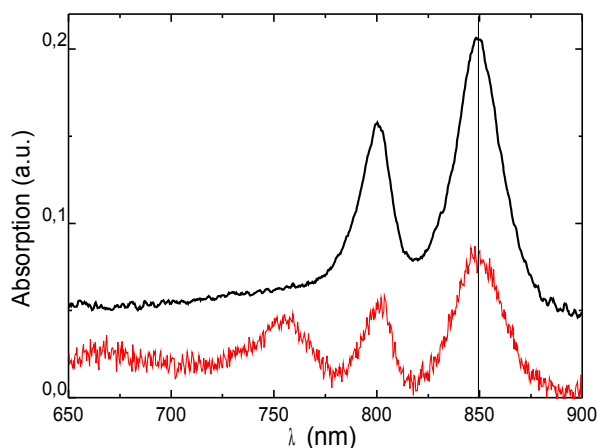


**Figure 4.5:** *In situ* absorption spectra of LH2 WT (black) and LH2  $\alpha\text{WT}_{\text{S-4/G}}$  (red). The spectra are taken of *Rb. sphaeroides* colonies directly on growth plates.

In addition, it has been observed that LH2 in LH2  $\alpha\text{WT}_{\text{S-4/G}}$  is expressed only transiently. In cells expressing LH2 WT, the assembled complex is detected during 10 days minimum, whereas in the cells expressing LH2  $\alpha\text{WT}_{\text{S-4/G}}$ , assembled complexes are observed only at the onset of growth but are absent from the cells beyond day two (figure 4.6). In addition, only ~ 5% of the colonies examined expressed LH2  $\alpha\text{WT}_{\text{S-4/G}}$  complex.

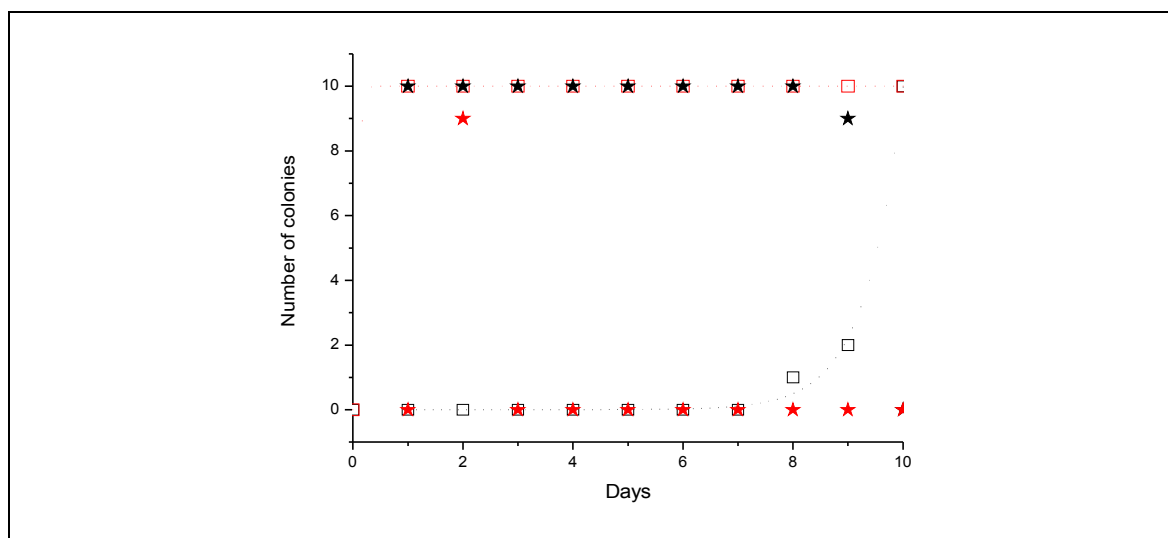


**Figure 4.6:** Number of colonies expressing LH2  $\alpha\text{WT}_{\text{S-4/G}}$  (red) in comparison to LH2 WT (black) over time. The square indicates the absorption bands at ~ 760 nm and the stars the band at ~ 850 nm (see text for further details).

This is further supported by directly quantifying the amount of assembled LH2 in the membrane. Quantification of total protein content *versus* LH2 content in the membrane indicates that the ratio of total protein to LH2 (as judged by the 850 content) is 10:2 for WT

LH2 and 10:0.5 for LH2  $\alpha$ WT<sub>S-4/G</sub> (table 4.1). Thus, LH2 WT seems to be approximately four times more abundant in the membranes than LH2  $\alpha$ WT<sub>S-4/G</sub>. This directly demonstrates that the replacement of serine with glycine results in reduced amounts of LH2 in the mutant cells. Moreover, the *in situ* absorption spectra in which the ratio of the 760/850 bands is increased, as well as the significantly shorter time span of LH2  $\alpha$ WT<sub>S-4/G</sub> expression support this finding.

	LH2 WT	LH2 $\alpha$ WT <sub>S-4/G</sub>
OD <sub>850</sub>	1.91	1.43
LH2 (g/l)	0.096	0.0714
Total protein (g/l)	0.495	1.529
LH2 content (% of total protein)	19	4.7

**Table 4.1: Quantification of LH2 of LH2 WT and LH2  $\alpha$ WT<sub>S-4/G</sub> in membranes.** For the estimation of LH2 protein content, the extinction coefficient of BChl-B850 is taken 120 mM<sup>-1</sup> cm<sup>-1</sup> (Clayton & Clayton 1981a) and 6000 kDa is taken as approximate MW for both subunits. The protein in the membrane is determined by using BCA™ kit (material and methods).

To test whether the replacement by glycine *per se* leads to assembly problems, two additional residues were replaced by glycine. One of them is  $\alpha$ -valine +3, which is in close contact with both the  $\alpha$ - and  $\beta$ -BChl-B850 in the modelled structure of *Rb. sphaeroides* and also in the crystal structure of *Rps. acidophila*. In particular, it has contact with in C8<sup>2</sup> of the ethyl group at the B ring of  $\alpha$ -BChl-B850 and with C8, C9 and C10 of  $\beta$ -BChl-B850 (figure 4.7). However, it is unlikely that valine participates in H-bonding, as valine does not have side chain groups which are likely to partake in strong H-bonding.

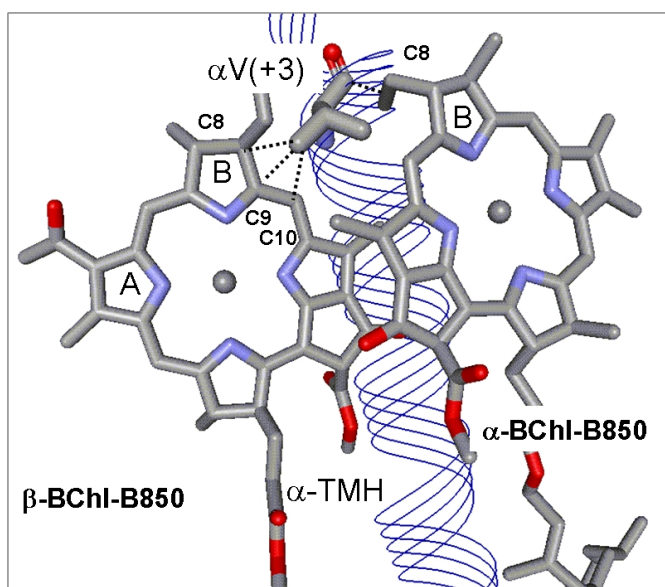


**Figure 4.7: Details of the contacts between BChls and  $\alpha$ -valine at position +3.** Depicted are the contacts to atoms are within a radius of  $\leq 5\text{\AA}$  in the modelled structure of *Rb. sphaeroides* as indicated by dotted lines.

The *in situ* absorption spectrum of LH2  $\alpha\text{WT}_{V+3/G}$  has the typical BChl-B850 and BChl-B800 absorption bands with maxima at  $\sim 850$  and  $\sim 800$  nm. A blue shift (from 850 to 845 nm) in the absorption band indicates some slight structural rearrangements in LH2  $\alpha\text{WT}_{V+3/G}$ . There is also a band at  $\sim 760$  nm, indicating that the assembly of this mutant is somewhat impaired (figure 4.8).

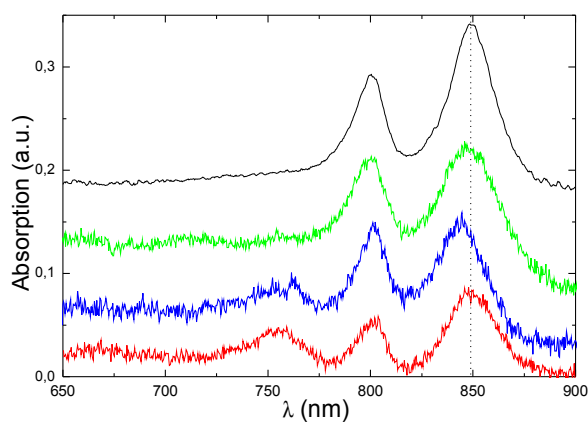


**Figure 4.8:** *In situ* absorption spectra of LH2 WT (black), LH2  $\alpha$ WT<sub>L+4/G</sub> (green), LH2  $\alpha$ WT<sub>V+3/G</sub> (blue) and LH2  $\alpha$ WT<sub>S-4/G</sub> (red). The spectra are taken of *Rb. sphaeroides* colonies directly on the growth plates LH2.

The other residue which has been tested by glycine scanning mutagenesis is the leucine at position +4, which is strictly conserved in the LH2- $\alpha$  (figure 3.4, chapter 3) however has no contacts with the dimer BChl-B850. The absorption spectrum of LH2  $\alpha$ WT<sub>L+4/G</sub> has two NIR absorption bands, typical for LH2 spectra, whereas the band at ~760 nm is entirely absent (figure 4.8). The packing values estimated are very different for glycine and valine (0.57 versus 0.49) as well as leucine (0.57 versus 0.47) at membrane embedded helix-helix interfaces, whereas they are rather similar for glycine and serine (0.57 versus 0.55). The altered packing values may thus account for the minor destabilization of the LH2  $\alpha$ WT<sub>V+3/G</sub> which closely interacts with BChl-B850.

In addition, glycine has been shown to be destabilizing when placed within the last 5 residues of a TM helix. Both, valine and leucine at position 3 and 4, respectively, are positioned close to the C-terminal end of the  $\alpha$ -TMH, in contrast to serine at position -4, which is close to the helix core. The glycine residues at positions +3 and +4 could thus entail multiple destabilizing affects unlikely to arise at position -4.

Nevertheless, replacement of serine with glycine has major effects on the stable expression of the LH2 pointing at the importance of the H-bond to the BChl-B850, which is ligated to BChl in the  $\beta$ -position. Taken together, these data indicate that the stable assembly of the antenna complexes is significantly impaired by the disruption of the H-bond to the BChl-B850, which is ligated to BChl in the  $\beta$ -position.

The H-bonding interaction state of the BChl of LH2 WT and LH2  $\alpha$ WT<sub>S-4/G</sub> has been further explored by RR spectroscopy. For a detailed discussion of the LH2 Raman spectrum of LH2 (figure 3.12, chapter 3). Here the interaction state of the C13<sup>1</sup> keto carbonyl is examined to further understand the role of  $\beta$ -ligated BChl in pigment-protein interactions. In figure 4.9, the resonance Raman spectrum of LH2 WT in comparison to LH2  $\alpha$ WT<sub>S-4/G</sub> is shown. The main change in the spectrum of LH2  $\alpha$ WT<sub>S-4/G</sub> is the considerable up-shift of the 1651 cm<sup>-1</sup> band to ~1674 cm<sup>-1</sup>, indicating that the H-bond to the C13<sup>1</sup> keto carbonyl has been disrupted or significantly weakened.

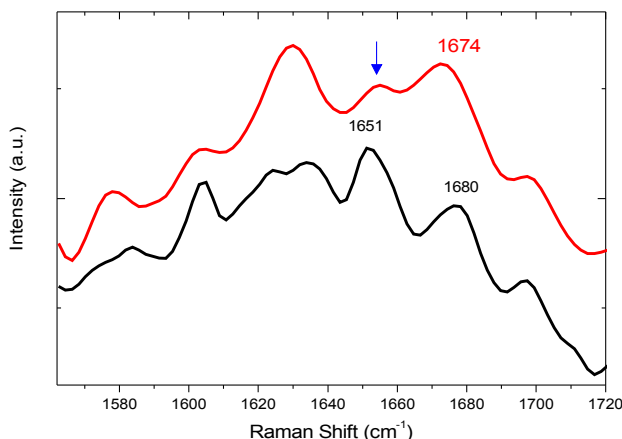


**Figure 4.9:** RR spectra of LH2 WT and LH2  $\alpha\text{WT}_{\text{S-4/G}}$ . The arrow indicates the band at  $1651\text{cm}^{-1}$ .

This value ( $1674\text{cm}^{-1}$ ) is still somewhat up-shifted as compared to the expected stretching frequency value of a free keto carbonyl group ( $1680\text{cm}^{-1}$ ). This may be due to a particularly polar environment around the keto carbonyl provided, for instance, by proximity of the imidazole ring of the histidine at position 0 of the  $\beta$  polypeptide. It is of note that, upon mutate serine to glycine a clear but minor component appears at  $1655\text{cm}^{-1}$  as a shoulder to the large  $1674\text{cm}^{-1}$  band. This component is also present in the spectra of the mutant LH2  $\alpha\text{WT}_{\text{S-4/A}}$  (figure 3.12, chapter 3), although less visible because of the larger shift of the  $1651\text{cm}^{-1}$ . The intensity of this smaller component is  $\sim 10\%$  of that of the main C=O stretching band. The origin of this minor component is unclear, and it could suggest some heterogeneity in the sample. However, it is not uncommon that such a minor component is found in the resonance Raman spectrum of bacterial light harvesting complexes. In LH1 WT, isolated or in the membrane, a small component at  $\sim 1680\text{cm}^{-1}$  has been described, although all of the stretching modes from the four groups of the two unequivalent BChls have been attributed in these complexes. These smaller components could be the molecular reflect of the intrinsic disorder in the LH structure, which, in the case of LH2, might result in the breathing of the H-bond in these complexes ( $1655\text{cm}^{-1}$  is the expected frequency for free-from-interaction acetyl carbonyl groups). In any case, the resonance Raman spectrum shows that the H-bond in the mutant LH2  $\alpha\text{WT}_{\text{S-4/A}}$  is strongly altered or disrupted.

#### 4.2.2 Thermal stability of the LH2 $\alpha\text{WT}_{\text{S-4/G}}$ complex

To examine the contribution of the H-bond between the serine -4 and the C13<sup>1</sup> keto carbonyl group of  $\beta$ -BChl-B850 to the structural stability of LH2, the thermal stability of the

LH2  $\alpha$ WT<sub>S-4/G</sub> has been determined by monitoring the CD signal of the BChl-B850 during heat denaturation. The cooperative thermal unfolding of LH2 complex is recorded of purified membranes and isolated complexes (figure 4.10).

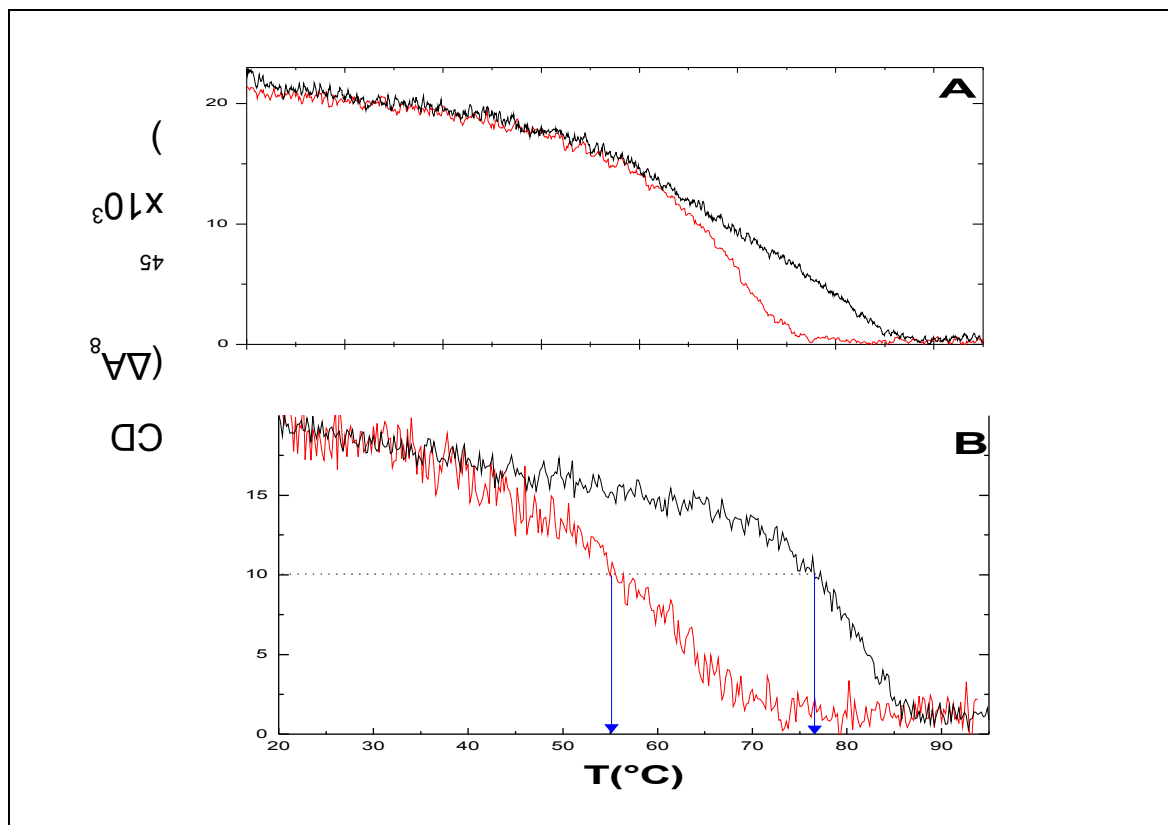


**Figure 4.10: Thermal denaturation of LH2 WT (black) and LH2  $\alpha$ WT<sub>S-4/G</sub> (red).** The changes of the CD signal at 845 nm during heating in membranes (A) and in isolated complexes (B). The arrows indicates the  $T_m$ .

The thermal stability of LH2  $\alpha$ WT<sub>S-4/G</sub> as compared with LH2 WT is clearly reduced in membrane and detergent (figure 4.10). Interestingly, the denaturation in native membranes covers a much wider temperature range in comparison to the process in detergent. In the membranes, the loss of BChl-B850 signal is accelerated for LH2  $\alpha$ WT<sub>S-4/G</sub> in particular at higher temperatures. This indicates changes in the unfolding pathways and/or denaturation rates in the mutant. Possibly, the rate of dissociation of BChl from the apoproteins is accelerated in LH2  $\alpha$ WT<sub>S-4/G</sub>, resulting in the altered cooperativity. Curiously, model LH2, in which the BChl-B850 binding site has been redesigned, also shows changed cooperativity. In this model LH2 most native contacts at the BChl-B850/protein interface have been reduced or eliminated and thus, the BChl are likely to be only weakly attached (figure 3.10 Chapter 3). In detergent, the difference in structural stability between LH2  $\alpha$ WT<sub>S-4/G</sub> and LH2 WT is even more pronounced. The  $T_m$  of LH2 WT (~ 76 °C) is approximately 20 °C higher than the  $T_m$  LH2  $\alpha$ WT<sub>S-4/G</sub>, (~ 55 °C). The major

difference in stability of the isolated complexes suggests that the decrease in structural stability is not related to changes in the membrane lipid composition or the protein/lipid ratio.

The acceleration of the decay of the CD signal and the shift of lower temperatures in LH2  $\alpha$ WT<sub>S-4/G</sub> in comparison with LH2 WT shows that the removal of the H-bond results in an inherently less stable complex. If, *a priori*, also less complex is assembled cannot be excluded at this point. The formation of H-bonds is energetically more favourable in the hydrophobic interior of the lipid bilayer than in a hydrophilic milieu, because of the low effective dielectric environment of the lipids. This has also been demonstrated experimentally by comparison to the formation of intramolecular H-bonding of model compounds in Me<sub>2</sub>SO and water (Shan & Herschlag 1996). Nevertheless, additional effects such as packing defects could contribute to the significantly impaired assembly of LH2 in the membrane. In any case, the acceleration of the decay in the CD signal and the shift to lower temperatures in LH2  $\alpha$ WT<sub>S-4/G</sub> in comparison to LH2 WT shows that the removal of the H-bond results in an inherently less stable complex.

The H-bonding motif involves BChls that are ligated in the  $\beta$ -position by a ligand attached to one TM helix and are H-bonded to residues from another adjacent helix. Thus, in LH2, the H-bond to the  $\beta$ -ligated BChl-B850 knots the two helices to another one. Only in the  $\beta$ -ligation state, the C13<sup>1</sup> keto carbonyl groups are facing away from the binding helices and thus are available for interhelical interactions. Therefore, (B)Chl molecules that are ligated in the  $\beta$ -position are likely to have a key structural impact, particularly on the packing of (B)Chl/helix associates with each other. Situated at a critical position, e.g. the interface between two subunits as in the oligomeric LH2 makes the H-bonding motif a key factor in the stable assembly of this BChl-proteins.

### 4.2.3 Statistical analysis of (B)Chl-protein interactions depending on the Chl ligation state

To explore whether the H-bonding motif involving the  $\beta$ -ligated (B)Chl is more widespread, a statistical analysis has been performed of the high resolution structures of PS I and PS II. The pigment in these PS is primarily Chl *a*, which has a structure very similar to BChl *a*, of the LH2 (figure 4.1). In particular ring C and E including the C13 substituents are identical in the two molecules. In reconstitution studies it has been shown Chl may perfectly well replace BChl in LH2. In these studies, however, it has been concluded that the C13 substituents which are identical in BChl and Chl may not be modified and thus have a critical role in stabilizing the binding of (B)Chl (Scheer & Hartwich 1995).

In PS I, there are 96 Chl *a* and only 14 of them are ligated in  $\beta$ -position (Oba & Tamiaki 2002, Balaban 2003). Thus, PS I constitutes a useful system to analyse the binding pockets of the Chl, and, particularly, the role of the stereochemistry in Chl binding. The Chls binding pockets have been analysed for the interactions of  $\alpha$ - and  $\beta$ -ligated Chl and their immediate protein environment within a radius  $\leq 4$  Å. The contacts (defined as atoms within a radius  $\leq 4$  Å) between the apoproteins and the  $\alpha$ - and  $\beta$ -ligated are similar at the first sight (figure 4.11A and C). (i) The major numbers of contacts occur most frequently with the long substituents of the Chl macrocycle, particularly, in the rings B, C, and E. Of these, the C13<sup>3</sup> methoxy, the C13<sup>1</sup> and the C13 C=O groups and the methyl group of C12 have the highest number of contacts to the apoprotein of the PS I. (ii) Relatively infrequent are the contacts with the ring D, the atoms that make up the tetrapyrrole rings, and methane bridges. (iii) The distribution of the amino acids at the contact points is also similar for  $\alpha$  and  $\beta$ -ligated Chl; the histidine residues are frequently close to the nitrogen atoms (bind the central Mg atom). Notably, the aromatic residue, phenylalanine, is often found to be close to Chl, in particular, around atoms that have little contact to histidine residues. Next to them, the aliphatic residues, alanine and the aromatic residues, tyrosine and tryptophan, make up most of the contact to the Chl in the binding pockets of PS I. Polar residues are also present to a lesser extent, and rarely, charged amino acid are close to the Chls (figure 4.11A and C).

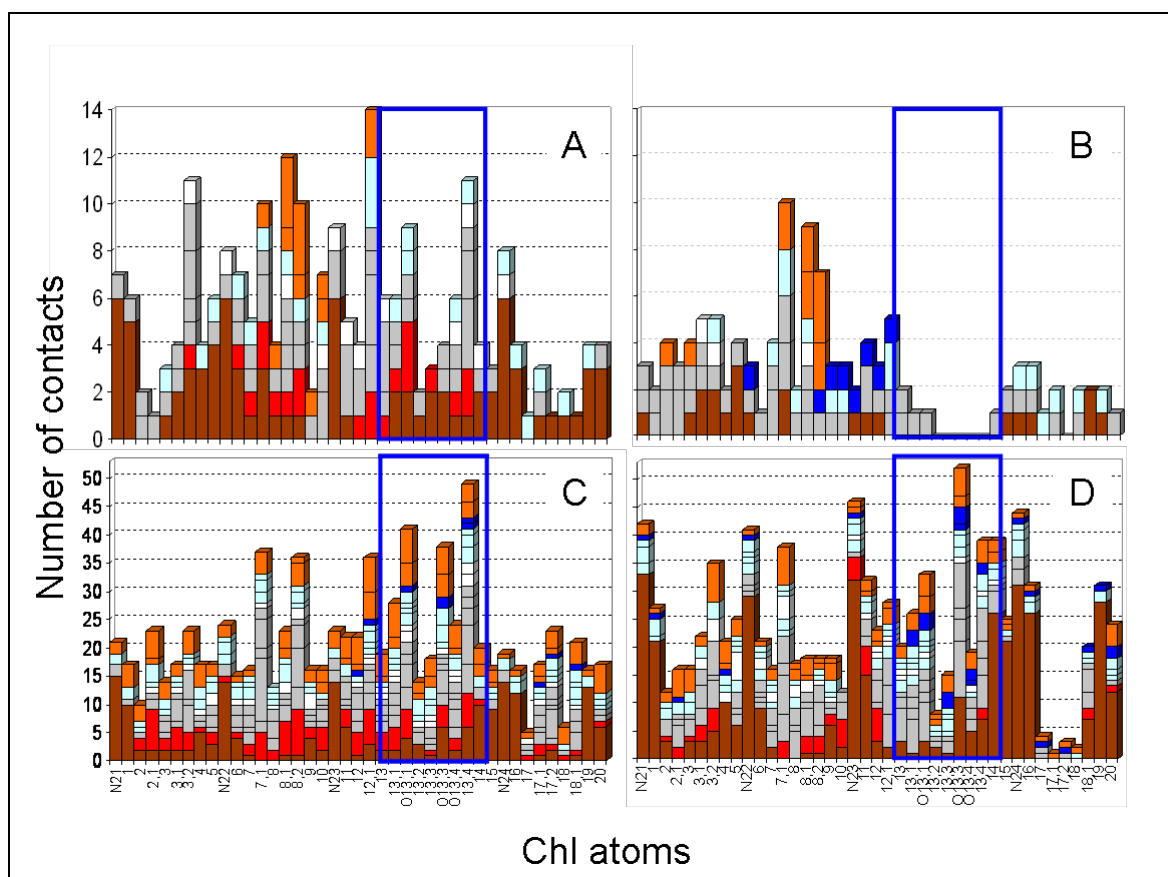


**Figure 4.11: Analysis of the Chl protein contacts in PSI.** Contacts to the proteinaceous environment, excluding contacts to binding helices, are shown for  $\beta$ -ligated Chls (A) and  $\alpha$ -ligated Chls (C). Contacts between residues of the binding-helices and the Chl atoms only are shown for  $\beta$ -ligated Chls (B) and  $\alpha$ -ligated Chls (D). The binding helices are defined as the helices that provide the ligand for the central magnesium atom. The colour coding is His (brown), Phe (red), Trp and Tyr (orange), Gly and Pro (white), polar (light blue), charged (dark blue) and the aliphatic residues (grey). The blue square enfolds the contacts to the atoms of the ring E.

There are major differences in the interaction of the two diastereotopic forms with their binding helices *i.e.* the helices that carry the ligating residue to the Mg of the Chl; (figures 4.11B and D). The major differences in interaction patterns are observed at the ring E and their substituents. In the case of  $\beta$ -ligated Chl (figure 4.11B), there exist very few close contacts between the residues of the helices and the atoms of the ring D of Chl. In particular, no contacts are observed between the keto carbonyl and methoxy groups of the C13<sup>3</sup> and C13<sup>1</sup> of the  $\beta$ -ligated Chls and atoms of surrounding polypeptide. In contrast, contacts between the  $\alpha$ -ligated Chl and these atoms, C13<sup>3</sup> and C13<sup>1</sup>, and also C13<sup>4</sup>, are very frequently observed. Additional differences in the Chl-binding sites are observed for the atoms of ring D and the initial C atoms of the 17-propionic phytol (figure 4.11D). In the case of the  $\alpha$ -ligated Chl, contacts are conspicuously low. These findings show that significant differences exist between the binding pockets of Chls, depending on the ligation state. The C13 substituents of Chls ligated in the  $\alpha$ -position are facing the binding helix, and thus, they are often in close contact with residues of these helices. The substituents of Chls ligated in  $\beta$ -position, however, face to the opposite side and are not in contact with the binding helix. Nevertheless there are a substantial number of contacts between the C13 substituents of the Chls ligated in the  $\beta$ -position and the protein environment as shown in figure 4.11A.

H-bonding between the C13<sup>1</sup> oxo of  $\beta$ -ligated Chl and protein residues of PS I and II are shown in the table 4.2. Remarkably, in the case of the C13<sup>1</sup> oxo from  $\beta$ -ligated Chl, almost every contact with the surrounding residues is identified as H-bonding interactions (~ 83 %). The majority of H-bonds are with neighboring helices and even the neighboring subunits majority of H-bond observed in the  $\beta$ -ligated Chl occur with neighboring residues which amount to 44% in PS I and 57% in PS II. Most of these H-bonds are thus with the neighboring helices and even the helices of neighboring subunits. The remaining C13<sup>1</sup> oxo atoms of the Chls ligated  $\beta$ -position are in close contact with other Chl and residues located in loop structures. Remarkably, the bindings of the C13<sup>1</sup> oxo in the  $\alpha$ -ligated Chl are significantly different. Most of contacts to the C13<sup>1</sup> oxo in the  $\alpha$ -ligated (47% in PS I and 39% in PS II) are to residues of adjacent loops structures, whereas contacts to

neighboring helices (10% PS I and 25% PS II) are less frequent, in particular to different subunits (3% in PS I and 7% in PS II). Most importantly, of the contacts between the protein and the  $\alpha$ -ligated Chl, few are identified as H-bond; (i) less than half of the contacts to the residues of the loops and binding helices in PS I, and (ii) less than 20% of the total contacts in PS II.

H-bonding to C13 <sup>1</sup> oxo								
	Chl $\beta$				Chl $\alpha$			
	PSI		PSII		PSI		PSII	
	H-bond	Contact	H-bond	Contact	H-bond	Contact	H-bond	Contact
Neighboring subunits <sup>a</sup>	14	14	14	14	0	3	0	7
Neighboring helices <sup>b</sup>	30	36	43	57	8	10	4	25
Binding helices <sup>c</sup>	0	0	0	0	6	14	7	18
Loops, parallel helices <sup>d</sup>	21	21	0	14	25	47	7	39
Neighboring pigment, H <sub>2</sub> O, etc <sup>e</sup>	ND	29	ND	14	ND	26	ND	7

**Table 4.2: H-bonding interactions of the Chl ligated in  $\beta$ - and  $\alpha$ - positions in PS I and PS II:** H-bonds and contacts of the Chl C13<sup>1</sup> oxo to polypeptide residues are listed as percentages of the total contacts. H-bonding interactions are identified by use of the graphics program WebLab View 3.7. (a) H-bonds between Chl molecules which are ligated by their central Mg to one subunit and residues of another subunit (e.g. Chl is ligated to subunit A, the C13<sup>1</sup> group makes a H-bond to a residue of subunit J); (b) H-bonds between Chl which are ligated to one TM-helix and the residues of neighbouring TM helices (other than the binding helices within one subunit); (c) H-bonds between Chl and residues of the binding helices; (d) H-bonds between Chl and residues from loop

structures (including helices parallel to the membrane); (e) H-bonds between Chl and neighbouring Chl or Cars (contacts to Chl are only included if no contacts to polypeptide are present).

Consequently, the statistical analyses of PS I and PS II suggests that the binding pockets of the two Chl ligation forms are clearly distinct: for  $\alpha$ -ligated Chl, the C13<sup>1</sup> oxo are observed to be in close vicinity of loops structures and the helices carrying the magnesium ligand as well as adjacent helices. Considerable percentage of H-bonding interactions, however, are only found to loops structures in PS I. In contrast, the C13<sup>1</sup> oxo of the Chls ligated in the  $\beta$ -position are predominantly in close contact with neighbouring helices and these are large identified as H-bond. It appears thus that the C=O groups of  $\beta$ -ligated Chls mediate interactions between adjacent helices, likely critically contributing to their packing and assembly.

### 4.3 Conclusions

The important role of H-bonding between (B)Chl ligated in the  $\beta$ -position and polypeptide for the assembly of (B)Chl-protein is demonstrated by site direct mutagenesis of the residue partaking in the H-bond. The disruption of the H-bond as evidenced by resonance Raman spectroscopy has a significant impact on (i) the stable expression of LH2 in the membrane and (ii) the structural stability of the LH2 complex. The decrease in the thermal stability is much more pronounced in the detergent as compared to the native membrane, indicating that the lipid environment elevates the resistance of the mutant LH2 complex against heat induced denaturation.

The statistical analysis of the PS I and II (figure 4.11, table 4.2) further support the finding that the  $\beta$ -ligated (B)Chls play a structural role in (B)Chl-proteins. It is found that the Chl ligated in the  $\beta$ -position in contrast to Chl ligated in the  $\alpha$ -position are frequently involved in H-bonding interactions with the adjacent helices even of neighbouring subunits.

The H-bonding motif characterised in this work involves (B)Chl that are ligated in the  $\beta$ -position by a ligand attached to one TM helix and are H-bonded to residues from adjacent helices. In the  $\beta$ -ligation state, the polar keto carbonyl and methoxy groups at the ring E point away from the binding helices and thus are available for tertiary interactions with structural elements other than their immediate binding helices. Therefore, (B)Chl molecules that are ligated in the  $\beta$ -position are likely to have a key structural impact, particularly, on the packing of (B)Chl/helix associates with each other. Situated at a critical position, such as the interface between two subunits, as in the oligomeric LH2 makes this motif a key factor in the stable assembly of this BChl-protein.



## CHAPTER 5

# Identification of critical factors for binding and functional modulation of carotenoids

### 5.1 Introduction

Cars are familiar to all of us, foremost through the orange-red and yellow colours of many foods like oranges, tomatoes, and carrots, and the yellow colours of many flowers. Cars occur widely in bacteria, fungi and algae, where they can be useful taxonomic markers. Some animals also use Cars for coloration, especially birds (yellow and red feathers), fish (gold fish and salmon), and a wide variety of invertebrate animals, where interaction with protein may modify their colour to blue, green or purple. They are also added as colorants to many manufactured foods, drinks and animal feeds, either in the form of natural extracts (e.g. annatto) or as pure compounds manufactured by chemical synthesis. The production of Cars by biotechnology is of increasing interest. In seaweed it already runs to hundreds of million tons per year.

Current Car research encompasses a wide variety of fields and interests including plant physiology, food science, environmental science, taxonomy, industrial chemical synthesis, biotechnology and medical research. Cars are important factors in human health. The essential role of  $\beta$ -carotene and others as the main dietary source of vitamin A has been known for many years. More recently, protective effects of Cars against serious disorders such as cancer, heart disease, and degenerative eye disease have been recognized, and have stimulated intensive research into the role of Cars as antioxidants and as regulators of the immune response system.

Cars are, along with Chls, the most abundant pigment found in nature. They are present in most organisms including humans, but can be synthesized only by plants and microorganisms. Cars are divided into two classes, the hydrocarbons (carotenes) and their oxygenated derivatives (xanthophylls). Both classes are, generally, made up of 40, sometimes to  $\pm 10$  carbons, which are composed of 7-8 isoprenoid units. They are joined in such a manner that the arrangement of isoprenoid units is reversed at the centre of the molecule so that the two central methyl groups are in a 1,6-position relationship and the

remaining non-terminal methyl groups are in 1, 5-positional relationship. Most of Cars may be formally derived from the acyclic  $C_{40}H_{56}$  structure (figure 3.1A,B).

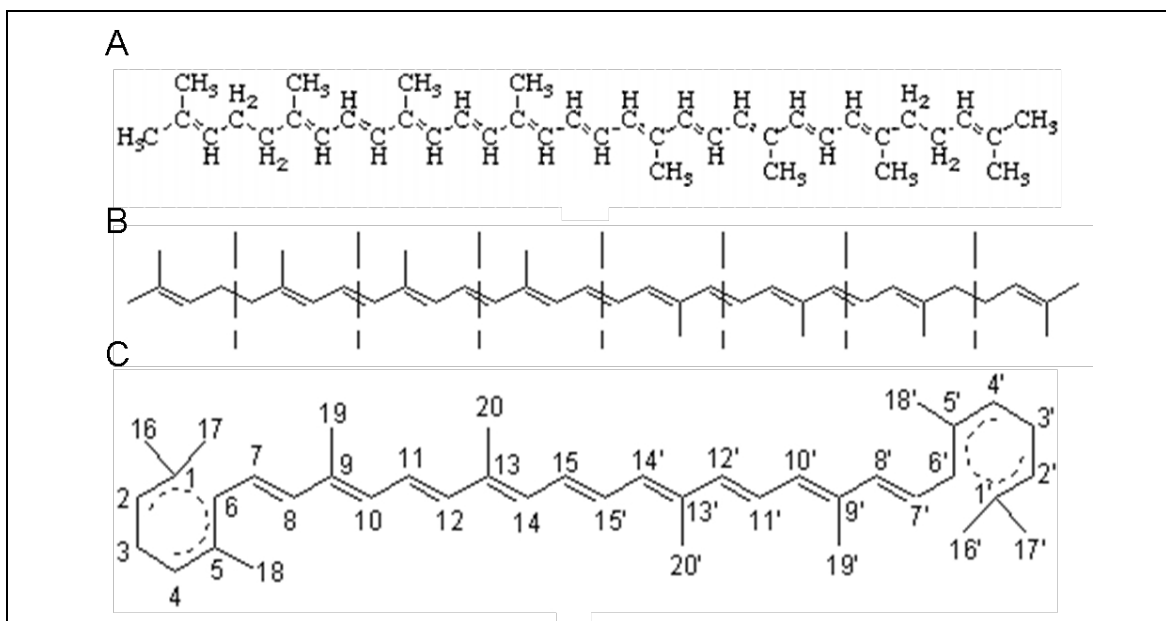


**Figure 5.1: Structure and nomenclature of Car according to IUPAC. (A)** Carbon skeleton of acyclic  $C_{40}H_{56}$ ; for convenience Car formulae are often written in a shorthand form as in **(B)** for  $C_{40}H_{56}$  and **(C)**. The broken lines indicate formal division into isoprenoid units of  $C_{40}H_{56}$ . All specific names are based on this stem name.

The central structural pattern which is repeated in every Car is the polyene backbone. Various numbers of alternating single and double bonds form a conjugated  $\pi$ -electron system which is responsible for most of the coloration and spectroscopic properties of Cars. In photosynthetic bacteria, the polyene chain maybe further modified by five different pathways (1) hydrogenation, (2) dehydrogenation, (3) cyclization, (4) oxidation, (5) glycosylation or (6) any combination of these processes, (see for example (Lang & Hunter 1994, Takaichi S 1999, Roszak et al. 2004)).

Principally the Cars have a dual role in LH systems: (i) they acts as photoprotective agents, preventing BChl from photodestructive reactions, by quenching of photosensitizer triplets, oxygen singlets and other radical species and (ii) they harvest light by collecting energy in the green-blue spectral region (between 450 and 570 nm) where the BChl do not absorb efficiently, and transfer it to the neighbouring BChls from where it ultimately makes it is way to the RC.

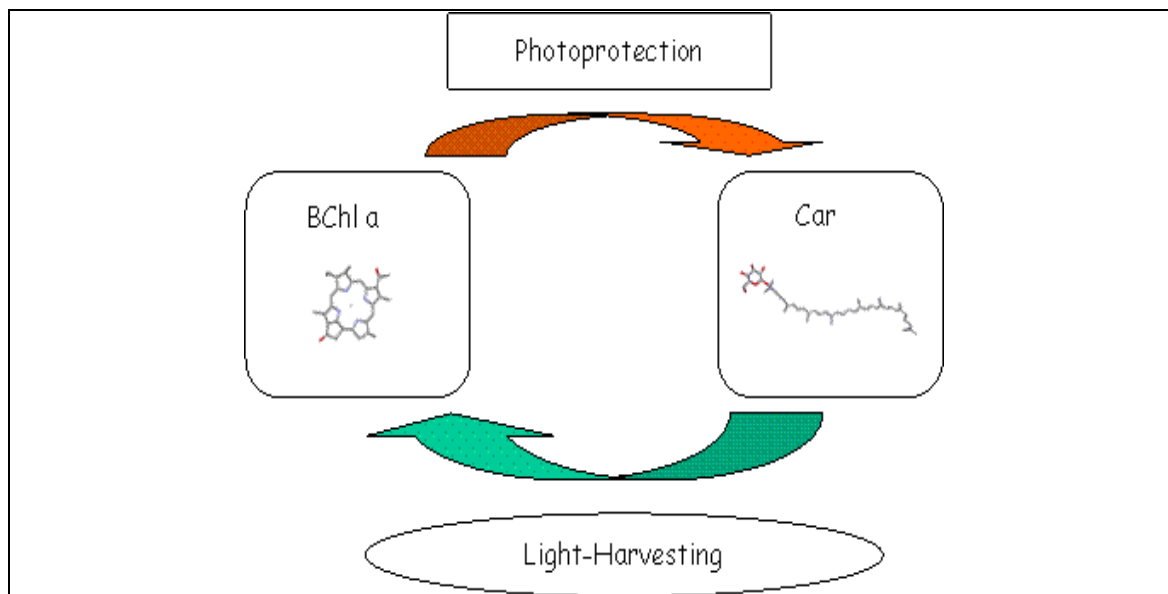


**Figure 5.2: Roles of Cars in photosynthesis.** Cars play a dual role (i) photoprotection, and (ii) light harvesting in photosynthetic system (see text). The arrows indicate the direction of energy transfer.

In photosynthetic proteins Cars occur in either *cis* or *trans* configuration. It has been proposed that the two isomers have different properties and possibly also different functions. Apparently, all the Cars, which function as LH pigments are found in *all-trans* configuration. In the RC of some photosynthetic bacteria, the Cars function exclusively in photoprotection, and are then found to be in *cis*-conformation only (Koyama & Fujii 1999, Koyama et al. 2004). Hitherto, there is only one exception to this rules, which has been observed in the high resolution of structure of LH2 from *Rps. acidophila*; there the existence of a second possible Car apparently in *cis*-conformation has been proposed . The potential second Car was detected at the cytoplasmatic wall of the LH2 ring, placed on the outside of the complex between the  $\beta$ -polypeptides. It is still controversial whether there are one or two Car molecules, because, the second Car has not been observed consistently and, in addition, appears to be in 15-*cis* configuration which has not been observed previously in light harvesting systems . However, this is still under dispute. In the very last works it has been concluded that the putative second Car in the crystal structure is not a Car but a detergent molecule .

Next to the photoprotective and light harvesting function, Cars play an important role in structural stabilization and assembly of the pigment-protein complexes. For instance, Cars have been shown to be critical for the proper folding of LHC proteins . In the photosynthetic bacterium, *Rb. sphaeroides*, the absence of Car molecules appears to inhibit the assembly of the peripheral antenna (LH2), but not that of the core (RC-LH1) complex (Jensen et al. 1958, Fuller & Anderson 1958). The absence of stable LH2 in cells

which lack Car has been interpreted by assuming that the assembly of LH2 requires the presence of the Car molecule. This, however, is still a matter of dispute. A Car-less *Rb. sphaeroides* mutant, R26, (Clayton & Smith 1960) entirely lacks LH2. This mutant has a tendency to revert to the strain R26.1, containing a modified LH2 complex which still lacks, at least coloured, Car (Davidson & Cogdell 1981).

Until now little is known about Car binding in the photosynthetic pigment-protein complexes. Based on the photosynthetic high resolution structures, and the orange Car protein (Kerfeld 2004), it has been suggested that Cars are bound to proteins by hydrophobic interactions. However, non-specific hydrophobic interactions alone fail to account for the fact that all Cars are specifically bonded in the pigment-protein complexes. Quantum chemical calculations suggest that intermolecular hydrogen bond interactions (C-H $\cdots$ O-C) between Car and the BChl-B800 in the LH2 complex may take place. Analyses of high resolution structure (Wang & Hu 2002) suggest that aromatic residues play an important role in the binding of Cars and (B)Chl in hydrophobic proteins regions, because of the high occurrence of these residues in close vicinity of these pigments. It was hypothesized that the existence of  $\pi$ - $\pi$  stacking interactions between Cars and aromatic residues are critical for binding of Car in photosynthetic pigment-protein complexes. However, this has not been demonstrated by experimental studies. In bacterial RC, replacement of phenylalanine by leucine resulted in steric hindrance and blockage of the Car binding pocket. A phenylalanine residue has thus been shown to determine the topology of spheroidene in the RC by functioning as a gate for the Car. Systematic mutations of the aromatic residues surrounding the Car in bacterial RC, however, did neither dramatically affect the binding nor the properties of the bound Car (Gall et al. 2004). The role of aromatic residues in Car binding thus remains to be substantiated.

This chapter focuses on the exploration of the role of aromatic residues in binding of Car to LH2 complex. To achieve this goal;

- putative Car binding interactions, in particular, interactions with aromatic residues are identified in the modelled structure of *Rb. sphaeroides* (chapter 1), based on the structure of *Rps. acidophila*,
- a model LH protein is used in which the native contacts at the Car-protein interface have been reduced and the contribution of distinct aromatic amino acids to the binding of Car can be readily assessed,
- the role of identified aromatic residues at the Car/protein interface is further explored in WT sequence context by mutagenesis of the LH2 complexes from *Rb.*

*sphaeroides*, and subsequent spectroscopic, chromatographic and thermal denaturation analyses

- the mutagenetic approach is complemented by statistical analyses of Car binding pockets in photosystems I and II

## 5.2. Results and Discussion

### 5.2.1 Modelling of the Car-protein interface in LH2 from *Rb. sphaeroides*

To identify putative residues which interact with Car in LH2, a model structure of LH2 from *Rb. sphaeroides* has been constructed as described in chapter 3. This is based on the backbone structure of *Rps. acidophila*. In essence, the backbone of the model structure has not altered, while the side chain conformations were optimised at positions where “mutations” took place. In this model structure, however, the Car and BChl positions and structural conformations are not changed, because no force field of the pigments is available (Linnanto et al. 2004, Palencar 2005). The Car, rhodophin glucoside, in the LH2 from *Rps. acidophila* is very similar to the Cars, SE and SO in *Rb. sphaeroides* (figure 5.3). In particular, the long central chain of isoprenoid units is very similar however; the number of conjugated double bonds may vary.

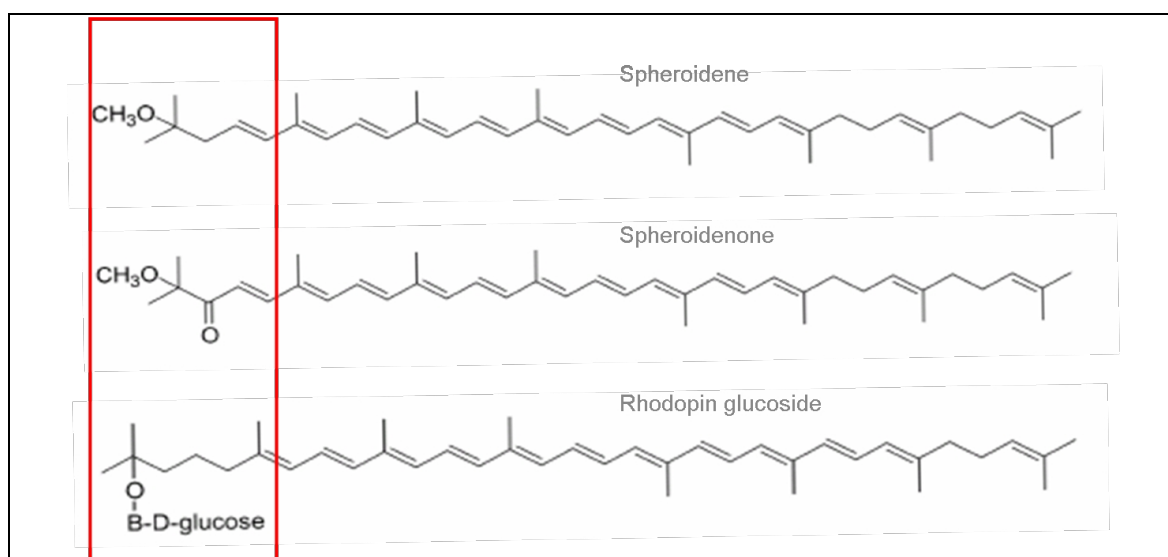


**Figure 5.3: Structure of major Cars in *Rps. acidophila* and *Rb. sphaeroides*:** The red square highlights the distinct headgroup regions. Note the difference in double bond location between SO, SE and rhodopine glucoside.

In figure 5.4 the residues of the  $\alpha$ -TMH are depicted that are in close vicinity (within a radius of 5 Å) of the Car in the model LH2 structure of *Rb. sphaeroides*. These residues are F(-12), L(-11), A(-6), V(-2), I(-1) and A(+2) (figure 5.4A). In the high resolution structure of *Rps. acidophila*, there are seven residues which are found to be in close contact with rhodopin glucoside. These are F(-12), L(-11), V(-6), I(-5), V(-2), I(-1) and A(+2). Contacts exits also with residues of  $\alpha$ -subunit of the neighbouring helix, these are A(-4), I(-3), H(0) and L(+1).

The Car-protein interface has been explored in the model structure in comparison to the structure of *Rps. acidophila*. The interface between the two structures is very similar, except for the residue at position -5, which is in contact only in the *Rps. acidophila*. In *Rps. acidophila* the residue is the long aliphatic isoleucine while in *Rb. sphaeroides* it is the relative small alanine.

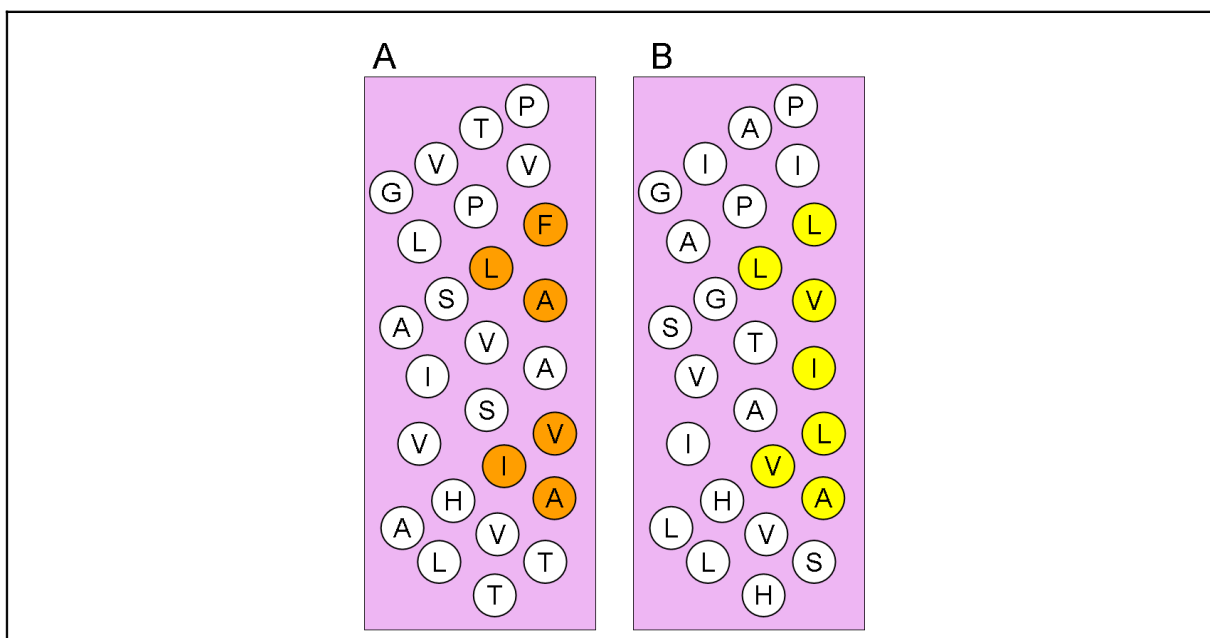


**Figure 5.4:** Car/protein interface in LH2  $\alpha$ -subunits. (A). AA sequence of TM helix of *Rb. sphaeroides* and (B) of TM helix of *Rps. acidophila*. The amino acids which interact with Car at a distance of  $\leq 5$  Å are shown in orange for *Rb. sphaeroides* and in yellow for *Rps. acidophila*.

This is readily explained by the similar polyene chains which predominantly interact with the TM helices of the LH2. Thus, the interface of the two structures appear closely similar. This suggests that the structure may be used as a first approximation for the exploration of the Car-protein interface.

As described in chapter 3, model TM sequences inserted into LH2 in place of the native ones can be employed to study cofactor-binding and assembly. Here, this approach has been used to study the factors of Car binding in LH2. To that end the model LH2 protein (chapter 3) is further modified. At the N-terminus of the TM helix of the  $\alpha$ -subunit in the

model protein LH2  $\alpha\text{AL}_{16/\text{S-4}}$  serine at position -10 is replaced by alanine and particularly, the aromatic residue, phenylalanine at position -12 is replaced by leucine resulting in LH2  $\alpha\text{AL}_{20/\text{S-4}}$  (figure 5.5).

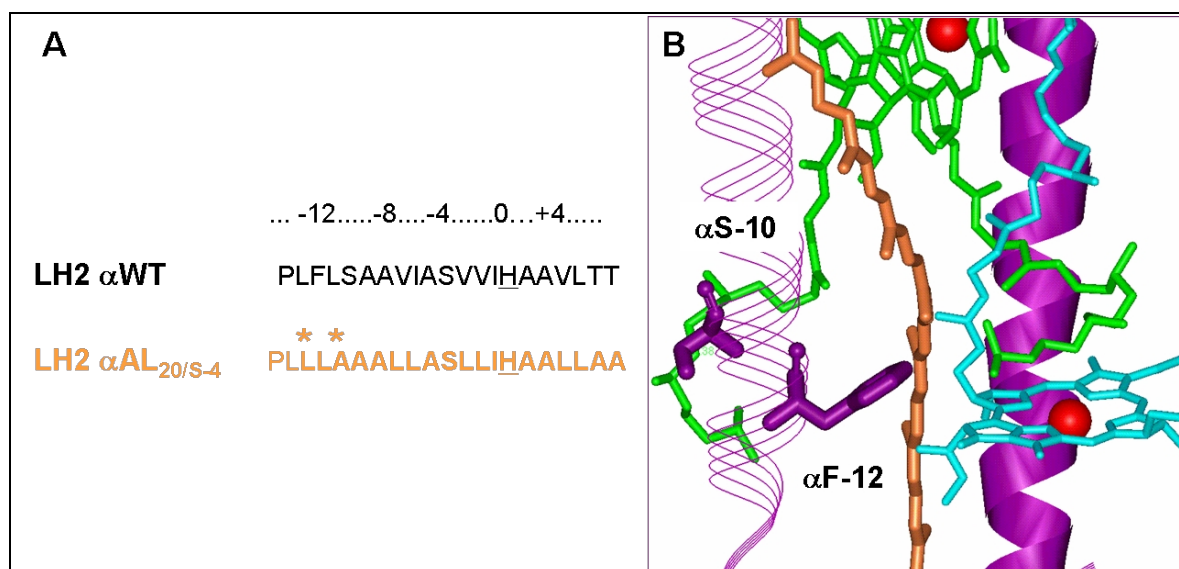


**Figure 5.5: Model TM helix of  $\alpha$ -subunit LH2  $\alpha\text{AL}_{20/\text{S-4}}$ :** (A) AA sequence of model helix. WT sequence is shown in black and the model sequence in orange. New residues replacing F(-12) and S(-10) are marked by an asterisks. (B) Detailed view of the modelled structure of *Rb. sphaeroides*,  $\alpha\beta$  subunits (purple), BChl-B850 (green), BChl-B800 (turquoise), and Car (orange). Note, that only the F(-12) is in close vicinity ( $\leq 4 \text{ \AA}$ ) of the Car.

### 5.2.2 Study of Car binding in model LH2 $\alpha\text{AL}_{20/\text{S-4}}$

In the model complex LH2  $\alpha\text{AL}_{16/\text{S-4}}$ , with serine -10 and, particularly, phenylalanine -12 in the TMH: (i) the BChl-B800 band is slightly reduced and (ii) the Car signal is somewhat altered (Chapter 3). The *in situ* absorption spectra of LH2  $\alpha\text{AL}_{20/\text{S-4}}$  compared to LH2 WT is, however, distinctively different. The BChl-B800 band is nearly lost, and the absorption band of BChl-B850 is red-shifted in comparison to LH2 WT (figure 5.6, inset).

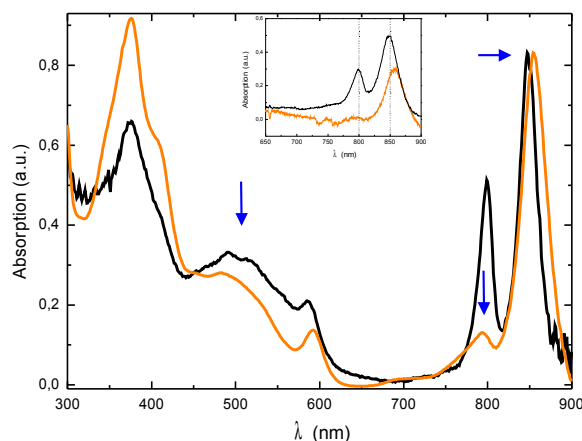


**Figure 5.6: Optical spectra of LH2 WT (black) and LH2  $\alpha$ AL<sub>20/S-4</sub> (orange).** The spectra are normalised at the maximum absorption of the Q<sub>y</sub> of BChl-B850. The inset shows the *in situ* absorption spectra of LH2 WT and LH2  $\alpha$ AL<sub>20/S-4</sub> taken of *Rb. sphaeroides* colonies. The arrows point at the spectral changes.

In the absorption spectra of purified membranes of LH2  $\alpha$ AL<sub>20/S-4</sub> (figure 5.6), the absorption band of BChl-B850 is ~8 nm red-shifted, and the BChl-B800 band is replaced by a minor slightly blue shifted band at ~793 nm. This band may originate either from BChl-B800 that should be structurally altered or from the high exciton component of BChl-B850 or a combination of the two. In addition, there is a reduction absorption of region of the Car at 450-550 nm. The absorption spectrum in the 450-550 nm range, is typical for SO, the major Car of LH2 grown under semi-aerobic conditions (Shneour et al 1962, Cogdell & Crofts 1978, Yeliseev & Kaplan 1997). The changes in the absorption spectra indicate either significant structural rearrangement of the pigments in LH2  $\alpha$ AL<sub>20/S-4</sub>, in particular, of the BChl-B800 and the Car sites or the substantial loss of BChl-B800 and Car molecules from the complex. This absorption range is already significantly affected by scattering effects and should thus be treated with care. Nevertheless, in LH2  $\alpha$ AL<sub>20/S-4</sub>, the red-shift from ~760 nm which is typical for “free” monomeric BChl (*i.e.* BChl that is not (tightly) bound to polypeptides and not assembled into pigment-protein complexes) to ~860 nm is entirely retained. This suggests that formation of the BChl-B850 is entirely supported by the alanine-leucine sequence in the model LH2  $\alpha$ AL<sub>20/S-4</sub> complexes, which replaces the entire TMH of the  $\alpha$ -subunit.

This is also obvious from the CD spectra of LH2  $\alpha$ AL<sub>20/S-4</sub> (figure 5.7). As BChl-BChl and Car-Car couplings, as well as Car-protein couplings mainly contribute to the typical CD-signal (Cogdell & Scheer 1985, Braun & Scherz 1991, Koolhaas et al. 1998,

Georgakopoulou et al. 2004), it is agreed that its exact shape serves as a fingerprint for the BChl and Car arrangement in the LH2 complex. The various intermolecular interactions experienced by the Car molecule makes it adopt a semi-helical structure, when viewed along its long axis. The twisted conformation is presumably responsible for the observed intense CD signal as compared with unbound Car .

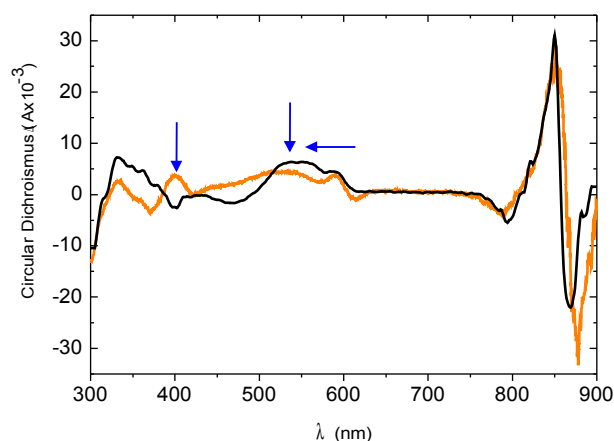


**Figure 5.7: CD spectra of LH2 WT (black) and LH2  $\alpha$ AL<sub>20/S-4</sub> (orange).** The CD spectra are taken of purified membrane preparations. The arrows indicate the changes between the spectra.

As shown in figure 5.8, the semi-conservative, S-shaped CD signal of the BChl-B850 is largely retained in LH2  $\alpha$ AL<sub>20/S-4</sub>. It has two bands, a positive one with extreme at ~ 850 nm (850 nm in LH2 WT), and a negative one with extrema at ~ 876 nm (~ 867 in LH2 WT). Thus it is similar to the one of LH2 WT except for the red-shift. Conspicuously, there is a clear negative trough with minimum at ~785 nm even though the BChl-B800 absorption band is nearly absent. In comparison to LH2 WT, the signal is somewhat reduced and shifted to the blue (from 792 to 785 nm). A CD signal with minimum at approximately 782 nm has been previously suggested by van Grondelle and co-workers to originate from the high excitation component of the BChl-B850 (Koolhaas et al 1998). The CD signal of LH2 WT complexes with minimum at ~ 784 nm should thus be contributed by both the BChl-B800 and the high excitation component of BChl-B850. In LH2  $\alpha$ AL<sub>20/S-4</sub>, the CD band in the region of BChl-B800 is reduced and blue shifted in comparison to LH2 WT reflecting loss of BChl-B800. The remaining signal may thus originate largely from the high excitation component of BChl-B850. The CD signal of LH2  $\alpha$ AL<sub>20/S-4</sub>, however, is significantly altered in the range of the Cars (450–550 nm): there is a clear reduction in the signal amplitude and it is much broader. Moreover, the slightly negative signal at ~485 nm is converted to a slightly positive one (figure. 5.7). The altered CD shape indicates an

altered interaction of the Car with surrounding polypeptide or/and pigment . In addition, the band at ~390 nm is positive in the mutant and negative in wild type. The CD in this range is too complex and as yet not clearly assigned. It maybe attributed by BChl-Car and/or Car-Car exciton coupling, or even to the Cyt bf6 complex . Curiously, in the CD spectra of LH2 in R26.1 which is devoid of Car, there is a positive band at ~ 400 nm, which is negative in LH2 complexes with Cars.

The reduction in CD intensity of the Car signal (450-550 nm) could be due to a reduction in Car, however, the changes in the shape of the CD clearly indicate alteration in Car bindings. The shape and magnitude of the signal may be altered by changes in the Car conformation, Car-Car interactions or by deformations of the entire LH ring structures . The change in the shape of the CD signal (figure 5.7) indicates that the interactions between the Car molecules and/or between Car and polypeptide have been altered in LH2  $\alpha$ AL<sub>20/S-4</sub> as compared with LH2 WT. Nevertheless, alterations in the interaction of Car with protein/pigments should not significantly affect the Car absorption bands. The observed reduction in the Car absorption bands of LH2  $\alpha$ AL<sub>20/S-4</sub>, thus likely reflects a substantial loss of Car from the complex.

The excitation spectra (figure 5.8) principally show similar features as the absorption spectrum when detecting fluorescence emission at 850 nm. In particular, the broad excitation band at 450-550 nm and the 800 nm excitation band show that ET takes place from the Car and BChl-B800 to BChl-B850. The broad absorption at 450-550 nm is typical for SO. In LH2  $\alpha$ AL<sub>20/S-4</sub>, the ET from the Cars is altered, as indicated by the slightly blue-shifted bands (from ~ 516 nm in LH2 WT to ~ 505 nm in LH2  $\alpha$ AL<sub>20/S-4</sub>) and the decrease in Car contributions relative to the BChl molecules as judged by Q<sub>x</sub>-excitation band of the BChl molecules at ~ 600 nm. Besides, the efficiency of ET from the Car to BChl-B850 decreases in LH2  $\alpha$ AL<sub>20/S-4</sub> to approximately 50% and ET from BChl-B800 to BChl-B850 is almost abolished (only 10% of activity). It has been shown previously that ET from Car proceeds both via the BChl-B800 and BChl-B850 in LH2 from *Rb. sphaeroides* (Polivka & Sundstroem 2004). As the efficiencies of the ET pathways, in particular, of the direct Car to BChl-B850 pathway are still a matter of dispute (Horvin Billsten et al. 2002, Polivka & Sundstrom 2004), the decrease in the amplitude of the Car excitation band could thus either reflect the loss in the ET due to the loss of B800-BChl , and/or the loss of Car from LH2.

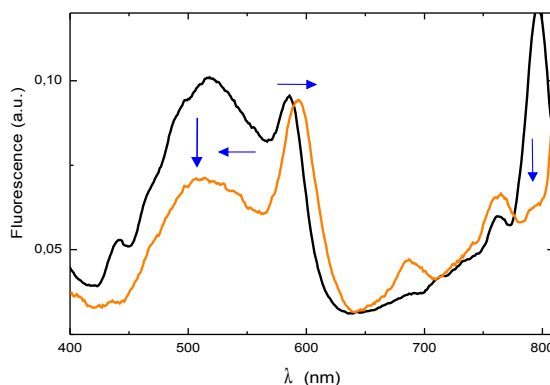


**Figure 5.8: Excitation spectra of LH2 WT (black) and LH2  $\alpha$ AL<sub>20/S-4</sub> (orange) of purified membranes from *Rb. sphaeroides* DD13.** The bands at ~800 nm arise from BChl-B800, at ~600 nm from the Q<sub>x</sub> transition of the BChl, and the bands at 450 to 550 nm arise from the Car. The fluorescence spectra are of purified membranes and are normalised to the Q<sub>x</sub> transition at ~600 nm. Fluorescence emission is detected at 850 nm. The arrows indicate at the major changes in the spectra.

Taken together, the absorption, CD, and fluorescence spectra indicate that Car binding has been altered in LH2  $\alpha$ AL<sub>20/S-4</sub>. In order to further examine the binding and interaction of the pigments with polypeptide, RR spectroscopy has been employed. Figure 5.10 displays the room temperature Fourier transform (FT) RR spectra in the higher frequency region of LH2 WT and LH2  $\alpha$ AL<sub>20/S-4</sub>. By use of RR spectroscopy precise information on both the conformations of and intermolecular interactions of bacteriochlorins may be obtained (Robert 1996, Nèveke et al. 1997, Lapouge et al. 1999, Robert 1999). The frequencies of six bacteriochlorin Raman modes, denoted R1 to R6, were shown to be sensitive to the BChl macrocycle conformation and they were used in particular to establish the conformations of the BChl molecules in LH proteins .

In these spectra the bands contributing between 1620 and 1710 cm<sup>-1</sup> arise from the carbonyl stretching modes of the C3 acetyl and C13<sup>1</sup> keto carbonyl groups of the different BChl molecules bound to the LH2 complexes. In the WT spectrum (figure 5.9), the BChl molecules responsible for the 850 nm absorption of these complexes contribute at 1627, 1632, 1651 and 1678 cm<sup>-1</sup>, while the carbonyl stretching modes of the 800 nm absorbing BChl molecule are observed at 1626 and 1699 cm<sup>-1</sup>.

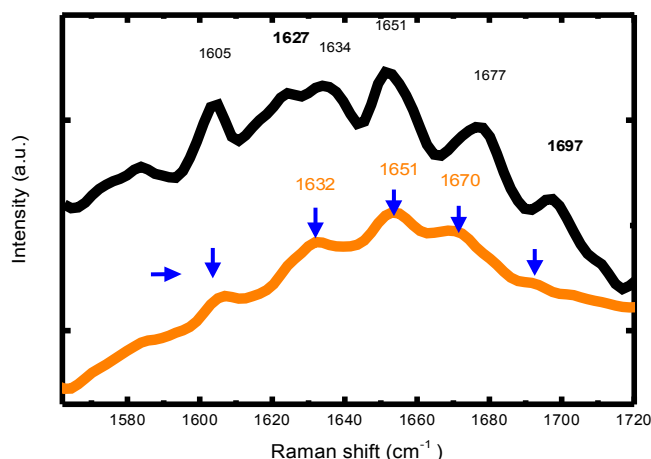


**Figure 5.9: RR spectra of WT LH2 (black), and LH2  $\alpha$ AL<sub>20/S-4</sub> (orange).** The arrows indicate the changes in Raman band of LH2  $\alpha$ AL<sub>20/S-4</sub> in comparison to LH2 WT.

In the FT-Raman spectrum of LH2  $\alpha$ AL<sub>20/S-4</sub> (figure 5.9), a number of changes is detected in comparison to the spectrum of LH2 WT. In particular, the bands of the BChl-B800 are altered, resulting in the loss of the band at 1697 cm<sup>-1</sup> and a decrease of intensity around 1628 cm<sup>-1</sup>. There are also changes related to the vibrational modes of BChl-B850; (i) the band at 1627 cm<sup>-1</sup> is shifted, and (ii) the bands at 1634, 1653 and 1677 cm<sup>-1</sup> are blue shifted to 1632, 1651 and 1670 cm<sup>-1</sup> respectively (figure 3.12, chapter 3). This indicates some reorganization of the BChl-B850 molecules in their binding sites, and suggests that, in addition to the removal of the BChl-B800, there are changes related to the Cars molecules, which affect the exact BChl-B850-protein interactions .

Thus far, it has been shown that BChl-B800 is lost and that there are significant changes in the Car content and binding in LH2  $\alpha$ AL<sub>20/S-4</sub> by spectroscopic means. In the native membrane, however, scattering effects obscure the spectra. In addition, Car maybe attached to mutated LH2 and membranes in a non-specific way. To further analyse Car content and properties in the model complex, it has been isolated in detergent and also expressed in of *Rb. sphaeroides* mutant strain which contains NE instead of SE as major Car. This Car has well resolved absorption bands in the visible range.

The absorption spectra of the isolated complex of LH2  $\alpha$ AL<sub>20/S-4</sub> are pronouncedly different as compared with the LH2 WT (figure 5.10A). There is (i) a red shift of the absorption maximum of the Q<sub>y</sub> transition (from 846 nm to 856 nm) of the BChl-B850, (ii) a reduction in the absorption bands of BChl-B800 and Cars and (iii) a blue shift of the Car absorption bands (from ~ 514 and ~ 490 nm to ~ 504 and ~ 482 nm respectively). Conspicuously, the spectral properties of LH2  $\alpha$ AL<sub>20/S-4</sub> are very similar to the spectroscopical properties of the

Car-less mutant LH2 complex of *Rb. sphaeroides* R26.1 (figure 5.10A). As in the case of LH2  $\alpha$ AL<sub>20/S-4</sub>, in the Car-less LH2 complex, the loss of Car is accompanied by a red shift the absorption maximum of BChl-B850 from 850 nm to 860 nm and the entire loss of the BChl-B800 absorption band. As observed in membranes, the major peak of the Car is blue shifted in isolated LH2  $\alpha$ AL<sub>20/S-4</sub> (figure 5.10A).

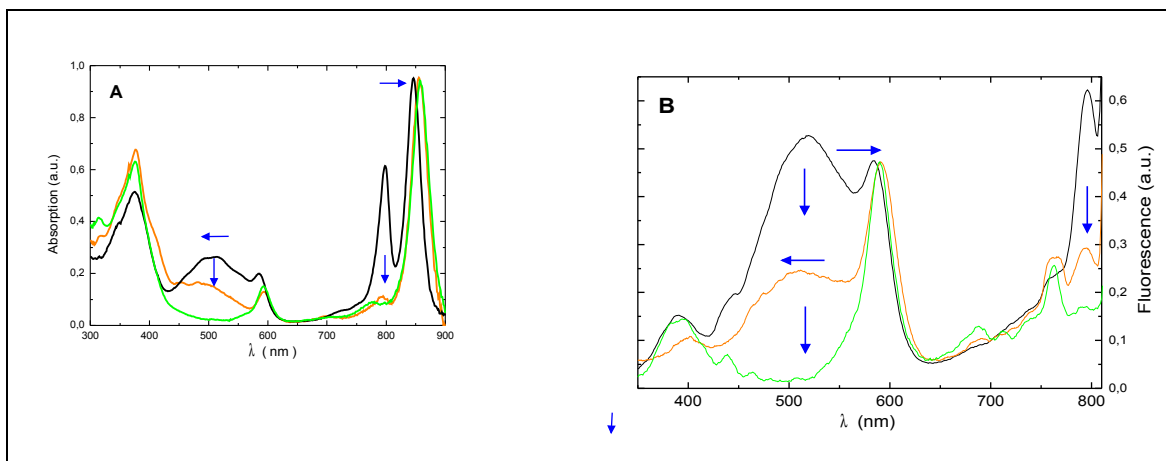


**Figure 5.10: Absorption (A) and excitation fluorescence (B) spectra of isolated LH2 WT (black), LH2  $\alpha$ AL<sub>20/S-4</sub> (orange) and LH2 R26.1 (green).** The optical spectra are normalised to the  $Q_y$  transition of BChl-B850. The excitation spectra are normalised to the BChl  $Q_x$  transition at 598 nm. The fluorescence emission is detected at 850 nm. The spectra are taken of isolated complexes LH2. The arrows indicate the major changes between spectra.

In comparison to the fluorescence spectra of purified membranes of LH2  $\alpha$ AL<sub>20/S-4</sub> (figure 5.8), the reduction in ET from the Car and BChl-B800 to BChl-B850 is even more pronounced in LH2  $\alpha$ AL<sub>20/S-4</sub>, isolated in detergent. The ET from Cars to BChl-B850 is approximately 40% and the ET from BChl-B800 to BChl-B850 is absent. The blue shift of the major Car excitation band, from ~518 nm in LH2 WT to ~500 nm in LH2  $\alpha$ AL<sub>20/S-4</sub> is clearly noticeable. The clear reduction in the Car absorption bands of LH2  $\alpha$ AL<sub>20/S-4</sub> in detergent likely reflects a substantial loss of Car from the complex. This is further supported by the comparison of the absorption spectra of LH2  $\alpha$ AL<sub>20/S-4</sub> to the spectra of Car-less LH2 from *Rb. sphaeroides* R26.1 (figure 5.10A). As shown, the BChl-B800 absorption band is absent, the  $Q_y$ -transition is shifted to ~ 860 nm and the absorption band of the Car is either absent (in Car-less LH2) or significantly reduced (in LH2  $\alpha$ AL<sub>20/S-4</sub>) in these complexes. Upon isolation of the complex from the membrane, the ET from Car to BChl-B850 is even further reduced, possibly indicating further loss of Car from LH2  $\alpha$ AL<sub>20/S-4</sub> due to the detergent treatment (figure 5.10B). In addition, there is a similar shift in the maximum of the  $Q_x$  band at ~600 nm in LH2  $\alpha$ AL<sub>20/S-4</sub> and LH2 R26.1.

To further explore the spectral changes of LH2  $\alpha$ AL<sub>20/S-4</sub> in comparison to LH2 WT, especially in the range of the Car, LH2  $\alpha$ AL<sub>20/S-4</sub> has been expressed in *Rb. sphaeroides* strain DG2 (see material and methods) which has as major Car NE. LH2 complexes from the strain DG2 are particularly useful as its major Car, NE, does not lack the resolved vibrational bands as is the case for SO.

In figure 5.11A, the absorption spectra of purified membranes for LH2 WT and LH2  $\alpha$ AL<sub>20/S-4</sub> in *Rb. sphaeroides* DG2 are shown. Principally, the spectra of the mutant LH2 show the same changes as in *Rb. sphaeroides* DD13; the red shift of the maximum absorption band of BChl-B850 by  $\sim 10$  nm, the loss of the band BChl-B800 absorption (see also in figure 5.8) the reduction in the range of the Car absorption and the blue shift of the Car absorption maxima. The major absorption bands of the NE are shifted by  $\sim 10$  nm. In LH2 WT the Car has maxima at  $\sim 479$  nm,  $\sim 448$  nm and  $\sim 431$  nm and LH2  $\alpha$ AL<sub>20/S-4</sub> at  $\sim 490$  nm,  $\sim 458$  nm. One peak is not resolved and/or masked by the Soret band. In addition, the Q<sub>x</sub> of LH2  $\alpha$ AL<sub>20/S-4</sub> is slightly blue shifted in comparison to LH2 WT (figure 5.11A).

The CD signal of LH2  $\alpha$ AL<sub>20/S-4</sub> in *Rb. sphaeroides* strain DG2 is closely similar to the CD signal of the LH2  $\alpha$ AL<sub>20/S-4</sub> in strain DD13 (figure 5.11 B). However, the blue shifts in the major NE peaks are clearly discernable, in LH2 WT the major peaks are at  $\sim 496$ ,  $\sim 464$  and  $\sim 436$  nm. In LH2  $\alpha$ AL<sub>20/S-4</sub> these peaks are blue shifted by  $\sim 10$ ,  $\sim 9$ , and  $\sim 3$  nm. In addition, there is also a reduction in the signal's intensity; in particular, the band at  $\sim 486$  nm is reduced while the band at  $\sim 433$  nm is increased (possibly due to the positive band at  $\sim 400$  nm).

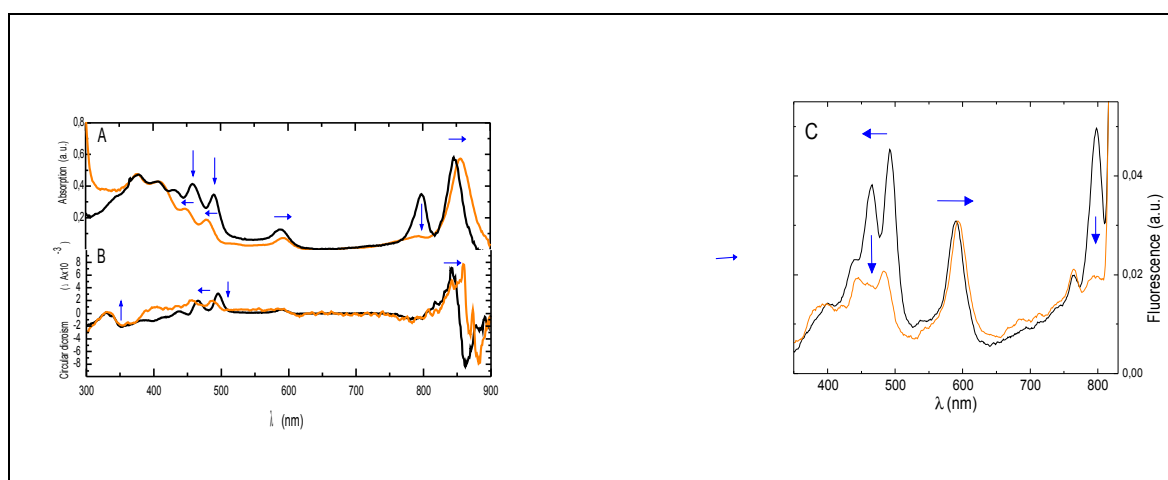


**Figure 5.11: Absorption (A), CD (B) and fluorescence excitation (C) spectra of LH2 WT (black) and LH2  $\alpha$ AL<sub>20/S-4</sub> (orange) expressed in DG2. Spectra are of membranes purified from**

*Rb. sphaeroides* DG2. The spectra are normalised to the maximal absorption of BChl-B850 expressed in DG2. Excitation fluorescence spectra, the band at ~ 800 nm arises from BChl-B800, the one at ~ 600 nm arises from the Q<sub>x</sub>-transition of the BChl, and the ones between 450 and 550 nm arise from NE. The fluorescence excitation spectra are normalised to the Q<sub>x</sub>-transition at ~ 600 nm. Fluorescence emission is detected at 850 nm. The arrows indicate the changes between the spectra.

In the fluorescence excitation spectra (figure 5.11C) of purified membranes of LH2  $\alpha$ AL<sub>20/S-4</sub>, major changes are observed in the Car region. The peaks are blue shifted in comparison to LH2 WT, from ~ 492 nm to ~ 483 nm, and ~ 439 nm to ~ 421 nm, whereas the peak at ~ 465 nm is not detected in LH2  $\alpha$ AL<sub>20/S-4</sub>. Furthermore, the ET of LH2  $\alpha$ AL<sub>20/S-4</sub> is reduced by approximately 50% as compared with LH2 WT, and ET from BChl-B800 to BChl-B850 is almost absent (only 10% of activity is retained). At present we lack an explanation for the change in the shape, in particular, the strong reduction of the band at 465 nm in the NE region of the fluorescence excitation spectra.

As is obvious from figures 5.10 and 5.11, the reduction in the Car content is accompanied by alteration in the spectra, in particular, blue shifting of the absorption, CD, and fluorescence spectra in the Car region.  $\pi$ - $\pi$  stacking interactions which may take place between aromatic residues and Car have been shown to be accompanied by red shifts in the Car main absorption bands. Moreover, the induction of the typical Car CD signal is related to specific binding in the protein site.

In summary, the changes observed in the spectra of LH2  $\alpha$ AL<sub>20/S-4</sub> strain DD13 are also shown in strain DG2. Due to the higher resolution of the spectra, the blue shifts are even better demonstrated in LH2 with the major Car NE. These blue shifts maybe related to disruption of  $\pi$ - $\pi$  interactions between the Car and the aromatic residues. However, also Car-BChl interactions may result in spectral shifting, and thus, at present, the underlying reason for the blue shift in Car absorption remains to be unravelled.

### 5.2.3 Carotenoid content in model LH2 $\alpha$ AL<sub>20/S-4</sub>

In order to quantify the amount of Car still bound in LH2  $\alpha$ AL<sub>20/S-4</sub>, the pigment contents has been determined by HPLC analysis. Quantitative extraction of the pigments from the LH2 proved difficult. The following obstacles had to be overcome: in the membranes the far too high Car/BChl ratios of LH2 WT suggested that pigments are non specifically bound to the complex or the lipid membrane. Thus, the extractions have been made from isolated complexes which have been washed excessively with detergent during purification. In addition, the choice of solvent for pigment extraction has been critical. Solubility of BChl a

is very different from the solubility of Car *i.e* acetone is optimal for BChl while ether is optimal for Car. The differences in solubility have been overcome by using a mixture of acetone and methanol (7:2, v/v) (see in material and methods).

In *Rb. sphaeroides*, the major Cars which accumulate are SO (red), which is the end product of the Car biosynthetic pathway, and SE (orange/yellow), which is the penultimate product of this pathway and a biosynthetic precursor of SO. In antenna complexes from *Rb. sphaeroides* 2.4.1 the composition is  $8 \pm 5.2$  for SO and  $5 \pm 0.4$  for SE per complex. In *Rb. sphaeroides* strain DD13 cell grown semi-aerobically, the content of SO relative to SE is much higher. The absorption spectra of the extracted pigments are shown in figure 5.12.

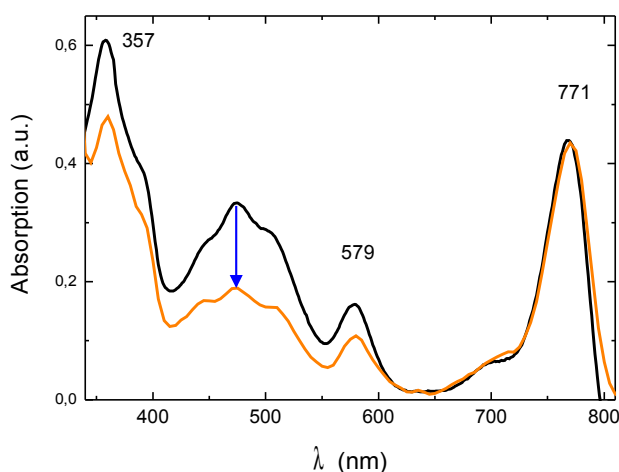


**Figure 5.12: Absorption spectra of extracted pigment from LH2 WT (black) and LH2  $\alpha$ AL<sub>20/S-4</sub> (orange).** The spectra are taken in ether and are normalised at  $\sim 771$ nm.

In order to determine the Car content relative to the BChl, the extracted pigments of isolated complexes of the LH2 WT and LH2  $\alpha$ AL<sub>20/S-4</sub> are analysed by HPLC. In LH2 WT about 93% of the Car relative to BChl is SO and  $\sim 7\%$  SE. As shown in figure 5.13, SE which is also detected LH2  $\alpha$ AL<sub>20/S-4</sub>, makes up less than 5-10% of total Cars, indicating that the SE content is very low in *Rb. sphaeroides* DD13 cells grown under semi-aerobic conditions (Yeliseev & Kaplan 1997). In LH2  $\alpha$ AL<sub>20/S-4</sub> the SO content is reduced by approximately 50%. The BChl/SO ratio amounts to  $2,8 \pm 0,4$  in LH2 WT and to  $5,6 \pm 0,7$  in LH2  $\alpha$ AL<sub>20/S-4</sub>. Curiously, the SE content is not changed relative to BChl, perhaps indicating that LH2  $\alpha$ AL<sub>20/S-4</sub> has a higher affinity to SE than LH2 WT. In spite of the considerable large deviations in the BChl/Car ratio (up to 12.5%) in different batches, it is

clear that the Car content is reduced in LH2  $\alpha\text{AL}_{20/\text{S-4}}$  as compared with LH2 WT. As the BChl-B800 is nearly absent, or at least strongly diminished, in LH2  $\alpha\text{AL}_{20/\text{S-4}}$ , the BChl/Car ratio should approach 2 instead of 3. The BChl/Car ratio of 5,6 in LH2  $\alpha\text{AL}_{20/\text{S-4}}$  should thus be even underestimated by up to 30%. These results indicate that in LH2  $\alpha\text{AL}_{20/\text{S-4}}$  the molar ratio of Car to BChl is strongly reduced, at least by 50%. That is, more than half of the Car binding sites are not occupied by Car molecules in the model LH2  $\alpha\text{AL}_{20/\text{S-4}}$ .

The Car/BChl content was independently assessed by the use of pre-resonance Fourier-Transform Raman spectroscopy (Mattioli et al.1993). In FT-Raman, the exciting beam used for producing the Raman effect is at 1064 nm, *i.e.* far from the electronic transitions of both the BChl and Car molecules. Under these conditions, the ratio between the Car and BChl signal may thus give a reasonable estimate of the Car content in the complexes. Using this technique, it is found that the Car content of the LH2  $\alpha\text{AL}_{20/\text{S-4}}$  is 2.2 times less than in the LH2 WT (not shown). This finding is in full agreement with the quantification results obtained by the HPLC analysis (figure 5.13).

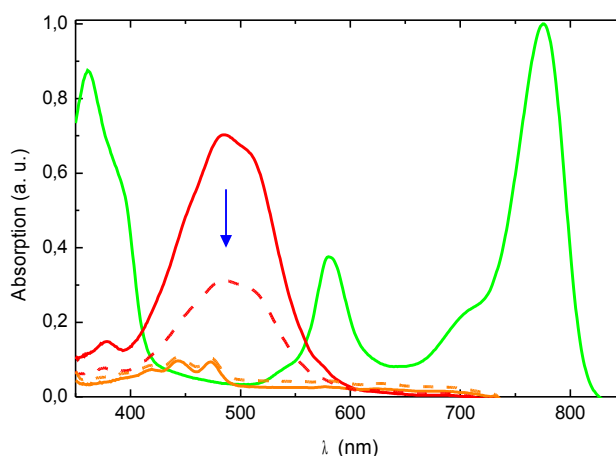


**Figure 5.13: Absorption spectra of LH2 WT and LH2  $\alpha\text{AL}_{20/\text{S-4}}$  pigment after HPLC.** BChl *a* (green), SO (red), SE (orange) in LH2 WT (solid line) and LH2  $\alpha\text{AL}_{20/\text{S-4}}$  (dotted line). The spectra are normalised to BChl absorption at  $\sim 771$  nm.

Up to here, it has been shown that the Car content is reduced in model  $\alpha\text{AL}_{20/\text{S-4}}$  complex. In addition, the spectral analysis indicates alteration in the binding of residual Car in the model complex. Raman experiments performed in resonance with the Car electronic transition yield specific information on the geometry of these molecules in LH2 complexes. RR spectra of Car contain four major groups of bands, termed  $\nu_1$  to  $\nu_4$  (for a review see (Robert 1999)). The frequency of the  $\nu_1$  band around  $1520\text{ cm}^{-1}$ , which arises from the stretching modes of the C=C double bonds, is very sensitive to the molecular

conformation of the Car molecules. The  $\nu_4$  band, around  $950\text{ cm}^{-1}$ , arises from the out-of-plane modes of the CH groups. It is forbidden by symmetry for planar molecules, and gains intensity when the Car molecules are twisted around the C-C bonds. RR spectra of LH2  $\alpha\text{AL}_{20/\text{S-4}}$  show small but definite differences as compared with LH2 WT (figure 5. 14). These differences mainly concern the frequency of the  $\nu_1$  band, which is slightly up shifted ( $3\text{ cm}^{-1}$ ) and the  $\nu_4$ , where an additional component at  $960\text{ cm}^{-1}$  appears, the reduction of the intensity at  $985\text{ cm}^{-1}$  is accompanied by the appearance of a new component at  $965\text{ cm}^{-1}$ . This band indicates some changes in the conformation of the Car. Similar changes observed upon depletion of the BChl-B800 molecules (Robert & Frank 1988) and were attributed to an isomerisation of the Car at the end of the polyene chain, accompanied by an out-of-plane torsion of the molecule. It is striking that the model LH2  $\alpha\text{AL}_{20/\text{S-4}}$  bound Car yield similar spectra as the Car bound to a BChl-B800-less LH2 WT.

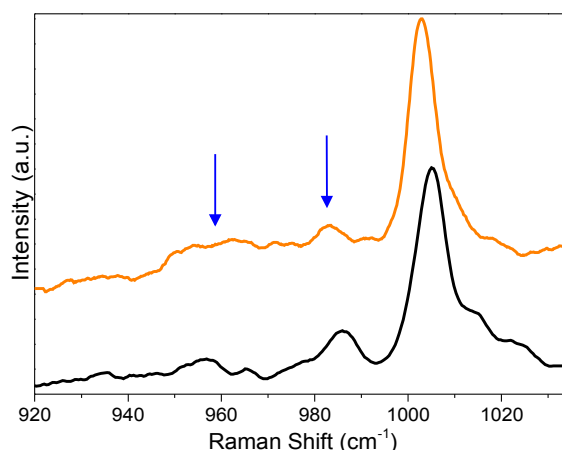


**Figure 5.14: RR spectra of LH2 WT (black), LH2  $\alpha\text{AL}_{20/\text{S-4}}$  (orange).** Excitation has been at 488 nm, experimental conditions, see material and methods of LH2 WT (black). The arrows indicate changes between spectra.

Taken together, this study shows that changing 10 out of the 20 residues which make up the pigment binding sites in LH2 does neither significantly change the geometry nor the functional properties of the BChl-B850. In contrast, the model TM helix LH2  $\alpha\text{AL}_{20/\text{S-4}}$  does not support efficient binding of the monomeric BChl-B800 and only partly supports binding of the Car molecules. BChl-B800 and Car have extensive van der Waals contacts and stable binding of BChl-B800 and Car apparently is substantially correlated in LH2. LH2 complexes which lack Car principally also lack BChl-B800, however, LH2 which lack BChl-B800 have been successfully reconstituted with Car. Furthermore, BChl-B800 can be selectively removed from LH2 without removing the Car. These findings suggest that

Car binding to LH2 is possible in the absence of BChl-B800 but not *vice versa*. In the model LH2  $\alpha\text{AL}_{16/\text{S}-4}$ , a considerable part of the BChl-B800 is absent, without significantly affecting Car content (figure 3.8, chapter 3). Mutating two more residues at the N-terminal part of the TM-helix of the  $\alpha$ -subunit, specifically,  $\alpha\text{F}(-12)$  and  $\alpha\text{S}(-10)$ , dramatically affects also the Car content in LH2 (figure 5.12 and 5.13). In addition, these mutations result in the loss of the BChl-B800, likely due to the substantial loss of the Car. BChl-B800 has neither close contacts with  $\alpha\text{F}(-12)$  nor  $\alpha\text{S}(-10)$  as based on the high resolution structure of *Rps. acidophila* and the modelled structure of LH2 of *Rb. sphaeroides* (figure 5.5). It cannot be excluded, however, that  $\alpha\text{S}(-10)$  makes an H-bond to BChl-B800 via a water molecule.

In summary, these results show that the model TM helix LH2  $\alpha\text{AL}_{20/\text{S}-4}$  does not support efficient binding of the monomeric BChl-B800 and the Car molecules. In contrast, neither the geometry nor the functional properties of the BChl-B850 are significantly disturbed. In the model LH2  $\alpha\text{AL}_{16/\text{S}-4}$ , a considerable part of the BChl-B800 is absent, without significantly affecting Car binding (chapter 3). Mutating two more residues at the N-terminal part of the LH2- $\alpha$  TM-helix, specifically, F (-12) and S (-10), dramatically affects also the Car content in LH2 (figure 5.8-5.8, 5.10-14). This points at the critical impact of these two residues for the assembly of LH2, specifically proper binding of the Car.

#### 5.2.4 Study of critical protein-carotenoid interactions in LH2 from *Rb. sphaeroides*

In the model protein LH2  $\alpha\text{AL}_{20/\text{S}-4}$ , it has been demonstrated that (i) the Car content is much reduced, and that (ii) the bindings of the residual Car is altered. Already in the model LH2  $\alpha\text{AL}_{16/\text{S}-4}$ , the changes in the Car properties are observed (10% of the ET is reduced and the major peaks of the Car are blue shifted), (figure 3.8-3.9, chapter 3), in LH2  $\alpha\text{AL}_{20/\text{S}-4}$  the changes in Car properties, however, are much more dramatic. In the mutant LH2  $\alpha\text{AL}_{20/\text{S}-4}$ , only two additional residues have been changed; the residue  $\alpha\text{S}(-10)$  is replaced for alanine and residue  $\alpha\text{F}(-12)$  is replaced for leucine. To investigate whether  $\alpha\text{F}(-12)$  or  $\alpha\text{S}(-10)$  are critical for the Car binding, either  $\alpha\text{F}(-12)$  or  $\alpha\text{S}(-10)$  have been mutated in LH2  $\alpha\text{AL}_{20/\text{S}-4}$  and LH2 WT (figure 5.15). In addition, a double mutant has been made, in this case  $\alpha\text{F}(-12)$  for leucine and  $\alpha\text{S}(-10)$  for glycine (figure 5.15B).

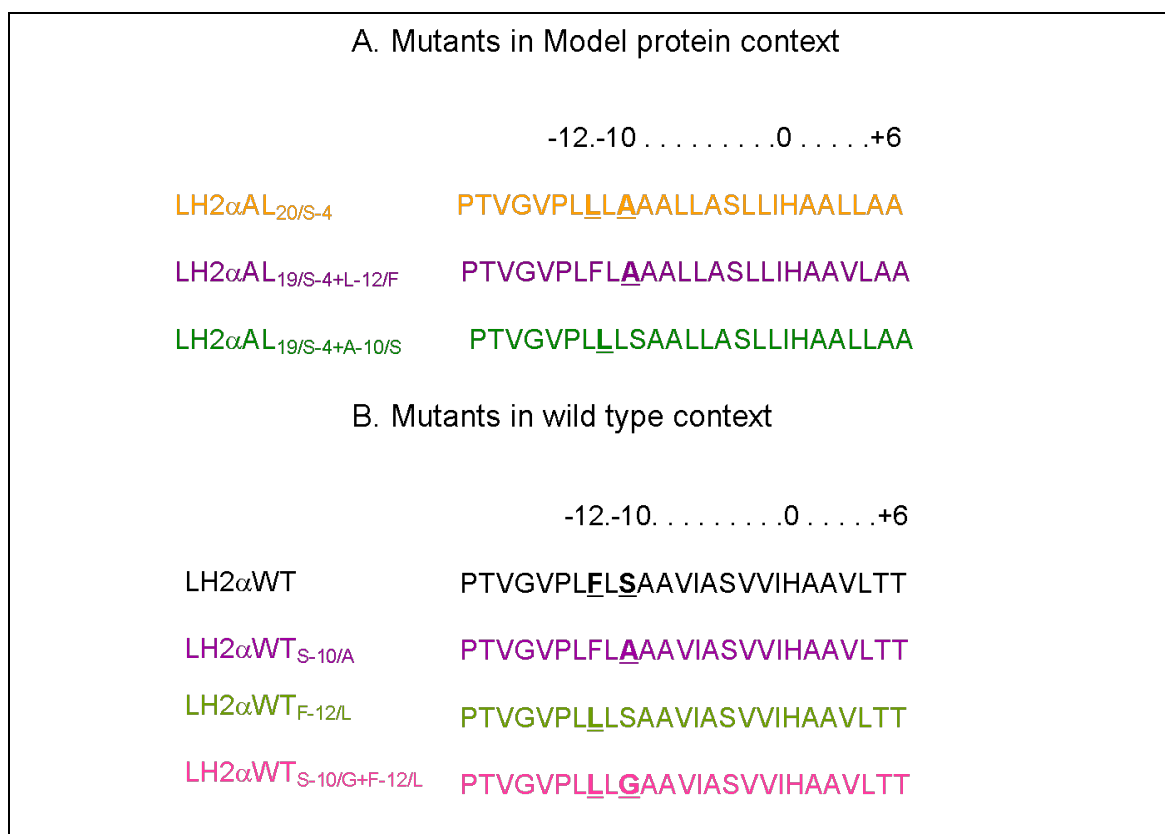


**Figure 5.15: Sequences of mutant LH2  $\alpha$ -TM helices used in this study.** The mutated residues are shown in bold and are underlined.

In order to determine the particular impact of  $\alpha$ F(-12) or  $\alpha$ S(-10) on the binding of SO, either  $\alpha$ F(-12) or  $\alpha$ S(-10) has been reinserted in LH2  $\alpha$ AL<sub>20/S-4</sub>, resulting in LH2  $\alpha$ AL<sub>19/S-4+L-12/F</sub> and LH2  $\alpha$ AL<sub>19/S-4+A-10/S</sub> (figure 5.15A, B). The absorption and fluorescence excitation spectra of LH2  $\alpha$ AL<sub>19/S-4+L-12/F</sub> and LH2  $\alpha$ AL<sub>19/S-4+A-10/S</sub> are shown in figure 3.16 A, B. As is obvious from the reduction in the fluorescence excitation band at 450-550 nm, the replacement of  $\alpha$ S(-10) by alanine does not significantly affect ET (~ 10%). In contrast, the replacement of  $\alpha$ F(-12) by leucine results in a considerable loss of ET (~ 50%) The loss of Car is obvious from the reduction in the absorption region of the Car, in particular, in case of LH2  $\alpha$ AL<sub>20/S-4</sub>. The spectra, however, are distorted due to scattering effects of the membranes and should thus be treated with some caution. The reduction in ET by ~ 40% in LH2  $\alpha$ AL<sub>19/S-4+A-10/S</sub> indicates that  $\alpha$ F(-12) has a critical input in the binding of SO in LH2  $\alpha$ AL<sub>20/S-4</sub>. In contrast, the ET in LH2  $\alpha$ AL<sub>19/S-4+L-12/F</sub> (*i.e.* if  $\alpha$ F(-12) is present but  $\alpha$ S(-10) is replaced by alanine) is only reduced by about 10% (figure 3.16 B). Nevertheless, the largest reduction in the ET from Car to BChl-B850 is observed when both  $\alpha$ F(-12) and  $\alpha$ S(-10) are simultaneously mutated (figure 5.16B), indicating that these residues synergistically contribute to the binding of Car to LH2.

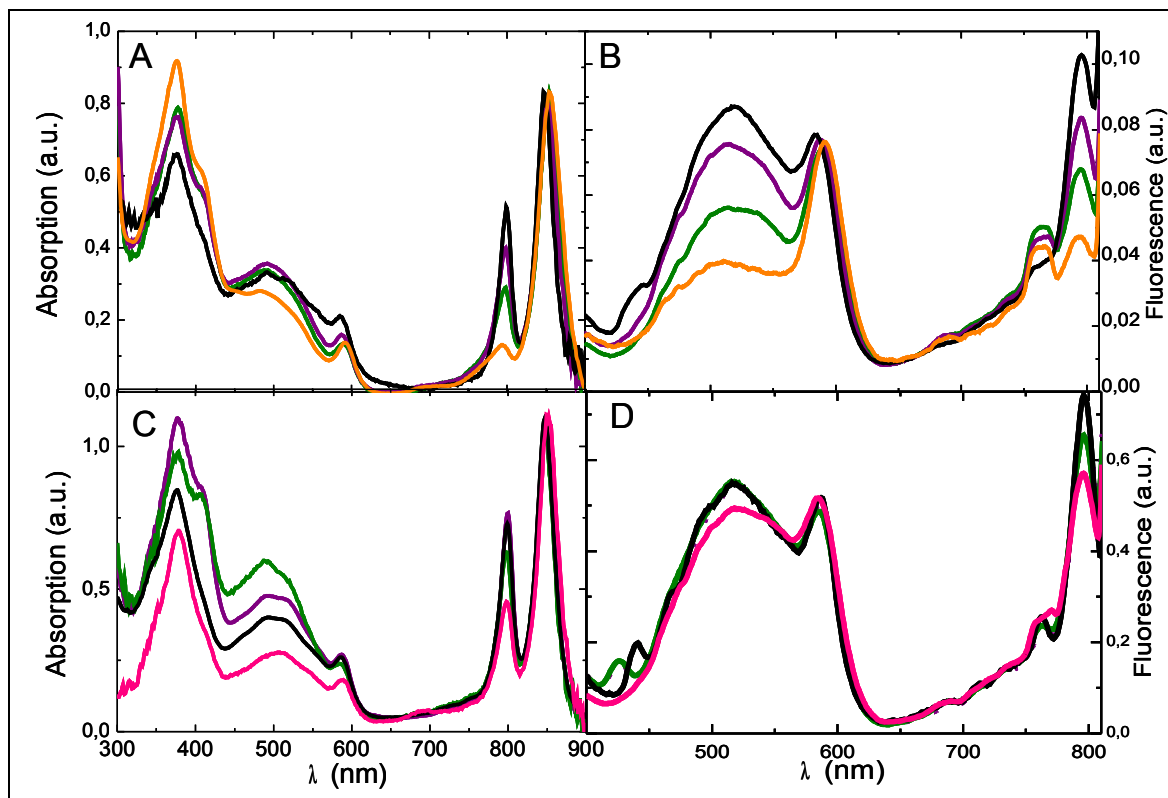


**Figure 5.16: Absorption (A) and fluorescence excitation (B) spectra of LH2  $\alpha$ AL<sub>20/S-4</sub> (orange), LH2  $\alpha$ AL<sub>19/S-4+A-10/S</sub> (olive) and LH2  $\alpha$ AL<sub>19/S-4+L-12/F</sub> (purple). Absorption (C) and fluorescence excitation (D) spectra of LH2 WT (black), LH2  $\alpha$ WT<sub>s-10/A</sub> (purple), LH2  $\alpha$ WT<sub>f-12/L</sub> (olive) and LH2  $\alpha$ WT<sub>s-10/G+f-12/L</sub> (pink). The absorption spectra are normalised at 850 nm. The fluorescence spectra are normalised by Q<sub>x</sub> band of BChl-B850 at 598 nm.**

Interestingly, mutating either  $\alpha$ F(-12) or  $\alpha$ S(-10) in WT sequence context does not affect ET between the Car and BChl-B850 (figure 3.17D). Mutation of both residues,  $\alpha$ S(-10) and  $\alpha$ F(-12), results in a mere 10-15% reduction in ET. Obviously, binding of Car is mediated by multiple interactions, which synergistically contribute to binding. In the model LH2, the impacts of single residues are amplified due to the simultaneous elimination of several native contacts contributing to Car binding in LH2 WT.

In summary, the site-directed mutational analysis of  $\alpha$ F(-12) and  $\alpha$ S(-10) in the model sequence and WT sequence context shows that both, serine and phenylalanine contribute to the binding of the Car. However, clearly  $\alpha$ F(-12) is more important for the binding of the Car pigments (figure 5.16). Based on the high resolution structure of LH2 of *Rps. acidophila* there are multiple polypeptide-polyene contacts with the residues distributed over the entire length of the  $\alpha$ - and  $\beta$ -subunits, particularly,  $\alpha$ I(-25),  $\alpha$ K(-26),  $\alpha$ V(-22)  $\beta$ W(-16),  $\alpha$ Q(-28),  $\beta$ V(-15),  $\alpha$ L(-12),  $\beta$ G(-12),  $\beta$ T(-11),  $\beta$ F(-8),  $\alpha$ V(-8),  $\alpha$ I(-5),  $\alpha$ A(-4),  $\alpha$ I(-3) and  $\alpha$ H(0) (Bowie 2005), , Considering such an extensive Car/protein interface (figure

5.4) it is surprising that mutation of only two residues,  $\alpha V(-3)$  and  $\alpha F(-12)$  which are in direct contact with the Car, results in such a significant loss of energy-transducing Car from the model LH complex (figure 5.16B). Previously, in LH2  $\alpha AL_{16/S-4}$ , the  $\alpha V(-3)$  has been replaced for alanine, however the changes in the Car binding are minor as compared to the changes in LH2  $\alpha AL_{20/S-4}$ . This points to a central role of the aromatic residue, phenylalanine, for the binding and assembly of LH active Car to this complex.

### 5.2.5 Study of the role of phenylalanine in carotenoid binding in LH2 from *Rb. sphaeroides*

In the RC from *Rb. sphaeroides*, there are seven phenylalanine residues in the close vicinity (within a distance of  $4 \leq \text{\AA}$ ) of the Car (Deber et al. 2001, . In the PsbS protein of PS II, which has been shown to bind with zeaxanthin, there are numerous phenylalanine residues . It appears that aromatic residues, in particular, phenylalanine, is in many cases located in the Car binding pockets of photosynthetic proteins. In the LH2 of *Rb. sphaeroides*, there is only one additional aromatic residue, namely F(-8) of the TM-helix of the  $\beta$ -subunit, in van der Waals ( $< 4\text{\AA}$ ) contacts with the Car (figure 5.17). To further investigate the role of aromatic residues in Car binding  $\beta F(-8)$  has been mutated in model LH2 and in WT LH2 from *Rb. sphaeroides*.

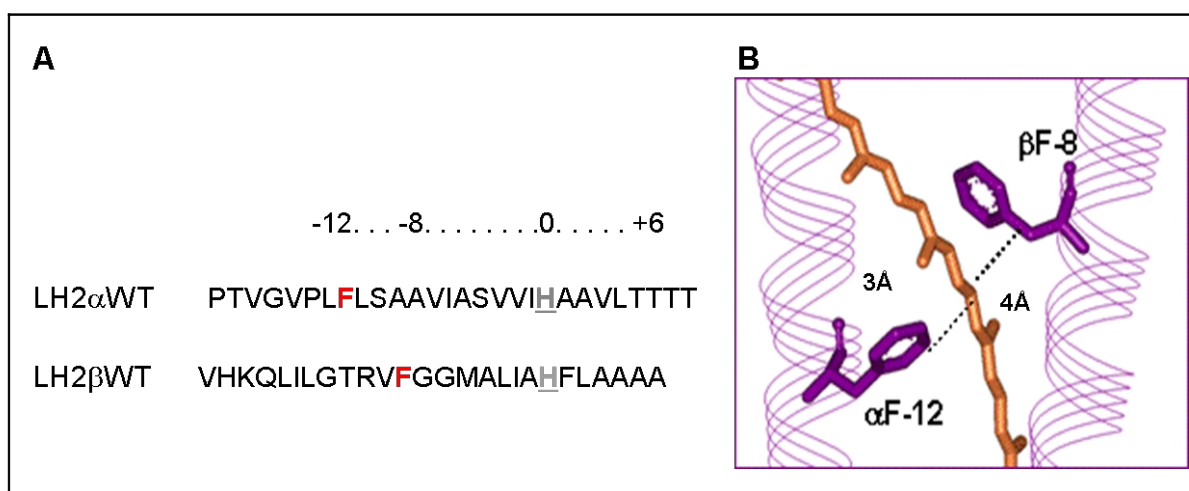


**Figure 5.17: Phenylalanine residues in close vicinity of the Car in the LH2 complex. (A) Amino acid sequences of LH2- $\alpha$  and  $\beta$  subunits (WT).** The residues,  $\alpha$ F(-12) and  $\beta$ F(-8) are shown in red. **(B) Detail view of the phenylalanine residues close to the Car in the model structure of *Rb. sphaeroides*  $\alpha\beta$  pair (purple) and Car (orange).** The phenylalanine residues are shown in stick model. Note that both phenylalanine residues are within a distance of  $\leq 4$  Å of the Car. The closest approach between Car and  $\alpha$ F(-12) is 3 Å and between Car and  $\beta$ F(-8) 4 Å respectively.

As shown in the figure 5.16, the replacement of  $\alpha$ F(-12) by leucine in WT LH2 exhibits no significant changes in the absorption or fluorescence excitation spectra (figures 5.16C, D). In contrast, the replacement of an additional phenylalanine, F(-8) to alanine results in the absence of assembled LH2 complex. Curiously, the replacement of  $\beta$ F(-8) with glycine does not result in the loss of the assembled LH2. In LH2  $\alpha$ WT<sub>F-12/A</sub>, there are, however, significant spectral changes (figure 5.18).

The substitution of phenylalanine by glycine in this position results in: (i) the absence of BChl-B800 and, (ii) red shift of the maximal absorption of BChl-B850 by  $\sim 10$  nm (figure 5.18). The aa glycine has been chosen because of the absence of any side chain in order to prevent potential blocking of this site to the Car. Here, alanine which is in the close vicinity (4.1 Å) of the Car may thus result in blocking of the site to the Car or lead to interactions which prevent the proper assembly of the LH2. However, it is not clear yet why glycine in position -8 of  $\beta$ -subunit permits complex assembly contrary to alanine. As shown by the statistical analysis, alanine interacts particularly often with the central carbon atoms of the polyene chain of the  $\beta$ -carotene in PS II (figure 5.28). Perhaps, alanine has a special role in the binding and assembly of Car. To study the effect of these two phenylalanine residues in close vicinity of the Car on LH2 assembly the double mutant,  $\beta$ F(-8)G and  $\alpha$ F(-12)L, LH2  $\alpha$ WT<sub>F-12/L</sub> +  $\beta$ WT<sub>F-8/G</sub>, is constructed and studied. The *in situ* absorption spectrum of this double mutant is shown in the figure 3.19. In the spectrum of LH2  $\alpha$ WT<sub>F-12/L</sub> +  $\beta$ WT<sub>F-8/A</sub> the band of BChl- B850 and BChl-B800 are absent while, a band around 760 nm appears that is typical for free BChl indicating either LH2 is not assembled properly or destabilized and thus disintegrating rapidly (figure 5.18).

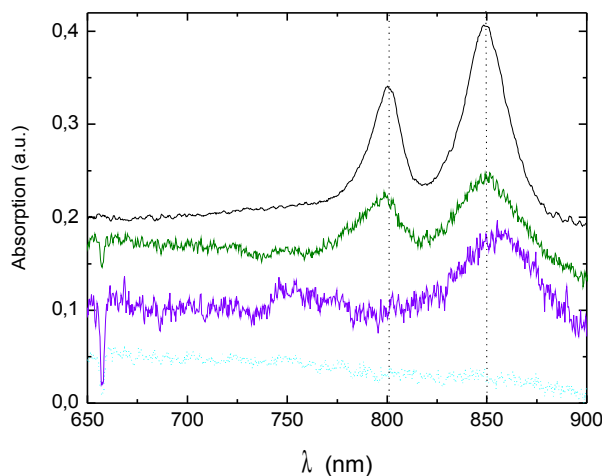


**Figure 5.18:** *In situ* absorption spectra of LH2 WT (black), LH2  $\alpha$ WT<sub>F-12/A</sub> (olive), LH2  $\alpha$ WT<sub>F-12/A</sub> +  $\beta$ WT<sub>F-8/G</sub> (violet) and LH2  $\alpha$ WT<sub>F-12/L</sub> +  $\beta$ WT<sub>F-8/A</sub> (cyan). The spectra were taken of *Rb. sphaeroides* colonies.

The absorption spectra of LH2  $\alpha$ WT<sub>F-12/L</sub> +  $\beta$ WT<sub>F-8/G</sub> in purified membranes is shown in figure 5.19A. The band at BChl-B800 is entirely lost and the band of BChl-B850 is ~ 8 nm red-shifted as compared with LH2 WT. It is not possible to properly assess the Car absorption bands in this mutant as this region is masked by the increased light scattering, due to the increase in membrane relative to mutant LH2 complex. The high level of scattering in the Soret region of the spectrum is obvious from the relative strength of the absorption bands in the near-IR and blue regions of the spectrum suggests that significantly less LH2 complex in LH2  $\alpha$ WT<sub>F-12/L</sub> +  $\beta$ WT<sub>F-8/G</sub> is assembled in the membrane in comparison to LH2 WT.

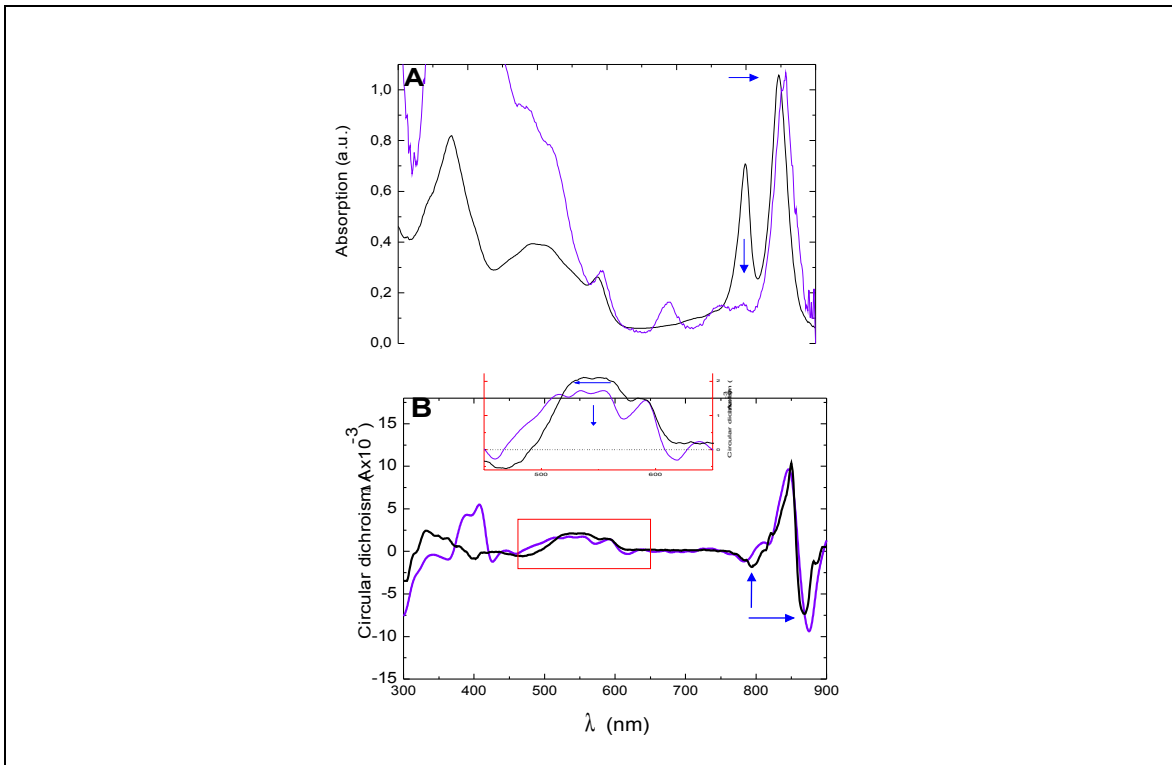


**Figure 5.19: Absorption (A) and CD (B) spectra of LH2 WT (black), and LH2  $\alpha\text{WT}_{F-12/L} + \beta \text{WT}_{F-8/G}$  (violet).** The spectra are normalised to the maximal absorption of the  $Q_y$  BChl-B850. Spectra are taken of purified membranes (material and methods). The arrows indicate changes between spectra.

The CD spectrum of LH2  $\alpha\text{WT}_{F-12/L} + \beta\text{WT}_{F-8/G}$  is recorded in figure 5.19B. The S-shaped, semi-conservative signal of the BChl-B850 is largely retained in LH2  $\alpha\text{WT}_{F-12/L} + \beta\text{WT}_{F-8/G}$ . It has two bands with extrema at  $\sim 848$  nm ( $\sim 850$  in LH2 WT) (+) and  $\sim 876$  ( $\sim 867$  in LH2 WT) nm (-) and a zero crossing at  $\sim 864$  nm ( $\sim 857$  in LH2 WT). This CD is largely similar to the CD of LH2 WT except for the red shift in the extrema (figure 5.19B). Conspicuously, there is a clear negative through at  $\sim 785$  nm even though, the BChl-B800 absorption band is nearly absent (figure 5.19B), which may either originate from residual BChl-B800 (which should then be structurally altered) or from the high exciton component of BChl-B850 (Leupold et al.1996, Koolhaas et al. 1998). In comparison to LH2 WT, this signal is somewhat reduced and shifted to the blue (from  $\sim 792$  nm to  $\sim 785$  nm). The CD signal of the Car is reduced and broadened. There is a shift of the maximum (from  $\sim 500$  nm to  $\sim 485$  nm), in comparison to LH2 WT (figure 5.19 inset), similar to the changes observed for the CD signal of LH2  $\alpha\text{AL}_{20/S-4}$  (figure 5.7). The significantly altered (reduced and modified) CD signal in the region 450-550 nm, indicates that either Car-protein or Car-Car interactions have been effectively changed in LH2, by the mutation of  $\alpha\text{F}(-12)$  and  $\beta\text{F}(-8)$  (figure 5.19B inset).

Energy transfer among the pigments LH2  $\alpha$ WT<sub>F-12/L</sub> +  $\beta$ WT<sub>F-8/G</sub> has been examined by fluorescence excitation spectroscopy (figure 5.20). The broad excitation band at 450-550 nm originates from SO, and the 800 nm excitation band from BChl-B800. However, the Car region of the LH2  $\alpha$ WT<sub>F-12/L</sub> +  $\beta$ WT<sub>F-8/G</sub> is reduced by approximately 50% in comparison to LH2 WT. This indicates a substantial loss of energy transducing Car from the complex upon the mutation of  $\alpha$ F(-12) and  $\beta$ F(-8) in the LH2 WT sequence context. The ET from BChl-B800 to BChl-B850 is nearly abolished.

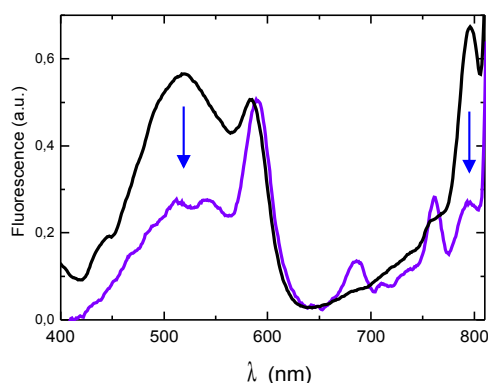


**Figure 5.20: Fluorescence excitation spectra of LH2 WT (black) and LH2  $\alpha$ WT<sub>F-12/L</sub> +  $\beta$ WT<sub>F-8/G</sub> (violet).** The spectra are normalised at  $Q_x$  of BChl 598nm. Spectra are taken of purified membranes.

This study shows that the mutation of only two phenylalanine residues, results in the significant reduction of the ET from Car to BChl in LH2. These mutations also cause changes in the absorbance of BChl-B800, suggesting a direct or indirect (via the Car molecule) effect on the binding of the BChl-B800. In the modelled structure of *Rb. sphaeroides* (figure 5.17),  $\alpha$ F(-12) is in the vicinity of BChl-B800 (closest approach is at  $\leq 5\text{\AA}$ ). Whereas  $\beta$ F(-8) is not in close vicinity of Car. It is near to the  $\beta$ R(-10), which is important for the binding of BChl-B800. Thus, it could be possible that the loss of the BChl-B800 is an indirect effect due to the alteration of the Car and/or critical residues in the BChl-B800 binding pocket.

It is also demonstrated, that the removal of the BChl-B800 causes blue shift in the absorbance peaks of the Car, however the Car is still bound and does not affect in the ET of the Car (Crielaard et al. 1994, Fowler et al. 1997). However, in this system, LH2, is quite difficult to separate the effect of the two pigments, BChl and Car.

The RR spectra of the LH2  $\alpha$ WT<sub>F-12/L</sub> +  $\beta$ WT<sub>F-8/G</sub> and LH2 WT is shown in figure 5.21. The replacement of the  $\alpha$ F(-12) and  $\beta$ F(-8) residues with leucine and glycine respectively,

results in significant changes in the RR bands of the Car molecule. These mutations induce a significant reduction of the major component present in the  $\nu_4$  region, at  $985\text{ cm}^{-1}$ . Interestingly, in this mutant LH2  $\alpha\text{WT}_{\text{F-12/L}} + \beta\text{WT}_{\text{F-8/G}}$  (figure 5.21), the reduction of the intensity at  $985\text{ cm}^{-1}$  is accompanied by the appearance of a new component at  $965\text{ cm}^{-1}$ , which indicates changes in the configuration of the Car. This band was also observed in the LH2  $\alpha\text{AL}_{20/\text{S-4}}$  mutant (figure 5.14). This indicates that the  $\alpha\text{F}(-12)$  and  $\beta\text{F}(-8)$  residues are necessary to keep the molecular conformation of Car as in the WT protein. It appears that these residues are in close contact with the Car molecule, and the phenylalanine residues lock it into a precise, well-defined, configuration. It is thus not surprising that these two aromatic residues strongly influence the specific binding of Car to LH2 (figure 5.27, 5.28).

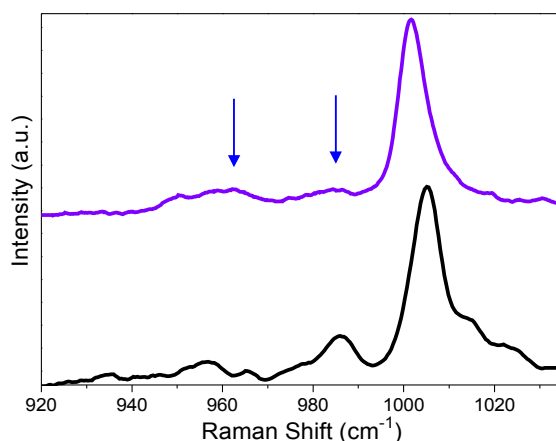


**Figure 5.21:** RR spectra of LH2 WT (black), LH2  $\alpha\text{WT}_{\text{F-12/L}} + \beta\text{WT}_{\text{F-8/G}}$  (violet). The arrows indicate changes between spectra.

To assess the influence of  $\beta\text{F}(-8)$  on the assembly, LH2  $\beta\text{WT}_{\text{F-8/G}}$  has been expressed with LH2  $\alpha\text{AL}_{20/\text{S-4}}$  as complement  $\alpha$ -subunit. The effect of  $\beta\text{F}(-8)$  is amplified in the model sequence context due to the reduction and elimination of native contact .

The *in situ* spectrum of LH2  $\alpha\text{AL}_{20/\text{S-4}} + \beta\text{WT}_{\text{F-8/G}}$ , (figure 5.22) shows that the BChl-B850 is red shifted  $\sim 7\text{ nm}$ , from  $\sim 854\text{ nm}$  to  $\sim 861\text{ nm}$ , in comparison to LH2  $\alpha\text{AL}_{20/\text{S-4}}$ .

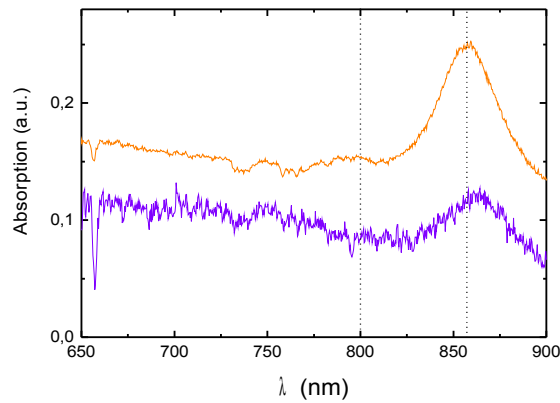


**Figure 5.22:** *In situ* absorption spectra of LH2  $\alpha\text{AL}_{20/\text{S-4}}$  (orange) and LH2  $\alpha\text{AL}_{20/\text{S-4}} + \beta\text{WTF}_{\text{F-8/G}}$  (violet). The spectra are taken of *Rb. sphaeroides* colonies.

As shown in the figure 5.23A the CD signal of LH2  $\alpha\text{AL}_{20/\text{S-4}} + \beta\text{WTF}_{\text{F-8/G}}$  is further reduced and broadened in the Car range as compared with the signal of LH2  $\alpha\text{AL}_{20/\text{S-4}}$  (figure 5.7A). Clearly, the CD spectra of LH2  $\alpha\text{AL}_{20/\text{S-4}} + \beta\text{WTF}_{\text{F-8/G}}$  resemble the CD spectra of Car-less LH2 complexes from *Rb. sphaeroides* R26.1 (figure 5.23A inset). There are some differences, particularly, in the blue region of the spectra. It should be noted that the increase in light scattering due to the low expression levels of this mutant may affect the CD in the blue region and should thus be treated with care. Nevertheless, the pronounced reduction in the CD signal in the Car range, indicate the near absence of the Car from LH2  $\alpha\text{AL}_{20/\text{S-4}} + \beta\text{WTF}_{\text{F-8/G}}$ .

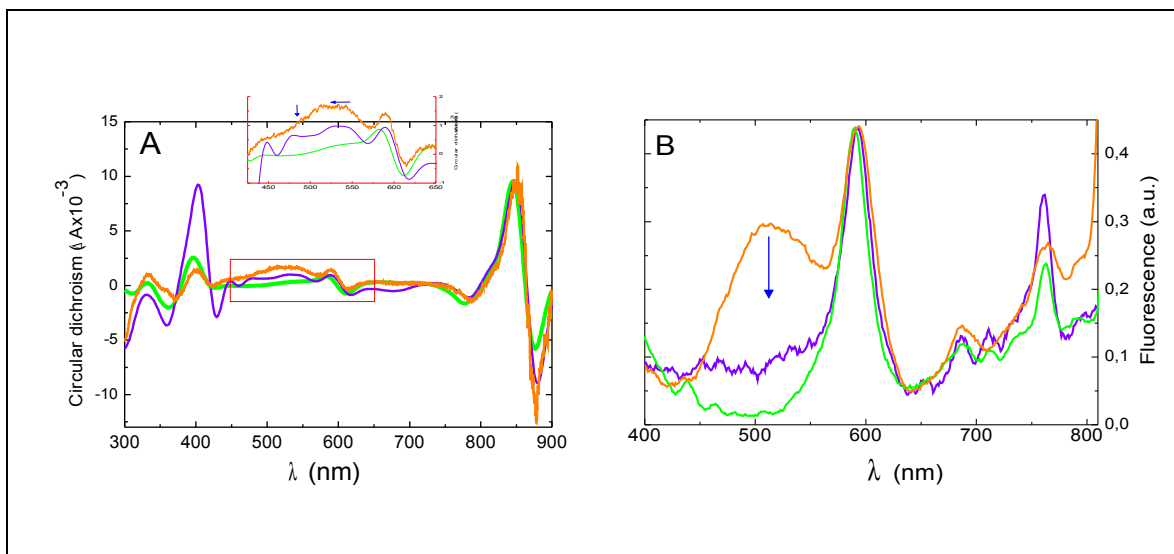


**Figure 5.23:** CD (A) and fluorescence spectra (B) of LH2  $\alpha\text{AL}_{20/\text{S-4}}$  (orange), LH2  $\alpha\text{AL}_{20/\text{S-4}} + \beta\text{WTF}_{\text{F-8/G}}$  (violet) and LH2 R26.1 (green). The spectra are taken from purified membranes. The fluorescence spectra are normalised at 598 nm.

Essentially, ET between the Car and BChl-B850 in model LH2  $\alpha\text{AL}_{20/\text{S-4}} + \beta\text{WT}_{\text{F-8/G}}$  is nearly lost similar to ET in the Car-less LH2 from *Rb. sphaeroides* R26.1 (figure 5.23B). In comparison to LH2 WT (not shown) only ~10% of the energy is transferred to BChl-850. In addition, the ET from BChl-B800 to BChl-B850 in the model complexes LH2  $\alpha\text{AL}_{20/\text{S-4}} + \beta\text{WT}_{\text{F-8/G}}$  is nearly absent as in R26.1 LH2 from *Rb. sphaeroides*.

Thus, the replacement of the two aromatic residues,  $\beta\text{F}(-8)$  and  $\alpha\text{F}(-12)$ , which are located in close vicinity of the Car in LH2 (figure 5.17), results in significant disturbance in the binding of Car. To the best of our knowledge, the significance of aromatic residues for Car binding has not been shown by an experimental approach. Based on recent model calculations of Car binding in LH2 from *Rps. molischianum* and in PS I from *Thermosynechococcus elongatus*, the importance of aromatic residues have been implicated (Wang & Hu 2002). Specifically, phenylalanine residues have been calculated to contribute up to 3.6 kcal/mol to the binding of Car in LH2 complexes from *Rps. molischianum*. Quantum chemical calculations also suggest that intermolecular hydrogen bond interactions (C-H $\cdots$ O-C) between Car and the B800-BChl in the LH2 complex may take place. It is not known, yet, whether these H-bonding interactions are widespread. In the LH2 complex from *Rps. molischianum*, the BChl-B800 adopts a different orientation from the one of BChl-B800 in *Rps. acidophila*. Mutational studies of bacterial RC already demonstrated that phenylalanine maybe critical for the binding of Car. In that case, however, rotation of the phenylalanine ring determined the topology of the Car in the TM-helices. Here, we show that Phe residues critically contribute to the binding of light harvesting active Car in LH2. In the model LH2 complex, binding of the Car is largely driven by two Phe residues,  $\beta\text{F}(-8)$  and  $\alpha\text{F}(-12)$ .

### 5.2.6 Statistical analysis of Car-protein interactions in photosystem I and II

An in depth statistical analysis of the membrane-embedded Car pockets of the photosystems I and II are made to further explore the role of aromatic residues in Car binding. In these two photosystems, there are in total 32  $\beta$ -carotenes bound which constitute thus a sizeable data base for a statistical analysis of Car binding pockets. As the Cars are generally rather similar, in particular, the central polyene chain  $\beta$ -carotene may serve as an approximate model for the binding of other Cars, such a SE and SO, present in *Rb. sphaeroides*. The differences between these Cars are at end group (figure 5.3), while the polyene backbone from carbon atom 6 to 6' are identical (figure 5.24).

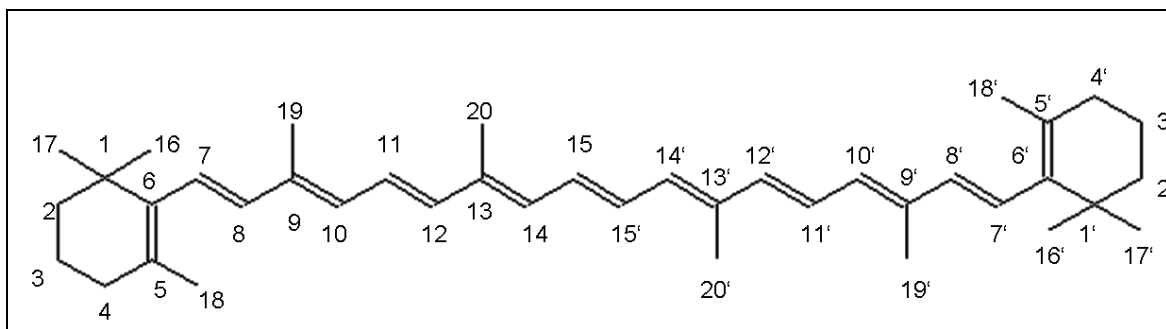


**Figure 5.24: Structure of  $\beta$ -carotene.** Nomenclature is according to IUPAC.

PS I binds a total of 22  $\beta$ -carotenes and PS II a total of 11  $\beta$ -carotenes. Here, the proteinaceous environments around the Cars of PS I (figure 5.27) and PS II (figure 5.28) have been analysed within a radius of  $\leq 5 \text{ \AA}$ . The contacts (defined as atoms within  $\leq 5 \text{ \AA}$ ) between the photosystem' apoproteins and the  $\beta$ -carotenes appear to be similar in the two photosystems. Contacts occur most frequently with the methyl groups of the polyene chain, in particular, at C16, 17, 18, 19 and 20 as well as C16', 17', 18', 19' and 20'. In PS II, the central carbons, 14, 14', 15, and 15' are also frequently in close contact with the protein environment. In addition, in both, PS I and PS II, the carbon atoms of the terminal  $\beta$ -ionylidene rings show elevated contact frequency with the surrounding proteins. Interestingly, the carbons in the centre of the polyene chain, C15, C16 and C17, of PS II have the highest number of contacts together with the protruding carbons of the methyl groups and ionylidene rings (figure 5.28). This difference in interaction frequency indicates a different arrangement of the Cars in the two systems possibly related to distinct functions. In PS I, some of the polyene chains of the  $\beta$ -carotenes run parallel to the membrane plane (figure 5.25), while in PS II, some of the polyene chains generally run perpendicular to the membrane plane (figure 5.26). The amino acid residues in the close vicinity of Car are largely similar for the two photosystems. The aromatic residue, phenylalanine is next to leucine residues most often found to be in close vicinity of the  $\beta$ -carotene. In PS I, 20% and in PS II, 27% of all contacts between  $\beta$ -carotene and polypeptide are made up of contacts to phenylalanine residues. Out of the total contacts between Cars and polypeptide residues, 22% are with leucine residues in both PS I and PS II. Approximately 10% of the TM residues of membrane proteins are phenylalanine residues. Thus, the Car-protein interaction frequency of 26 % and 20 % is significantly higher, than would be expected from a random distribution of phenylalanine residues in the membrane. Also leucine residues are slightly overrepresented in the Car vicinity.

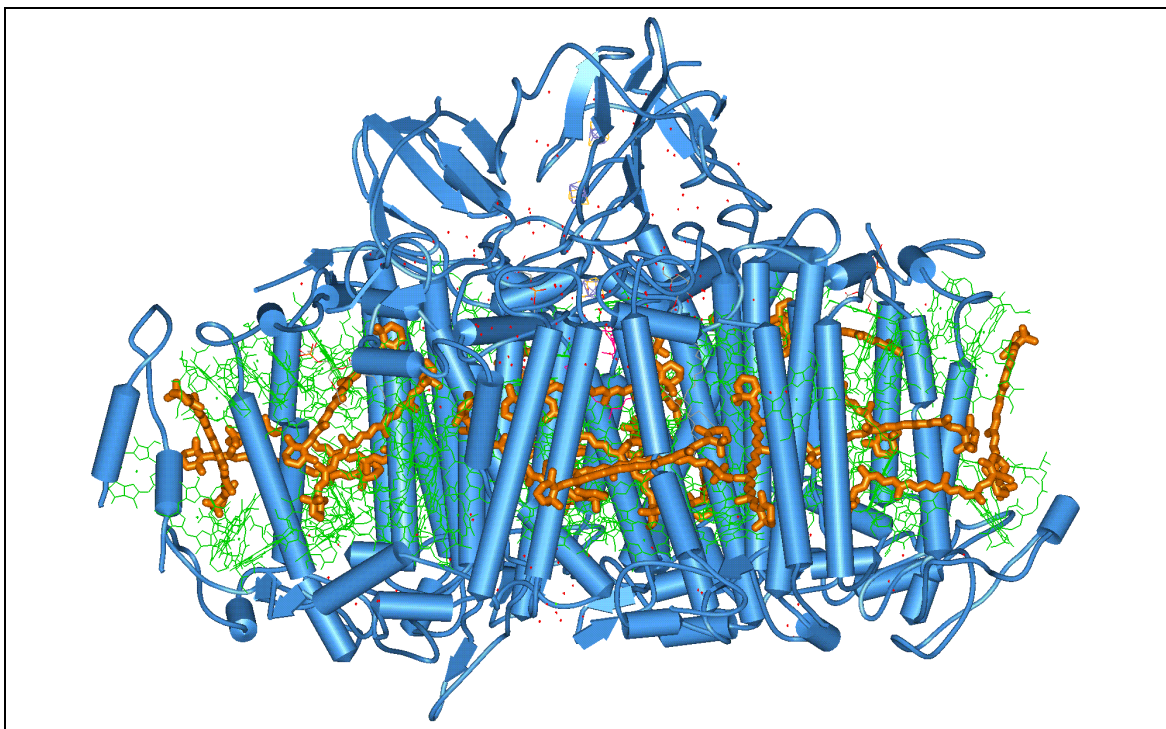


**Figure 5.25: Crystal structure of PS I .** Note that there are Cars both parallel and perpendicular to the membrane plane.

This, however, is clearly more pronounced for phenylalanine. In PS II, the contacts between some of the carbons of the carotenes such as C1, 17, 7, and phenylalanine, can even make up more than 2/3 of the contacts at this particular carbon. In analogy, tyrosine and tryptophan are also frequently found in close vicinity of the Cars, particularly, at the carbon atoms of the ionylidene rings (figure 5.28). These are often located at the membrane interface where the occurrence of phenylalanine is slightly reduced and that of tyrosine and tryptophan residues is elevated. Curiously, alanine makes up a considerable part of the contact surface between apoprotein and  $\beta$ -carotenes. Alanine residues, which make up about 13% of the residues of TM-helices are found to make up 9% in PS I and 14% in PS II of the total contacts to  $\beta$ -carotene. This appears to reflect a random distribution of alanine residues around the  $\beta$ -carotenes. However, in PS II, alanine residues are primarily found to interact closely with the central carbon atoms of the polyene chain (figure 5.28). At some of the Car carbons, the contacts between alanine and Car contacts make up nearly 1/3 of the contacts to polypeptide. This may indicate that the polyene chain from C12 to C20 tightly packs with the helices. Polar residues are clearly underrepresented in the  $\beta$ -carotene binding pockets while charged residues are entirely absent except for few lysine and arginine residues in PS I (figure 5.27).

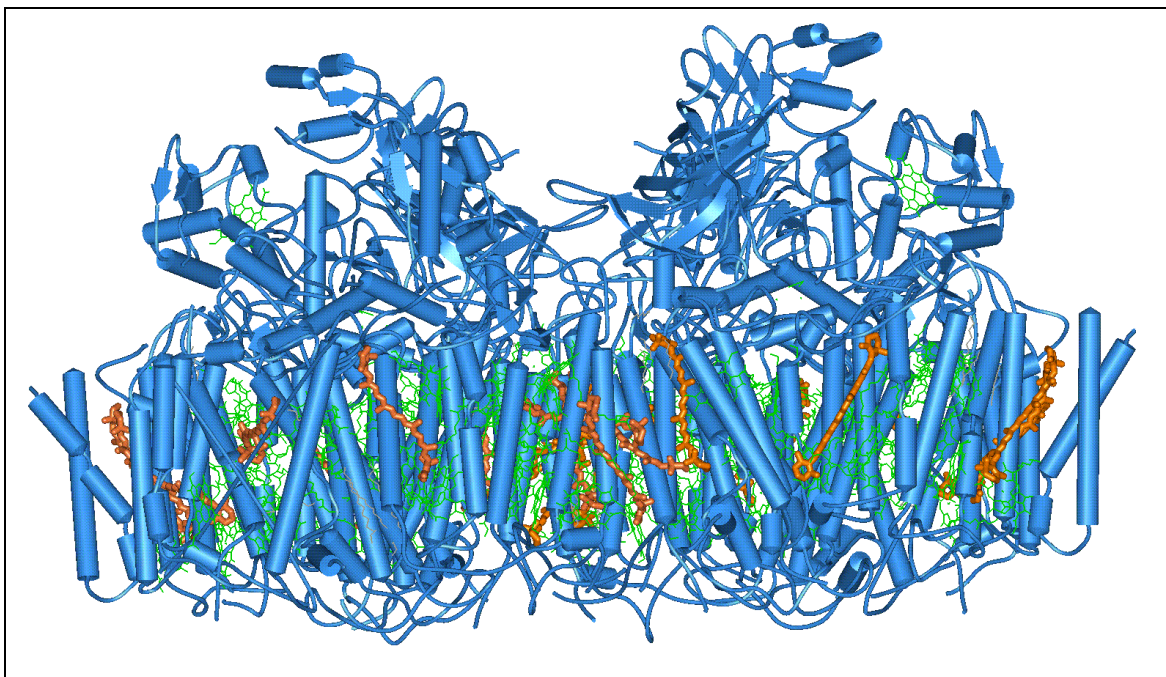


**Figure 5.26: Crystal structure of PS II .** Note that the Cars are generally oriented perpendicular to the membrane plane.

Phenylalanine, as well as tryptophan and tyrosine, may partake in  $\pi$ - $\pi$  stacking interactions. The strength of these interactions depends on the distance and geometry of the interacting molecules (Wang & Hu 2002). The residues tryptophan and tyrosine may have additional interactions *e.g.* H-bonding which has not been further analysed in the scope of this study. Next to the aromatic residues, the aliphatic residues leucine, isoleucine and valine are frequently close to the  $\beta$ -carotene. Curiously, the short residues, alanine, and serine make up a considerable part of the contact surface of Car/apoprotein. This is particularly pronounced for the polyene chains of the  $\beta$ -carotenes in PS II, but not in PS I. Considering that in PS II, the Car orientations are closely similar to the TMH orientations; it may indicate that the chain from atom C12 to C20 tightly pack with the TM helices. Glycine residues are also found around the atoms of the polyene chain further supporting the idea of tight packing even with the polypeptide backbone. In any case, the aromatic residues, in particular, phenylalanine, are frequently in close contact with the  $\beta$ -carotene molecules of PS I and PS II. This has been shown previously , and further supports the experimental finding that aromatic residues play a critical role in binding of the  $\beta$ -carotenes to polypeptide.

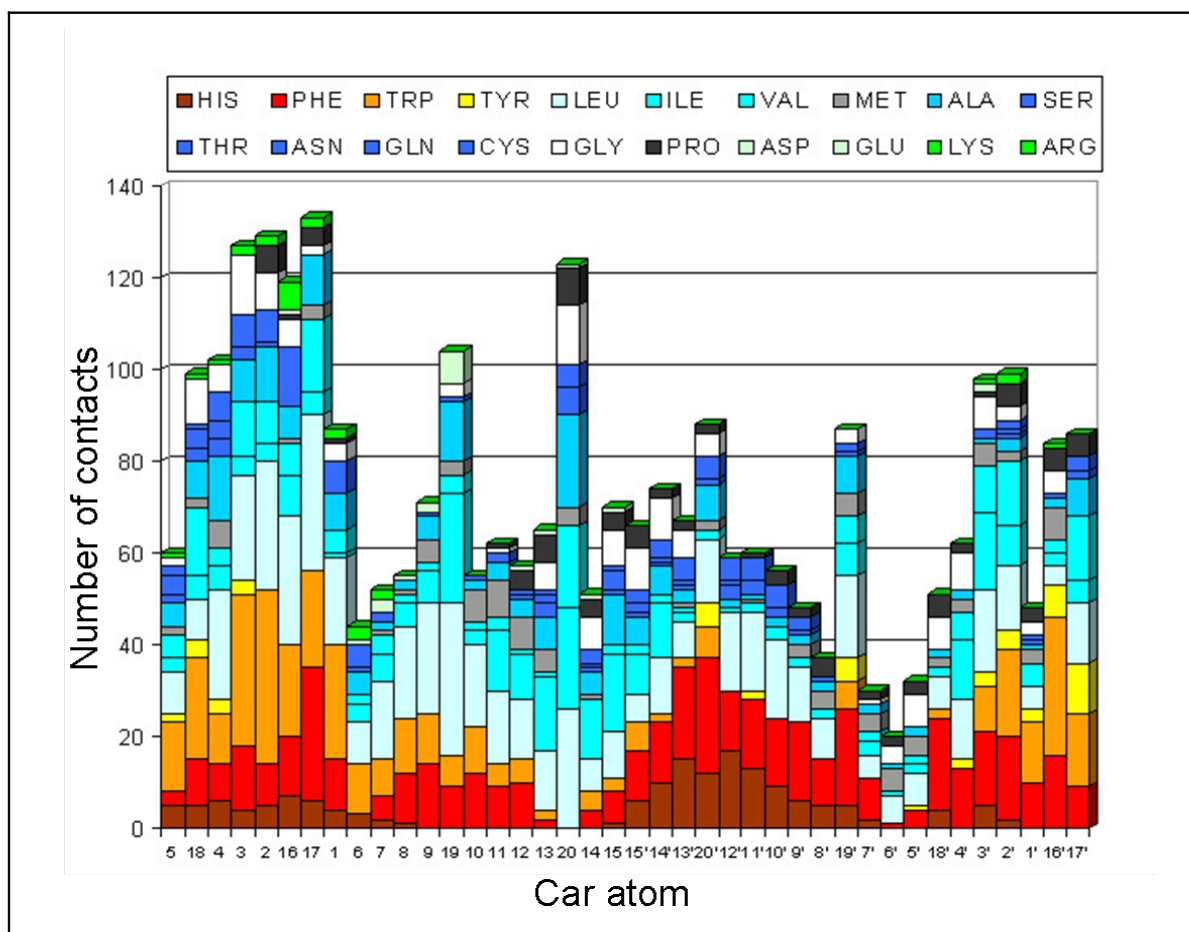


**Figure 5.27: Statistical analyses of Car binding sites.** Residues distribution in the Car binding sites of PS I . Contacts are determined within a radius of  $\leq 5\text{\AA}$ . Colour codes are as indicated.

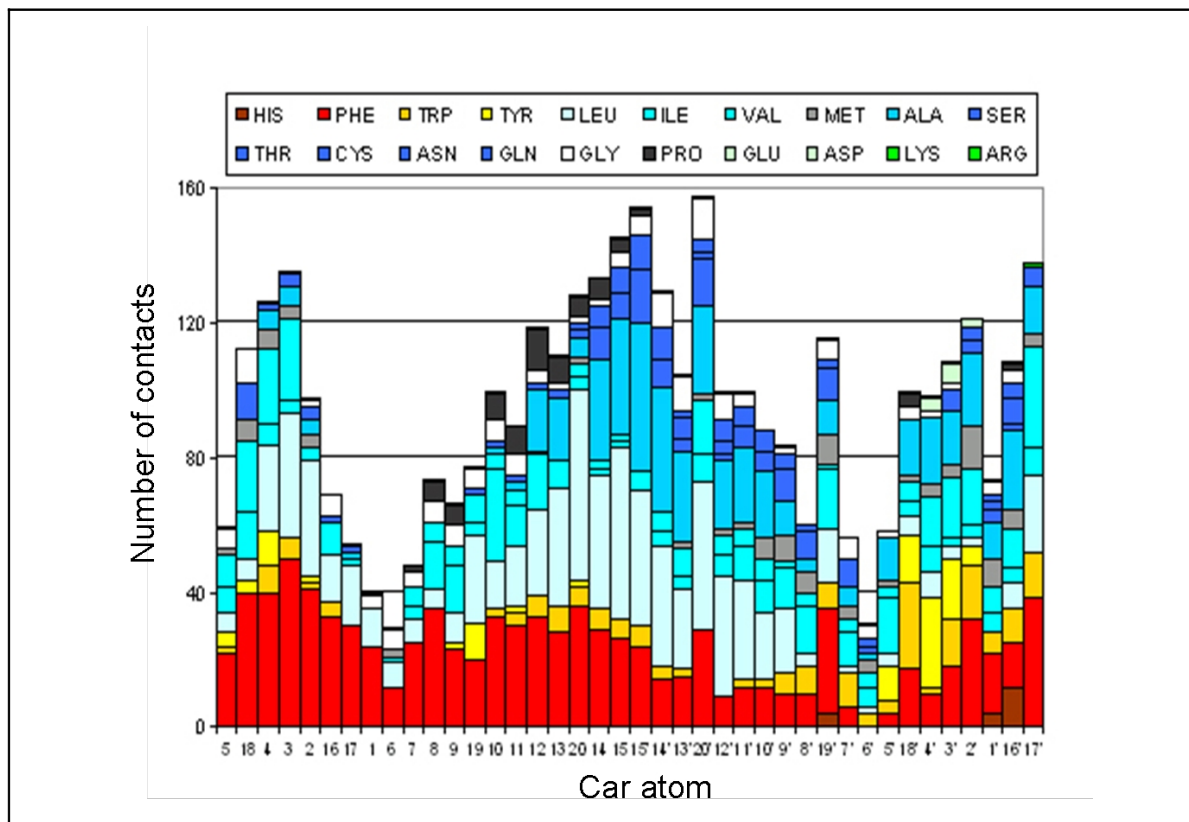


**Figure 5.28: Statistical analyses of Car binding sites.** Residues distribution in the Car binding sites of PS II. Contacts are determined within radius of  $\leq 5$  Å. Colour codes are as indicate.

In any case, the clear overrepresentation of the aromatic residues, in particular, phenylalanine points towards a particular role of the phenylalanine residues in the binding of Car.

### 5.2.7 Thermal stability of the LH2 depending on the Car contents

A number of investigations suggest that the stable assembly of LH2 requires the presence of the Car molecules: Car deficient purple non sulphur bacteria generally lack LH2 complexes (Cohen-Bazire & Stanier 1958, Fuller & Anderson 1958, Lang & Hunter 1994). For instance, the Car-less *Rb. sphaeroides* mutant strain, R26, entirely lacks LH2 (Clayton & Smith 1960). This mutant strain, however, has a tendency to revert to the strain R26.1, containing a modified LH2 complex which still lacks (at least colored) Cars. In this LH2, BChl-B800 is absent, and the arrangement of BChl-B850 is altered (Davidson & Cogdell 1981, Gall et al. 2003). Thus, the additional modification in R26.1 somewhat compensates for the absence of Car, as yet not understood manner. In addition, the extraction of Car from assembled LH2 complex from *Rb. capsulatus* have been shown to result in destabilization.

To further explore the effect of the Car on the structural stability of LH2, the decay of CD signal of LH2 WT and the LH2 mutant complexes, which lack Car or contain reduced amounts of Car, is monitored during heat denaturation. The thermal stability of LH2  $\alpha$ AL<sub>20/S-4</sub>, as compared with LH2 WT, is clearly reduced (figure 5.29). The  $T_m$  is shifted from  $\sim 68^\circ\text{C}$  in LH2 WT to  $\sim 50^\circ\text{C}$  in LH2  $\alpha$ AL<sub>20/S-4</sub>, indicative of a pronounced decrease in structural stability. In addition, the cooperativity (see chapter 3) of denaturation is altered for the model LH2 as compared to LH2 WT. In the model LH2, the loss of the BChl-B800 and Car both result in the reduction of packing surface between the pigment and the helices. In addition, the mutant LH2  $\alpha$ AL<sub>16/S-4</sub>, in which 8 residues have been changed (chapter 3), exhibits already a decrease in the  $T_m$  in comparison to LH2 WT ( $\sim 56^\circ\text{C}$  in LH2  $\alpha$ AL<sub>16/S-4</sub>) ( $\sim 67^\circ\text{C}$  in LH2 WT). The alterations in the denaturation curves, in particular the shift in  $T_m$  of LH2  $\alpha$ AL<sub>20/S-4</sub> is significant as compared to LH2  $\alpha$ AL<sub>16/S-4</sub> and LH2 WT, and emphasizes the important role of the Car and BChl-B800 molecules for the LH2 stability. Considering, that both the BChl-B800 and the Car are strongly altered in LH2  $\alpha$ AL<sub>20/S-4</sub>, the contribution of each of those pigments cannot be determined by use of these mutants. As binding of BChl-B800 is compulsory coupled to the binding of the Car, it is as yet impossible to produce a mutant complex which lacks Car only.

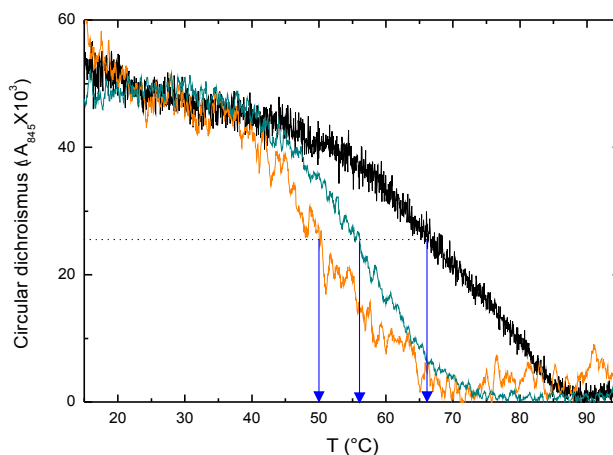


**Figure 5.29:** Thermal denaturation of LH2 WT (black), LH2  $\alpha$ AL<sub>16/S-4</sub> (dark cyan), and LH2  $\alpha$ AL<sub>20/S-4</sub> (orange). Changes of the CD signal are monitored at 845 nm during heating of suspended membranes.

The thermal stability of the double mutant LH2  $\alpha$ WT<sub>F-12/L</sub> +  $\beta$ WT<sub>F-8/G</sub> (figure 5.30) is clearly reduced as compared with WT LH2. The midpoint of transition is shifted to lower temperatures,  $\sim 67^\circ\text{C}$  in LH2 WT and  $\sim 49^\circ\text{C}$  in the mutant. Interestingly, the cooperativity of denaturation is not altered in LH2  $\alpha$ WT<sub>F-12/L</sub> +  $\beta$ WT<sub>F-8/G</sub> and thus the change in

cooperativity is apparently related to the model sequences in these artificial complexes. As shown above the double mutation,  $\alpha$ F(-12) and  $\beta$ F(-8), in WT context results in the reduction of the Car content (by 50%) and in the loss of BChl-B800 (figure 5.18,5.19). Thus as in the case of model LH2  $\alpha$ AL<sub>20/S-4</sub> the decrease in thermal stability cannot be assigned to the reduction of Car only.

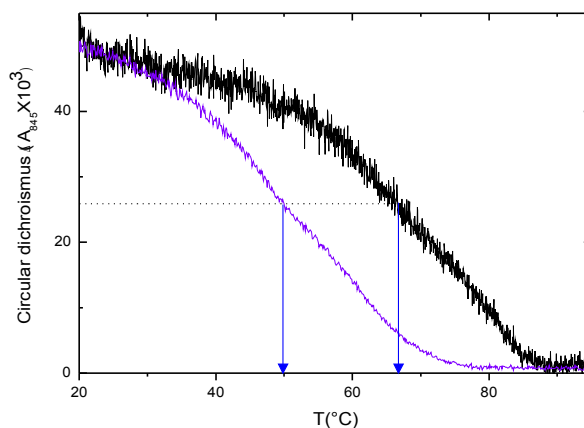
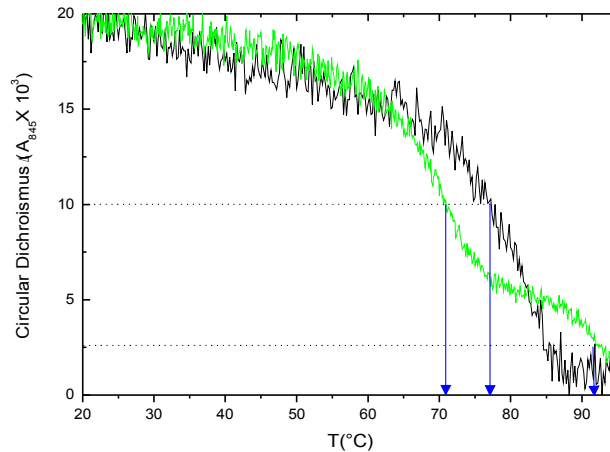


**Figure 5.30: Thermal denaturation of LH2 WT (black) and LH2  $\alpha$ WT<sub>F-12/L</sub> +  $\beta$ WT<sub>F-8/G</sub> (violet).** Changes of the CD signal at 845 nm during heating of suspended membranes.

Interestingly, the LH2 from R26.1 which does neither contain BChl-B800 nor Car (figure 5.31) shows a fairly slight decrease in thermal stability relative to WT LH2. Naturally, the complexes are isolated in detergents to remove LH1 and RC. The thermal stability of LH2 complexes in detergent is elevated compared to the stability in the native membrane. The  $T_m$  of LH2 WT in detergent is  $\sim 77^\circ\text{C}$  and of the  $T_m$  of LH2 R26.1 is  $\sim 71^\circ\text{C}$ . The denaturation curve of LH2 from R26.1, however, is clearly biphasic, in contrast, to the denaturation curves of WT LH2, double mutant and model LH2 complexes. At present, we do not have an explanation for the biphasic behaviour of R26.1. Possibly, the absorption properties of LH2 R26.1 are altered during denaturation resulting in apparent biphasic decay. This, however, has not been investigated further here. In any case, the thermal stability of R26.1 is affected by the removal of Car and BChl-B800 but apparently still high in comparison to pronounced reduction in stability observed in double mutant LH2. The mutation in R26.1 thus appears to compensate for the loss of BChl-B800 and Car in a not understood manner (Lang & Hunter 1994).



**Thermal denaturation of LH2 WT (black) and LH2 R26.1 (green).** Changes of the CD signal at 845 nm during heating of LH2 complexes isolated in detergents. Note, that the denaturation curve of LH2 R26.1 is biphasic. The  $T_m$  are indicated by the arrows (blue).

The model complex LH2  $\alpha$ AL<sub>20/S-4</sub> and LH2  $\alpha$ AL<sub>20/S-4</sub> +  $\beta$ WT<sub>F-8/G</sub> contain distinct amounts of Car (figure 3.23B). In both complexes, BChl-B800 is depleted but in LH2  $\alpha$ AL<sub>20/S-4</sub> +  $\beta$ WT<sub>F-8/G</sub>, the content of light harvesting active Car is nearly entirely depleted as well (figure 5.23B). The thermal stability of LH2  $\alpha$ AL<sub>20/S-4</sub> +  $\beta$ WT<sub>F-8/G</sub>, is further decreased in comparison to LH2  $\alpha$ AL<sub>20/S-4</sub>, (from  $\sim 49$  to  $\sim 42^\circ\text{C}$ , respectively (figure 5.32)). The further decrease in the midpoint of transition, in model LH2  $\alpha$ AL<sub>20/S-4</sub> +  $\beta$ WT<sub>F-8/G</sub> nearly depleted of Car shows that the residue  $\beta$ F(-8) contributes to the stability of LH2.

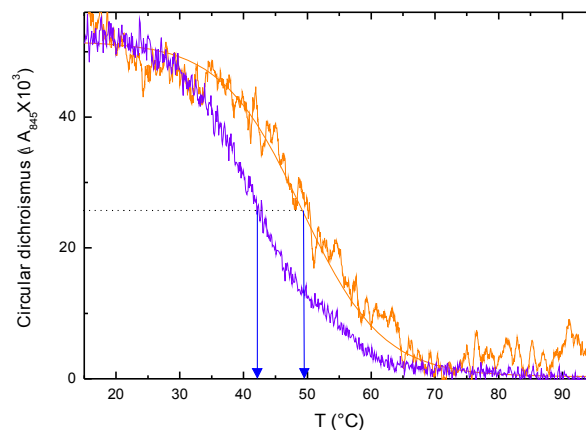


**Figure 5.32: Thermal denaturation of LH2  $\alpha$ AL<sub>20/S-4</sub> (orange) and LH2  $\alpha$ AL<sub>20/S-4</sub> +  $\beta$ WT<sub>F-8/G</sub> (violet).** Changes of the CD signal at 845 nm during heating of suspended membranes.

One of the effects of the removal of the aromatic side chain of  $\beta F(-8)$  is the loss of Car in this complex. This is accompanied by further the destabilisation and supports the notion that Car-protein interactions are critical for the structure stabilisation of LH2. The additional destabilisation, however, is not very pronounced as already LH2  $\alpha AL_{20/S-4}$  is only marginally stable. Nevertheless additional reduction in Car content results in further destabilisation. The absence of helix-helix interaction in the TM region of LH2 , , which usually drive stable assembly of membrane protein devoid of pigments, is obviously complemented by helix-pigment interaction. Here, it is shown that interaction between the Car and a single phenylalanine may considerable elevate the structural stability of such a complex.

### 5.3 Conclusions

In this study a possible Car binding pocket is identified in which the aromatic residue phenylalanine plays a crucial role in functional binding of Car. This is demonstrated by site direct mutagenesis of the phenylalanine residues which are in the immediate environment of the complexes' Car in the TM helices of native and model LH2 complexes from *Rb. sphaeroides*. The significant contribution of phenylalanine residues to Car binding pockets is further supported by statistical analyses of high resolution structures of photosystems I and II with 32 Car binding pockets. Aromatic residues are frequently part of the Car binding environment with phenylalanine residues making up to 40% of the total number of contacts between some of the Car atoms, in particular, of the polyene chains, and the polypeptides.

The Car/protein interface in LH2 is extensive, including also protein subunits from neighbouring  $\alpha\beta$  subunits. In LH2  $\alpha AL_{20/S-4}$ , only two residues that interact with Car are changed, one of them is phenylalanine -12. The carotenoid content is reduced by approximately 50%. Furthermore, the alterations in functional binding of Car are significant resulting in a largely reduced energy transfer from Car to BChl-B850.

Equally, in WT sequence context the replacement of the two phenylalanine residues in the close vicinity of membrane embedded Car results in the significant reduction in the content of the light harvesting active Car. Resonance Raman spectroscopy shows that removal of the aromatic side chain results in an altered configuration of the Car. The phenylalanine residues thus contribute to the Car binding and modulation of its molecular configuration. This points at a central role of the aromatic residue, phenylalanine, in the binding and assembly of light-harvesting active Car in transmembrane proteins.

## 6. SUMMARY

The presented thesis has focused on the interactions between protein and pigments in photosynthetic membrane proteins, and the significance of these interactions in membrane protein assembly. The thesis has been divided into 3 Chapters, two are focused on the interactions between (bacterio)chlorophyll and proteins, and one is focused on the interactions, between carotenoid and proteins. In order to explore these interactions model proteins have been designed based on the peripheral antenna of *Rhodobacter sphaeroides*. In the model LH2 complexes, portions of the transmembrane helices, in particular, at the pigment binding sites, are replaced simplified alternating by alanine-leucine stretches. In the model sequence context, the effects of particular amino acids are amplified, and thus allow for convenient identification of potentially critical interaction motifs. This approach is employed to study the factors that contribute to pigment binding and pigment-protein assembly. To confirm the significance of thus identified motifs, they are subsequently also examined in the WT sequence context.

In Chapter 3, it is shown that the residue at position -4 of the  $\alpha$ -subunit has a critical structural role for the proper organisation of the excitonically coupled BChl dimer in the antenna complex. In WT LH2, the residue at this position makes an H-bond to the C13<sup>1</sup> keto carbonyl group of one of the dimeric BChl molecules. The potential importance of such a H-bonding motif at the BChl/protein interface is demonstrated by use of the model LH2 in which the H-bond drives the folding and assembly of this transmembrane BChl-protein. The structural role of this residue at the BChl/protein interface is further demonstrated by the linear correlation between the LH2 spectral tuning and the residue-BChl contact.

In Chapter 4, the aspect of diastereotopic ligation to the central Mg of BChl is explored, in particular, the consequences of BChl-ligation for folding and assembly of BChl-proteins. The analysis of H-bonding patterns in Chl-binding photosystem I and II showed that H-bonding at the (B)Chl-protein interface is structurally distinct depending on the ligation type. In essence, the C13<sup>1</sup> keto groups of (B)Chl ligated in the  $\beta$ -position, contrary to those ligated in the  $\alpha$ -position, are frequently employed to associate Chl-helix units and thus involved in tertiary interactions. Disruption of such H-bonding interactions by site directed mutagenesis significantly altered the structural stability and assembly of the LH2 complex in the membrane. These findings suggest that H-bonding to  $\beta$ -ligated bacteriochlorophyll is a key structural motif for the correct assembly of (bacterio)chlorophyll proteins.

In Chapter 5, it is shown by mutational analysis of the carotenoid binding pocket of native and model LH2 complexes that the aromatic residues, in particular phenylalanine, are a key factor for carotenoid binding. The phenylalanine not only contributes to the stable Car binding but also lock the Car into a particular molecular configuration. The importance of aromatic residues in Car binding is further supported by statistical analyses of the plant photosystems which show that phenylalanine residues are frequently in the close vicinity of Car molecules. This study provides, to the best of our knowledge, the first experimental evidence for the central role of aromatic residues in carotenoid binding and functional specification.

## 7. References

- Adamian L, Liang J (2001) Helix-helix packing and interfacial pairwise interactions of residues in membrane proteins. *J Mol Biol* 311: 891-907
- Adamian L, Liang J (2002) Interhelical hydrogen bonds and spatial motifs in membrane proteins: polar clamps and serine zippers. *Proteins* 47: 209-218
- Allen JP, Feher G, Yeates TO, Komiya H, Rees DC (1987) Structure of the reaction center from *Rhodobacter sphaeroides* R-26: the protein subunits. *Proc Natl Acad Sci U S A* 84: 6162-6166
- Allen SJ, Kim JM, Khorana HG, Lu H, Booth PJ (2001) Structure and function in bacteriorhodopsin: the effect of the interhelical loops on the protein folding kinetics. *J Mol Biol* 308: 423-435
- Aspinall-O'Dea M, Wentworth M, Pascal A, Robert B, Ruban A, Horton P (2002) *In vitro* reconstitution of the activated zeaxanthin state associated with energy dissipation in plants. *Proc Natl Acad Sci U S A* 99: 16331-16335
- Balaban TS (2003) Are syn-ligated (bacterio)chlorophyll dimers energetic traps in light-harvesting systems? *FEBS Lett* 545: 97-102
- Balaban TS (2005) Relevance of the diastereotopic ligation of magnesium atoms of chlorophylls in the major light-harvesting complex II (LHC II) of green plants. *Photosynth Res* 86: 251-262
- Balaban TS, Fromme P, Holzwarth AR, Krauß N, Prokhorenko VI (2002) Relevance of diastereotopic ligation of magnesium atoms of chlorophylls in photosystem I. *Biochim. Biophys. Acta* 1556: 197-207
- Bandilla M, Uecker B, Ram M, Simonin I I, Gelhaye E, McDermott G, Cogdell RJ, Scheer H (1998) Reconstitution of the B800 bacteriochlorophylls in the peripheral light harvesting complex B800-850 of *Rhodobacter sphaeroides* 2.4.1 with BChl a and modified (bacterio)chlorophylls. *Biochem Biophys Acta* 1364: 390-402
- Bassi R, Croce R, Cugini D, Sandona D (1999) Mutational analysis of a higher plant antenna protein provides identification of chromophores bound into multiple sites. *Proc Natl Acad Sci U S A* 96: 10056-10061
- Booth PJ, Paulsen H (1996) Assembly of light-harvesting chlorophyll a/b complex *in vitro*. Time-resolved fluorescence measurements. *Biochem* 35: 5103-5108
- Bowie JU (2005) Solving the membrane protein folding problem. *Nature* 438: 581-589
- Braun P, Greenberg BM, Scherz A (1990) D1-D2-cytochrome b559 complex from the aquatic plant *Spirodela oligorrhiza*: correlation between complex integrity, spectroscopic properties, photochemical activity, and pigment composition. *Biochem* 29: 10376-10387
- Braun P, Olsen J, Strohmann B, Hunter CN, Scheer H (2002) Assembly of light-harvesting bacteriochlorophyll in a model transmembrane helix in its natural environment. *J. Mol. Biol.* 318: 1085-1095
- Braun P, Scherz A (1991) Polypeptides and bacteriochlorophyll organization in the light-harvesting complex B850 of *Rhodobacter sphaeroides* R-26.1. *Biochem* 30: 5177-5184

- Braun P, Vegh A, Strohmann B, Hunter N, Robert B, Scheer H (2003) Hydrogen bonding between the C13<sup>1</sup> keto group of bacteriochlorophyll and intramembrane serine residue  $\alpha$  27 stabilizes LH2 antenna complex Biochim. Biophys. Acta 1607: 19-26
- Braun P, von Heijne G (1999) The aromatic residues Trp and Phe have different effects on the positioning of a transmembrane helix in the microsomal membrane. Biochemistry 38: 9778-9782
- Britton G, Young AJ (1993) Methods for the isolation and analysis of carotenoids Carotenoids in Photosynthesis. Young AJ, Britton G (eds). Carotenoids in Photosynthesis. Chapman & Hall, London: 409-459.
- Brunisholz RA, Zuber H (1992). Structure, Function and Organization of Antenna Polypeptides and Antenna Complexes from the 3 Families of Rhodospirillaneae. J. Photochem. Photobiol. B. 15, 113-140.
- Cherezov V, Clogston J, Papiz MZ, Caffrey M (2006) Room to move: crystallizing membrane proteins in swollen lipidic mesophases. J Mol Biol 357: 1605-1618
- Choma C, Gratkowski H, Lear JD, DeGrado WF (2000) Asparagine-mediated self-association of a model transmembrane helix. Nat Struct Biol 7: 161-166
- Chothia C (1976) The nature of the accessible and buried surfaces in proteins. J Mol Biol 105: 1-12
- Cinque G, Croce R, Bassi R (2000) Absorption spectra of chlorophyll  $\alpha$  and  $\beta$  in Lhcb protein environment. Photosynth Res 64: 233-242
- Clayton RK, Clayton BJ (1981b) B850 pigment-protein complex of *Rhodopseudomonas sphaeroides* - extinction coefficients, circular dichroism and the reversible binding of Bacteriochlorophyll. Proc. Natl. Acad. Sci. USA 78: 5583-5587
- Clayton RK, Smith C (1960) *Rhodopseudomonas sphaeroides*: high catalase and blue-green double mutants. Biochem Biophys Res Commun 3: 143-145
- Cogdell RJ, Crofts AR (1978) Analysis of the pigment content of an antenna pigment-protein complex from three strains of *Rhodopseudomonas sphaeroides*. Biochim Biophys Acta 502: 409-16
- Cogdell RJ, Isaacs NW, Freer AA, Howard TD, Gardiner AT, Prince SM, Papiz MZ (2003) The structural basis of light-harvesting in purple bacteria. FEBS Lett 555: 35-39
- Cogdell RJ, Parson WW, Kerr MA (1976) The type, amount, location, and energy transfer properties of the carotenoid in reaction centers from *Rhodopseudomonas sphaeroides*. Biochim Biophys Acta 430: 83-93
- Cogdell RJ, Scheer H (1985) Circular dichroism of light-harvesting complexes from purple photosynthetic bacteria. Photochem. Photobiol. 42: 669-678
- Cohen-Bazire G, Stanier RY (1958) Specific inhibition of carotenoid synthesis in a photosynthetic bacterium and its physiological consequences. Nature 181: 250-252
- Crielaard W, Visschers RW, Fowler GJS, van Grondelle R, Hellingwerf KJ, Hunter CN (1994) Probing the B800 bacteriochlorophyll binding site of the accessory light-harvesting complex from *Rhodobacter sphaeroides* using site-directed mutants. I. Mutagenesis, effects on binding, function and electrochromic behavior of its carotenoids (1994) Biochem Biophys Acta 1183, 473-482.

- Croce R, Weiss S, Bassi R (1999) Carotenoid-binding sites of the major light-harvesting complex II of higher plants. *J Biol Chem* 274: 29613-29623
- Davidson E, Cogdell RJ (1981) Reconstitution of carotenoids into the light-harvesting pigment-protein complex from the carotenoidless mutant of *Rhodospseudomonas sphaeroides* R26. *Biochim Biophys Acta* 635: 295-303
- Davis CM, Bustamante PL, Todd JB, Parkes-Loach PS, McGlynn P, Olsen JD, McMaster L, Hunter CN, Loach PA (1997) Evaluation of structure-function relationships in the core light-harvesting complex of photosynthetic bacteria by reconstitution with mutant polypeptides. *Biochemistry* 36: 3671-3679
- Dawson JP, Weinger JS, Engelman DM (2002) Motifs of serine and threonine can drive association of transmembrane helices. *J Mol Biol* 316: 799-805
- de Ruijter WP, Oellerich S, Segura JM, Lawless AM, Papiz M, Aartsma TJ (2004) Observation of the energy-level structure of the low-light adapted B800 LH4 complex by single-molecule spectroscopy. *Biophys J* 87: 3413-3420
- Deber CM, Wang C, Liu LP, Prior AS, Agrawal S, Muskat BL, Cuticchia AJ (2001) TM Finder: a prediction program for transmembrane protein segments using a combination of hydrophobicity and nonpolar phase helicity scales. *Protein Sci* 10: 212-219
- DeGrado WF, Gratkowski H, Lear JD (2003) How do helix-helix interactions help determine the folds of membrane proteins? Perspectives from the study of homo-oligomeric helical bundles. *Protein Sci* 12: 647-665
- Deisenhofer J, Epp O, Miki K, Huber R, Michel H (1984) X-ray structure analysis of a membrane protein complex. Electron density map at 3 Å resolution and a model of the chromophores of the photosynthetic reaction center from *Rhodospseudomonas viridis*. *J Mol Biol* 180: 385-398
- Desamero RZB, Chynwat V, van der Hoef I, Jansen FJ, Lugtenburg J, Gosztola D, Wasielewski MR, Cua A, Bocian DF, Frank HA (1998) Mechanism of energy transfer from carotenoids to bacteriochlorophyll: light-harvesting by carotenoids having different extents of  $\pi$  electron conjugation incorporated into the B850 antenna complex from the carotenoidless bacterium *Rhodobacter sphaeroides* R-26.1. *J. Phys. Chem. B* 102: 8151-62
- Desiraju GR (2002) Hydrogen bridges in crystal engineering: interactions without borders. *Acc Chem Res* 35: 565-573
- Eilers M, Patel AB, Liu W, Smith SO (2002) Comparison of helix interactions in membrane and soluble alpha-bundle proteins. *Biophys J* 82: 2720-2736
- Eilers M, Shekar SC, Shieh T, Smith SO, Fleming PJ (2000) Internal packing of helical membrane proteins. *Proc Natl Acad Sci U S A* 97: 5796-57801
- Engelman DM, Chen Y, Chin CN, Curran AR, Dixon AM, Dupuy AD, Lee AS, Lehnert U, Matthews EE, Reshetnyak YK, Senes A, Popot JL (2003) Membrane protein folding: beyond the two stage model. *FEBS Lett* 555: 122-125
- Engelman DM, Steitz TA (1981) The spontaneous insertion of proteins into and across membranes: the helical hairpin hypothesis. *Cell* 23: 411-422
- Fowler GJ, Gardiner AT, Mackenzie RC, Barratt SJ, Simmons AE, Westerhuis WH, Cogdell RJ, Hunter CN (1995) Heterologous expression of genes encoding bacterial light-

harvesting complexes in *Rhodobacter sphaeroides*. J Biol Chem 270: 23875-23882

Fowler GJ, Hess S, Pullerits T, Sundstrom V, Hunter CN (1997) The role of betaArg-10 in the B800 bacteriochlorophyll and carotenoid pigment environment within the light-harvesting LH2 complex of *Rhodobacter sphaeroides*. Biochemistry 36: 11282-91

Fowler GJ, Sockalingum GD, Robert B, Hunter CN (1994) Blue shifts in bacteriochlorophyll absorbance correlate with changed hydrogen bonding patterns in light-harvesting 2 mutants of *Rhodobacter sphaeroides* with alterations at alpha-Tyr-44 and alpha-Tyr-45. Biochem J 299 695-700

Fowler GJ, Visschers RW, Grief GG, van Grondelle R, Hunter CN (1992) Genetically modified photosynthetic antenna complexes with blueshifted absorbance bands. Nature 355: 848-850

Freer A, Prince S, Sauer K, Papiz M, Hawthornthwaite-Lawless A, McDermott G, Cogdell R, Isaacs NW (1996) Pigment-pigment interactions and energy transfer in the antenna complex of the photosynthetic bacterium *Rhodospseudomonas acidophila*. Structure 4: 449-462

Frese RN, Siebert CA, Niederman RA, Hunter CN, Otto C, van Grondelle R (2004) The long-range organization of a native photosynthetic membrane. Proc Natl Acad Sci U S A 101: 17994-17999

Fromme P, Jordan P, Krauss N (2001) Structure of photosystem I. Biochim Biophys Acta 1507: 5-31

Fuller RC, Anderson IC (1958) Suppression of carotenoid synthesis and its effect on the activity of photosynthetic bacterial chromatophores. Nature 181: 252-254

Gall A, Cogdell RJ, Robert B (2003) Influence of carotenoid molecules on the structure of the bacteriochlorophyll binding site in peripheral light-harvesting proteins from *Rhodobacter sphaeroides*. Biochemistry 42: 7252-7258

Gall A, Fowler GJ, Hunter CN, Robert B (1997) Influence of the protein binding site on the absorption properties of the monomeric bacteriochlorophyll in *Rhodobacter sphaeroides* LH2 complex. Biochemistry 36: 16282-16287

Gall A, Gardiner AT, Cogdell RJ, Robert B (2006) Carotenoid stoichiometry in the LH2 crystal: no spectral evidence for the presence of the second molecule in the alpha/beta-apoprotein dimer. FEBS Lett 580: 3841-3844

Gall A, Henry S, Takaichi S, Robert B, Cogdell RJ (2005) Preferential incorporation of coloured-carotenoids occurs in the LH2 complexes from non-sulphur purple bacteria under carotenoid-limiting conditions. Photosynth Res 86: 25-35

Gall A I, Ridge JP., Robert B, Cogdell RJ, Jones MR, Fyfe PK (2004) Effects of mutagenesis on the detailed structure of spheroidenone in the *Rhodobacter sphaeroides* reaction centre examined by resonance Raman spectroscopy Photosynthesis Research 59: 223-230

Garcia-Martin A, Kwa LG, Strohmam B, Robert B, Holzwarth AR, Braun P (2006a) Structural role of (bacterio)chlorophyll ligated in the energetically unfavorable  $\beta$ -position. J Biol Chem 281: 10626-10634

- Garcia-Martin A, Kwa LG, von Jan M, Braun P (2006b) Assembly of Model bacteriochlorophyll proteins in the native lipid environment. In Chlorophylls and Bacteriochlorophylls: Biochemistry, Biophysics, Functions and Applications B Grimm, W Porra, W Rüdiger, H Scheer (eds) Series: Advances in Photosynthesis (Govindjee ed.) Springer, Dordecht: 387-96
- Garcia-Martin A, Kwa LG, von Jan M, Vegh A, Robert B, Scheer H, Braun P (2005) H-bonding drives assembly of model bacteriochlorophyll protein in the native membrane. In: PS2004 Proceedings: 13th International Congress on Photosynthesis: Fundamental Aspects to global, van der Est A and Bruce D (eds) Allen Press, Montreal, Canada: 138-140
- Georgakopoulou S, Frese RN, Johnson E, Koolhaas C, Cogdell RJ, van Grondelle R, van der Zwan G (2002) Absorption and CD spectroscopy and modeling of various LH2 complexes from purple bacteria. *Biophys J* 82: 2184-2197
- Georgakopoulou S, van Grondelle R, van der Zwan G (2004) Circular dichroism of carotenoids in bacterial light-harvesting complexes: experiments and modeling. *Biophys J* 87: 3010-3022
- Germain C, Larbouret C, Cesson V, Donda A, Held W, Mach JP, Pelegrin A, Robert B (2005) MHC class I-related chain A conjugated to antitumor antibodies can sensitize tumor cells to specific lysis by natural killer cells. *Clin Cancer Res* 11: 7516-7522
- He Z, Sundstrom V, Pullerits T (2001) Intermolecular hydrogen bonding between carotenoid and bacteriochlorophyll in LH2. *FEBS Lett* 496: 36-39
- Heinemann B, Paulsen H (1999) Random mutations directed to transmembrane and loop domains of the light-harvesting chlorophyll a/b protein: impact on pigment binding. *Biochemistry* 38: 14088-93
- Henderson R, Baldwin JM, Ceska TA (1990) Model for the structure of Bacteriorhodopsin based on high-resolution electron cryo-microscopy. *J Mol Biol* 213: 899-929
- Ho B, Curmi PM (2002) Twist and shear in beta-sheets and beta-ribbons. *J Mol Biol* 317: 291-308
- Horvin Billsten H, Herek JL, Garcia-Asua G, Hashoj L, Polivka T, Hunter CN, Sundstrom V (2002) Dynamics of energy transfer from lycopene to bacteriochlorophyll in genetically-modified LH2 complexes of *Rhodobacter sphaeroides*. *Biochemistry* 41: 4127-4136
- Hu Q, Sturgis JN, Robert B, Delagrave S, Youvan DC, Niederman RA (1998) Hydrogen bonding and circular dichroism of bacteriochlorophylls in the *Rhodobacter capsulatus* light-harvesting 2 complex altered by combinatorial mutagenesis. *Biochemistry* 37: 10006-10015
- Hughes JM, Hutter MC, Reimers JR, Hush NS (2001) Modeling the bacterial photosynthetic reaction center. 4. The structural, electrochemical, and hydrogen-bonding properties of 22 mutants of *Rhodobacter sphaeroides*. *J Am Chem Soc* 123: 8550-8563
- Hunter CN, McGlynn P, Ashby MK, Burgess JG, Olsen JD (1991) DNA sequencing and complementation/deletion analysis of the bchA-puf operon region of *Rhodobacter sphaeroides*: *in vivo* mapping of the oxygen-regulated puf promoter. *Mol Microbiol* 5: 2649-2661
- Ivancich A, Artz K, Williams JC, Allen JP, Mattioli TA (1998) Effects of hydrogen bonds on

the redox potential and electronic structure of the bacterial primary electron donor. *Biochemistry* 37: 11812-11820

Janovjak H, Muller DJ, Humphris AD (2005) Molecular force modulation spectroscopy revealing the dynamic response of single bacteriorhodopsins. *Biophys J* 88: 1423-1431

Jensen SL, Cohen-Bazire G, Nakayama TO (1958) The path of carotenoid synthesis in a photosynthetic bacterium. *Biochim Biophys Acta* 29: 477-498

Jones MR, Fowler GJ, Gibson LC, Grief GG, Olsen JD, Crielaard W, Hunter CN (1992) Mutants of *Rhodobacter sphaeroides* lacking one or more pigment-protein complexes and complementation with reaction-centre, LH1, and LH2 genes. *Mol Microbiol* 6: 1173-1184

Jones MR, Visschers RW, van Grondelle R, Hunter CN (1992) Construction and characterization of a mutant of *Rhodobacter sphaeroides* with the reaction center as the sole pigment-protein complex. *Biochemistry* 31: 4458-4465

Jordan P, Fromme P, Witt HT, Klukas O, Saenger W, Krauss N (2001) Three-dimensional structure of cyanobacterial photosystem I at 2.5 Å resolution. *Nature* 411: 909-917

Karrasch S, Bullough PA, Ghosh R (1995) The 8.5 Å projection map of the light-harvesting complex I from *Rhodospirillum rubrum* reveals a ring composed of 16 subunits. *EMBO J* 14: 631-638

Kashiwada A, Nishino N, Wang Z-H, Nozawa T, Kobayashi M, Nango M (1999) Molecular Assembly of Bacteriochlorophyll *a* and its Analogues by Synthetic 4  $\alpha$ -Helix Polypeptides. *Chem Lett*: 1301-1302

Keen NT, Tamaki S, Kobayashi D, Trollinger D (1988) Improved broad-host-range plasmids for DNA cloning in gram-negative bacteria. *Gene* 70: 191-197

Kehoe JW, Meadows KA, Parkes-Loach PS, Loach PA (1998) Reconstitution of core light-harvesting complexes of photosynthetic bacteria using chemically synthesized polypeptides. 2. Determination of structural features that stabilize complex formation and their implications for the structure of the subunit complex. *Biochemistry* 37: 3418-3428

Kerfeld CA (2004) Water-soluble carotenoid proteins of cyanobacteria. *Arch Biochem Biophys* 430: 2-9

Kim JM, Booth PJ, Allen SJ, Khorana HG (2001) Structure and function in bacteriorhodopsin: the role of the interhelical loops in the folding and stability of bacteriorhodopsin. *J Mol Biol* 308: 409-422

Kleiger G, Grothe R, Mallick P, Eisenberg D (2002) GXXXG and AXXXA: common alpha-helical interaction motifs in proteins, particularly in extremophiles. *Biochemistry* 41: 5990-5997

Koepke J, Hu X, Muenke C, Schulten K, Michel H (1996) The crystal structure of the light-harvesting complex II (B800-850) from *Rhodospirillum molischianum*. *Structure* 4: 581-597

Koolhaas MHC, Frese RN, Fowler GJS, Bibby TS, Georgakopoulou S, van der Zwan G, Hunter CN, van Grondelle R (1998). Identification of the upper exciton component of the B850 bacteriochlorophylls of the LH2 antenna complex, using a B800-free mutant of *Rhodobacter sphaeroides*. *Biochemistry* 37: 4693-4698

Koyama Y, Fujii R (1999) Cis-trans carotenoids in photosynthesis: Configurations,

excited-state properties and physiological functions. In *The photochemistry of carotenoids* HA Frank, AJ Young, G Britton, RJ Cogdell (eds). Kluwer Academic Publishers, Dordrecht: 161-188.

Koyama Y, Rondonuwu FS, Fujii R, Watanabe Y (2004) Light-harvesting function of carotenoids in photosynthesis: the roles of the newly found 1(1)Bu- state. *Biopolymers* 74: 2-18

Kühlbrandt W, Wang DN, Fujiyoshi Y (1994) Atomic model of plant light-harvesting complex by electron crystallography. *Nature* 367: 614-621

Kwa LG, Garcia-Martin A, Vegh AP, Strohmann B, Robert B, Braun P (2004) Hydrogen bonding in a model bacteriochlorophyll-binding site drives assembly of light harvesting complex. *J Biol Chem* 279: 15067-15075

Laemmli UK (1970) Cleavage of structural proteins during the assembly of the head of bacteriophage T4. *Nature* 227: 680-685

Landin JS, Katragadda M, Albert AD (2001) Thermal destabilization of rhodopsin and opsin by proteolytic cleavage in bovine rod outer segment disk membranes. *Biochemistry* 40: 11176-11183

Landolt-Marticorena C, Williams KA, Deber CM, Reithmeier RA (1993) Non-random distribution of amino acids in the transmembrane segments of human type I single span membrane proteins. *J Mol Biol* 229: 602-608

Lang HP, Hunter CN (1994) The relationship between carotenoid biosynthesis and the assembly of the light-harvesting LH2 complex in *Rhodobacter sphaeroides*. *Biochem J* 298: 197-205

Lapouge K, Naveke A, Gall A, Ivancich A, Seguin J, Scheer H, Sturgis JN, Mattioli TA, Robert B (1999) Conformation of bacteriochlorophyll molecules in photosynthetic proteins from purple bacteria. *Biochemistry* 38: 11115-11121

Lapouge K, Naveke A, Robert B, Scheer H, Sturgis JN (2000) Exchanging cofactors in the core antennae from purple bacteria: structure and properties of Zn-bacteriopheophytin-containing LH1. *Biochemistry* 39: 1091-1099

Law CJ, Prince SM and Cogdell (1998). Crystallizing of LH1-RC core complex of purple bacteria. *Biochem Soc Trans* 26: 160

Law CJ, Roszak AW, Southall J, Gardiner AT, Isaacs NW, Cogdell RJ (2004) The structure and function of bacterial light-harvesting complexes. *Mol Membr Biol* 21: 183-191

Leupold D, Stiel H, Teuchner K, Nowak F, Sandner W, Ucker B, Scheer H (1996) Size enhancement of transition dipoles to one- and two-exciton bands in a photosynthetic antenna. *Phys Rev Let* 77: 4675-4678

Liebl U, Nitschke Wa, Mattioli TA (1996) Pigment-Protein Interactions in the Antenna-Reaction Center Complex of *Heliobacillus mobilis*. *Photochem. Photobiol.* 64: 38-45

Linnanto, J. and Korppi-Tommola, J. (2004) Structural and Spectroscopic Properties of Mg-Bacteriochlorin and Methyl Bacteriochlorophyllides a, b, g, and h Studied by Semiempirical, ab Initio, and Density Functional Molecular Orbital Methods. *J Phys Chem A* 108: 5872- 5882.

- Loll B, Kern J, Saenger W, Zouni A, Biesiadka J (2005). Towards complete cofactor arrangement in the 3.0 Å resolution structure of photosystem II. *Nature* 438: 1040-1044
- Mattioli TA, Gray KA, Lutz M, Oesterhelt D, Robert B (1991) Resonance Raman characterization of *Rhodobacter sphaeroides* reaction centers bearing site-directed mutations at Tyrosine M210. *Biochem* 30: 1715-1721.
- Mattioli TA, Hoffmann, A., Sockalingum, D.G., Schrader, B., Robert, B., Lutz, M (1993) Application of near IR Fourier-Transform resonance Raman spectroscopy to the study of photosynthetic systems. *Spectrochim Acta* 49A: 785-99.
- McDermott G, Prince SM, Freer AA, Hawthornthwaite-Lawless AM, Papiz MZ, Cogdell RJ, Isaacs NW (1995) Crystal structure of an integral membrane light-harvesting complex from photosynthetic bacteria. *Nature* 374: 517-521.
- McLuskey K, Prince SM, Cogdell RJ, Isaacs NW (2001). The crystallographic structure of the B800-820 LH3 light-harvesting complex from the purple bacteria *Rhodospseudomonas acidophila* strain 7050. *Biochem* 40: 8783-8789
- Meadows KA, Parkes-Loach PS, Kehoe JW, Loach PA (1998) Reconstitution of core light-harvesting complexes of photosynthetic bacteria using chemically synthesized polypeptides. 1. Minimal requirements for subunit formation. *Biochem* 37: 3411-3417
- Moenne-Loccoz P, Robert B, Ikegami I, Lutz M (1990) Structure of the primary electron donor in photosystem I: a resonance Raman study. *Biochem* 29: 4740-4746
- Monne M, Nilsson I, Elofsson A, von Heijne G (1999) Turns in transmembrane helices: determination of the minimal length of a "helical hairpin" and derivation of a fine-grained turn propensity scale. *J Mol Biol* 293: 807-814
- Monne M, Nilsson I, Johansson M, Elmhed N, von Heijne G (1998) Positively and negatively charged residues have different effects on the position in the membrane of a model transmembrane helix. *J Mol Biol* 284: 1177-1183
- Montoya G, Cyrklaff M, Sinning I (1995) Two-dimensional crystallization and preliminary structure analysis of light harvesting II (B800-850) complex from the purple bacterium *Rhodovulum sulfidophilum*. *J Mol Biol* 250: 1-10
- Moss G (1998) IUPAC-IUB Joint commission biochemical nomenclature. *Eur J. Biochem* 178: 277-328
- Näveke A, Lapouge K, Sturgis JN, Harwich G, Simonin I, Scheer H, Robert B (1997) Resonance Raman spectroscopy of metal-substituted bacteriochlorophylls: Characterization of Raman bands sensitive to bacteriochlorin conformation. *J Raman Spectr* 28: 599-604
- Niedermann RA (1974) Membranes of *Rhodospseudomonas sphaeroides*: Interactions of Chromatophores with the Cell Envelope. *J Bacteriol* 117: 19-28
- Oba T, Tamiaki H (2002) Which side of the  $\pi$ -macrocycle plane of (bacterio)chlorophylls is favoured for binding of the fifth ligand. *Photosynth Res* 74: 1-10
- Olsen JD, Robert B, Siebert CA, Bullough PA, Hunter CN (2003) Role of the C-terminal extrinsic region of the alpha polypeptide of the light-harvesting II complex of *Rhodobacter sphaeroides*: a domain swap study. *Biochem* 42: 15114-15123
- Olsen JD, Sockalingum GD, Robert B, Hunter CN (1994) Modification of a hydrogen bond

- to a bacteriochlorophyll a molecule in the light-harvesting I antenna of *Rhodobacter sphaeroides*. Proc Natl Acad Sci U S A 91: 7124-7128
- Olsen JD, Sturgis JN, Westerhuis WH, Fowler GJ, Hunter CN, Robert B (1997) Site-directed modification of the ligands to the bacteriochlorophylls of the light-harvesting LH1 and LH2 complexes of *Rhodobacter sphaeroides*. Biochem 36: 12625-12632
- Palencar P, Vacha F, Kutý M (2005) Force field development on pigments of photosystem 2 reaction center. Photosynthetic 43: 417-420
- Papagiannakis E, Kennis JT, van Stokkum IH, Cogdell RJ, van Grondelle R (2002) An alternative carotenoid-to-bacteriochlorophyll energy transfer pathway in photosynthetic light harvesting. Proc Natl Acad Sci U S A 99: 6017-6022
- Papiz MZ, Prince SM, Howard T, Cogdell RJ, Isaacs NW (2003) The structure and thermal motion of the B800-850 LH2 complex from *Rhodospseudomonas acidophila* at 2.0 Å resolution and 100K: new structural features and functionally relevant motions. J Mol Biol 326: 1523-1538
- Polivka T, Sundstrom V (2004) Ultrafast dynamics of carotenoid excited States-from solution to natural and artificial systems. Chem Rev 104: 2021-2071
- Popot JL, Engelman DM (1990) Membrane protein folding and oligomerization: the two-stage model. Biochem 29: 4031-4037
- Popot JL, Engelman DM (2000) Helical membrane protein folding, stability, and evolution. Annu Rev Biochem 69: 881-922
- Popot JL, Engelman DM, Zaccai G, de Vitry C (1990) The "microassembly" of integral membrane proteins: applications & implications. Prog Clin Biol Res 343: 237-262
- Porra RJ, Schaefer W, Gadon N, Katheder I, Drews G, Scheer H (1996). Origin of the two carbonyl oxygens of bacteriochlorophyll alpha - Demonstration of two different pathways for the formation of ring E in *Rhodobacter sphaeroides* and *Roseobacter denitrificans*, and a common hydratase mechanism for 3-acetyl group formation. Eur J Biochem 239: 85-92
- Porra RJ, Urzinger M, Winkler H, Bubenzer C, Scheer H (1998) Biosynthesis of the 3-Acetyl and 13<sup>1</sup>-Oxo groups of bacteriochlorophyll a in the facultative aerobic bacterium, *Rhodovulum sulfidophilum*: the presence of both oxygenase and hydratase pathways for isocyclic ring formation. Eur J Biochem 257: 185-191
- Prince SM, Howard TD, Myles DA, Wilkinson C, Papiz MZ, Freer AA, Cogdell RJ, Isaacs NW (2003) Detergent structure in crystals of the integral membrane light-harvesting complex LH2 from *Rhodospseudomonas acidophila* strain 10050. J Mol Biol 326: 307-315
- Prince SM, Papiz MZ, Freer AA, McDermott G, Hawthornthwaite-Lawless AM, Cogdell RJ, Isaacs NW (1997) Apoprotein structure in the LH2 complex from *Rhodospseudomonas acidophila* strain 10050: modular assembly and protein pigment interactions. J Mol Biol 268: 412-423
- Rau HK, Snigula H, Struck A, Robert B, Scheer H, Haehnel W (2001) Design, synthesis and properties of synthetic chlorophyll proteins. Eur J Biochem 268: 3284-3295
- Remelli R, Varotto C, Sandona D, Croce R, Bassi R (1999) Chlorophyll binding to monomeric light-harvesting complex. A mutation analysis of chromophore-binding residues. J Biol Chem 274: 33510-33521

- Robert B (1996) Application of resonance Raman spectroscopy in photosynthesis. In *Biophysical Techniques in Photosynthesis*. J Amesz, A Hoff (eds). Kluwer Academic Publisher, Amsterdam: 161-176
- Robert B (1999) The electronic structure, stereochemistry and resonance Raman spectroscopy of carotenoids. In *The photochemistry of carotenoids*. HA Frank, AJ Young, G Britton, RJ Cogdell (eds) Vol 8 of 'Advances in Photosynthesis', series editor Govindjee Kluwer, Dordrecht: 189-201
- Robert B, Frank HA (1988) A resonance raman investigation of the effect of Lithium Dodecyl-sulfate on the B800-850 light-harvesting protein of *Rhodospseudomonas acidophila* 7750. *Biochem Biophys Acta* 934: 401-405
- Robert B, Lutz M (1985) Structures of antenna complexes of several *Rhodospirillales* from their resonance Raman spectra *Biochem Biophys Acta* 807: 10-23
- Roszak AW, McKendrick K, Gardiner AT, Mitchell IA, Isaacs NW, Cogdell RJ, Hashimoto H, Frank HA (2004) Protein regulation of carotenoid binding; gatekeeper and locking amino acid residues in reaction centers of *Rhodobacter sphaeroides*. *Structure* 12: 765-773
- Russ WP, Engelman DM (2000) The GxxxG motif: a framework for transmembrane helix-helix association. *J Mol Biol* 296: 911-919
- Saenger W, Jordan P, Krauss N (2002) The assembly of protein subunits and cofactors in photosystem I. *Curr Opin Struct Biol* 12: 244-54
- Sambrook J, Fritsch EF, Maniatis T (1989) *Molecular cloning: a laboratory manual* (2nd ed.). Cold Spring Harbour Laboratory Press, New York
- Sauer K, Cogdell RJ, Prince SM, Freer AA, Isaacs NW, Scheer H (1996) Structure-based calculations of the optical spectra of the LH II Bacteriochlorophyll-protein complex from *Rhodospseudomonas acidophila*. *Photochem Photobiol* 64: 564-576
- Sauer PR, Lottspeich F, Unger E, Mentele R, Michel H (1996) Deletion of a B800-850 light-harvesting complex in *Rhodospirillum molischianum* DSM119 leads to "revertants" expressing a B800-820 complex: insights into pigment binding. *Biochem* 35: 6500-6507
- Scheer H (2006) An overview of chlorophylls and bacteriochlorophylls: biochemistry, biophysics, functions and applications. In *Chlorophylls and Bacteriochlorophylls: Biochemistry, Biophysics, Functions and Applications* B Grimm, RJ Porra, W Rüdiger and Scheer (eds). *Advances in Photosynthesis and Respiration*, vol 25. Springer, Dordrecht, 1-26
- Scheer H, Hartwich G (1995) Bacterial reaction centers with modified tetrapyrrole chromophores. R Blankenship, MT Madigan, and CE Bauer (eds) In *Anoxygenic Photosynthetic Bacteria*. Dordrecht, Kluwer: 649-663.
- Scherz A and Parson W W (1986) Interactions of the bacteriochlorophylls in antenna bacteriochlorophyll-protein complexes of photosynthetic bacteria. *Photosyn res* 9: 21-32
- Scheuring S, Seguin J, Marco S, Levy D, Breyton C, Robert B, Rigaud JL (2003) AFM characterization of tilt and intrinsic flexibility of *Rhodobacter sphaeroides* light harvesting complex 2 (LH2). *J Mol Biol* 325: 569-580
- Senes A, Gerstein M, Engelman DM (2000) Statistical analysis of amino acid patterns in transmembrane helices: the GxxxG motif occurs frequently and in association with beta-

branched residues at neighboring positions. *J Mol Biol* 296: 921-36

Shan SO, Herschlag D (1996) The change in hydrogen bond strength accompanying charge rearrangement: implications for enzymatic catalysis. *Proc Natl Acad Sci U S A* 93: 14474-14479

Shlyk-Kerner O, Samish I, Kaftan D, Holland N, Sai PS, Kless H, Scherz A (2006) Protein flexibility acclimatizes photosynthetic energy conversion to the ambient temperature. *Nature* 442: 827-830

Shneour EA (1962) Carotenoid pigment conversion in *Rhodopseudomonas sphaeroides*. *Biochim Biophys Acta* 62: 534-540

Simon R.P, Priefer U, Puhler A (1983) A broad host range mobilization system for *in vivo* genetic engineering: transposon mutagenesis in Gram-negative bacteria. *Biol/Technology* 1: 784-791

Sipos L, von Heijne G (1993) Predicting the topology of eukaryotic membrane proteins. *Eur J Biochem* 213: 1333-1340

Sturgis JN, Hagemann G, Tadros MH, Robert B (1995) Biochemical and spectroscopic characterization of the B800-850 light-harvesting complex from *Rhodobacter sulphidophilus* and its B800-830 spectral form. *Biochem* 34: 10519-10524

Sturgis JN, Jirsakova V, Reiss-Husson F, Cogdell RJ, Robert B (1995) Structure and properties of the bacteriochlorophyll binding site in peripheral light-harvesting complexes of purple bacteria. *Biochem* 34: 5175-23

Sturgis JN, Olsen JD, Robert B, Hunter CN (1997) Functions of conserved tryptophan residues of the core light-harvesting complex of *Rhodobacter sphaeroides*. *Biochem* 36: 2772-2778

Sturgis JN, Robert B (1996) The role of chromophore coupling in tuning the spectral properties of peripheral light-harvesting protein of purple bacteria. *Photosynth. Res.* 50: 5-10

Sturgis JN, Robert B (1997) Pigment binding site and electronic properties in light-harvesting proteins of purple bacteria. *J. Phys. Chem.* 101: 7227-7231

Takaichi S (1999) Carotenoids and carotenogenesis in anoxygenic photosynthetic bacteria. In *The photochemistry of carotenoids*. HA Frank, AJ Young, G Britton, RJ Cogdell (eds)(Kluwer Academic Publishers, Dordrecht: 36-39

Todd JB, Parkes-Loach PS, Leykam JF, Loach PA (1998) *In vitro* reconstitution of the core and peripheral light-harvesting complexes of *Rhodospirillum rubrum* from separately isolated components. *Biochem* 37: 17458-17468

van Grondelle R (1985) Excitation energy transfer, trapping and annihilation in photosynthetic systems. *Biochim Biophys Acta* 811: 147-195

Visschers RW, Crielaard W, Fowler GJS, Hunter CN, van Grondelle R (1994). Probing the B800 bacteriochlorophyll binding site of the accessory light-harvesting complex from *Rhodobacter sphaeroides* using site-directed mutants. II. A low-temperature spectroscopy study of structural aspects of the pigment-protein conformation. *Biochim Biophys Acta* 1183, 483-490.

von Heijne G (1994) Membrane proteins: from sequence to structure. *Annu Rev Biophys*

Biomol Struct 23: 167-192

Walz T, Jamieson SJ, Bowers CM, Bullough PA, Hunter CN (1998) Projection structures of three photosynthetic complexes from *Rhodobacter sphaeroides*: LH2 at 6 Å, LH1 and RC-LH1 at 25 Å. *J Mol Biol* 282: 833-845

Wang Y, Hu X (2002) A quantum chemistry study of binding carotenoids in the bacterial light-harvesting complexes. *J Am Chem Soc* 124: 8445-8451

White SH, Wimley WC (1999) Membrane protein folding and stability: physical principles. *Annu Rev Biophys Biomol Struct* 28: 319-365

Witt H, Schlodder E, Teutloff C, Niklas J, Bordignon E, Carbonera D, Kohler S, Labahn A, Lubitz W (2002) Hydrogen bonding to P700: site-directed mutagenesis of threonine A739 of photosystem I in *Chlamydomonas reinhardtii*. *Biochem* 41: 8557-8569

Yeliseev AA, Eraso JM, Kaplan S (1996) Differential carotenoid composition of the B875 and B800-850 photosynthetic antenna complexes in *Rhodobacter sphaeroides* 2.4.1: involvement of spheroidene and spheroidenone in adaptation to changes in light intensity and oxygen availability. *J Bacteriol* 178: 5877-5883

Yeliseev AA, Kaplan S (1997) Anaerobic carotenoid biosynthesis in *Rhodobacter sphaeroides* 2.4.1: H<sub>2</sub>O is a source of oxygen for the 1-methoxy group of spheroidene but not for the 2-oxo group of spheroidenone. *FEBS Lett* 403: 10-14

Zeng X, Choudhary M, Kaplan S (2003) Second and unusual *pucBA* operon of *Rhodobacter sphaeroides* 2.4.1: genetics and function of the encoded polypeptides. *J Bact* 185: 6171-6184

Zamyatin AA (1972) Protein volume in solution. *Prog Biophys Mol Biol* 24: 107-123

Zhou FX, Cocco MJ, Russ WP, Brunger AT, Engelman DM (2000) Interhelical hydrogen bonding drives strong interactions in membrane proteins. *Nat Struct Biol* 7: 154-160

Zhou FX, Merianos HJ, Brunger AT, Engelman DM (2001) Polar residues drive association of polyleucine transmembrane helices. *Proc Natl Acad Sci U S A* 98: 2250-2255

Zsila F, Molnar P, Deli J, Lockwood SF (2005) Circular dichroism and absorption spectroscopic data reveal binding of the natural cis-carotenoid bixin to human alpha1-acid glycoprotein. *Bioorg Chem* 33: 298-309

Zuber H (1986) Primary structure and function of the light-harvesting polypeptides from cyanobacteria, red algae, and purple photosynthetic bacteria. In *Photosynthesis III: Photosynthetic Membranes and Light-Harvesting Systems*. LA Staehelin and CJ Arntzen (eds). Springer Verlag, Berlin:238-251

Zuber H, Cogdell RJ (1995). Structure and Organization of Purple Bacterial Antenna Complexes. In *Anoxygenic Photosynthetic Bacteria*. R Blankenship, MT Madigan and CE Bauer (eds). Dordrecht, Kluwer Academic Publishers: 315-348

Zurdo J, Fernandez-Cabrera C, Ramirez JM (1993). A Structural Role of the Carotenoid in the Light-Harvesting II-Protein of *Rhodobacter capsulatus*. *Biochem J* 290, 531-537

# Ehrenwörtliche Versicherung

Die vorliegende Dissertation wurde von Dipl. Biol. Adela García-Martín selbständig und ohne unerlaubte Hilfe angefertigt. Der Verfasser hat zuvor nicht versucht, anderweitig eine Dissertation einzureichen oder sich einer Doktorprüfung zu unterziehen. Die Dissertation wurde keiner weiteren Prüfungskommission weder in Teilen noch als Ganzes vorgelegt.

Adela García Martín, München 09/02/2007

## Publications list

**Garcia-Martin A**, Kwa LG, Strohmann B, Robert B, Holzwarth AR, Braun P (2006) Structural role of (bacterio)chlorophyll ligated in the energetically unfavorable  $\beta$ -position. *J Biol Chem* 281: 10626-34

**Garcia-Martin A**, Kwa LG, von Jan M, and Braun P (2006) Assembly of Model bacteriochlorophyll proteins in the native lipid environment. In *Chlorophylls and Bacteriochlorophylls: Biochemistry, Biophysics, Functions and Applications* (Grimm B, Porra W, Rüdiger W, Scheer H (eds). Series: *Advances in Photosynthesis* (Govindjee ed.) Springer, Dordecht: 387-96

**Garcia-Martin A**, Kwa LG, von Jan M, Vegh A, Robert B, Scheer H, and Braun P (2005) H-bonding drives assembly of model bacteriochlorophyll protein in the native membrane. In: *PS2004 Proceedings: 13th International Congress on Photosynthesis: Fundamental Aspects to global*, van der Est A and Bruce D (eds) Allen Press, Montreal, Canada: 138-140

Kwa LG\*, **Garcia-Martin A\***, Vegh AP, Strohmann B, Robert B, Braun P (2004) Hydrogen bonding in a model bacteriochlorophyll-binding site drives assembly of light harvesting complex. *J Biol Chem* 279: 15067-75

**García-Martín A**, Pazur A, Wilhelm B, Robert B, and Braun P The aromatic residue, phenylalanine, drives binding of carotenoid in model light harvesting complex submitted to *J Mol Biol*

\*These authors contributed equally to this work.

# *Curriculum vitae*

Adela García Martín

25/04/1975, Córdoba, Spain

e-mail:tgm-75@hotmail.de

## **School education**

1989-1993 Secondary School, at “Sagrado Corazón”, Córdoba, Spain

## **University education**

1993-1999 Licenciatura en Biología (Diplom biologie) at Córdoba University, Spain

## **Scholarships**

2000-2001 Erasmus scholarship, Eichstätt University, Germany

## **Graduate studies**

Since June 2001 at the laboratory of PD. Dr. P. Braun, Department Biologie I, Bereich Botanik; Ludwig-Maximilians Universität, München, Germany